Reconstructing Late Holocene Environmental Change in the Pevensey Levels: Stratigraphic and Paleoenvironmental Insights from Horse Eye and North Eye, UK

by

Kian Leonard Drew

A thesis

presented to the University of Waterloo

in fulfilment of the

thesis requirement for the degree of

Master of Science

in

Earth Sciences

Waterloo, Ontario, Canada, 2025

© Kian Leonard Drew 2025

Author's Declaration

This thesis consists of material all of which I authored or co-authored: see Statement of Contributions included in the thesis. This is a true copy of the thesis, including any required final revisions, as accepted by my examiners.

I understand that my thesis may be made electronically available to the public.

Statement of Contributions

The following contributors assisted in the analysis, collection, or display of data for the specified sections. All other parts of this thesis are my own work.

Field Work:

- Dr. John Johnston and Dr. Ben Pears assisted with fieldwork conducted at North Eye (2022).
- Dr. Johnston, Dr. Ben Pears, and two field assistants, Wilfrid Laurier University student Anna Cassell and University of Waterloo student Kira Bourque, assisted with fieldwork conducted at Horse Eye (2023).

Laboratory Analysis:

- LOI and pXRF analysis was conducted by Dr. Ben Pears at the University of Southampton.
- XRD analysis was conducted by both the author (supervised by Dr. Atindra Sapkota) and by Dr. Atindra Sapkota at the Groundwater Geochemistry Remediation Group at the University of Waterloo and was supported by University of Waterloo student Ehsan Niknam.

Figures:

- Dr. Ben Pears aided with the development of age-depth models (Figures 4.27, 4.28, 4.29, and 4.30) in Section 4.3.10: Geochronology Results, and the climatic model in Figure 5.8 Section 5.3.1: Climatic Variability Across Part of the Holocene.
- University of Waterloo student Nicholas Mesich assisted in plotting the cumulative grain size plot in Figure 5.8 in section 5.3.1: Climatic Variability Across Part of the Holocene.

Abstract

This thesis investigates the stratigraphic framework and paleoenvironmental evolution of the Pevensey Levels, focusing on the depositional histories of the sediment covering the bedrock-cored islands Horse Eye and North Eye in East Sussex, United Kingdom (UK). Low-lying coastal systems such as the Pevensey Levels are sensitive to climatic variability, geomorphological changes, and human interaction, yet detailed stratigraphic and environmental reconstructions are limited for these landscapes. By combining field observations, sedimentological analyses, and laboratory analyses, this research enhances the understanding of climatic events, geomorphological factors, and anthropogenic influences that have shaped this low-lying coastal-lagoonal landscape over the Holocene.

A multiproxy laboratory approach- including laboratory methods that include laser diffraction grain size analysis, portable X-ray fluorescence (pXRF), loss on ignition (LOI), X-ray diffraction (XRD), and AMS radiocarbon dating- was applied to create a stratigraphic framework for reconstructing the stratigraphy and environmental history of the sediment on these bedrock-cored islands. The stratigraphic analyses reveal a broadly consistent depositional sequence across both islands, transitioning from lower marine silty clays at the base to organic-rich peat layers and finally to upper terrestrial clayey silts. Despite this similarity, there are differences that emerge: North Eye's stratigraphy includes sand-dominated units, attributed to its thinner sediment cover, bedrock exposure, and localized sediment contributions during episodic higher-energy depositional events. In contrast, Horse Eye's thicker sediment cover and more continuous peat layers indicate prolonged lower-energy deposition and water-logged conditions. Additionally, the lithologic and stratigraphic analyses conducted in this thesis offer a higher level of detail compared to earlier studies, providing localized depositional variability. These findings distinguish this research from earlier work in the area, which provided generalized stratigraphic data for North Eye and focused on broader regional depositional sequences within the Pevensey Levels.

The integration of results from the different techniques identified a temporal alignment between localized responses in the sediment with key climatic events, such as the globally recognized 4.2 ka event- a period characterized by dry climates in some regions but has remained poorly understood in Western Europe. At the Pevensey Levels, the stratigraphy during this period reveals an increase in sand content, indicative of heightened depositional energy and fluctuating hydrological conditions, providing new insights into how this global climatic phase may have influenced low-lying coastal landscapes in the UK. The findings also align temporally with documentation of human modifications during the late Holocene, including drainage and land reclamation. For example, lenticular laminations and an increase in sand content in the upper stratigraphy align with documented medieval drainage efforts in this region. This thesis situates these modifications within a regional context, noting how anthropogenic activities may have influenced sedimentary processes in dynamic coastal environments.

This thesis provides a new framework for understanding the evolution of the Pevensey Levels within a broader regional context by drawing comparisons with adjacent systems such as the Romney Marsh and Somerset Levels. While the Pevensey Levels exhibit broadly similar depositional patterns to adjacent systems, including marine-to-terrestrial transitions, there are localized differences in sediment depositional processes due to geomorphological controls, such as the differences in size and shape of the bedrock islands, as well as their location with respect to their proximity to sediment sources. The Pevensey Levels' stratigraphy is more influenced by bedrock-controlled sedimentation near the bedrock-cored islands, landforms that are not present in the Romney Marsh. These regional comparisons reveal variations in depositional energy, peat development, and anthropogenic modifications, offering new insights into the factors shaping coastal-lagoonal systems during the Holocene.

Acknowledgements

I would like to extend my deepest gratitude to those who have supported and guided me throughout this thesis journey. First and foremost, I would like to thank my supervisors, Dr. John Johnston and Dr. Martin Ross. John has been an unwavering source of guidance and encouragement, seeing this project grow from an undergraduate thesis into the MSc thesis it is today. Your mentorship and support have been invaluable. Martin, your insights have greatly shaped this work, and I am grateful for your guidance. To my committee members, Dr. Keith Delaney and Dr. Ben Pears, thank you for your invaluable feedback and support. Our committee meetings were always productive and encouraging, providing me with the direction and confidence to move forward. Ben, your advice and support throughout the project, both in and outside of meetings, was especially helpful, and I deeply appreciate your mentorship. I would also like to express my gratitude to the residents and landowner of Horse Eye and North Eye for access to the sites.

The Environments of Change (EOC) project was instrumental in enabling this research, providing funding and the opportunity to conduct fieldwork in England. I am very grateful for the field assistants who supported me during my work in the Pevensey Levels, as well as Dr. Simon Coppard, for his help and advice during my time at the Herstmonceux Castle. A special thank you to Dr. Steven Bednarski, the primary investigator of the EOC project and a dear colleague whose professional guidance and encouragement have been a cornerstone of this journey. To my colleagues at the DRAGEN Lab, thank you for your support, collaboration, and assistance with the historical review of the Pevensey Levels. Your input has been instrumental in shaping this work.

To my family, your support and encouragement have kept me motivated throughout this journey. To my friend Emma, thank you for being a support throughout my master's and for helping take care of the animals while I was away in England. Finally, to my wife, Shannon, thank you for your endless patience, love, and understanding throughout the process of this thesis, especially during my fieldwork in the UK. Your support has been my foundation, and I could not have achieved this without you.

Table of Contents:

Author's Declaration ..... **ii**

Statement of Contributions ..... **iii**

Abstract ..... **iv**

Acknowledgements ..... **vi**

List of Figures ..... **x**

List of Tables ..... **xvii**

Chapter 1: Introduction, Rationale, and Description of Study and the Study Site **1**

1.1.0. Introduction 1

1.2.0. Rationale 1

1.3.0. Location of Study and Site Descriptions 3

1.4.0. Conclusion 7

Chapter 2: Review of Previous Research and Scope and Objectives of Thesis **8**

2.1.0. Introduction 8

2.2.0. Regional Bedrock Geology 9

2.3.0. Regional Surficial Geology 10

2.4.0. East Sussex Coastal Sediment and Development 13

2.5.0. Comparative Case Study: Somerset Levels 19

2.6.0. Comparative Case Study: The Brede-Pett Level 22

2.7.0. Pevensey Levels Borehole Data 24

2.8.0. Pevensey Levels Historiography 30

2.9.0. Summary of Existing Research 35

2.9.0. Scope and Objective of Thesis 37

Chapter 3: Methodologies of Field and Laboratory Work **39**

3.1.0. Introduction 39

3.2.0. Geographic / Geomorphologic Analysis 40

3.3.0. Fieldwork Methods 41

3.3.1. Transects 41

3.3.2. Coring 42
3.3.3. Stratigraphic and Sediment Description 44
3.3.4. Sediment Sampling 46
3.4.0. Laboratory Methods 48
3.4.1. Grain Size Analysis 48
3.4.2. Portable X-ray Fluorescence (pXRF) Analysis 50
3.4.3. Loss on Ignition (LOI) 51
3.4.4. X-Ray Diffraction Analysis (XRD) 52
3.4.5. Geochronology 54
3.5.0. Summary of Methodologies 56
Chapter 4: Results of Fieldwork and Laboratory Analyses (North Eye and Horse Eye) 58
4.1.0. Introduction 58
4.2.0. North Eye 58
4.2.1. Preliminary Fieldwork 58
4.2.2. Facies Analysis and Stratigraphic Patterns 61
4.2.3. Laser Diffraction Grain Size Analysis 68
4.3.0. Horse Eye 73
4.3.1. Site Description 73
4.3.1.1. Field Work Methodology 75
4.3.1.2. The Transects 76
4.3.2. Stratigraphy of Each Transect 79
4.3.3. Summary of Stratigraphy Across Transects 83
4.3.4. Detailed Stratigraphy of Transect 4 87
4.3.5. Laser Diffraction Grain Size Analysis 96
4.3.6. Portable X-ray Fluorescence (pXRF) Analysis 116
4.3.6.1. Spatial and Elevation Relationships 117
4.3.6.2. Depth and Composition Trends in Core HE23T4C4B 121
4.3.7. Loss on Ignition (LOI) 127
4.3.7.1. Spatial and Elevation Relationships 127

4.3.7.2. Depth and Composition Trends in Core HE23T4C4B 129
4.3.8. X-Ray Diffraction Analysis (XRD) of Core HE23T4C4B 132
4.3.9. Stratigraphic Units of Core HE23T4C4B 142
4.3.10. Geochronology Results 149
Chapter 5: Reconstructing the Depositional History in the Pevensey Levels (Horse Eye and North Eye) 165
5.1.0. Introduction 165
5.2.0. Synthesis of Stratigraphy of Horse Eye and North Eye: Building on Regional Context 169
5.3.0. Climatic and Anthropogenic Influences 181
5.3.1. Climatic Variability in Part of the Holocene 181
5.3.2. Anthropogenic Contributions 191
5.4.0. Summary of Data Compilation 194
Chapter 6: Conclusions & Opportunities for Future Research 196
6.1.0. Thesis Contributions 196
6.2.0. Future Research Directions 199
References: 201
Appendix A – North Eye Field Notes 212
Appendix B – Horse Eye Field Notes 231
Appendix C – GRADISTAT grain size distribution output (phi) 290

List of Figures

Figure 1.1 - A map displaying the United Kingdom (UK), the location of London, UK is shown, the area representing the county of East Sussex is highlighted in red on the South-east coast. Data source: (GADM, 2022) 3
Figure 1.2 - A map displaying the south-eastern portion of the United Kingdom (UK) showing the outline of East Sussex as a dashed line and outlining the boundary of Pevensey Levels within the red box (Figure 1.4), adjacent to the English Channel. The area of this map is represented by the dotted black square in the overlying map of the UK in the top left-hand corner. 4
Figure 1.3 - Two metre resolution Light Detection and Ranging (LiDAR) hill shade digital terrain model (DTM) (UK Ordinance Survey, 2020) with a colourized raster to show the elevation of the Pevensey Levels (UK) and surrounding uplands. Illustrating contrast between the low-lying embayed area, known as the Levels, and the higher elevated Weald to the north, east, and west, contour intervals representing changes in elevation are illustrated. 5
Figure 1.4 - Two-metre resolution LiDAR hill shade digital terrain model (DTM) (UK Ordinance Survey, 2020) of the Pevensey Levels' Site of Special Scientific Interest (SSSI) boundary. Isolated areas with higher elevation can be seen as raised portions of the DTM, these areas were previously islands when water in the English Channel was relatively higher in the past. 6
Figure 1.5 - Two metre resolution LiDAR hill shade digital terrain model (DTM) (UK Ordinance Survey, 2020) with a colourized raster to show the elevation of Pevensey Levels (UK). Indicating and naming the locations of six islands within Pevensey Levels. 6
Figure 2.1 - Geologic map showing bedrock geology of the Pevensey Levels and surrounding area. Modified from (BRITISH GEOLOGICAL SURVEY (BGS), 1988). The outline of the Pevensey Levels are shown in red, and the approximate shape and location of both Horse Eye and North Eye are illustrated. 10
Figure 2.2 - A map showing the superficial deposits of the proposed study area including and surrounding the Pevensey Levels (BGS, 2023). The colour overlying the base map correlate to superficial deposits outlined in the legend. The Pevensey Levels are outlined with a thick black line, and Horse Eye and North Eye are outlined with a dashed black line. 11
Figure 2.3 - Bedrock geology and superficial deposit map of the Pevensey Levels and surrounding area. Modified from (BRITISH GEOLOGICAL SURVEY (BGS), 2006). 12
Figure 2.4 - A schematic representation of the stratigraphy of coastal lagoons of the region encompassing the southern North Sea region (Waller and Kirby, 2020). 14

Figure 2.5 - Location of the Somerset Levels in Southwest England, UK, as indicated by the black rectangle on the map. Modified from (S.K. Haslett et al., 1998). 19
Figure 2.6 - Location of Pett Level in East Sussex as indicated by the red box outline, modified from (Timpany et al., 2021)..... 22
Figure 2.7 - This map depicts the locations of each borehole that the BGS (2020) have in their system for the Pevensey Levels and surrounding area. Each colour symbol corresponds to different lengths of boreholes, a legend is shown in the top right. 25
Figure 2.8 - Seven borehole records that have the units defined by Jones (2002) expanded to boreholes retrieved from BGS (2020). (L-R: PL transect (Jones, 2002), P-B I transect (TP) (BGS, 2020), AH series (BGS, 2020)), (Drew, 2021). 26
Figure 2.9 - Cross sectional representation of the stratigraphy of the "bedrock island" of North Eye (Champness, 2009)..... 29
Figure 2.10 - A map of the county of Sussex produced in 1910 that depicts how the shoreline would appear if the sea-banks and shingle were removed. Modified from (Ballard, 1910). 31
Figure 2.11 - A map depicting Sussex during the 17th century. The Pevensey Levels are labelled as "Pevensey Marsh", and the Medieval chapel on North Eye is located in the red circle as "Nordy Chap". Modified from Hewett (2018). 32
Figure 2.12 - The Domesday Book entry for Horsey (Horse Eye), recorded in 1086 within the hundred of Pevensey and the county of Sussex. The red oval highlights the word “Horsey” in Latin. This entry documents the presence of a settlement with a recorded population of 1 household (from Powell-Smith et al., 2011)..... 33
Figure 2.13 - Timeline of major flooding and drainage history of the Pevensey Levels. Green events are records of natural events caused by the environment, and yellow events are records of human interaction and manipulation of the natural landscape. Modified from (Moore, 2020). 34
Figure 3.1 - A photograph showing the start of a transect indicated at the bottom of the photo by a red marker flag, with field assistant, Kira, in the distance indicating the end of the transect. Kira is circled in red with a red arrow pointing at her for emphasis. 41
Figure 3.2 - Photograph of the two-piece gouge auger set showing all pieces included in the set. Obtained from (Two-Piece Gouge Auger Set with Bayonet Connection for Soft Soils, 2023). 42
Figure 3.3 - Grain size card showing measurements in centimeters, millimeters, and phi placed next to a sediment core sample..... 44
Figure 3.4 - Photograph of a sediment core with a measuring tape adjacent to it. This is completed to record the depth of each sediment core and each unit within the cores. 46
Figure 3.5 – Photograph of the Fritsch Analysette 22 MicroTec Plus in the Quaternary Geology Lab at the University of Waterloo. 48

Figure 3.6 - An agate mortar and pestle used to finely powder sediment samples and a weighing paper with finely powdered sample. 53
Figure 3.7 - Image of the Malvern Panalytical Aeris XRD machine from the Groundwater Geochemistry Remediation Group at the University of Waterloo. 54
Figure 4.1 - A map of North Eye showing the transect of boreholes collected during the preliminary fieldwork in May 2022. 60
Figure 4.2 - A map displaying the borehole locations along the transect at North Eye, collected during preliminary fieldwork in May 2022 with a two-metre resolution LiDAR hill shade digital terrain model (DTM) (UK Ordinance Survey, 2020). 60
Figure 4.3 - A cross-section detailing the 14 units assigned to each borehole collected along the North Eye transect, demonstrating the spatial distribution of lithologies. 65
Figure 4.4 - A cross-section illustrating the simplified lithological units (sand, silt, clay, topsoil, iron pan) identified in the boreholes along the North Eye transect. 66
Figure 4.5 - (A) A photograph of plant material that was collected in borehole NE22T1C5 (depth: 163-167 cm). (B) A photograph of a shell fragment found in the same core (depth: 367 cm), indicating a predominantly marine depositional environment. 68
Figure 4.6 - A cross-section illustrating the simplified lithological units (sand, silt, clay, topsoil, iron pan) identified in the boreholes along the North Eye transect, displaying the approximate location of samples which were used for LDM grain size analysis. 69
Figure 4.7 - Grain size distribution (%) for units sampled from North Eye, showing the relative proportions of clay, silt, and sand as determined by Laser Diffraction Grain Size Analysis (LDM). Note that the samples are from different cores and depths, as detailed in Table 4.2, and should not be interpreted as representing a continuous vertical sequence. 71
Figure 4.8 - Map of Horse Eye showing transect locations of boreholes collected during fieldwork in May 2023. The map includes a two-meter resolution LiDAR hill shade digital terrain model (DTM) (UK Ordinance Survey, 2020). 74
Figure 4.9 - Boreholes collected along four transects on Horse Eye during fieldwork in May 2023. (A) Transect 1, running north-south on the southern side of the island; (B) Transect 2, running east-west on the western portion; (C) Transect 3, running north-south in the central part of the island on the northern side; and (D) Transect 4, running north-south in the central part of the island on the southern side. Elevation is indicated in meters above Ordnance Datum (OD) with contour intervals of 1 and 2.5 meters. The maps include a two-meter resolution LiDAR hill shade digital terrain model (DTM) (UK Ordinance Survey, 2020). 79
Figure 4.10 - A cross-section detailing the 26 lithofacies assigned to each borehole collected along the Transect 4 on Horse Eye, demonstrating the spatial facies distribution. 90

Figure 4.11 - A cross-section illustrating the simplified stratigraphic beds (silt, clay, peat, and minerogenic pan) identified in the boreholes along Transect 4 on Horse Eye. 92
Figure 4.12 - Grain size distribution bar chart for borehole HE23T4C1 along Transect 4, showing the percentage of clay, silt, and sand at various depths below the ground surface. The figure also includes the simplified cross-section of Transect 4 based on field observations, as well as a map view of the transect, both of which highlight the location of borehole HE23T4C1 circled in red. The cross-section and map provide spatial context, illustrating the borehole's position..... 98
Figure 4.13 - (A) Grain size distribution bar chart for borehole HE23T4C2 along Transect 4, showing the percentage of clay, silt, and sand at various depths below the ground surface. The figure also includes (B) the simplified cross-section of Transect 4 based on field observations, and (C) a map view of the transect, both of which highlight the location of borehole HE23T4C2 circled in red. The cross-section and map provide spatial context, illustrating the borehole's position..... 100
Figure 4.14 - (A) Grain size distribution bar chart for borehole HE23T4C35.5m along Transect 4, showing the percentage of clay, silt, and sand at various depths below the ground surface. The figure also includes(B) the simplified cross-section of Transect 4 based on field observations, and (C) a map view of the transect, both of which highlight the location of borehole HE23T4C35.5m circled in red. The cross-section and map provide spatial context, illustrating the borehole's position. 102
Figure 4.15 - (A) Grain size distribution bar chart for borehole HE23T4C45.5m along Transect 4, showing the percentage of clay, silt, and sand at various depths below the ground surface. The figure also includes (B) the simplified cross-section of Transect 4 based on field observations and (C) a map view of the transect, both of which highlight the location of borehole HE23T4C45.5m circled in red. The cross-section and map provide spatial context, illustrating the borehole's position. 104
Figure 4.16 - (A) Grain size distribution bar chart for borehole HE23T4C3 along Transect 4, showing the percentage of clay, silt, and sand at various depths below the ground surface. The figure also includes (B) the simplified cross-section of Transect 4 based on field observations (C) and a map view of the transect, both of which highlight the location of borehole HE23T4C3 circled in red. The cross-section and map provide spatial context, illustrating the borehole's position..... 106
Figure 4.17 - (A) Grain size distribution bar chart for borehole HE23T4C4B along Transect 4, showing the percentage of clay, silt, and sand at various depths below the ground surface as well as brackets showing the divisions discussed in the text. The figure also includes the simplified cross-section of Transect 4 based on field observations (B) and a map view of the transect (C), both of which highlight the location of borehole HE23T4C4B circled in red. The cross-section and map provide spatial context, illustrating the borehole's position..... 110

Figure 4.18 - Detailed grain size distribution analysis for borehole HE23T4C4B, showing six down-profile graphs. The first three graphs display the percentage of sand, silt, and clay at various depths below the ground surface, with their average values and standard deviations indicated. The sand fractions chart (D) breaks down the total sand percentage into very coarse sand (vCS, 1-2 mm) and coarse sand (CS, 500 µm - 1 mm), while the silt fractions chart (E) subdivides the total silt percentage into very fine (v.f, 2-4 µm), fine (f, 4-8 µm), medium (med, 8-16 µm), coarse (c, 16-31 µm), and very coarse (v.c, 31-62.5 µm) silt fractions. The final graph (F) depicts the normalized relationship between very coarse sand (vCS) and coarse silt (cS). 115
Figure 4.19 - Map view of Horse Eye Transect 4 with sampling locations indicated along the topographic gradient from the hilltop of the bedrock island to the Levels. Each site along the transect is marked with its respective sampling depth and pie charts that display the relative proportions of each proxy (Coarse + Fine Clastic, Redox, Carbonate, Proxy Organic, Heavy Metals/Pollutants, and Atmospheric Radioactive) at each location. This spatial overview provides context for understanding the relationship between a sample's spatial locations, elevation, and subsequent geochemical evaluation from the pXRF analyses. 118
Figure 4.20 – Cross-section of Horse Eye Transect 4 showing the elevation profile and pXRF elemental composition of topsoil samples (0-10 cm depth) at the hilltop of Horse Eye, mid-slope of Horse Eye, and within the levels at the threshold of the bedrock island. Pie charts display the relative proportions of each proxy (Coarse + Fine Clastic, Redox, Carbonate, Proxy Organic, Heavy Metals/Pollutants, and Atmospheric Radioactive) at each location. The transect demonstrates the transition from higher to lower elevations (with a 22x Vertical Exaggeration) and associated geochemical variations in topsoil along the landscape. 119
Figure 4.21 - pXRF analysis results for core HE23T4C4B, displaying the relative proportions of each geochemical proxy (Coarse + Fine Clastic, Redox, Carbonate, Proxy Organic, Heavy Metals/Pollutants, and Atmospheric Radioactive) across three depth intervals: topsoil (0-10 cm), Upper Peat (120-130 cm), and Lower Peat (173-180 cm). 123
Figure 4.22 - Sampling depths of XRD analysis for core HE23T4C4B, providing context for the sampled locations, showing lithological units defined in the field. 132
Figure 4.23 - A line graph showing the depth profile of quartz, calcite, and illite, allowing visualization of the mineral trends with increasing depth in the core. 135
Figure 4.24 - XRD mineral composition pie charts for each sampled interval in core HE23T4C4B from 30 cm to 110 cm, showing the relative percentages of all identified minerals 138
Figure 4.25 - XRD mineral composition pie charts for each sampled interval in core HE23T4C4B from 148 cm to 235 cm, showing the relative percentages of all identified minerals 139

Figure 4.26 - Combined calibrated radiocarbon age distributions for samples collected on Horse Eye, (A) Upper Peat (Unit 4) in core HE23T4C4B, (B) Lower Peat (Unit 2) in core HE23T4C4B, and (C) an additional peat sample collected nearby core HE23T4C4B. Calibrated using OxCal v4.4 (Bronk Ramsey, 2001, 2017) and the IntCal20 calibration curve (Reimer et al., 2020). 150
Figure 4.27 - Age-depth model for Scenario A. Modelled age (cal BP). 156
Figure 4.28 - Age-depth model for Scenario B. Modelled age (cal BP). 157
Figure 4.29 - Age-depth model for Scenario C. Modelled age (cal BP). 158
Figure 4.30 - Age-depth model for Scenario D. Modelled age (cal BP). 159
Figure 4.31 - Age-depth model for Scenario A, showing modeled ages (cal BP), labeling each segment as a stratigraphic unit, with the blue labels aligning with age-dated peat samples in the core HE23T4C4B. 163
Figure 5.1 - Topographic map of the Pevensey Levels showing the locations of Horse Eye and North Eye, providing spatial context while highlighting the relative locations and elevations of the two bedrock islands. Contour intervals highlight elevation changes, with Horse Eye and North Eye outlined in red. 167
Figure 5.2 - Topographic map of North Eye showing the locations of boreholes from Fieldwork 2022 transect and Champness' (2009) transect, with 2 m and 5 m contours... 171
Figure 5.3 - Full cross-section (top) of North Eye, and detailed cross section of the western side of the bedrock island (bottom) (modified from Champness (2009)). 172
Figure 5.4 - Cross-section of North Eye transect, showing stratigraphic units and assumed bedrock contact. This cross-section illustrates stratigraphic units defined at Horse Eye, predominantly terrestrial, transitional, and predominantly marine. Elevation (m OD) is indicated on the y-axis, with 22.2x vertical exaggeration. 174
Figure 5.5 - Cross-section of Transect 4 at Horse Eye, showing the stratigraphic units defined at Horse Eye. Elevation (m OD) is indicated on the y-axis with 22x vertical exaggeration. Stratigraphic units include predominantly marine, peat, transitional, and predominantly terrestrial. The figure demonstrates spatial variability in stratigraphy and elevation across the transect. 175
Figure 5.6 - Photograph of Tunbridge Wells Sand Formation (TWS) bedrock exposed on the eastern portion of North Eye. 177
Figure 5.7 - Topographic map showing boreholes collected along 2022 North Eye transect, with 1- and 2-meter interval contours. Inset map shows the entire bedrock island of North Eye with a red triangle indicating the location of the TWS bedrock exposure (Figure 5.6). 178
Figure 5.8 - Holocene stratigraphic and climatic context of core HE23T4T4B from Horse Eye. Displayed are the stratigraphic units defined, grain size distributions (% sand, % silt, % clay), cumulative grain size distribution (%), and $\delta^{18}O$ records from the NGRIP ice core (NGRIP 2004- Andersen et al. (2004)) to interpret depositional and climatic variability.

Climatic phases (e.g., 4.2 kiloyear event, Middle Bronze Age Cold Epoch (MBACE), Bronze Age Optimum (BAO), Roman Warm Period (RWP), Dark Age Cold Period (DACP), Medieval Climate Anomaly (MCA), Little Ice Age (LIA), and Anthropocene Warm Period (AWP)) are shown to provide chronological context. Calibrated radiocarbon dates (cal. BP) are provided alongside archaeological and geological ages for reference..... 183
Figure 5.9 – A plot showing $\delta^{18}O$ data (%) from the NGRIP ice core (50-yr intervals) (Andersen et al., 2004), a global proxy for climate variability, warmer periods are indicated in pink and cooler periods are indicated in blue, alongside averaged sand percentages(50-yr intervals) derived from core HE23T4C4B at Horse Eye, both plotted against calibrated years before present (cal BP) on the x-axis. Average % Sand is plotted on the primary y-axis, $\delta^{18}O$ data is plotted on the secondary y-axis..... 186
Figure 5.10 - Stratigraphic profile and mineralogical composition of core HE23T4C4B. The stratigraphic units (left) span the Holocene, showing transitions between marine, paludal, and terrestrial environments. The pie charts (right) display XRD-derived mineral compositions at selected depths, refer to figures 4.24 and 4.25 for a larger legend for the XRD pie charts. 189

List of Tables

Table 2.1 - Summary table of geologic formations and their corresponding descriptions (BGS, 2023) that make up the geologic setting of Pevensey Levels, the broad area of this thesis' study sites. 9
Table 2.2 - Summary of lithological descriptions and observations from Jones (2002), established from Jones' (2002) sample core, modified from (Drew, 2021). 28
Table 4.1 - Description of the 14 primary facies/units identified at North Eye during 2022 preliminary fieldwork. The table includes unit numbers, names, field descriptions, and corresponding facies codes based on Farrell et al. (2012). 62
Table 4.2 - Sample details for Laser Diffraction Grain Size Analysis, including the unit, core associated with the sample, and the depth range of the sample collected. Four cores (NE22T1C2, NE22T1C3, NE22T1C5, and NE22T1C6) were sampled. 70
Table 4.3 - Summary table of transects completed on Horse Eye during fieldwork in May 2023, including the number of boreholes completed and samples collected, the elevation difference, length, and orientation of each transect. 76
Table 4.4 - Lithological summary of Selected Boreholes Across Transects Conducted on Horse Eye. 85
Table 4.5 - Lithofacies Codes and Descriptions Identified in Transect 4 based upon field descriptions following Farrell et al. (2012). 87
Table 4.6 - Groupings of Lithofacies Codes (following Farrell et al. (2012)) Identified in Transect 4. 89
Table 4.7 - Elemental categories and their associated elements identified through Portable X-ray Fluorescence (pXRF) analysis along Transect 4 on Horse Eye, after (Davies et al., 2015). 117
Table 4.8 - Portable X-ray Fluorescence (pXRF) analysis of topsoil samples (0-10 cm) from Horse Eye Transect 4, showing elemental composition by proxy category (Coarse + Fine Clastic, Redox, Carbonate, Proxy Organic, Heavy Metals/Pollutants, and Atmospheric Radioactive) across varying elevations. The table highlights the relationship between elevation and elemental concentrations in the topsoil at hilltop, mid-slope, and in the Levels. 121
Table 4.9 - Portable X-ray Fluorescence (pXRF) analysis of core HE23T4C4B, showing elemental concentrations across three depth intervals: Lower Peat (173 - 180 cm), Upper Peat (120 - 130 cm), and topsoil (0 - 10 cm). Each row provides the specific values for each geochemical proxy category: Coarse + Fine Clastic, Redox, Carbonate, Proxy Organic, Heavy Metals/Pollutants, and Atmospheric Radioactive, illustrating the changes in elemental composition with depth from the organic-rich peat layers to the mineral-dominated topsoil. 126

Table 4.10 - Loss on Ignition (LOI) data for topsoil samples (0-10 cm) collected from three elevations along Horse Eye Transect 4, including hilltop, mid-slope, and in the Pevensey Levels. The table displays elevation range, moisture, organic, and carbonate content. ... 127
Table 4.11 - Loss on Ignition (LOI) data for core HE23T4C4B, showing elevation range, moisture, organic, and carbonate content across three depth intervals: topsoil (0-10 cm), Upper Peat (120-130 cm), and Lower Peat (173-180 cm). This table illustrates depth-specific variations in LOI analysis, reflecting compositional differences between the minerogenic-rich topsoil and the organic-rich peat layers. 129
Table 4.12 - A summary table of the mineral percentages at each sampled depth, showing the variation of primary minerals (quartz, calcite, and illite) and trace minerals throughout core HE23T4C4B. 134
Table 4.13 - Stratigraphic units of core HE23T4C4B. 143
Table 4.14 - Summary table of samples from Horse Eye that were processed at 14Chrono Centre for Climate, the Environment and Chronology at Queen's University Belfast. The stratigraphy, depth, material, laboratory reference, uncalibrated and calibrated dates for each sample are summarized. 151
Table 4.15 - Summary table of calibrated age ranges (cal BP) for each stratigraphic unit across age-depth model scenarios A, B, C, and D. 154
Table 4.16 - Summary of average age ranges (cal BP) for Scenario A across the stratigraphic units for core HE23T4C4B. 161

Chapter 1: Introduction, Rationale, and Description of Study and the Study Site

1.1.0. Introduction

Climate variations have impacted societies in many ways throughout human history, influencing agricultural productivity, public health, and conflicts (Büntgen et al., 2011). In medieval Europe, humid and mild summers between ~1000 and 1200 C.E. (950 and 750 BP) are thought to have contributed to rapid cultural and political growth, whereas wetter and colder summers in the Late Middle Ages (1350-1500 C.E., approximately 600-450 BP) are associated with periods of widespread economic turmoil, famine, and pandemics (Büntgen et al., 2011). Reconstructing paleoclimates and paleoenvironmental change are thus critical to understanding the potential influence of natural conditions on and the relationships with human history. Coastal areas are particularly sensitive to climate variability due to their highly dynamic nature and human occupation and activity (e.g. Degeai et al. 2015). Yet, little is known about the paleoenvironments of many coastal areas that have been occupied by humans over the last several millennia.

1.2.0. Rationale

During a literature review for an undergraduate thesis (Drew, 2021) focusing on the late Holocene and ancient lagoonal area presently named the Pevensey Levels ('Levels' are a large, flat expanse of land), along the south coast of East Sussex (UK), it was found that limited information is available regarding the depositional environments during the medieval period of that area. This helped identify several gaps in knowledge that are needed to understand the relationship between human activity and the environment within the Pevensey Levels during the High and Late Middle Ages (1000 to 1500 C.E., approximately 950 to 450 BP), as well as the geological evolution extending back through the late Holocene (4200 – 0 BP, Cohen et al., 2022). The research herein is part of a larger

project: The Environments of Change multidisciplinary research project, which is studying the south coast of East Sussex between about 1000 and 1550 C.E. (approximately 950-400 BP), a place and time of vast environmental and cultural variation. This is done to understand the complex relationship between humans and their changing environment (*Environments of Change*, 2023). To achieve this, one must understand what the natural environment was during that time interval. Doing so requires many experts from different fields of study. One outcome of this large research project is to advance and supplement education for school-aged children and the general public through implementing technology such as educational video games, AR (augmented reality) / VR (virtual reality), and 3D models. However, developers require guidance regarding what the natural environment looked like and how it functioned during this time period. Quaternary geoscientists can provide both a long-term (millennial) and short-term (centennial to decadal) perspective from clues preserved in stratigraphic layers necessary to reconstruct past processes and environments.

1.3.0. Location of Study and Site Descriptions

The study site is in south-east United Kingdom (UK), south-east of London by about 80 km, in the county of East Sussex, and is depicted by the red polygon in Figure 1.1.

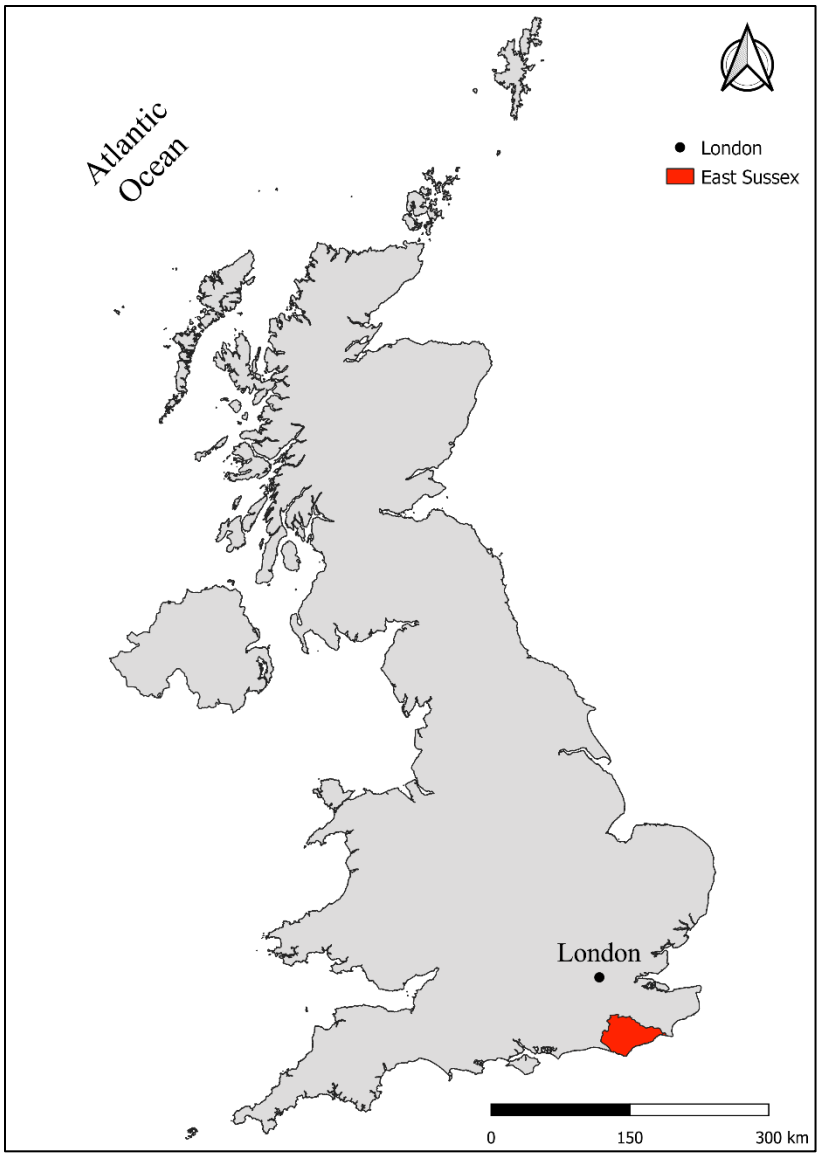


Figure 1.1 - A map displaying the United Kingdom (UK), the location of London, UK is shown, the area representing the county of East Sussex is highlighted in red on the South-east coast. Data source: (GADM, 2022)

The site is also within the Pevensey Levels, a designated biological Site of Special Scientific Interest (SSSI), as well as a wetland of international significance, otherwise known as a Ramsar site (*Pevensey Levels | Ramsar Sites Information Service*, 1999). The Pevensey Levels area is situated on the south-east coast of the UK, northeast of the town of

Eastbourne. Site boundaries for the Pevensey Levels and central position within East Sussex are shown in Figure 1.2.

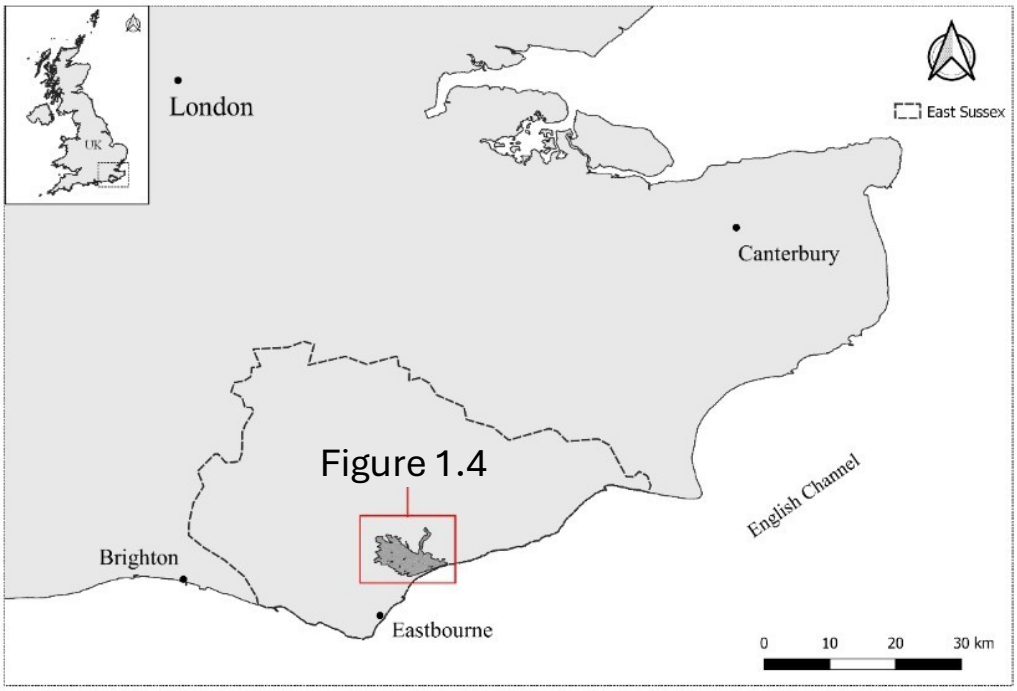


Figure 1.2 - A map displaying the south-eastern portion of the United Kingdom (UK) showing the outline of East Sussex as a dashed line and outlining the boundary of Pevensey Levels within the red box (Figure 1.4), adjacent to the English Channel. The area of this map is represented by the dotted black square in the overlying map of the UK in the top left-hand corner.

The Pevensey Levels can be described as a low-lying embayed or lagoonal area relative to water levels in the English Channel to the south and is surrounded by higher elevated land commonly called *uplands* or *weald* to the North, East, and West. An elevated beach barrier extends across the mouth of the embayed area, parallel to the English Channel. This elevation difference highlights the unique topographical setting of the Pevensey Levels, the relationship between the low-lying Pevensey Levels and the surrounding uplands is depicted in Figure 1.3.

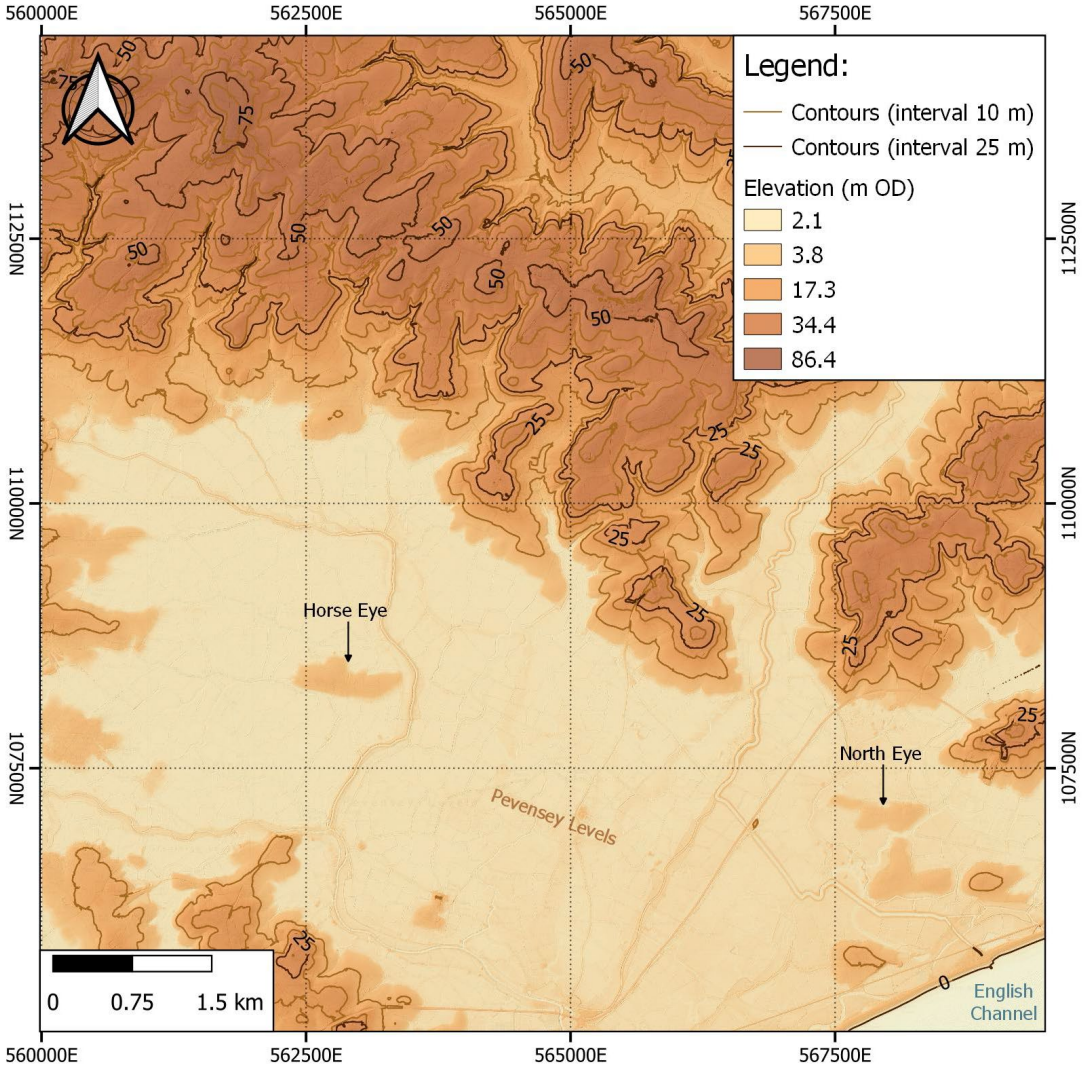


Figure 1.3 - Two metre resolution Light Detection and Ranging (LiDAR) hill shade digital terrain model (DTM) (UK Ordinance Survey, 2020) with a colourized raster to show the elevation of the Pevensey Levels (UK) and surrounding uplands. Illustrating contrast between the low-lying embayed area, known as the Levels, and the higher elevated Weald to the north, east, and west, contour intervals representing changes in elevation are illustrated.

Figure 1.4 focuses only on the Pevensey Levels and shows a hillshade representation of relief in the Levels, highlighting elevated areas that are isolated or resemble islands when compared to adjacent areas. Figure 1.5 offers a more detailed view of elevations in the Pevensey Levels using 2 m resolution LiDAR data (UK Ordinance Survey, 2020). The study sites focus on the flanks of- and the individual- elevated areas (islands) that are found within the Pevensey Levels. These islands are visualized in Figure 1.4 and labelled with the respective names of each island in Figure 1.5.

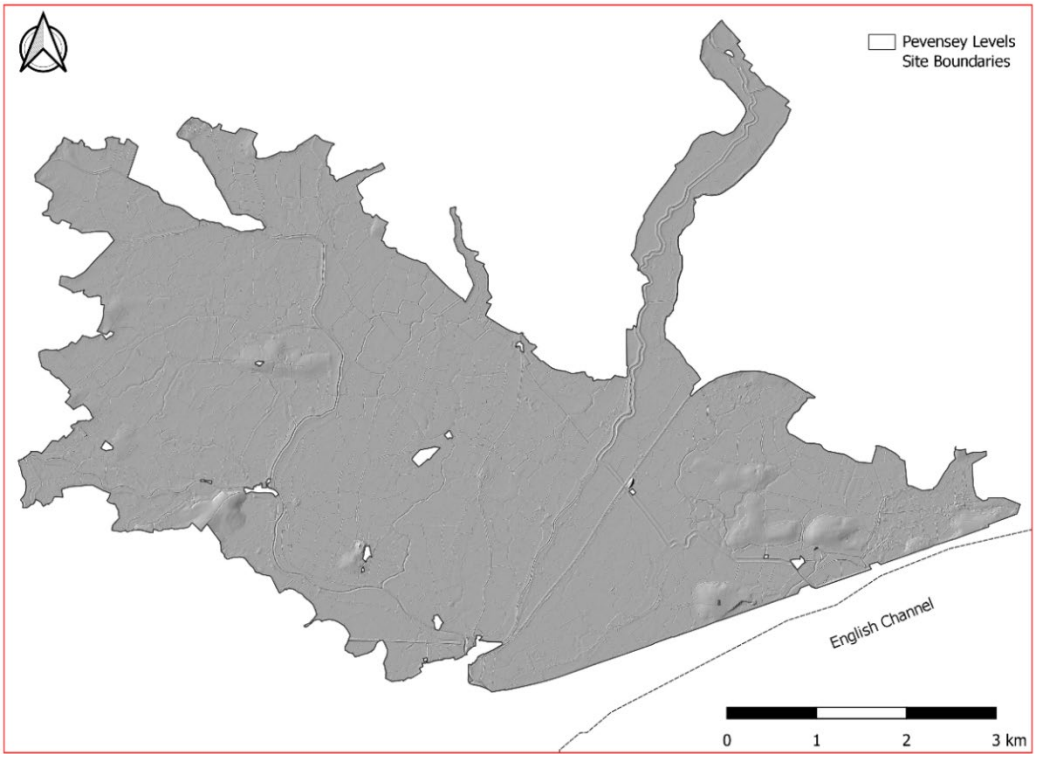


Figure 1.4 - Two-metre resolution LiDAR hill shade digital terrain model (DTM) (UK Ordinance Survey, 2020) of the Pevensey Levels' Site of Special Scientific Interest (SSSI) boundary. Isolated areas with higher elevation can be seen as raised portions of the DTM, these areas were previously islands when water in the English Channel was relatively higher in the past.

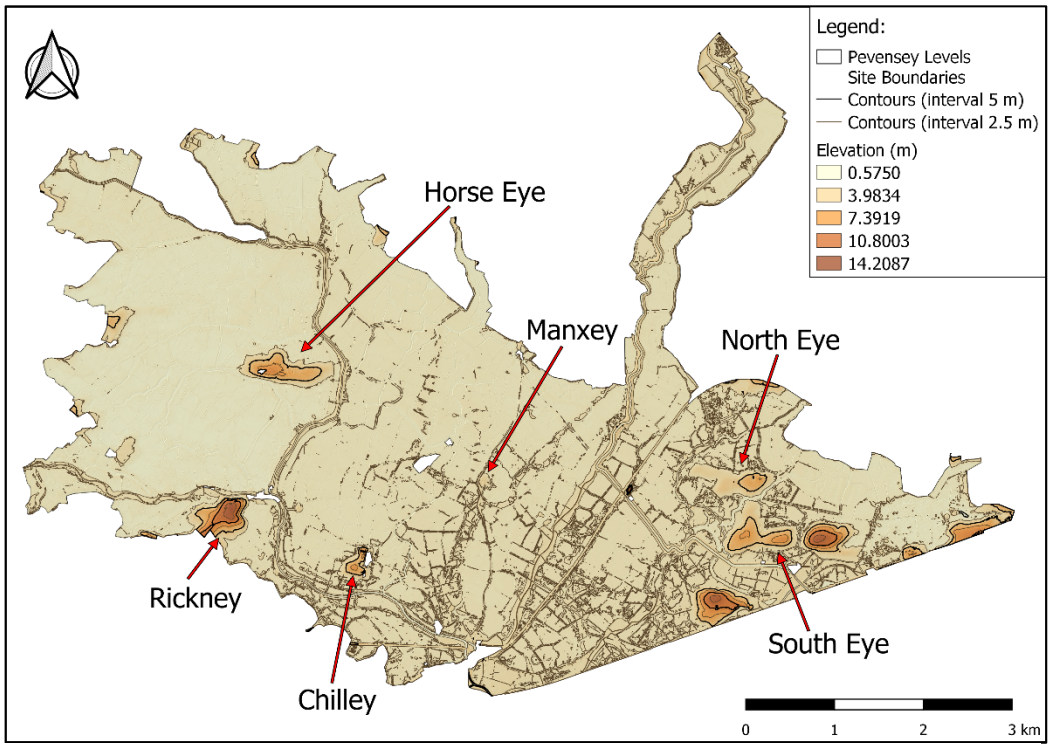


Figure 1.5 - Two metre resolution LiDAR hill shade digital terrain model (DTM) (UK Ordinance Survey, 2020) with a colourized raster to show the elevation of Pevensey Levels (UK). Indicating and naming the locations of six islands within Pevensey Levels.

1.4.0. Conclusion

This chapter introduced the Pevensey Levels, a dynamic coastal embayment with scientific and historic significance providing context for the stratigraphic and paleoenvironmental investigation conducted in this thesis. The Levels' designation as both a Ramsar site and an SSSI highlights its ecological importance, while its stratigraphic and historical record offers insight into the interaction between natural and anthropogenic processes over millennia. The geographical and topographical context of the Pevensey Levels, characterized by its low-lying lagoonal nature surrounded by elevated uplands and isolated elevated areas that resemble islands within the Levels, provides a setting to study paleoenvironmental changes. The visualizations of the site, including the use of LiDAR data, emphasize the variability in elevation within the Levels, as well as the spatial distribution of isolated elevated areas in the Levels.

This chapter has outlined the rationale for this study as shown through gaps in the understanding of the depositional environments and paleoenvironmental changes in the Pevensey Levels during the late Holocene, particularly the High and Late Middle Ages. These centuries were characterized by significant climatic and cultural shifts, yet the relationships between natural processes and human activities in the region remain underexplored. Part of the larger multidisciplinary Environments of Change research project, this study complements broader efforts to understand the relationship between humans and the environment in southeast England from approximately 1000 to 1550 CE by investigating the paleoenvironmental history of this period through analyzing the stratigraphy. The following chapters will build upon this foundation, integrating field and laboratory methodologies to reconstruct the paleoenvironmental history of the Pevensey Levels.

Chapter 2: Review of Previous Research and Scope and Objectives of Thesis

2.1.0. Introduction

This chapter provides an overview of the literature review for this thesis. Initially, a summary and visual representation of the mapped upper and lower Cretaceous bedrock geology and Quaternary surficial geology of the Pevensey Levels is presented to provide a general context for the geologic material that comprises the Levels that is necessary for this new detailed paleoenvironmental study. Next, the previously published research relevant to understanding the coastal development of the regional area pertinent to the study site is presented and helps identify knowledge gaps. Then, comparative analyses with similar environments, such as the Somerset Levels and the Brede-Pett Level, are included to provide context and highlight similarities and differences in their respective geological and historical developments. Lastly, the historical background of the Pevensey Levels is introduced, focusing on the ways that humans have interacted with the natural environment (including manipulation), as well as an introduction to how the islands within the Levels have been previously indicated throughout human-recorded history.

2.2.0. Regional Bedrock Geology

The bedrock geology of the area within and surrounding the Pevensey Levels comprises of primarily sandstones, siltstones, and mudstones, with minimal amounts of shale (BGS, 2023). The geologic setting of the Pevensey Levels is composed of the Wealden Group, the geological formations that make up the Pevensey Levels and their brief descriptions are shown in Table 2.1.

Table 2.1 - Summary table of geologic formations and their corresponding descriptions (BGS, 2023) that make up the geologic setting of Pevensey Levels, the broad area of this thesis' study sites.

Formation Name	Description
Tunbridge Wells Sand Formation (TWS)	Primarily sandstone (fine- to medium-grained), siltstone, and rhythms of silty sand. Includes some thin limestones and thinly bedded mudstones.
Weald Clay (WC)	Thinly bedded dark grey mudstones (shales), sandstones (fine- to medium-grained), clay ironstones, and shelly limestones.
Ashdown Formation (ASD)	Predominantly siltstones, and silty sandstones (fine-grained), with small amounts of thinly bedded mudstones. Commonly formed in rhythmites divided by thin beds of pebbles.
Wadhurst Clay (WdC)	Dark grey, soft, and thinly bedded mudstones (shales). As well as mudstones with pale grey beds of siltstone, sandstone (fine-grained), clay ironstone, and shelly limestone. Pebble beds are rarely found.
Lower Greensand Group (LGS)	Predominantly sandstones (poorly sorted and medium- to coarse-grained, to well-sorted and fine-grained) and sands, with smaller intervals of clays and silts.

The predominant geologic formations in the Pevensey Levels (outlined in red in Figure 2.1) are the Tunbridge Wells Sand (TWS) Formation and the Weald Clay (WC) Formation. TWS is widely distributed throughout the Levels and is the predominant lithostratigraphic unit on the northern and eastern sides of the Levels. WC is the predominant unit on the west and southwest portion of the Levels. These rock formations form the pre-depositional surface of the Levels before the deposition of surficial sediment. The bedrock geology of the area surrounding and containing Pevensey Levels is presented

in Figure 2.1. Where the two main bedrock formations that comprise the study area are shown in the figure with the locations of both Horse Eye and North Eye, these bedrock formations are lithologically similar, with a generally coarser formation (TWS) in the south and southeast portion of the levels, and a generally finer formation (WC) in the north and

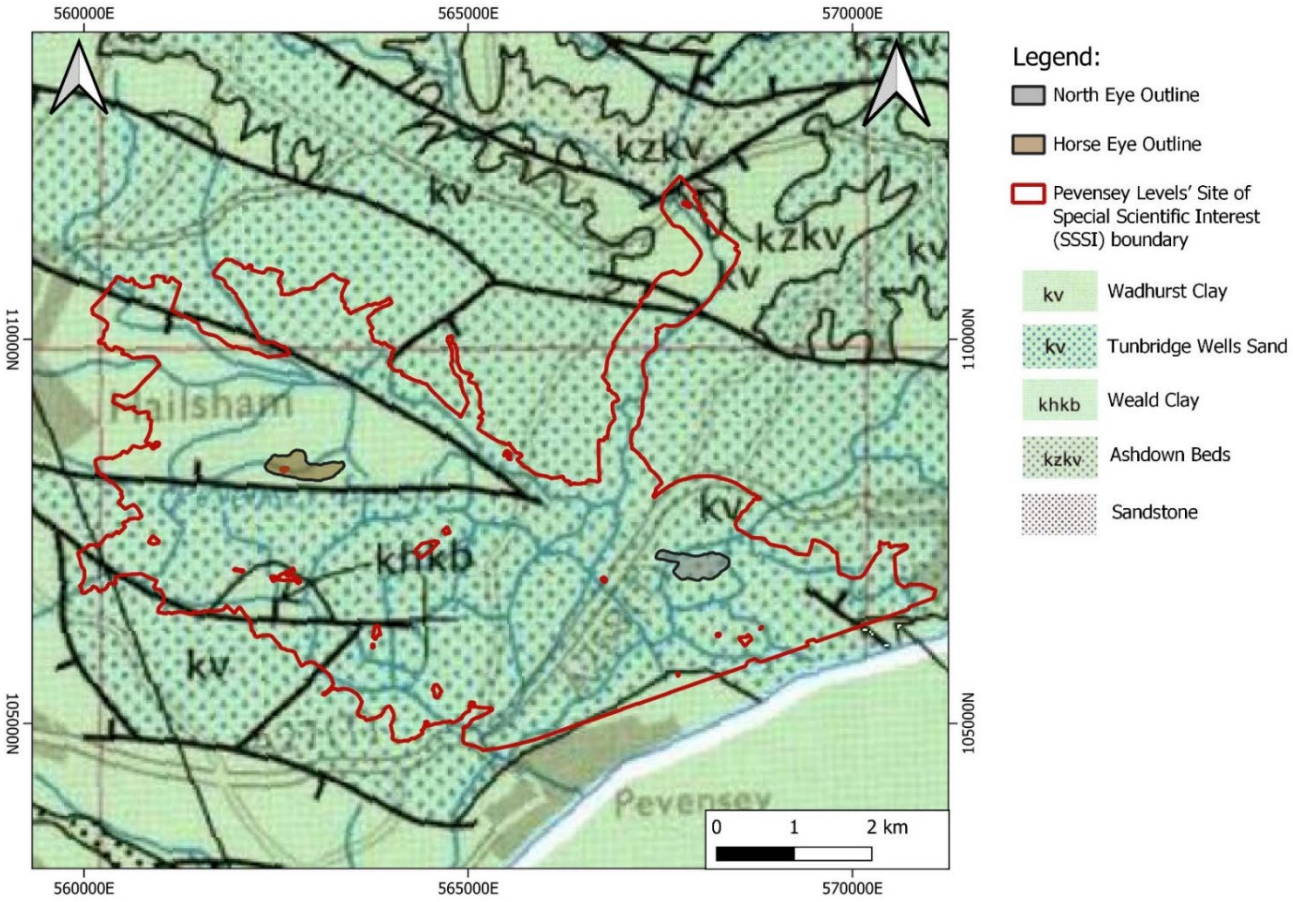


Figure 2.1 - Geologic map showing bedrock geology of the Pevensey Levels and surrounding area. Modified from (BRITISH GEOLOGICAL SURVEY (BGS), 1988). The outline of the Pevensey Levels are shown in red, and the approximate shape and location of both Horse Eye and North Eye are illustrated.

northwest portion of the levels.

2.3.0. Regional Surficial Geology

The surficial or superficial (UK terminology) sediment distributed throughout the Pevensey Levels falls within the British Geological Survey's (BGS) Alluvium general classification. This classification includes soft to firm consolidated detrital material deposited by a body of running water, such as clay, silt, sand, gravel, and peat (BGS, 2023).

A simplified view of the surficial sediment that outlines the Pevensey Levels is depicted in Figure 2.2. A lack of alluvium and surficial sediment can be observed in the isolated areas of higher elevation (islands), which were previously outlined in Figure 1.5 in Section 1.3.0: Location of Study and Site Descriptions. This mapped surficial sediment may suggest that bedrock is exposed at the ground surface on the islands, or that surficial sediment is relatively thin compared to adjacent sediment in the Levels or a combination of both scenarios.

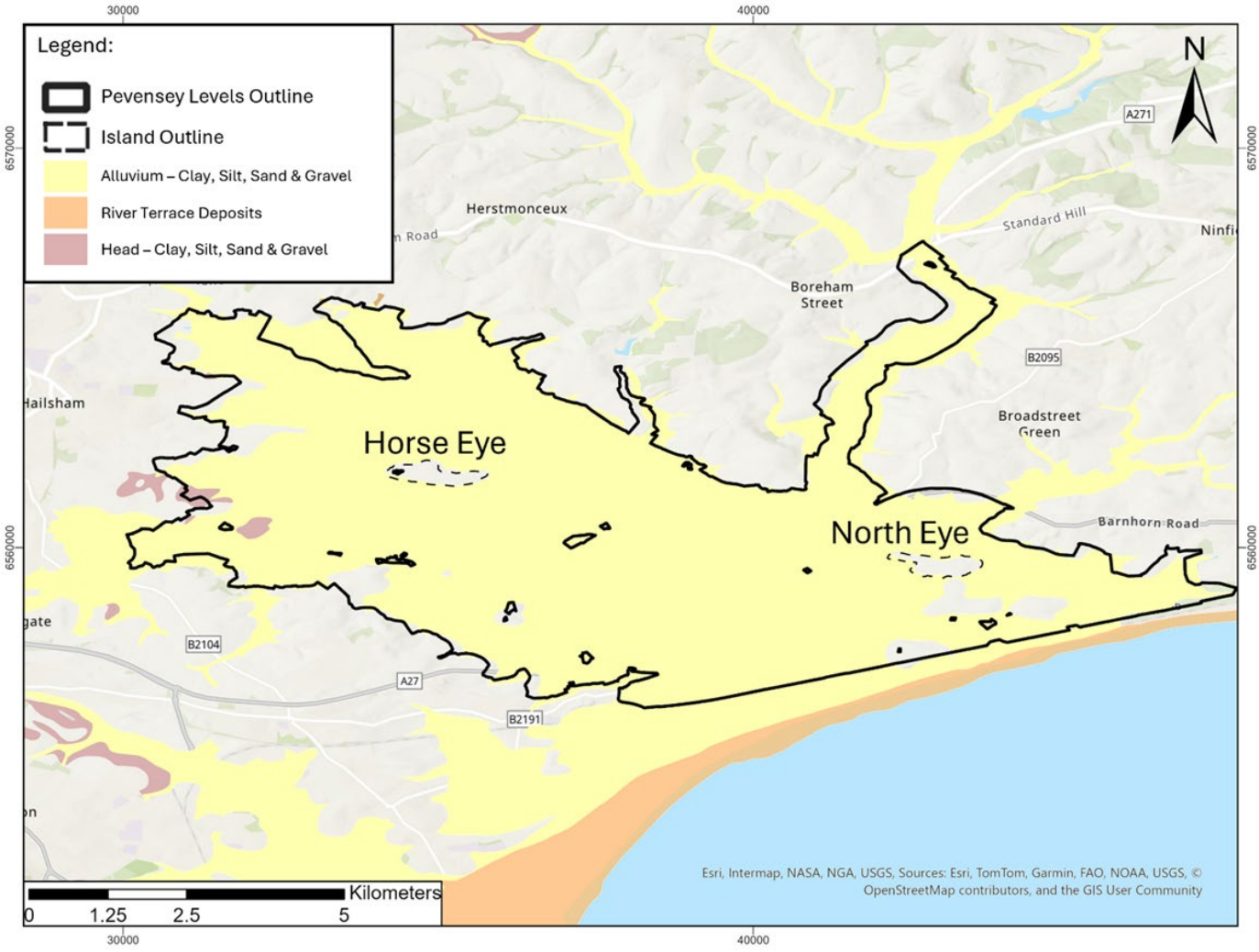


Figure 2.2 - A map showing the superficial deposits of the proposed study area including and surrounding the Pevensey Levels (BGS, 2023). The colour overlying the base map correlate to superficial deposits outlined in the legend. The Pevensey Levels are outlined with a thick black line, and Horse Eye and North Eye are outlined with a dashed black line.

A more detailed view of the sediment distribution in the Levels outlining the islands is shown in Figure 2.3. It can be observed that for the majority of these areas, the islands in the Pevensey Levels are mapped as bedrock. Figure 2.3 outlines these islands, it depicts North Eye, South Eye, and Chilley as the TWS bedrock formation, and Horse Eye and Rickney depicted as the WC bedrock formation. The remaining portion of the Levels that surround the islands (lower elevation), with the exception of the beach barrier (shown in light orange along the coastline), are depicted as Alluvium (clay, silt, sand, and peat), similar to the surficial geology map shown in Figure 2.2.

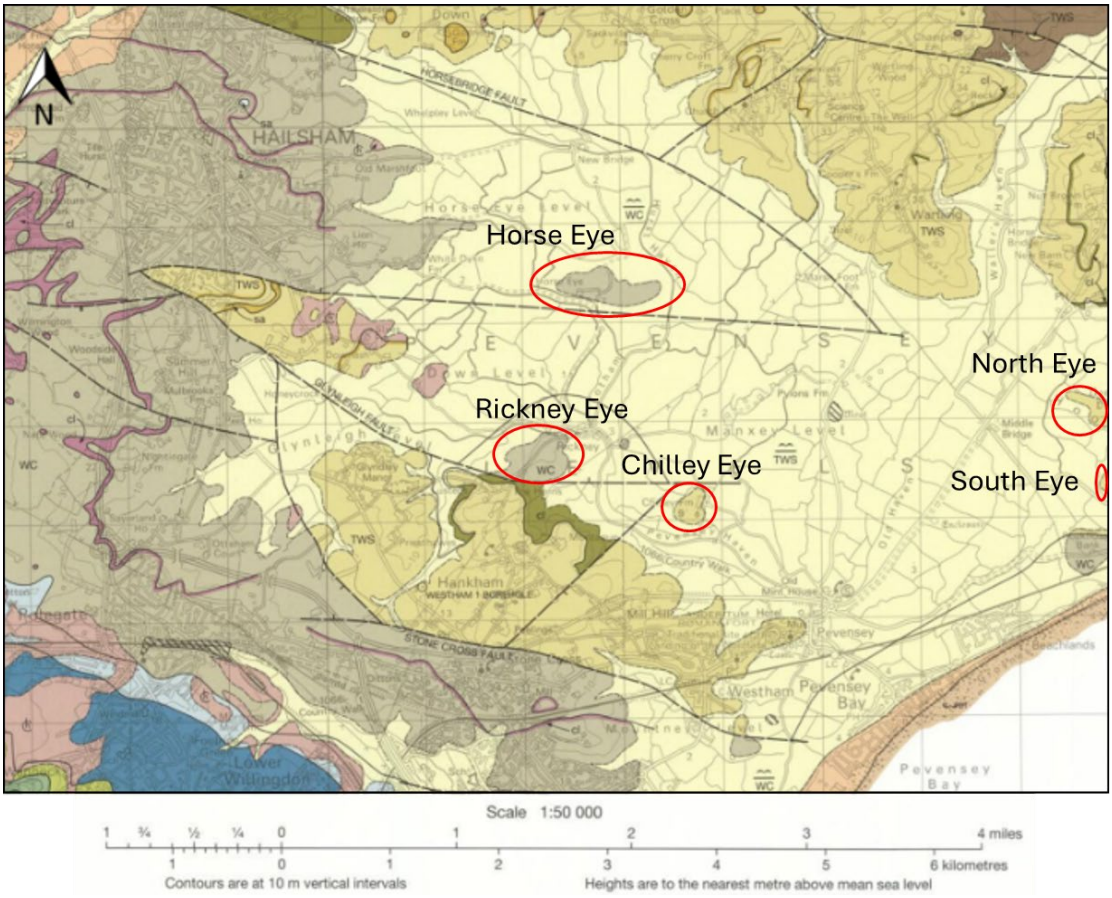


Figure 2.3 - Bedrock geology and superficial deposit map of the Pevensey Levels and surrounding area. Modified from (BRITISH GEOLOGICAL SURVEY (BGS), 2006).

2.4.0. East Sussex Coastal Sediment and Development

To further identify knowledge gaps and develop specific research objectives, it is essential to review previous work completed in the study area and surrounding regions. This section presents an overview of the development of the coastal sediment in East Sussex and previous paleoenvironmental work conducted within the surrounding area. Lastly, this section introduces publications that employ methodologies such as sediment core analysis, radiocarbon age-dating, and geochemical analyses, which are important to reconstructing paleoenvironmental conditions. These methodologies align with the objectives of this study, offering a foundation for understanding previous research efforts and situating the current research within a broader field. The reviewed publications help identify the scope of past work and knowledge gaps in the existing literature and provide context for this study.

A preliminary literature review completed by undergraduate colleagues at the University of Waterloo hired by the Environments of Change research team, and subsequent literature review completed by the author (Drew, 2021) as part of an undergraduate thesis study, found an abundance of studies in a wetland adjacent to the Pevensey Levels called the Romney Marsh. The Pevensey Levels and the Romney Marsh are relatively close to each other (approximately 40 km away), share a common coastline adjacent to the English Channel (a narrow branch of the Atlantic Ocean), and are similar complex coastal systems. Both areas are embayments which have been infilled with sediment through geologic time, representing an oscillating transitional zone between marine and continental conditions. Each area contains a beach barrier separating an embayed lagoonal area from the English Channel.

Waller & Kirby (2020) provide a generalized cross-section representing the stratigraphy of common coastal lagoonal areas of the southern portion of the North Sea, an area on the opposite side of the North Sea to the Pevensey Levels (Figure 2.4) but is representative of many coastal embayments south and north (i.e., Pevensey Levels) of the

North Sea. This schematic and the authors' interpretation provide a conceptual model for both the type and distribution of sediment that form common coastal lagoons in the region.

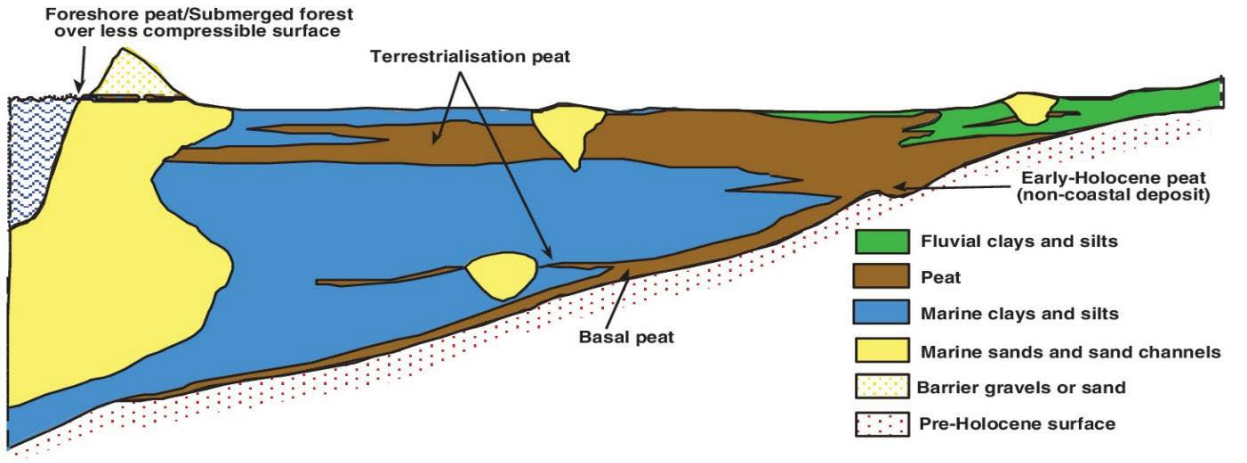


Figure 2.4 - A schematic representation of the stratigraphy of coastal lagoons of the region encompassing the southern North Sea region (Waller and Kirby, 2020).

The ancient lagoon represented in Figure 2.4 shows a beach barrier composed of marine sands and a coastal lagoon that includes marine and fluvial clays and silts, peat, and marine sand. A common pattern observed in this context is the transition from marine clays and silts to fluvial clays and silts further inland, away from the North Sea. The schematic highlights the variation in both the lateral extent and thickness of peat, with layers thickening and joining together inland. Similar sediment facies transitions are expected within the Pevensey Levels, as shown in Figure 2.3, which includes a geological map of the area. Specifically, at the study sites depicted in Figure 2.3 (Horse Eye and North Eye), it is predicted that there would be deposits of marine silts and clays, peat, and, depending on each individual island's proximity to rivers, fluvial silts and clays. Additionally, marine sand and coastal barriers, either gravel or sand, are anticipated along the coast (depicted by the light orange deposit on the coastline in Figure 2.3), which is consistent with the sedimentary patterns described by Waller and Kirby (2020).

Jennings and Smyth (1987) present a model of the coastal evolution of Eastbourne (East Sussex), a town that is roughly 10 km southwest of the Pevensey Levels (seen in Figure 1.2 in Section 1.3.0: Location of Study and Site Descriptions). The authors describe a change in the type of sediment that was transported into their study area, originally silty

clay, then sand, and lastly gravel, forming a coarsening-upward sequence (Jennings & Smyth, 1987).

The authors describe six coastline developmental stages for the Holocene coastline within East Sussex near Eastbourne, these six stages are briefly explained below in ascending chronological order (Jennings & Smyth, 1987):

- Stage 1: Organic material is deposited into low-lying areas.
- Stage 2: Peat is fully established; sand banks and dunes are developing.
- Stage 3: Offshore sand banks grew vertically, sediment accretion continued in the coastal zone. Fine-grained sediments accumulated behind sand banks.
- Stage 4: Coastline shifted seawards with a slow sea-level rise leading to significant sediment transfer from offshore. This developed stable depositional features such as spits and barriers.
- Stage 5: A major coastline retreat, sediment was released onto the Levels. By the end of this stage, gravel accumulated as spits, and a continuous line of gravel had developed.
- Stage 6: Gravel spits and tombolo's (sand or shingle bars connected to the mainland) developed rapidly into an extensive beach barrier. The shoreline shifted seawards due to gravel accretion.

Within these stages, Jennings and Smyth (1987) described three distinct phases of maximum sediment accretion (time periods of maximum sediment deposition) during the Holocene. The combination of the coastline developmental stages and the phases of maximum sediment accretion ultimately led to the development of the modern-day coastline near Eastbourne in East Sussex.

In their later study, Jennings and Smyth (1990), refine their earlier six-stage model into a five-stage framework, focusing on the relationship between sediment supply, sea-level change, and the evolution of gravel coastlines in the region. These stages are primarily

linked to variations in sediment availability and hydrodynamic conditions and are summarized with their appropriate time periods below:

- **Stage 1 (11,000 – 10,000 BP):** During the later part of the Late-glacial period, rising sea levels reworked material from the English Channel floor, transporting sediments through river systems into coastal environments. These sediments formed initial sedimentary drift cells and may have supported episodic beach barrier formation.
- **Stage 2 (10,000 – 5000 BP):** As sea levels continued to rise during the early Holocene, drowned river valleys filled with sediment, while terrace deposits were reworked into developing coastal systems. An open drift system was established as sea levels overtopped valley systems, enabling sediment to disperse alongshore.
- **Stage 3 (5000 – 300 BP):** Stabilized sea-levels during the mid-to-late Holocene facilitated sediment transfer that maintained shallow nearshore zones, creating dissipative wave environments where sediment accretion dominated. In earlier phases, accretion was sand-dominant, and cliff erosion was limited.
- **Stage 4 (300 BP – Present):** Exhaustion of sediment supply marked a transition to longshore redistribution as offshore-onshore sediment transfer diminished. This shift resulted in the dominance of reflective wave regimes, leading to the erosion of previously accreted structures, such as the Crumbles Shingle.
- **Stage 5 (The Future):** Projected future developments include the redistribution of gravel into sediment traps and sinks, which may create an indented coastline with tidal inlets reminiscent of pre-gravel stages. This stage highlights challenges for coastal management in maintaining the current coastline.

These refined stages show the interactions between sediment availability and sea-level dynamics in shaping the East Sussex coastline. The Jennings and Smyth (1990) framework also aids in understanding the role and development of beach barriers in ancient coastal lagoons, such as those found near the Pevensey Levels.

These stages describe how rising sea levels reworked, deposited, and moved sediment, influencing the formation and evolution of beach barriers. These studies help give an understanding of the role and development of beach barriers with respect to embayment development in ancient lagoons within East Sussex, an area that includes the Pevensey Levels.

In Figure 2.3, the mapped geological features of the Pevensey Levels include a beach barrier, consistent with the coastal depositional sequences proposed by Jennings and Smyth. This barrier, shown on the map, aligns with their stages of coastal evolution, highlighting the processes of sediment reworking and deposition along the coast. The presence of this barrier in the map reinforces the connection between mapped geological features and the theoretical depositional sequences described in these studies.

Roberts and Plater (2007) reconstructed the progradation and development of the Late Holocene gravel foreland named the Dungeness foreland, a site that is located roughly 40 km northeast of the Pevensey Levels, immediately south of the Romney Marsh, and adjacent to the English Channel. This publication utilized both Optically Stimulated Luminescence (OSL) and radiocarbon dating from multiple sites within the Dungeness foreland. This article provides a detailed chronology of the formation and evolution of the Dungeness gravel barrier, which separates the Romney Marsh and the Walland Marsh saltmarshes from the English Channel, the chronology of the gravel deposition for the foreland dated to between about 5000 and 1000 years ago.

The study is significant as it utilizes radiocarbon age dating to establish a timeline for coastal development, which is one of the methodologies applied to this study. The geographic proximity and similar depositional environments of the Dungeness foreland to the Pevensey Levels make this publication particularly relevant. Thus, Roberts and Plater's (2007) study offers valuable comparative data for understanding the Late Holocene coastal changes and the role of beach barriers in shaping coastal landforms in Southeast England.

To better understand the sedimentary development of East Sussex, Pears et al. (2020) provide valuable insights into the late Holocene flood history at the confluence of

the Teme and Severn rivers in south and central UK. Although this study area differs geographically from the Pevensey Levels, the use of detailed stratigraphic and multiproxy sedimentological analyses, including OSL and X-ray Fluorescence (XRF), offers a comprehensive approach to reconstructing past environmental changes during the late Holocene. The application of these methodologies provides one of the most detailed chronologies available, which is crucial for understanding the timing and impact of historical flood events.

This study is significant because it demonstrates how advanced stratigraphic and sedimentological analyses can enhance our understanding of sedimentary records and floodplain development on stratigraphies that have been flooded by marine waters. For the Pevensey Levels, adopting similar methodologies could help refine the analysis and interpretation of stratigraphic layers, potentially revealing new insights into the region's coastal evolution and flood history. This approach aligns with the broader objectives of this research, which aims to contextualize and understand the sedimentary processes shaping the coastal landscape of the Pevensey Levels.

2.5.0. Comparative Case Study: Somerset Levels

The Somerset Levels, located in Somerset in Southwest England (UK) (indicated by the black rectangle in Figure 2.5), provide a relevant comparative case study due to their similar environmental setting of low-lying coastal plains with isolated areas of higher elevation (the "Lost Somerset' archipelago) that have been historically occupied by humans. This region was selected as a case study due to its distinct geomorphological features, including the presence of named islands, such as the Isle of Wedmore, which mirror the bedrock islands within the Pevensey Levels. Additionally, the Somerset Levels' well-documented Holocene depositional history provides valuable comparative data for understanding coastal wetland evolution.



Figure 2.5 - Location of the Somerset Levels in Southwest England, UK, as indicated by the black rectangle on the map. Modified from (S.K. Haslett et al., 1998).

S. K. Haslett et al. (1998) investigated Holocene relative sea-level changes at Nyland Hill in the Somerset Levels. The lithostratigraphy comprises turf peat underlying marine clay, both onlapping a sloping Upper Palaeozoic basement. This study highlighted significant sediment compaction and continuous relative sea-level rise throughout the

deposition of the clay unit, contrasting with previous models that suggested stabilized sea levels by 3000 BP (S. K. Haslett et al., 1998). Allen (1990) provides a broader regional context for sedimentary processes in the Severn Estuary and the adjacent Somerset Levels, describing the role of fine-grained sediment deposition, marine transgressions, and the impact of estuarine hydrodynamics on Holocene stratigraphy. This complements Haslett's findings and highlights the complexity of marine and terrestrial influences in shaping the Somerset Levels.

S. Haslett et al. (1998) also reconstructed Holocene sea-level change in the Severn Estuary and Somerset Levels using Sea-Level Index Points (SLIPs) based on foraminiferal analysis. This study demonstrated that sediment compaction is a significant factor affecting sea-level reconstructions, and accurate sea-level curves must consider compaction and other local factors (S. Haslett et al., 1998). Similarly, Allen (1990) highlights the variability of sediment compaction and depositional rates across estuarine and coastal systems, further validating the importance of these factors in regional sea-level reconstructions. The findings from these studies provide valuable insights into similar processes and environmental changes that might have occurred in the Pevensey Levels.

Rippon et al. (2000) examined the Romano-British exploitation of coastal wetlands in the Somerset Levels, revealing how these landscapes were used for agricultural purposes and settlement. The study provides insights into the human adaptation and modification of these environments, similar to the historical occupation and modification seen in the Pevensey Levels. Like the Pevensey Levels, the Somerset Levels experienced significant historical drainage efforts. These efforts aimed to reclaim the land primarily for agricultural use and human settlement. The "Lost Somerset" archipelago includes village names ending in "-ey" (such as Muchelney and Godney); this mirrors the bedrock islands present in the Pevensey Levels (like Rickney, Manxey, and Pevensey). These parallels highlight the common environmental and historical challenges that were faced when utilizing and managing low-lying coastal environments. Allen (1990) adds to this understanding by discussing the influence of anthropogenic factors, such as reclamation and drainage, on the geomorphology and stratigraphy of lowland estuarine systems.

The Isle of Wedmore in the Somerset Levels, similar to North Eye, shows evidence of human presence from at least the Neolithic period. Flint artifacts found on the Isle of Wedmore indicate human activity dating back thousands of years. Moreover, wooden trackways between the Isle of Wedmore and the Polden Hills, approximately 11 km to the south, dating from the first millennium BC, further support the existence of settlements on these uplands (Newell & Peacock, 2023).

While the Somerset Levels were chosen for their unique features and parallels to the Pevensey Levels, future studies could benefit from a broader analysis of other lowland UK wetlands such as The Wash, the Humberhead Levels, or the Solent, to provide more context for regional Holocene depositional variation. This could enhance the interpretation of similarities and differences between sites and improve the overall understanding of lowland marsh development across diverse environmental settings.

Utilizing the Somerset Levels as a comparative case study offers valuable parallels for understanding similar paleoenvironmental processes and history in the Pevensey Levels as the Somerset Levels have detailed reconstructions of Holocene sea-level changes, environmental management, and human adaption. These parallels not only better the understanding of past coastal dynamics, but also highlight the importance of integrating geological, archaeological, and historical perspectives when studying these complex landscapes.

2.6.0. Comparative Case Study: The Brede-Pett Level

The Brede-Pett Level, located in East Sussex, Southeast England, is on the southern edge of the Romney Marsh depositional complex bordering the English Channel and is indicated by the red box outline in Figure 2.6 below.

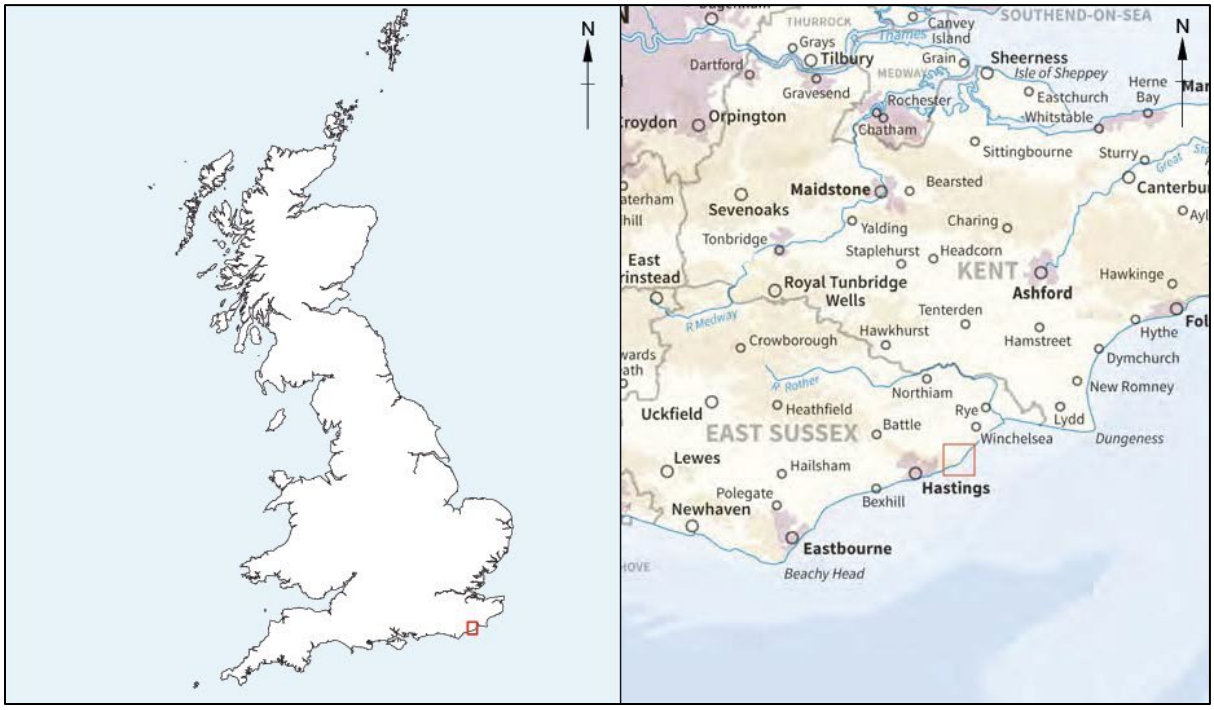


Figure 2.6 - Location of Pett Level in East Sussex as indicated by the red box outline, modified from (Timpany et al., 2021).

Approximately 26 km northeast of the Pevensey Levels, the Brede-Pett Level provides a useful comparative case study due to its geographic proximity and similar environmental conditions of low-lying reclaimed coastal plains. This site was selected for its significance within the Romney Marsh depositional complex, offering insight into nearby Holocene stratigraphy and palaeoecology. Unlike the Pevensey Levels, the Brede-Pett Level lacks bedrock islands but also features a stratigraphically complex sequence of interbedded peat, clay, and silty deposits, and demonstrate the importance of sedimentary processes and anthropogenic influences in shaping reclaimed marshlands.

Waller (1998) and Waller et al. (1998) describe the Brede-Pett Level's stratigraphy as comprising detrital peat layers overlain by intertidal and mudflat sediments. These sequences reflect the gradual reduction of marine influence, marked by transitions

between hyposaline environments and fen carr vegetation. The stratigraphy illustrates the dynamic environmental changes characteristic of reclaimed coastal wetlands in southeastern England.

Further palaeoecological investigations by Waller & Marlow, 1994 and Timpany et al. (2021) highlight the importance of the Brede-Pett Level for reconstructing Holocene environmental and vegetational History. Declines in Ulmus and Tilia pollen within the Brede Valley correlate with regional anthropogenic activity and shifts in wetland vegetation. Such records provide insight into how human activity and climatic factors have influenced the development of lowland landscapes.

The Brede-Pett Level, like the Pevensey Levels, underwent significant anthropogenic modifications, particularly during the post-medieval period. Drainage and reclamation efforts have reshaped the marshland, facilitating its use for agriculture and settlement. These interventions are similar to modifications in the Pevensey Levels and demonstrate the broader human impact on reclaimed coastal environments in southeastern England.

While the Brede-Pett Level provide valuable comparative data for understanding the Pevensey Levels, future research could benefit from considering additional lowland marshland examples, such as The Wash, or even Northern France. These broader comparisons could offer a more comprehensive framework for understanding regional Holocene depositional variation and the influence of marine and terrestrial processes.

Despite its lack of bedrock islands, the Brede-Pett Level's stratigraphic and palaeoecological records offer key parallels with the Pevensey Levels, such as the interaction between marine transgressions and fenland development. These similarities highlight the importance of integrating geological, ecological, and archaeological perspectives to reconstruct complex embayed landscapes. This case study complements the Pevensey Levels by demonstrating regional variability in depositional processes, sedimentation patterns, and anthropogenic influences.

2.7.0. Pevensey Levels Borehole Data

The studies and data that are presented in this section help with the understanding of some stratigraphic (litho-, bio-, and chrono-) information across the Pevensey Levels and one specific bedrock island named North Eye to aid in the understanding of the current configuration of the land and the development of the stratigraphy in the Levels.

The British Geological Society (BGS) display geologic information in the form of static and interactive, bedrock and surficial (superficial) geologic maps and borehole records. All boreholes in the Pevensey Levels that the BGS have available are shown in Figure 2.7, where the Pevensey Levels is the embayment labelled “Pevensey Levels” with a high density of water courses (drainage ditches). It can be observed from Figure 2.7 that a large number of boreholes were collected along roadways, with a clear concentration in and around the town of Eastbourne. Additionally, boreholes outside the Levels are spread more unevenly, with some clustering observed, and the average length of boreholes is generally longer outside the Levels than within. Apart from one borehole transect, most boreholes that are recorded within the Levels are shallow in depth (between 0 and 10 meters), and were collected along roadways, leaving many large gaps without any borehole data within the Pevensey Levels.

Borehole Records

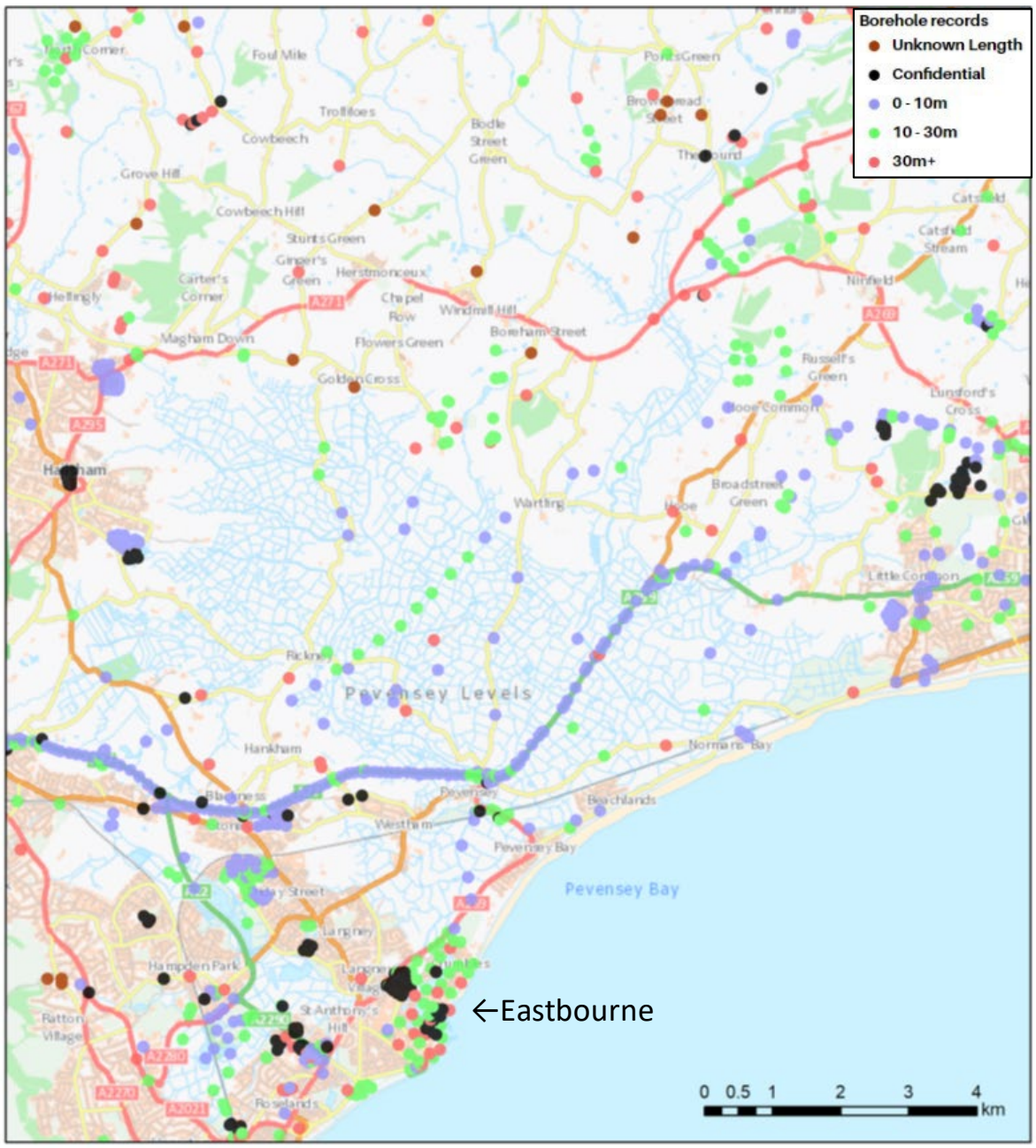


Figure 2.7 - This map depicts the locations of each borehole that the BGS (2020) have in their system for the Pevensey Levels and surrounding area. Each colour symbol corresponds to different lengths of boreholes, a legend is shown in the top right.

The most detailed stratigraphic research completed in the study area on sediment layers deposited during the late Holocene is by Jones (2002). This study provided a new dataset of sea-level index points, which determine the approximate position of the relative sea level in both time and space (Engelhart et al., 2011). This study aimed to compare these results with pre-existing geophysical models of relative sea-level change. Jones' thesis included new detailed borehole data for the Pevensey Levels, offering descriptive lithologies for each unit defined. It also presented a relatively detailed stratigraphic survey and data from multiple proxies, such as pollen, foraminifera, and diatoms, which helped reconstruct paleoenvironments associated with recorded biostratigraphy.

Units defined in Jones (2002) were compiled into a summary table that encapsulated the thickness of each unit, lithology, biostratigraphy, organic material, and depositional environments associated with each unit. These units were compared and expanded to the remainder of Jones' and BGS' cores in Drew (2021), an example of the comparison and expansion of units is visualized in Figure 2.8 below.

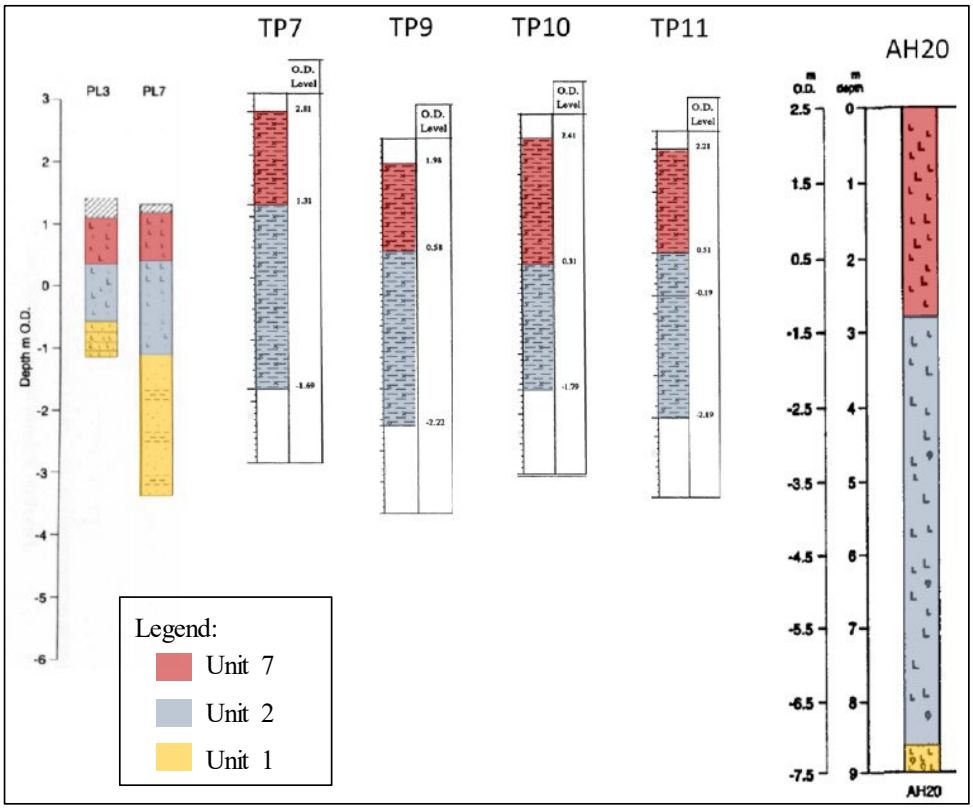


Figure 2.8 - Seven borehole records that have the units defined by Jones (2002) expanded to boreholes retrieved from BGS (2020). (L-R: PL transect (Jones, 2002), P-B I transect (TP) (BGS, 2020), AH series (BGS, 2020)), (Drew, 2021).

Drew (2021) interpreted Jones' (2002) multiproxy analysis and applied this knowledge to adjacent BGS boreholes within the Levels to better understand spatial and temporal patterns within the stratigraphy for potential predictive capabilities. The interpretation provided in Drew (2021) was an aid in connecting the stratigraphy, depositional environments, and processes during the late Holocene with the uppermost stratigraphy in the Levels. Table 2.2 shows a summary table from Drew (2021) summarizing, compiling, and calculating the work from Jones (2002) outlining and describing the lithologies, thicknesses, and observations of the main units that would be expected to appear within the Pevensey Levels.

Table 2.2 - Summary of lithological descriptions and observations from Jones (2002), established from Jones' (2002) sample core, modified from (Drew, 2021).

Unit	Approx. Thickness (m)	Lithological Description	Comments and Observations
7	Max: 1.9 Min: 0.6 Avg: 1.2	Upper Silty Clay (Oxidized): **Very hard** brown part clay, part silt with some **orange mottling** (oxidization)	Oxidization present in this unit implies a return to shallow pasture lane conditions, in other words, **similar to present-day conditions**. This unit is common throughout the Levels and is similar to uppermost sediments found throughout Southeast England.
6	Variable	Transition Silty Peat: No specific lithological description provided.	**Thin** transition layer between units 5 and 7.
5	Variable: 0.2 – 0.7	Upper Peat (woody): **Well decomposed woody peat** with **large pieces of wood** near the lower contact.	Lack of phragmites when compared with unit 3.
4	Variable	Silt and Clay (with some sand): Silty clay **with some sand** with major variations in thickness and altitude.	**Thin** layer that separates the two peat layers. Sand suggests a potential rise in relative sea-level. Layer tended to be absent from cores closest to the modern-day coastline, and further inland.
3	Max: 0.8 Min: 0.1 Avg: 0.3	Lower Peat (phragmites): Thin layer of **humified** peat, often containing **Phragmite** and **wood remains**.	Typically followed by blue-grey silty clay in many cores and tend to be located towards the center of the ancient lagoonal area.
2	Max: 2.3 Min: 0.5 Avg: 1.4	Lower Silty Clay: Very fine, soft, wet, and sticky sediment with a blue grey colour.	Becomes gradually less sandy from Unit 1. Average depth ranged from -4m OD to 0m OD with an average -2m OD.
1	Max: 4.7 Min: 0.3 Avg: 1.5	Sand, Silt, and Clay: Silty clay with the presence of sand	The lowest unit observed in all boreholes in Jones' stratigraphic survey. Sand suggests strong tidal influence. Some **organic material may be present** in **lower portions** of this unit.

A geoarchaeological assessment report of the site of a Medieval (500–1500 CE, 1450 to 450 BP) village on North Eye in the Pevensey Levels is presented by Champness (2009). This report provided six additional detailed borehole records that were not in the BGS database, new age dates of the peat sequences using multiple biostratigraphic proxies, and a cross-sectional representation of the stratigraphy of North Eye (Figure 2.9).

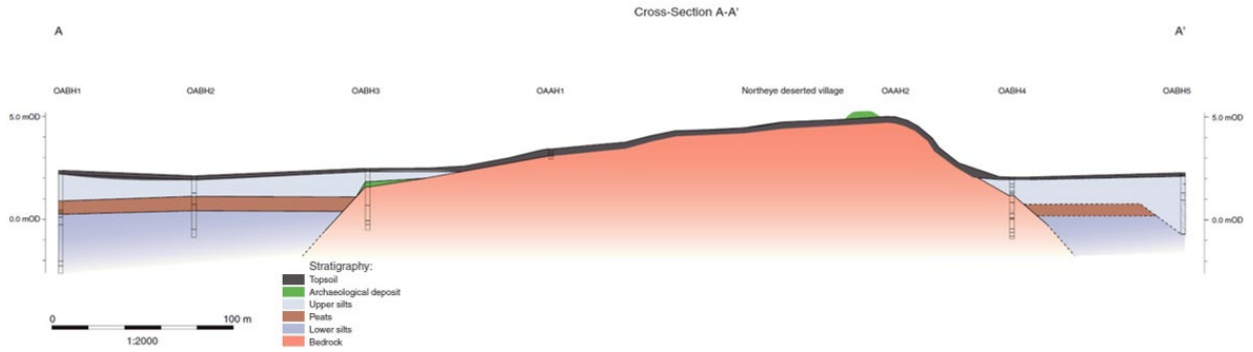


Figure 2.9 - Cross sectional representation of the stratigraphy of the "bedrock island" of North Eye (Champness, 2009).

Champness' (2009) report identified the following key stratigraphic units:

- Topsoil
- Archaeological fills
- Upper silty clays
- Peat/organics
- Lower clayey silts/sands
- Bedrock.

The lower units were characterized by blueish-grey clayey silt and sand, indicative of tidal influences, while the peat and organic deposits were interstratified with light blueish-grey clay, suggesting a more complex depositional history.

The stratigraphic summary provided by Drew (2021) (shown above in Table 2.2), which summarizes the work of Jones (2002), aligns with Champness' observations. The descriptions of upper silty clay units, peat layers, and lower silty clay units in Table 2.2 from Drew (2021) correspond with those found by Champness (2009), highlighting consistent sedimentary processes across the Pevensey Levels, thereby enhancing the understanding of the region's geological and archaeological history.

2.8.0. Pevensey Levels Historiography

While the primary objective of this thesis focuses on geology and stratigraphy, the historical background plays an important role in providing essential human context. This section examines some of the oldest known maps or predictive maps of the Pevensey Levels, analyzes the place name history of the bedrock islands within the Levels, and discusses an entry from the Domesday Book, a comprehensive survey of England that was ordered by William the Conqueror in 1086 (Green, 2021). The Domesday book is a significant historical record that provides detailed information about human settlements, land use, and resources during that time. Additionally, this section covers a timeline of flooding and drainage events in the Levels based on historical records. This historical perspective not only augments the understanding and comprehension of the Levels' previous state during the targeted time period for this study, but it also provides a better understanding of the lasting effects of human manipulation and interaction with the Levels. Furthermore, this section contributes to a holistic understanding of the evolution and challenges of the Pevensey Levels.

The Pevensey Levels are an area of frequent and extreme environmental fluctuations that have greatly impacted humans over several centuries (Moore, 2020, 2021). Fluctuations may be expected in such a coastal depositional system, although a natural sand and gravel beach barrier separating the Pevensey Levels from the English Channel helps protect the inland areas. However, historically, the low-lying embayed area landward of the beach barrier has been naturally flooded by relatively high river discharge and extreme storm surges from the North Sea. Figure 2.10 depicts a predicted arrangement of the land and sea at the Pevensey Levels and surrounding area during the year 1910 if the shingle and sand beach barrier modified by human interaction were to be removed (Ballard, 1910).

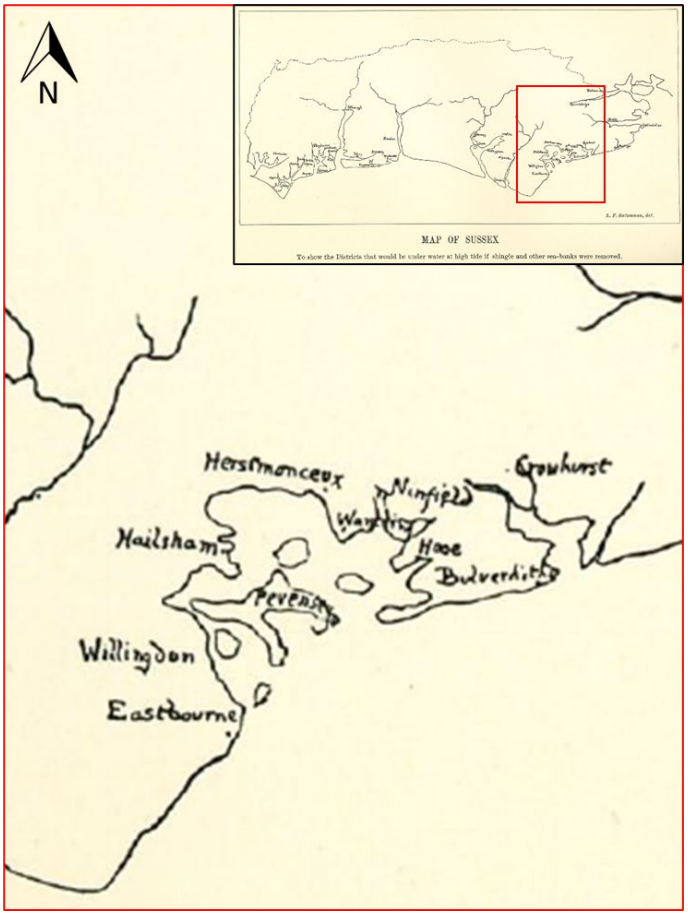


Figure 2.10 - A map of the county of Sussex produced in 1910 that depicts how the shoreline would appear if the sea-banks and shingle were removed. Modified from (Ballard, 1910).

This interpretation illustrates a coastal embayment with islands in the Pevensey Levels. This visual shows islands that are separated by standing water connected to the English Channel because of elevation differences between the relatively lower marshland and higher islands.

Hewitt (2018) identified a lack of historical maps during the eleventh century within accessible literature in his article that explored a human perspective of the Pevensey Levels. During Hewett's (2018) process of completing a map regression (viewing maps of the same area backwards from most recent to increasingly older maps) of the Levels, a seventeenth century map of Sussex (Figure 2.11) was found. This map depicts a simplified view of the Pevensey Levels (also called Pevensey Marsh), where the Medieval chapel, "Nordy Chap" was recorded and is the name of the chapel that was discovered in the

abandoned Medieval village on North Eye. Archaeological evidence of this was displayed above in Champness' (2009) archaeological report (see Figure 2.9).



Figure 2.11 - A map depicting Sussex during the 17th century. The Pevensey Levels are labelled as "Pevensey Marsh", and the Medieval chapel on North Eye is located in the red circle as "Nordy Chap". Modified from Hewett (2018).

Islands within Pevensey Levels have been indicated previously throughout history recorded by humans. The names of each area of higher elevation (island) that were shown in an earlier figure (Figure 1.5 in Section 1.3.0: Location of Study and Site Descriptions), as well as an alternative name presented above in Figure 2.10 (Nordy), each name ends in "-ey", "-y" or "Eye". These endings are common elements in English placenames and are derived from the Old Norse word "Ey" which translates to "island" (Arthur, 2002; Cameron, 1961), or to "dry land in a marshy area" (Higham et al., 2011).

Lastly, Horsey (Horse Eye) was a settlement recorded in the Domesday Book within the hundred of Pevensey and the county of Sussex (seen in Figure 2.12). In 1086, Horsey had a recorded population of 1 household and 1 men's plough team (Powell-Smith et al., 2011), indicating its small size at the time. This recorded history provides evidence of early human settlement and activity on the islands within the Pevensey Levels.

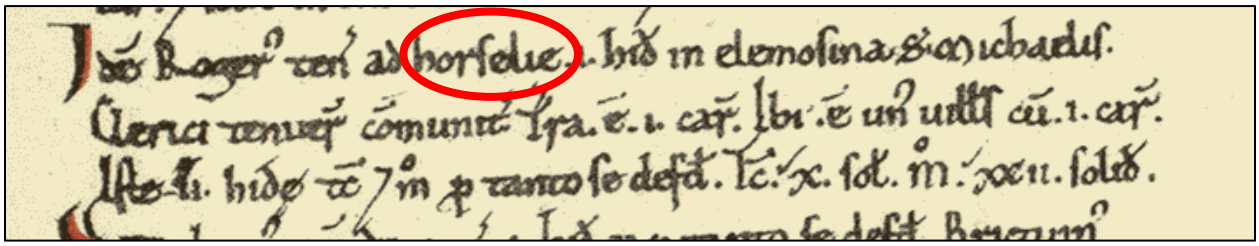


Figure 2.12 - The Domesday Book entry for Horsey (Horse Eye), recorded in 1086 within the hundred of Pevensey and the county of Sussex. The red oval highlights the word "Horsey" in Latin. This entry documents the presence of a settlement with a recorded population of 1 household (from Powell-Smith et al., 2011).

A timeline, which contains the time period discussed above in Figure 2.10 (17th century), of the historic record of flooding events and drainage efforts documented by humans ranging from the 10th century to the late 16th century has been compiled by Moore (2020) and was simplified into Figure 17 below. Historians have focused on the period spanning 950 – 400 BP or 1000 – 1550 CE, which is encompassed in the time range of Figure 2.12, within the Pevensey Levels because there is documentation of excessive amounts of human manipulation of the natural environment, such as the construction of drainage ditches and canals in the Pevensey Levels, and the silting up of the mouth of the Pevensey watercourse. Examples of human modification of the natural environment in the Levels are shown below in Figure 2.12 as the yellow boxes along the timeline.

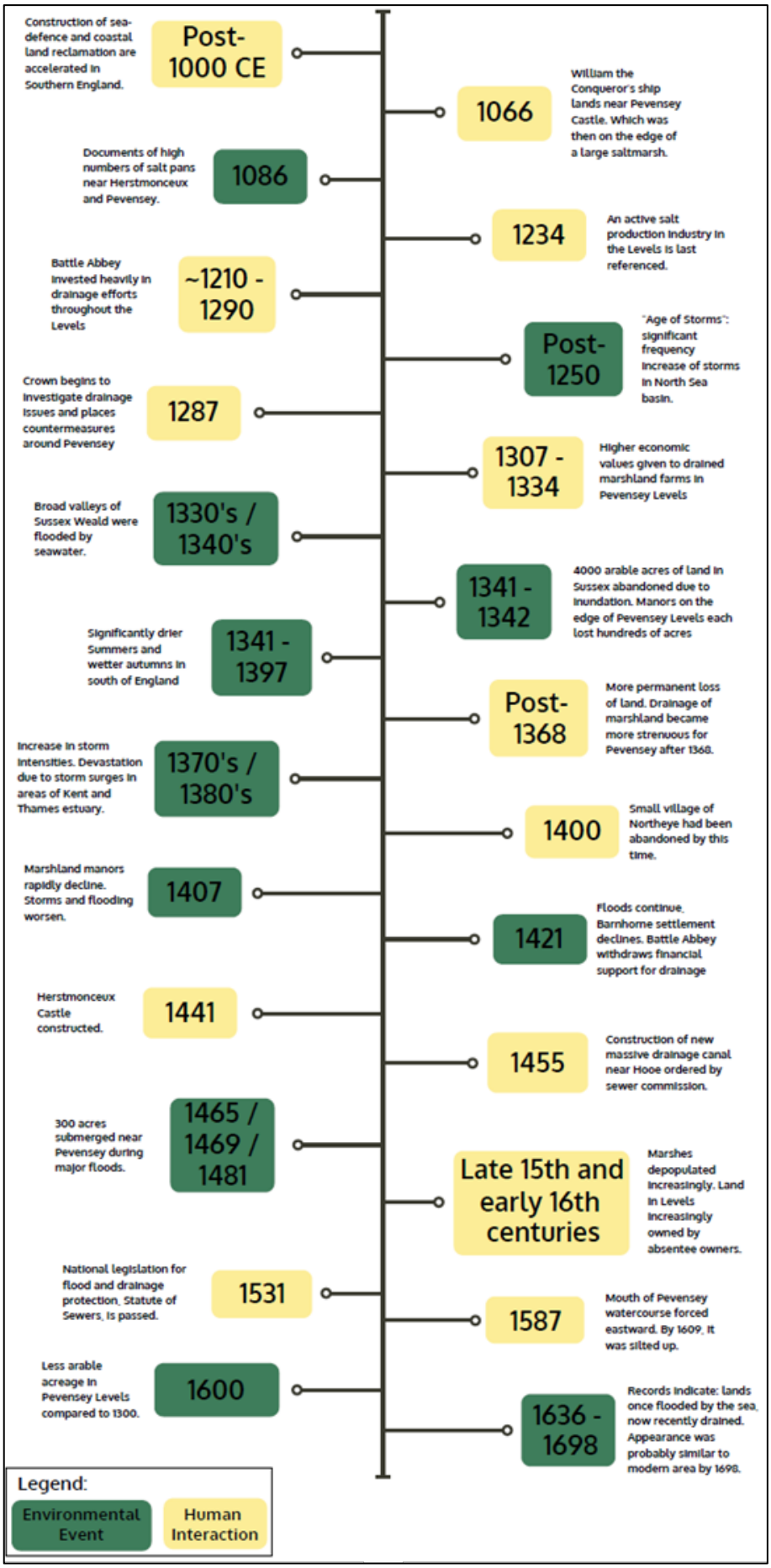


Figure 2.13 - Timeline of major flooding and drainage history of the Pevensey Levels. Green events are records of natural events caused by the environment, and yellow events are records of human interaction and manipulation of the natural landscape. Modified from (Moore, 2020).

2.9.0. Summary of Existing Research

The Pevensey Levels are a unique ancient lagoonal landscape that has been heavily influenced by both human interaction and environmental changes throughout time. While existing literature has advanced the understanding of coastal development in East Sussex and comparable environments such as the Somerset Levels, significant gaps remain in the Late Holocene stratigraphy and paleoenvironmental history of the Pevensey Levels, particularly concerning its isolated elevated areas, or "bedrock islands", such as Horse Eye and North Eye.

Regional studies have detailed the stratigraphic sequences within comparable embayed environments, such as Romney Marsh and Somerset Levels, utilizing methodologies such as sediment core analysis, radiocarbon age-dating, and geochemical analyses. These studies have highlighted the importance of integrating geological, archaeological, and historical data to reconstruct paleoenvironmental changes and interactions between human activities and natural processes. Similarly, work on the Pevensey Levels has provided a foundation into the sedimentary processes, beach barrier dynamics, and the impact of sea-level changes, yet there remains limited focus on the stratigraphy and the paleoenvironmental evolution of its bedrock islands.

Historical and geological records emphasize the dynamic nature of the Pevensey Levels, including transitions from marine and terrestrial conditions, sediment reworking, and human-driven landscape modifications such as drainage systems and agricultural adaptations. Comparative case studies like those of Jennings and Smyth (1987, 1990) and Roberts and Plater (2007) highlight the need for high-resolution stratigraphic analyses to contextualize these processes. Furthermore, the inclusion of the Somerset Levels as a comparative case study highlights parallels in environmental changes, sedimentary processes, and human interactions within low-lying coastal environments.

Existing studies provide valuable frameworks and methodological approaches, but they highlight the need for site-specific research to address stratigraphic and paleoenvironmental variations at finer scales. By focusing on underexplored aspects of the

Pevensey Levels' geological history, this thesis builds upon the established literature while contributing new perspectives to the understanding of coastal and lagoonal landscapes in southeastern England.

2.9.0. Scope and Objective of Thesis

The Pevensey Levels, a landscape rich in historical and environmental significance, presents a unique opportunity to explore the dynamic relationship between human settlement and natural processes. Building upon existing research conducted at North Eye, and within the Pevensey Levels, this study aims to deepen our understanding of the environmental processes shaping the former island settlement sites within the Pevensey Levels.

The primary objective of this research is to **1) develop a comprehensive stratigraphic framework specifically focusing on the isolated elevated areas**, referred to as bedrock islands, within the Pevensey Levels. These bedrock islands, exemplified by Horse Eye and North Eye, offer distinct geological features that serve as archives of past environmental dynamics and natural conditions. By closely mapping, age-dating, and analyzing sediments in relation to these island sites, this study seeks to **2) reconstruct the paleoenvironmental context of these landscapes from their formation through periods of use and abandonment**. The targeted time for investigation spans the geological Late Holocene Epoch, or Meghalayan Age (4200 BP to present, Cohen et al., 2022). Particularly emphasizing the lead up to and potentially during the historical High and Late Middle Ages (950 – 400 BP, 1000 – 1550 CE). This age range aligns with the objectives of the Environments of Change multidisciplinary research project.

The rationale for selecting bedrock islands as the focal point of this study stems from their unique geological characteristics and their historical significance as settlement sites. These elevated areas not only provide a distinct stratigraphic record but also offer insights into the interactions between human activity and environmental processes over time. By developing a stratigraphic framework encompassing sediment analysis, bedrock composition, structural features, and historical evolution, this study aims to enhance our understanding of the geological processes that shaped the development of these bedrock islands and their broader implications for the landscape evolution of the Pevensey Levels.

Developing and applying this stratigraphic framework aids in a deeper understanding of the paleoenvironmental variations and geological processes that may have played a crucial role in the formation of not only the Pevensey Levels but also the bedrock islands Horse Eye and North Eye. Developing this framework is one method to help understand the complex history of the Levels and these bedrock islands, in addition to a better understanding of the naturally dynamic landscape that humans occupied and depended upon for habitat and subsistence.

Chapter 3: Methodologies of Field and Laboratory Work

3.1.0. Introduction

To develop a stratigraphic framework (Objective 1) and reconstruct the paleoenvironmental context of Horse Eye and North Eye (Objective 2) within the Pevensey Levels, a structured approach comprising both fieldwork and laboratory analyses was employed. This study utilized a combination of geographic, geomorphologic, and sedimentological methods to achieve these objectives.

The initial step involved geographic and geomorphologic analysis using LiDAR data to remotely assess the landscape of the bedrock islands prior to fieldwork, as shown in Section 3.2.0. This was followed by the determination and establishment of transects during fieldwork, which are explained in sections 3.3.1. Subsequently, coring, stratigraphic and sediment description, and sediment sampling were conducted during fieldwork, as elaborated in Sections 3.3.2, 3.3.3, and 3.3.4.

The collected samples were then subjected to various laboratory analyses as described in section 3.4.0. Grain size analysis was performed using the Laser Diffraction Method (LDM) as described in Section 3.4.1. For the peat layers, Portable X-ray Fluorescence (pXRF) and Loss on Ignition (LOI) analyses were conducted to determine elemental composition and organic content, respectively, as detailed in Sections 3.4.2 and 3.3.3. The mineralogical composition of the detrital material was determined through X-ray Diffraction (XRD) analysis, as explained in Section 3.4.4. Finally, the geochronology of the peat layers was established using AMS radiocarbon dating (C-14), as outlined in Section 3.4.5.

To address Objective 2, the compiled field and laboratory data were synthesized into a comprehensive facies analysis. These facies were categorized based on predominant lithology and sedimentary attributes, such as roots, mottling, and sedimentary structures, following Farrell et al. (2012). Climatic data from the NGRIP $\delta^{18}O$ dataset (Andersen et al., 2004) was also incorporated to aid in the paleoenvironmental interpretation of Horse Eye. Sand fractions identified within the stratigraphy were correlated with fluctuations in the

NGRIP $\delta^{18}O$ record to contextualize sedimentary processes in relation to climatic variations. These analyses are discussed in Chapter 5: Reconstructing the Depositional History in the Pevensey Levels (Horse Eye and North Eye).

3.2.0. Geographic / Geomorphologic Analysis

Elevation data in the form of Light Detection and Ranging (LiDAR) obtained from the UK Ordinance Survey (UK Ordinance Survey, 2020) provided the most detailed surface elevations (1 m resolution) in the Pevensey Levels and were used to define the modern-day ground surface in maps (shown in Figure 1.4 in Section 1.3.0 Location of Study and Site Descriptions) and cross-sectional views. LiDAR is a remote sensing technique that uses laser light to measure distances to a target, producing high-resolution three-dimensional information about the surface being scanned (Wang, 2020). Physical descriptions of the landscape were recorded in a field notebook and through photographs, noting land use, vegetation, and potential bedrock outcrops.

These LiDAR-derived elevation data were analysed using QGIS version 3.16.5-Hannover and processed in the OSGB 1936 / British National Grid coordinate reference system. The hillshade model, used to visualize topographic relief, was created from the LiDAR raster image using standard parameters, including a sun altitude of 45˚ and an azimuth of 315˚. These elevation data and descriptions aided in recording the dimensions and orientation of each island, as well as analyzing the topographic and geomorphologic features to identify potential coring locations and to contextualize the stratigraphic findings within the broader landscape.

3.3.0. Fieldwork Methods

3.3.1. Transects

Transects were established using a Garmin GPSMAP 62s Global Positioning System (GPS) device, referencing the Ordnance Survey National Grid reference system (OSGB), otherwise known as the British National Grid (BNG). The planning process involved setting up roughly N-S and E-W transects, with transects perpendicular or parallel to the modern-day coastline. The lengths of the transects were not static and were determined by ensuring boreholes started on the hilltop of the bedrock island and ended in the bottom of the slope; in the Levels, the length depended on the slope of the island. The orientation of each transect was chosen to find the transition from marine to terrestrial environments. Lastly, the location of each transect was marked with the GPS, a marker flag, and a 100-meter-long tape measure was used for accuracy.



Figure 3.1 - A photograph showing the start of a transect indicated at the bottom of the photo by a red marker flag, with field assistant, Kira, in the distance indicating the end of the transect. Kira is circled in red with a red arrow pointing at her for emphasis.

Figure 3.1 shows the start of one transect that is marked by a red marker flag and shows field assistant Kira Bourque, indicating the end of the transect. This visual representation can help illustrate the process of setting up and marking transects in the field.

3.3.2. Coring

Coring was performed along the established transects using a 20 cm diameter, 100 cm long two-piece bayonet gouge auger, and a 60 cm diameter, 50 cm long two-piece gouge auger, as shown in Figure 3.2 below. These gouge augers were used to extract soft sediment cores along multiple transects on Horse Eye and North Eye.



Figure 3.2 - Photograph of the two-piece gouge auger set showing all pieces included in the set. Obtained from (Two-Piece Gouge Auger Set with Bayonet Connection for Soft Soils, 2023).

A total of 11 boreholes were collected across one transect on North Eye and 25 boreholes across four transects on Horse Eye, spanning both island and edge deposits. The transects for both islands were strategically placed to capture the transition from higher elevations to the lower-lying Pevensey Levels. The transects on Horse Eye, being the primary focus, aimed to cover the perimeter of the island where sediment layers potentially increase in thickness and number away from the island. This strategy allowed for the collection of samples both on and off the island, providing a comprehensive understanding of the stratigraphy along the edge of the islands.

The 60 cm diameter, 50 cm long gouge auger was used to collect additional sediment samples from harder and deeper strata. The coring process entailed driving the corer into the ground, marking the level of the ground surface with tape, turning the corer in a clockwise or counterclockwise manner, and then carefully lifting the corer out of the ground, attempting to have no sediment lost into the core hole. The tape marker was then aligned with a tape measure to keep track of the depth of each sediment layer or stratigraphic feature.

The placement of transects prioritized areas where sediment layers were expected to vary in thickness and composition based on topography, with a focus on potential transition zones between marine and terrestrial paleoenvironments. Spatial data for the boreholes and transects, as well as descriptions of the sedimentary sequences, are presented in Chapter 4: Results of Fieldwork and Laboratory Analyses (North Eye and Horse Eye), with North Eye's coring locations and results presented in 4.2.1: Preliminary Fieldwork, and Horse Eye's in 4.3.1: Site Description.

3.3.3. Stratigraphic and Sediment Description

The identification and classification of the lithology and grain size of the sediment in the field were crucial to developing the stratigraphic framework of the study site. In the field, visual inspection of the sediment grain size and lithology was completed using a hand lens and a grain size card, following Boggs (2012) for grain size classification using the Wentworth scale. An image of a sediment core sample placed next to a grain-size card is included to illustrate the process (Figure 3.3). The colour of the sediment was recorded using colour names from a Munsell soil colour chart (Munsell, 1988).

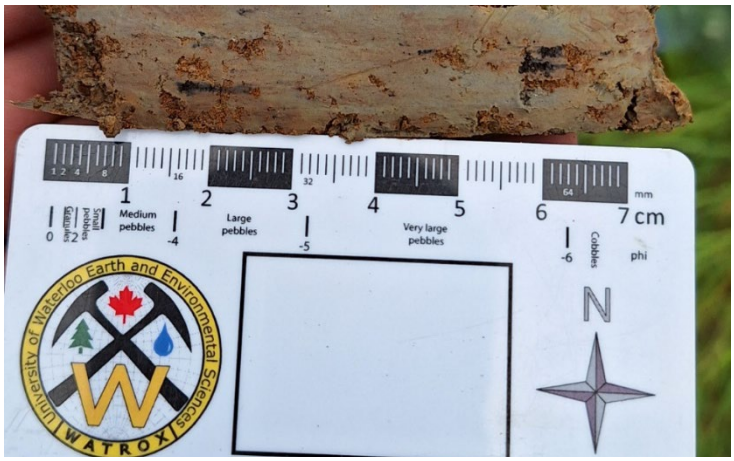


Figure 3.3 - Grain size card showing measurements in centimeters, millimeters, and phi placed next to a sediment core sample.

Additionally, the depth of each sample collected was recorded by placing a measuring tape beside the sediment core, ensuring a precise depth reference within each sediment core (seen in Figure 3.4).

A detailed stratigraphic description (Appendix A – North Eye, Appendix B – Horse Eye) and sampling of each core was conducted in the field using a working checklist. This included the following steps:

1. Photograph of core (cellular phone) and depth recorded (tape measure)
2. Colour (Munsell soil colour chart [Munsell, 1988]) and plasticity (guided by the Unified Soil Classification System [USCS] [Howard, 1986])
3. Visible contacts (gradational or abrupt and planar or undulating)
4. Visible grain size (Wentworth scale [Wentworth, 1922]) and sedimentary structures or other features (guided by Boggs, 2012)
5. Density and compaction (guided by the USCS)
6. Collect representative samples in labelled plastic bags
7. Record core location using a GPS Waypoint (Garmin GPSMAP 62s)

3.3.4. Sediment Sampling

Sediment samples were collected for each section being described, especially if there was a new characteristic that distinguished it from the adjacent unit. However, if a long section of the core looked homogenous, a few samples were collected to follow a somewhat regular sampling interval and allow for exploration of non-visible changes in grain size. The top portion of each core, including the topsoil and uppermost soil horizons, was not collected to avoid sampling topsoil material, whose importation into Canada is restricted and was not the focus of this study.



Figure 3.4 - Photograph of a sediment core with a measuring tape adjacent to it. This is completed to record the depth of each sediment core and each unit within the cores.

Samples were cut from the core with a clean spatula, then removed from the core (seen in Figure 3.4) and placed in a zipper storage plastic bag labelled with the core they corresponded to and the depth at which they were collected. Peat material was placed in aluminum foil to contain it in a pouch before being put in a labelled zipper storage plastic bag. Peat and topsoil were transported to the University of Southampton, United Kingdom, for analyses. Detrital sediment was transported to the University of Waterloo, Canada. Note that half of each sediment core sample was archived in the UK in case samples were

lost or destroyed during transport to Canada. However, all detrital samples were transported successfully to Canada.

3.4.0. Laboratory Methods

3.4.1. Grain Size Analysis

Grain size analysis was conducted using the Laser Diffraction Method (LDM) with the Fritsch Analysette 22 MicroTec Plus (Figure 3.5) (FRITSCH, 2009) at the Quaternary Geology Lab at the University of Waterloo. The LDM is a widely used method for determining particle size distributions. LDM determines particle size based on the principle that the intensity and angle of light diffracted is inversely proportional to the particle size (Di Stefano et al., 2010). In LDM, a monochromatic laser passes through a suspension of particles flowing in a closed circulation loop; the resulting diffraction pattern is captured by detectors. The diffraction pattern, which is focused by a Fourier lens, determines particle size distributions (Di Stefano et al., 2010; Wen et al., 2002).



Figure 3.5 – Photograph of the Fritsch Analysette 22 MicroTec Plus in the Quaternary Geology Lab at the University of Waterloo.

The workspace, including all necessary equipment, was thoroughly cleaned to ensure a contamination-free environment prior to analysis. To minimize flocculation, a pre-prepared 4% w/v sodium metaphosphate solution was used. This solution was mixed with the sediment samples at room temperature to create a slurry consisting of approximately 75% sediment and 25% sodium metaphosphate solution.

Samples underwent necessary pretreatment prior to analysis. If grains larger than 2mm were present, the sample was wet sieved using a 2mm sieve, settled in a beaker, and

once the sediment had settled, the water was removed, and the sample dried in an oven at 70°C to remove any remaining water. In cases where there was organic matter that could impact the LDM analysis, organic matter was removed using a 30% hydrogen peroxide solution, following the procedure from Papuga et al. (2022).

The Fritsch Analysette 22 MicroTec Plus, with a full wet range of 2000 µm to 0.08 µm, was utilized to determine the grain size of samples collected, using two semiconductor lasers with a wavelength of 532 nm or 940 nm. Approximately one gram of each sample was used for the analysis, but the exact quantity varies depending on the grain size (coarser material requires more sample). The samples were dispersed in deionized water and flowed through the system's sample cell.

The raw grain size data from the MaScontrol software, associated with the Fritsch Analysette 22 MicroTec Plus, was output as individual .xls files for each sample. These files included data columns for Size Low [µm] and dQ3(x) [%], which were used to calculate grain size distributions. The calculations employed the Fraunhofer equation for particle size determination. The data was categorized according to the Wentworth scale (Boggs, 2012) into three size fractions: sand (62.5 - 2000 µm), silt (2 - 62.5 µm), and clay (0.6 - 2 µm). The sum of the frequencies for each fraction was calculated in Microsoft Excel to produce percentage values (% sand, % silt, and % clay) for each sample.

These percentage values were compiled into a master Excel spreadsheet to facilitate comparison across all sampled depths. Grain size distribution plots were created as bar charts for individual cores from Horse Eye Transect 4 and North Eye Transect. Additionally, down-profile line charts were created to visualize the relationship between grain size distributions (% sand, % silt, % clay) and depth. Normalized plots of sand and silt fractions were also created to highlight trends in sediment composition with depth.

The grain size data for Core HE23T4C4B was further analysed using GRADISTAT (Blott & Pye, 2001) (see Appendix C), a grain size distribution and statistics package that runs within an Excel spreadsheet. This provided complementary grain size distribution plots alongside statistical summaries including statistics such as mean, mode, and

sorting. These additional outputs helped to validate the results obtained from Excel and offered insights into the sedimentary characteristics of the samples for this core. Together, the Excel-based and GRADISTAT analyses ensured a comprehensive understanding of the grain size distributions of core HE23T4C4B, contributing to broader interpretations of Horse Eye's paleoenvironmental history.

3.4.2. Portable X-ray Fluorescence (pXRF) Analysis

Elemental analysis of the core sediment samples was conducted using a Niton XL3t GOLDD+ portable X-Ray Fluorescence (pXRF) analyzer at the University of Southampton by Dr. Ben Pears. This technique provides a rapid and quantifiable (ppm) assessment of the elemental composition, this analysis is based on the procedure from Pears et al. (2020) and Pennington et al. (2019). The procedure involved:

1. **Sample Preparation:** A total of 8 samples were placed into plastic pots and covered with 160µm Ultralene film.
2. **Analysis:** Samples were placed in a mounted test stand under laboratory conditions. Readings were taken using the 'Geochem' mode with a dwell time of 120 seconds divided into four filters: main (0-100keV), low (0-40keV), high (40-100keV), and light (0-10keV).
3. **Elemental Identification:** The pXRF identified 21 key elements associated with various sediment characteristics, including:
    - **Clastic Indicators:** Titanium (Ti), Silicon (Si), Zirconium (Zr) are proxies for coarser sediments; Potassium (K), Aluminium (Al), Rubidium (Rb) for finer sediments.
    - **Carbonates:** Calcium (Ca) and Strontium (Sr) indicate carbonates.
    - **Organic Proxies:** Sulfur (S) indicates the presence of organic material.
    - **Redox Indicators:** Iron (Fe) and Manganese (Mn) reflect variations in redox conditions.

- **Heavy Metals/Pollutants:** Lead (Pb), Zinc (Zn), Copper (Cu), among others indicate anthropogenic influences and pollution.

The elemental analysis using pXRF allows for mapping the variability in depositional and post-depositional processes, ultimately deriving from changing environmental conditions. Key elements like Ti, Si, Zr, and others were chosen based on their associations with different depositional environments, as detailed in the referenced works by Davies et al. (2015).

According to Davies et al. (2015):

- **Aluminium (Al)** is indicative of flood/detrital layers and detrital silicates.
- **Calcium (Ca)** can indicate increased evaporative concentration, primary productivity, or marine influence.
- **Iron (Fe)** is associated with detrital inputs, redox conditions, and clay-rich layers in varved sediments.
- **Potassium (K)** reflects increased detrital input and flood layers.
- **Strontium (Sr)** can be an indicator of in-lake carbonate precipitation or erosion of carbonatite-rich material.
- **Titanium (Ti)** indicates increased runoff/rainfall and detrital input

3.4.3. Loss on Ignition (LOI)

Loss on Ignition (LOI) is commonly utilized to determine the organic and carbonate content in different types of samples (Mu et al., 2017). This method involves heating a sample to specific temperatures to measure the mass loss, which corresponds to the volatilization of organic matter and decomposition of carbonates. The principle underlying LOI is that when a sample is heated, it loses weight at specific temperatures, reflecting the loss of particular components such as moisture, organic matter, and carbonates (Bensharada et al., 2022; Mu et al., 2017).

LOI analysis was conducted at the University of Southampton by Dr. Ben Pears on peat samples and topsoil sediment samples to determine the percentage of organic matter and carbonate content. Each sample was initially oven-dried at 105°C for 12 hours to determine water content and calculate Dry Bulk Density (DBD). The organic content was then determined by combusting the samples at 550°C for 2 hours. Finally, carbonate content was measured by further combusting at 950°C for 4 hours. The resulting values were used to calculate the organic and carbonate content using standard relative equations.

3.4.4. X-Ray Diffraction Analysis (XRD)

XRD analysis was carried out using the Malvern Panalytical Aeris within the Groundwater Geochemistry Remediation Group at the University of Waterloo to determine the mineralogical composition of the sediment units surrounding the peat layers. By understanding the mineral composition of the silt and clay units, insights into the depositional environment and post-depositional processes were gained. The method involved:

1. **Wet Sieving**: Samples were wet sieved with a 63 µm mesh sieve to remove coarse grains, nodules, and organics.
2. **Sedimentation**: The wet sieved samples were allowed to settle for 3-5 days. After the sediment had settled, water was removed from the top of the beaker using a syringe.
3. **Drying**: Samples with minor amounts of water left were dried in an oven at 70°C.

4. **Powdering**: Dried samples were powdered using a mortar and pestle and re-powdered in an agate mortar and pestle to ensure they were finely powdered (seen in Figure 3.6)



Figure 3.6 - An agate mortar and pestle used to finely powder sediment samples and a weighing paper with finely powdered sample.

5. **Mounting**: Powdered samples were mounted onto back-loaded steel sample holders.
6. **Analysis**: The Aeris X-Ray diffractometer (pictured in Figure 3.7) was used for analysis, and the HighScore software was utilized to plot the XRD data. This technique utilizes the Rietveld method for phase identification and quantification (Makvandi et al., 2023).

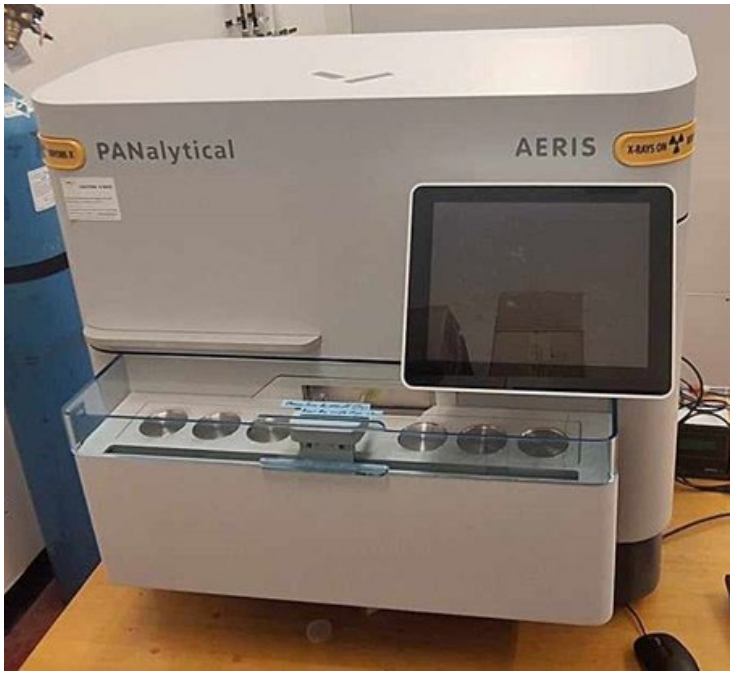


Figure 3.7 - Image of the Malvern Panalytical Aeris XRD machine from the Groundwater Geochemistry Remediation Group at the University of Waterloo.

3.4.5. Geochronology

There are two methods to measure Carbon-14 (^{14}C) atoms, one of the three naturally occurring isotopes of Carbon (^{12}C, ^{13}C, ^{14}C), in organic material and obtain an age from it. The first method, called conventional radiocarbon dating, consists of detecting and counting beta particles, which are electrons emitted by ^{14}C atoms due to radioactivity, to establish the activity of a sample (Povinec et al., 2009). The second method, Accelerator Mass Spectrometry (AMS) radiocarbon dating, measures the isotopic ratio of ^{14}C to ^{12}C or ^{13}C (Povinec et al., 2009). Results are then standardized for 'modern carbon' using reference material and the age is obtained based on the decay constant. Raw results are then corrected to account for isotopic fractionation because the $\delta^{13}C$ of the sample may differ from the convention used in the calculation. Finally, results must be calibrated using the International Calibration Curve to account for variable ^{14}C production through time (Reimer et al., 2020).

The main chronological method used in this study to determine the age of the uppermost strata associated with the bedrock island known as Horse Eye within the Pevensey Levels was AMS radiocarbon dating. This method involved using plant material, such as peat. Samples were collected using a gouge auger, packaged in aluminum foil, and sent to the 14Chrono Centre for Climate, the Environment and Chronology at Queen's University Belfast for analyses. Pretreatment procedures followed at the 14Chrono Centre included the following:

1. Cleaning samples to remove any contaminants.
2. Removal of carbonates and secondary organics through an acid-base-acid (ABA) treatment.
3. Graphitization, converting the samples to graphite targets for AMS measurement.

The radiocarbon dates provided by the 14Chrono Centre were calibrated using two software packages: OxCal version 4.4 (Bronk Ramsey, 2001, 2017) and Bacon (rbacon) v.3.3.1 (Blaauw, 2010) within R version 4.4.1 (R Core Team, 2024) with the IntCal20 calibration curve. Each provided distinct advantages and disadvantages. Both software's produced age-depth models and accumulation rate graphs.

- OxCal: Offers a versatile and comprehensive tool for calibrating radiocarbon ages. It supports classical calibration using standard radiocarbon calibration curves (e.g., IntCal20) as well as an option to employ Bayesian statistical techniques to combine prior information with radiocarbon data, facilitating precise age modeling (Bronk Ramsey, 2009).
- Bacon: Uses Bayesian statistics to develop age-depth models from radiocarbon ages. It segments the core into multiple sections and applies millions of Markov Chain Monte Carlo (MCMC) iterations to estimate the accumulation rates for each section, thereby constructing a detailed age-depth model (Blaauw, 2010).

3.5.0. Summary of Methodologies

This study employed a multi-method or multi-proxy approach to achieve the objectives of developing a stratigraphic framework and reconstructing the paleoenvironmental context for Horse Eye and North Eye within the Pevensey Levels. Initial geographic and geomorphologic analyses were conducted using high-resolution LiDAR data to define the surface elevations of the Pevensey Levels and inform the placement of field transects. These data were processed in QGIS to generate topographic visualizations, aiding in the identification of coring locations and providing essential context for stratigraphic analyses.

Fieldwork involved the extraction of 36 boreholes- 11 at North Eye and 25 at Horse Eye- using two-piece gouge augers of varying dimensions. Boreholes were strategically positioned along transects to capture the stratigraphic transitions between the bedrock islands and the surrounding Pevensey Levels. Stratigraphic descriptions recorded key attributes such as grain size, sedimentary structures, and sediment colour, while sediment samples were collected systematically to ensure representation of the variability observed across the sites.

Laboratory analyses were conducted primarily on samples from Horse Eye Transect 4, with additional limited data from North Eye. Grain size analysis, using the Laser Diffraction Method (LDM), was conducted on samples from both Horse Eye Transect 4 and the North Eye transect, though only a limited number of samples were collected from North Eye. Portable X-ray Fluorescence (pXRF) and Loss on Ignition (LOI) analysis quantified elemental compositions and organic and carbonate content of topsoil and peat samples from Horse Eye Transect 4. X-ray Diffraction analysis (XRD) and AMS radiocarbon dating were conducted specifically on core HE23T4C4B from Horse Eye Transect 4. These methods identified the mineralogical composition and chronological context of key sedimentary units within core HE23T4C4B.

The integration of fieldwork observations and data with laboratory results enables the development of a stratigraphic framework for Horse Eye and North Eye, categorizing sediment into distinct units based on lithological, textural, and compositional

characteristics. These units, which are detailed in Chapter 4, and specifically Section 4.3.9 for stratigraphic units of core HE23T4C4B. Together, these methodologies form the basis for understanding the depositional history and paleoenvironmental evolution of the Pevensey Levels.

Chapter 4: Results of Fieldwork and Laboratory Analyses (North Eye and Horse Eye)

4.1.0. Introduction

The following section presents the results of the fieldwork and laboratory analyses conducted on North Eye and Horse Eye. The aim is to develop a comprehensive stratigraphic framework and paleoenvironmental analysis for the islands or isolated elevated areas called Horse Eye and North Eye within the Pevensey Levels, addressing the objective of understanding the sedimentary sequences and their depositional environments. The results are organized by site and methods and are followed by a data integration section where results and interpretation from both islands are compared to each other as well as with data from relevant publications.

4.2.0. North Eye

Situated in the southeastern portion of the Pevensey Levels, North Eye offers a baseline for understanding the stratigraphy of the southern part of the Levels, complementing the northernmost site, Horse Eye. Fieldwork at North Eye focused on identifying key transitions between marine and terrestrial depositional environments. These deposits offer valuable information about the changes in depositional conditions and processes over time, contributing to the broader objective of reconstructing the paleoenvironmental history of the Pevensey Levels. This section presents the stratigraphic results from North Eye, using observations from fieldwork and laboratory analyses to explore the depositional environments represented in the sequence. The results set a foundation for comparison with Horse Eye, highlighting regional variations in sedimentary processes and paleoenvironmental conditions.

4.2.1. Preliminary Fieldwork

Preliminary fieldwork was completed from May 23rd to May 25th, 2022, with the guidance of Dr. John Johnston and Dr. Ben Pears. The six islands in the Pevensey Levels (labelled in Figure 1.5 in Section 1.3.0: Location of Study and Site Descriptions) were investigated in the field to identify which locations were the most feasible for analysis.

Attributes that were investigated in the field included access to each site, vegetation, natural versus disturbed ground cover, land ownership, and the physical characteristics of each island (i.e., elevation, shape, and slope). North Eye was the focus of the preliminary fieldwork in May 2022 because permission to conduct fieldwork was granted by the landowner, and previous stratigraphic work had been completed nearby (Champness, 2009).

During this initial fieldwork, a total of 11 boreholes were completed along a linear east-west transect on the western portion of the island (location of transect shown in Figure 4.1). This transect, spanning approximately 100 meters in distance with a gentle slope of approximately 2 meters in relief (0.02 slope), targeted a potential transition zone between preserved material reflecting oscillating marine and terrestrial paleoenvironments. Core samples were extracted using a 20 cm diameter, 100 cm long two-piece bayonet gouge auger. Sediment descriptions of each sample were recorded in detail, resulting in the identification of 14 primary facies (shown in Table 4.1). These descriptions, alongside photographs, were documented in a field notebook and later compiled into a table (Table 4.1) for analysis. Spatial relationships of the boreholes are shown in Figure 4.2, while the initial facies descriptions are illustrated in Table 4.1.

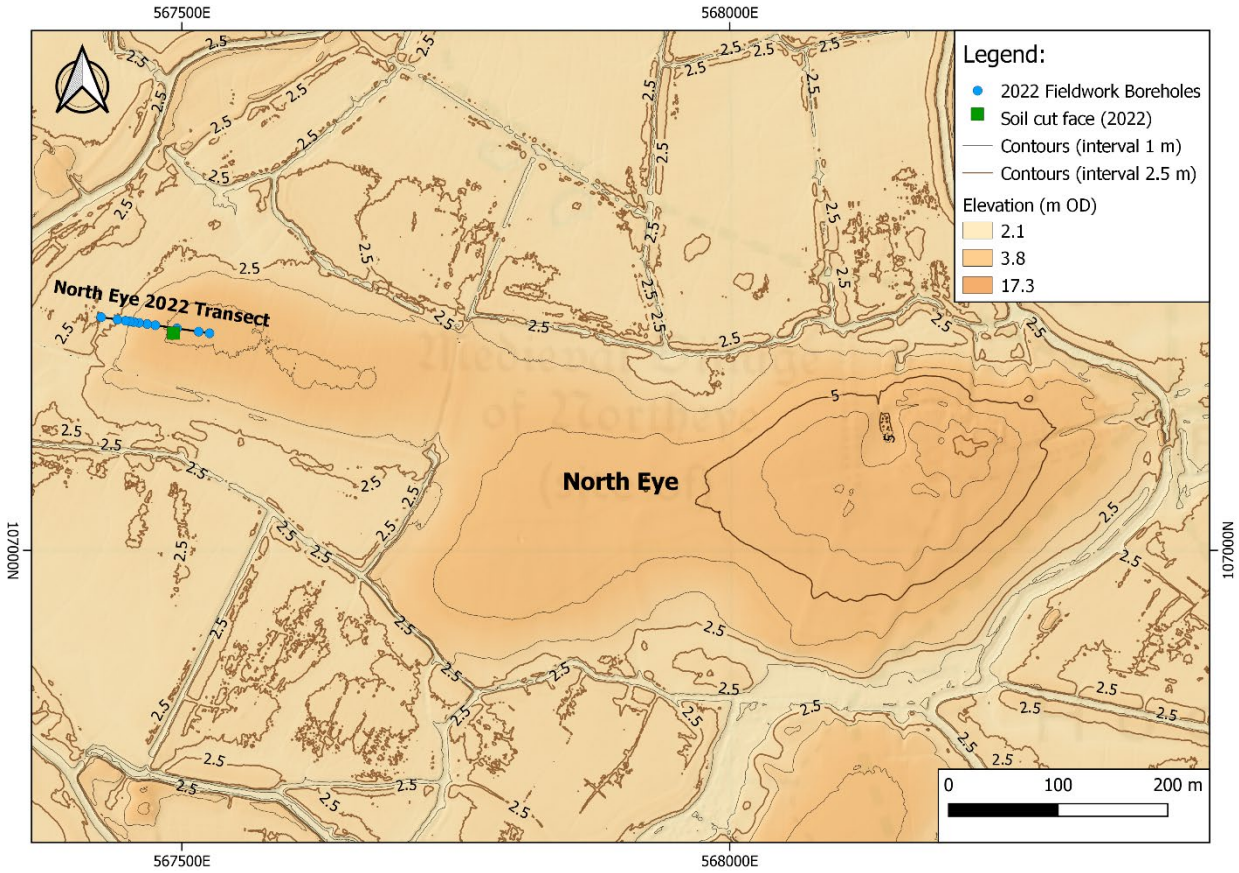


Figure 4.1 - A map of North Eye showing the transect of boreholes collected during the preliminary fieldwork in May 2022.

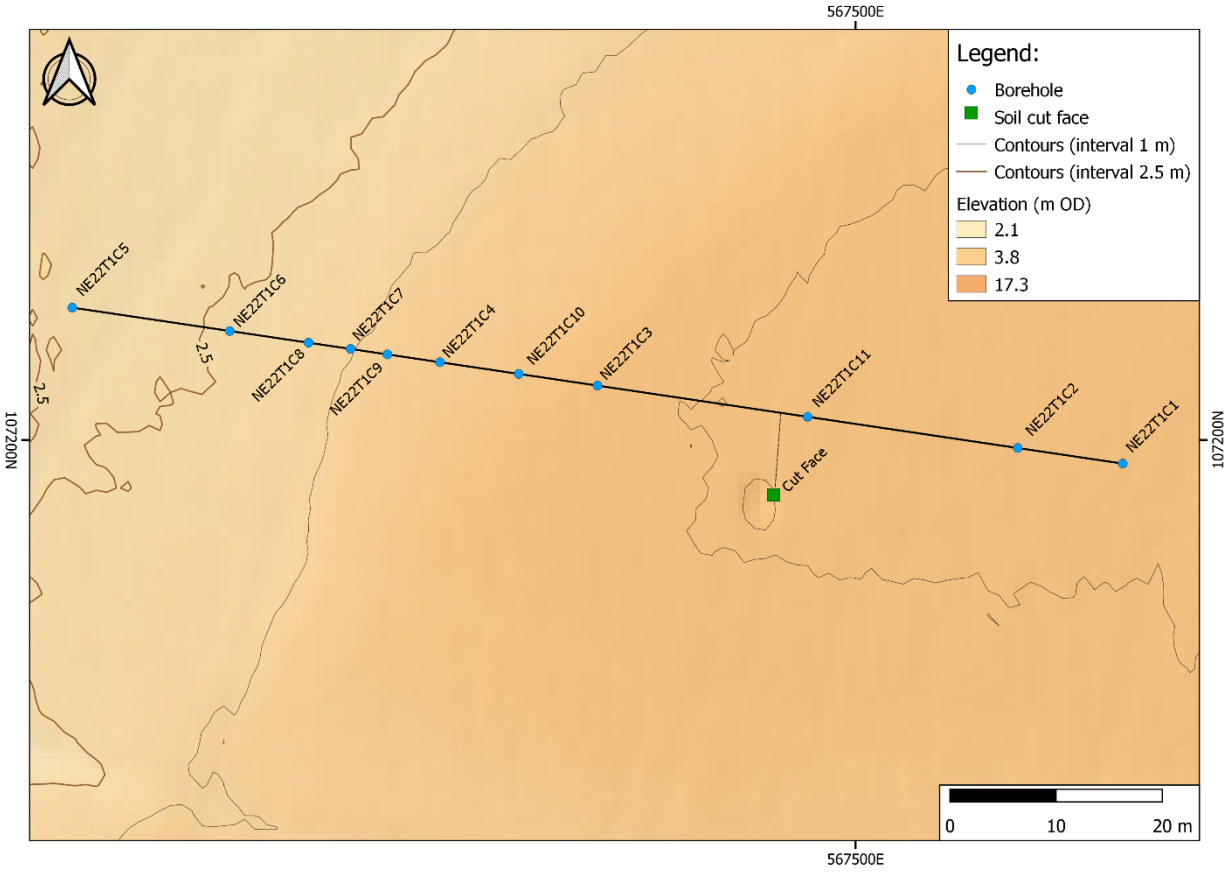


Figure 4.2 - A map displaying the borehole locations along the transect at North Eye, collected during preliminary fieldwork in May 2022 with a two-metre resolution LiDAR hill shade digital terrain model (DTM) (UK Ordinance Survey, 2020).

4.2.2. Facies Analysis and Stratigraphic Patterns

A facies analysis, primarily based on lithology and field descriptions, was conducted to help summarize the sedimentary sequences identified at North Eye. The 14 facies were categorized by texture (sand, silt, clay) and additional attributes such as sedimentary structures, organic material, and iron pan formations. These facies range from clay-dominated units to sand and silty-clay mixtures, providing evidence of the variability in depositional conditions at the transition between the island and the Pevensey Levels. While sands were relatively less common and thinner compared to silts and clays, they were predominantly observed in distinct layers at higher elevations, particularly on the western summit of the island, as well as inter-laminated with finer sediment. Clays, by contrast, were generally found at lower elevations along the edge of the island, where they exhibited greater thicknesses. These facies were categorized based on predominant lithology and sedimentary attributes, such as roots, mottling, and sedimentary structures following Farrell et al. (2012) and are presented in Table 4.1. This classification revealed variability within the depositional sequence, with sand appearing in an isolated unit (Unit 6), and fine-grained silts and clays dominating most of the transect (such as Units 8- Clayey silt, and 13- Sandy silt with clay lenticular laminations). Notably, the spatial patterns reflect a trend of coarser sediments at higher elevations and finer-grained sediments at lower elevations.

Table 4.1 - Description of the 14 primary facies/units identified at North Eye during 2022 preliminary fieldwork. The table includes unit numbers, names, field descriptions, and corresponding facies codes based on Farrell et al. (2012).

Unit #	Name	Description	Facies Code After Farrell et al. (2012)
1	Topsoil (Sandy silt)	Medium brown sandy silt, with roots.	sZ_{rt}
2	Subsoil (Clayey sandy silt)	Compacted orange mottled light grey-brown clayey sandy silt with roots.	$csZ_{rt\text{-}mot}$
3	Iron Pan 1	Brown / black iron pan, oxidized sandy clayey silt with sesquioxide concretions.	scZ
4	Sandy clayey silt	Orange mottled light grey-brown sandy clayey silt.	$scZ_{rt\text{-}mot}$
5	Transition Unit		
6	Sand	Clean, well sorted, light grey/white f. sand.	S
7	Iron Pan 2	Dark brown iron pan, oxidized, with orange mottled sand.	S_{mot}
8	Clayey silt	Light grey, orange mottled, clayey silt	$(z)C_{mot}$
9	Transition Unit 2		
10	Sandy clay with sand laminations	Inter-laminated clay with v.f. to f sand.	$C_{org}/s_{lam\text{-}mot}$
11	Silty clay 1	Dark grey-blue silty clay.	zC
12	Clayey silt with sand laminations	Inter-laminated clayey silt with v.f. sand.	$cZ/(s)_{lam}$
13	Sandy silt with clay lenticular laminations	Light grey sandy silt with clay lenticular laminations.	sZ/c_{l}
14	Silty Clay 2	Light grey silty clay with shells and shell fragments.	zC

To better visualize spatial relationships, the primary 14 facies were compiled into an initial cross section (Figure 4.3), which highlights lateral changes in lithology across the transect. This cross-section demonstrates key features, such as the localized sand unit (Unit 6) near the islands crest, and the continuous clay and silt layers extending along the flanks. To simplify this analysis, these 14 facies were simplified into five predominant units: sand, silt, clay, topsoil, and iron pans. These simplified units were then correlated across all borehole logs to form a geological cross-section Figure 4.4 that illustrates the 2-D stratigraphic framework and geometry across the island. These simplified units offer a clearer visualization of the dominant grain size and their distribution. In Figure 4.3, the colours used for the stratigraphic units are intentionally chosen to visually represent the dominant sediment type that was recorded in the field within each unit: a range of oranges is used for silt-dominant units, a range of blues for clay-dominant units, and yellows for sand and sand-dominant units. This consistent colour scheme aids in distinguishing sediment types across the stratigraphic profile.

The facies analysis further reveals that clays dominant units (such as Units 10 and 14) are typically found at lower elevations and are thickest along the edges of the island, reflecting prolonged deposition under low-energy conditions. Silts (e.g., Unit 4) occupy transition zones, particularly at mid-elevations, and often form the transition into the thicker clay units below.

Sand deposits (such as Unit 6) occur in localized areas near higher elevations, or within finer-grained units as laminations or lenticular laminations, suggesting episodes of higher-energy deposition or sediment transport. Lenticular laminations were observed in the core as small, isolated packets or lenses of silt or sand, approximately 1-3 mm in size, within a finer-grained matrix. These laminations are characterized by their discontinuous and lens-like geometry, consistent with lenticular bedding typically found in tidal or mixed-energy depositional environments. This arrangement suggests alternating periods of higher-energy conditions, capable of transporting and depositing coarser material, followed by lower-energy conditions favouring the accumulation of finer sediment. This

analysis highlights a vertical and lateral progression from coarser sands, at a higher elevation and on the island, to silts and clays, at lower elevations and on the flanks of the island, driven by decreasing depositional energy conditions and elevation.

These observations provide a foundation for understanding the sedimentary processes that shaped deposition of sediment on North Eye, emphasizing the role of elevation and depositional energy in controlling sediment distribution. The patterns observed here are important for drawing comparisons with Horse Eye (Section 4.3.0) and interpreting the broader paleoenvironmental history of the Pevensey Levels.

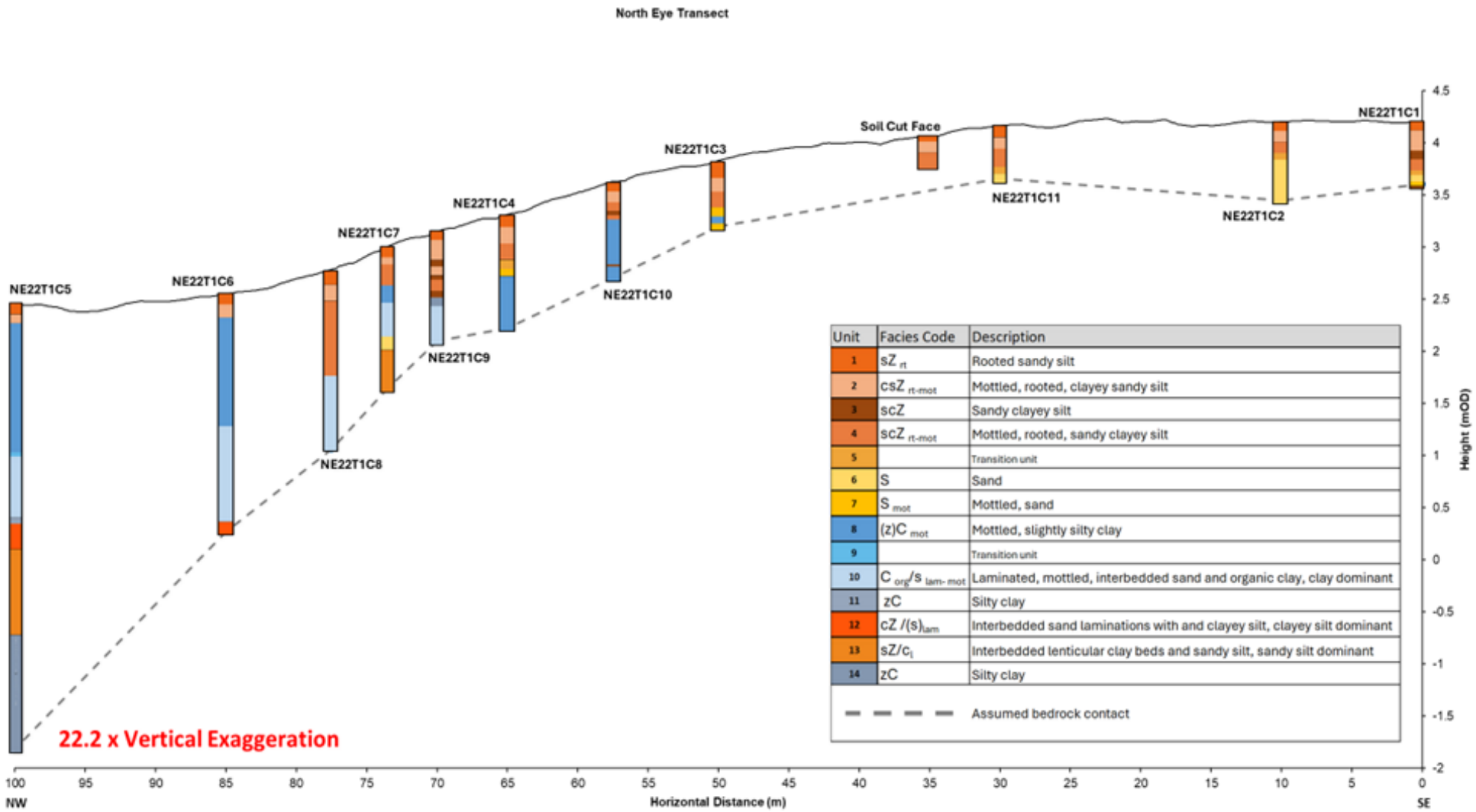


Figure 4.3 - A cross-section detailing the 14 units assigned to each borehole collected along the North Eye transect, demonstrating the spatial distribution of lithologies.

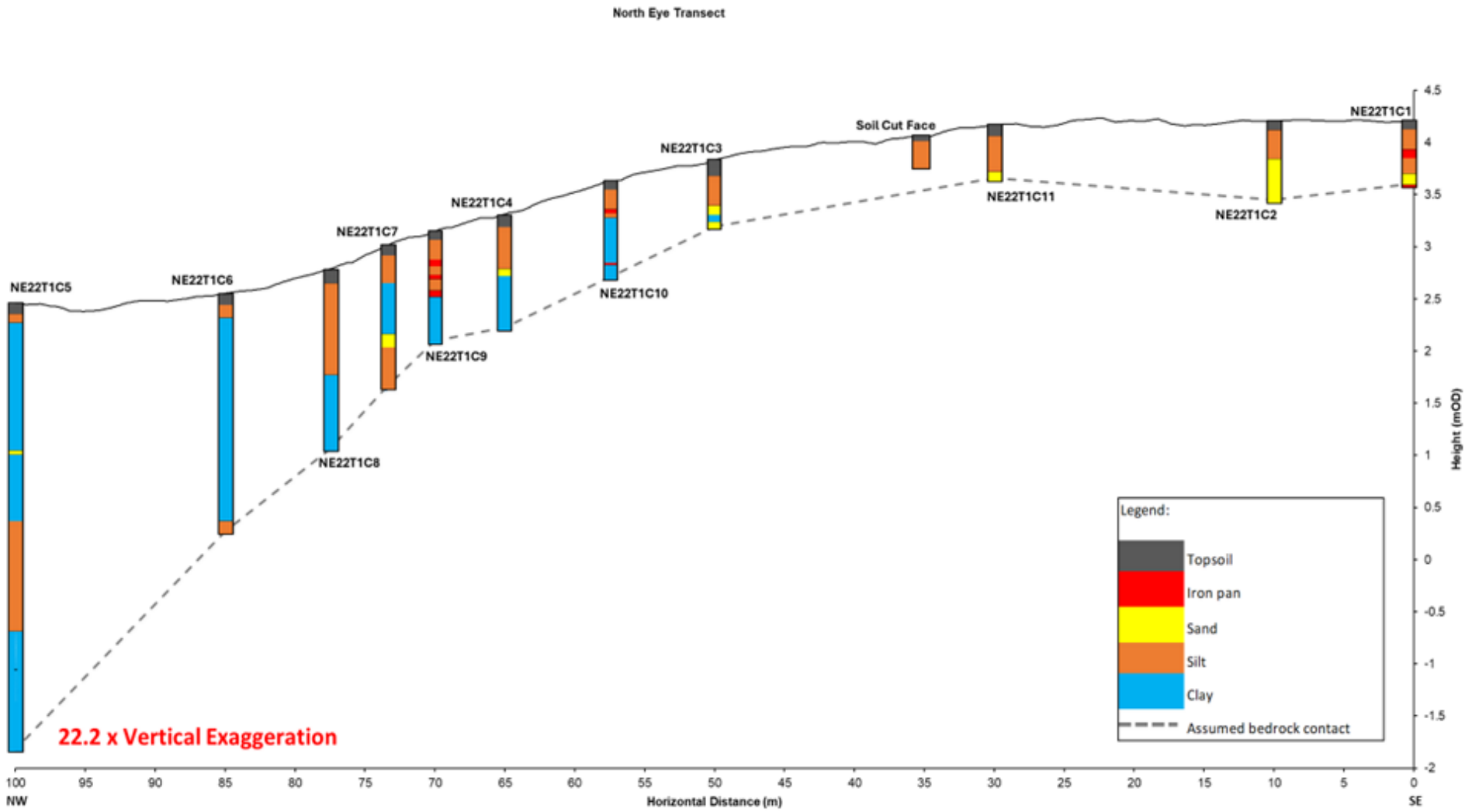


Figure 4.4 - A cross-section illustrating the simplified lithological units (sand, silt, clay, topsoil, iron pan) identified in the boreholes along the North Eye transect.

During preliminary fieldwork, several significant observations were made, which provide insights into the stratigraphy and depositional history of North Eye. One key finding includes shell fragments from within the sediment layers, roughly 315 – 380 cm deep in core NE22T1C5 (Figure 4.5B). Due to local context, these shells are indicative of a marine paleoenvironment, suggesting this core's location was once subject to rising water levels from the nearby ocean into Pevensey Levels (an ancient, embayed area along the coastline). Additionally, the discovery of well-preserved plant material (macro and fibrous), found in Unit 10 in NE22T1C5, most notably, macro plant material found 165 cm deep (Figure 4.5A). The plant material, consisting of intact-macro and fibrous structures, likely represent vegetation that grew in-situ (macro) or was deposited in a low-energy depositional environment (fibrous). Its presence is indicative of periods of terrestrial environmental conditions when water levels were sufficiently low to expose land, allowing for vegetation growth.

The general trend of shells and then plant material up the core indicates a lagoonal system exhibiting a potential paleoenvironmental shift from predominantly marine to predominantly terrestrial conditions. Although these findings suggest one relatively long-term shift in paleoenvironments, multiple smaller variations in the core suggest dynamic conditions at North Eye and in Pevensey Levels with many phases of terrestrial and marine influence.

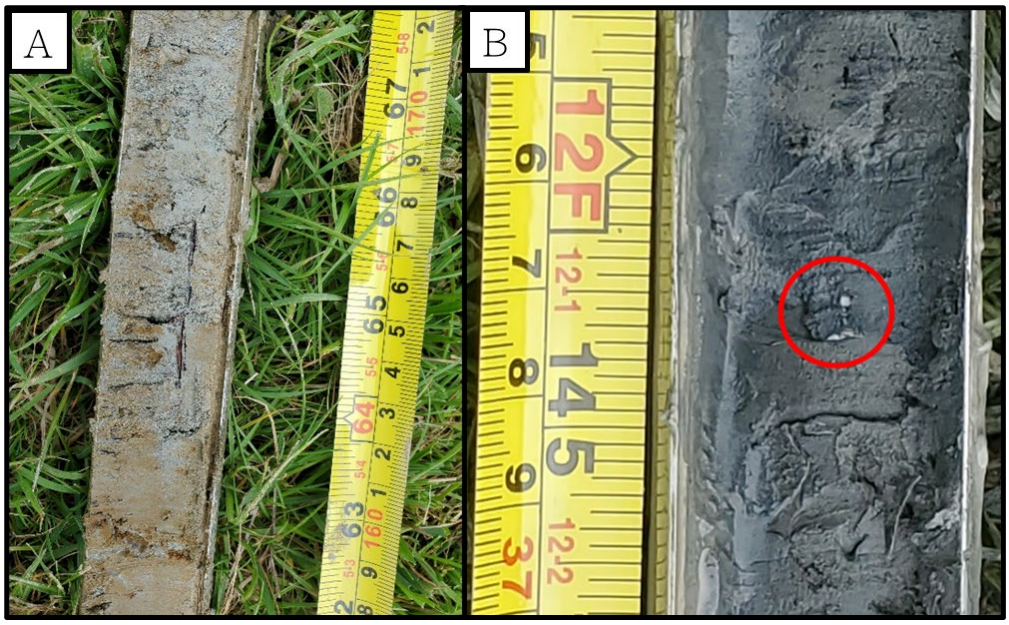


Figure 4.5 - (A) A photograph of plant material that was collected in borehole NE22T1C5 (depth: 163-167 cm). (B) A photograph of a shell fragment found in the same core (depth: 367 cm), indicating a predominantly marine depositional environment.

4.2.3. Laser Diffraction Grain Size Analysis

Laser Diffraction (LDM) Grain Size Analysis was conducted on six samples collected from four cores (NE22T1C2, NE22T1C3, NE22T1C5, NE22T1C6) at varying depth ranges (shown in Table 4.1) to characterize sediment properties and grain size distribution. The samples were intentionally selected from specific depths and units to represent a range of depositional environments identified during fieldwork. Unit 6, a shallow unit in NE22T1C2 was sampled to evaluate coarse-grained materials, while deeper units (Units 10, 12, 13, and 14 in NE22T1C5 and NE22T1C6) were selected to examine finer-grained sediment at greater depths. Their approximate locations in relation to the cores are illustrated in Figure 4.6 below, with LDM sample depths indicated by the red arrows in the simplified cross-section.

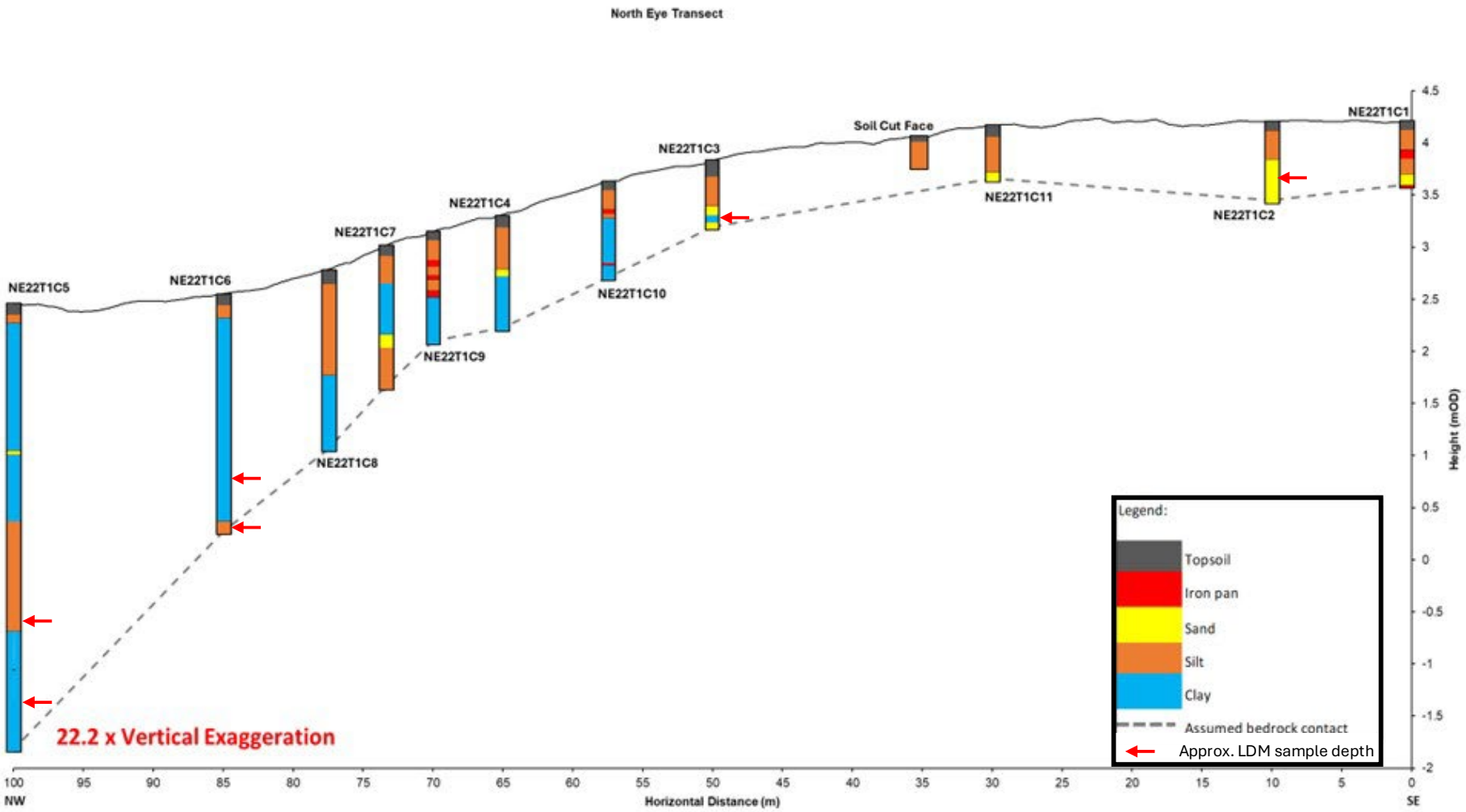


Figure 4.6 - A cross-section illustrating the simplified lithological units (sand, silt, clay, topsoil, iron pan) identified in the boreholes along the North Eye transect, displaying the approximate location of samples which were used for LDM grain size analysis.

The details of the sampled units (from Table 4.1), corresponding core, and depth ranges are presented in Table 4.2 below. This analysis aimed to characterize the sediment properties and grain size distribution of each unit that was sampled, providing insights into the depositional environment and associated sedimentary processes at North Eye. By selecting units across different depths and cores, the samples represent both coarse-grained and fine-grained units, aiding in a broader understanding of the stratigraphic variability of the island.

Table 4.2 - Sample details for Laser Diffraction Grain Size Analysis, including the unit, core associated with the sample, and the depth range of the sample collected. Four cores (NE22T1C2, NE22T1C3, NE22T1C5, and NE22T1C6) were sampled.

Unit	Core	Depth (cm)
6	NE22T1C2	36 – 39
8	NE22T1C3	49 – 55
10	NE22T1C6	160 – 170
12	NE22T1C6	218 – 229
13	NE22T1C5	245 – 250
14	NE22T1C5	249 – 320

The results of the Laser Diffraction Grain Size Analysis (LDM) are presented in Figure 4.7, which illustrates the grain size distribution as a bar plot for each sampled unit from North Eye, providing the percentages of sand, silt, and clay within each unit. This data spans multiple cores (NE22T1C2, NE22T1C3, NE22T1C5, and NE22T1C6) and reflect a general trend of increasing depth across the sampled units (Units 6, 8, 10, 12, 13, and 14), though not all units are represented in each core. These samples, collected from four cores, represent sedimentary deposits from different depths and elevations across the transect that was conducted on North Eye, capturing variations in depositional environments on and on the flanks of the island.

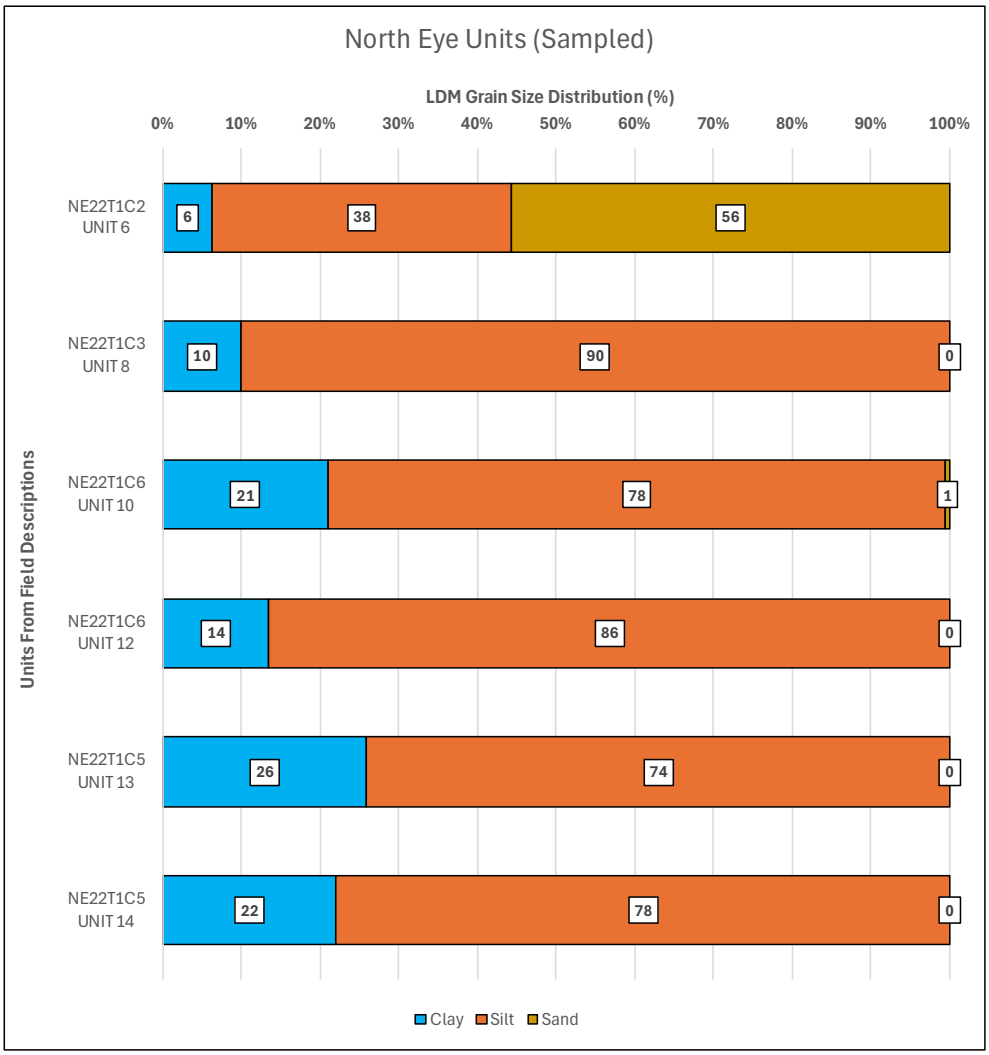


Figure 4.7 - Grain size distribution (%) for units sampled from North Eye, showing the relative proportions of clay, silt, and sand as determined by Laser Diffraction Grain Size Analysis (LDM). Note that the samples are from different cores and depths, as detailed in Table 4.2, and should not be interpreted as representing a continuous vertical sequence.

The grain size analysis of the sampled units at North Eye reveals a pattern of coarser grain sizes being concentrated at higher elevations within shallow samples, while finer grain sizes (silt and clay) dominate deeper samples, at lower elevations, deposited by lower-energy depositional settings. Unit 6, sampled from 36-39 cm depth in core NE22T1C2. Exhibits the highest proportion of sand (56%) among all sampled units. This relatively shallow sample was collected from the highest elevation on the island (approximately 4 meters OD). The higher sand content suggests relatively higher depositional energy conditions where finer particles like clay and silt were less likely to settle in such conditions. In contrast, the deeper units (Unit 8 sampled from NE22T1C3, Units 10 and 12 from NE22T1C6, and Units 13 and 14 from NE22T1C5), show a predominance of silt (74-90%) and lesser amounts of clay (10-26%), with minimal sand (1%

in Unit 10). These patterns suggest that deeper, finer-grained units were deposited under lower-energy depositional conditions.

When comparing the grain size distributions across the sampled units, two main groups emerge: Unit 6, a shallower unit with its distinct sand dominance, stands out as a coarser grained deposit likely reflecting higher-energy depositional conditions. In contrast, the deeper units (8, 10, 12, 13, and 14), which are predominantly silt and clay, represent finer-grained sediment which are typically associated with lower-energy depositional conditions. This contrast suggests a stratigraphic transition from a low-energy depositional conditions in deeper portions of the stratigraphy, to a higher-energy depositional setting, possibly influenced by proximity to the islands crest, or sediment source. These observations highlight both vertical changes in grain size and imply spatial differences in depositional processes.

The grain size results at North Eye highlight a clear distinction between shallower, sand-dominated sediments and deeper, finer-grained silt and clay units. These findings reflect a vertical and spatial variation in sediment composition, with coarser material concentrated at higher elevations and finer grains dominating at depth. This distribution provides a foundation for understanding the sedimentary processes that shaped North Eye, setting the stage for further interpretation of depositional environments and comparisons with Horse Eye.

4.3.0. Horse Eye

Located near the Herstmonceux Castle, Horse Eye offers a unique perspective on the depositional history of the northern portion of the Levels, contrasting with the previously studied southern island, North Eye. Through a combination of field observations and laboratory analyses, this section describes the geomorphology, stratigraphy, and sedimentology of Horse Eye, highlighting the transitions between marine and terrestrial environments that have shaped its development.

4.3.1. Site Description

The island of Horse Eye, located in the northern portion of the Pevensey Levels, is an elongated bedrock "island" extending predominantly in an east-west trend, it is shown below in Figure 4.8. Horse Eye is characterized by a relatively narrow width (approximately 300 m) and considerable length (approximately 1000 m). Two relatively short sections, measuring about 80 and 150 meters, jut out along the northern side, adding to the island's irregular shape. The highest elevation on Horse Eye reaches approximately 9.4 meters above Ordnance Datum (OD) in the west-central part of the island, which is significantly higher than the surrounding Pevensey Levels, where the elevation is approximately near 0 meters OD. Ordinance Datum is a vertical datum and is the UK's national levelling reference at the Newlyn Tidal Observatory, Cornwall (Jones, 2002).

The relief of the island varies, with the steepest slopes generally located on the western portion, particularly on the southern side. From the high point in the west-central area, the elevation gradually decreases towards the edges of the island, where the island connects to the Pevensey Levels, where the elevation is around one meter OD.

The topography of Horse Eye is characterized by a subtle, rounded elevation profile extending east-west. The highest point is in the western central portion of the island, and from this area, the elevation gently decreases towards the island's edges. The western-central portion of the island features a steeper slope, particularly on the southern side, as indicated by the contour lines in Figure 4.8. This area, near Transect 1 marks one of the more pronounced declines in elevation as the island slopes towards the southern

boundary of the island. In contrast, the northern extensions, where Transect 3 is located, exhibits a more gradual decline in elevation.

Overall, while the elevation differences on Horse Eye are subtle, the variation in slope across different parts of the island plays an important role in shaping its geomorphological features, including aspects such as water drainage and sediment deposition.

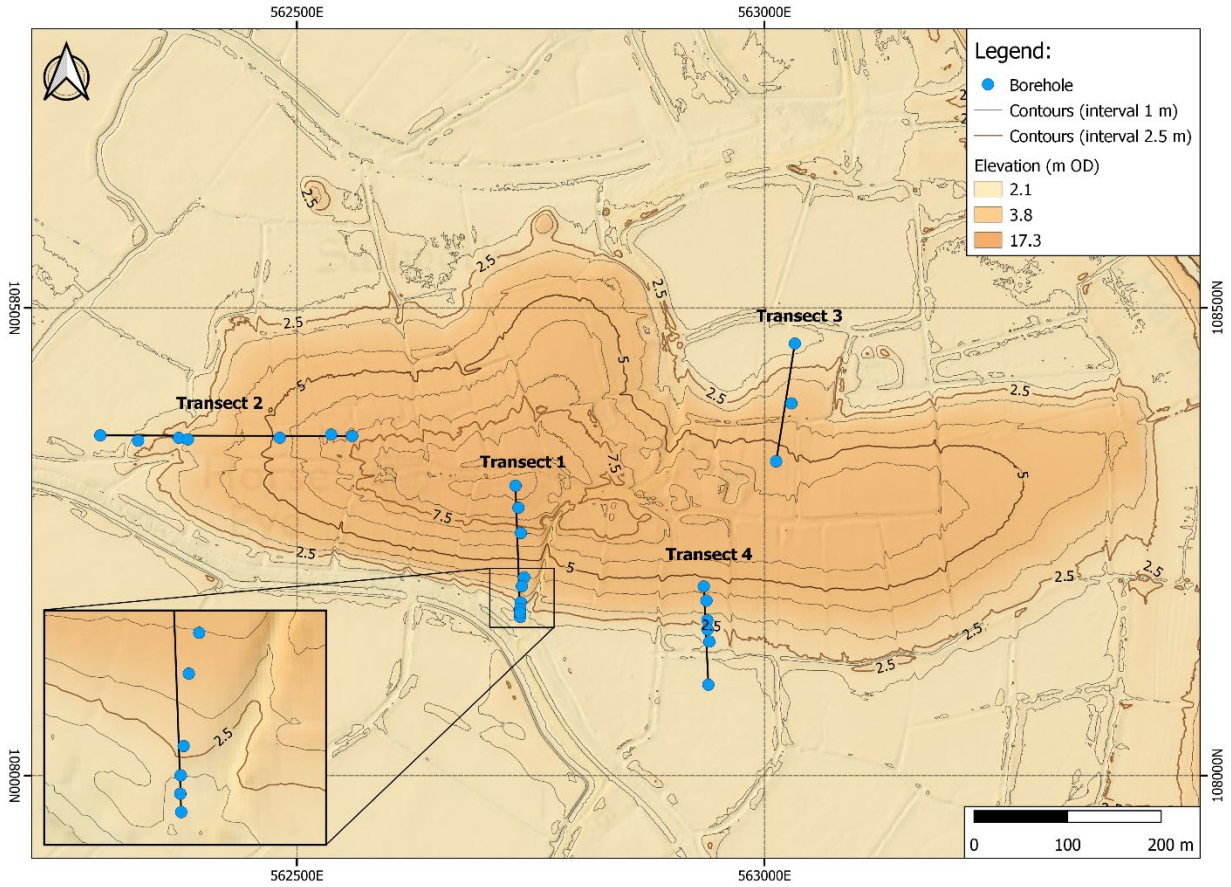


Figure 4.8 - Map of Horse Eye showing transect locations of boreholes collected during fieldwork in May 2023. The map includes a two-meter resolution LiDAR hill shade digital terrain model (DTM) (UK Ordinance Survey, 2020).

Horse Eye was the focus of fieldwork during May 2023 for this study and was chosen for several reasons. As one of the most northerly islands within the Pevensey Levels, Horse Eye provided a unique opportunity to gather stratigraphic information for the northern

portion of the Levels. Unlike the southern islands, Horse Eye had not been the subject of any published or unpublished research, despite its position in the Levels.

Pre-existing field research at North Eye (Champness, 2009) had already established a baseline for the stratigraphy of the southern portion of the Pevensey Levels. By studying Horse Eye, it became possible to interpret and compare the stratigraphy of both the northern and southern parts of the Levels. This comparison could help create a comprehensive stratigraphic framework applicable to the other bedrock islands within the Pevensey Levels.

Additionally, Horse Eye is also the largest island in the Levels and is closest in proximity to Bader College (Queen's University) on the Herstmonceux Castle Estate, which served as the accommodation location during fieldwork, further facilitating easier access. Lastly, Horse Eye lacks a scheduled area, unlike North Eye, meaning consent from the Secretary of State or submitting applications for Scheduled Monument Consent are not needed.

4.3.1.1. Field Work Methodology

Fieldwork on Horse Eye was conducted from May 9th to May 26th, 2023, with support from several team members. Field assistant Kira Bourque provided support during the initial phase of fieldwork between May 9th and May 12th. Field assistant Anna Cassell continued assistance comprising support in sediment coring and note-taking during fieldwork from May 16th to May 26th. Dr. John Johnston and Dr. Ben Pears offered guidance and support during fieldwork between May 23rd and May 26th, their collective efforts were instrumental in the successful completion of fieldwork.

During fieldwork on Horse Eye, four transects were completed to capture the stratigraphic transition from the island to the surrounding Pevensey Levels. These transects were strategically positioned to cover the different parts of the island (i.e., north, south, and west) and oriented perpendicular to the slope. The boreholes along these transects were collected using two types of two-piece bayonet gouge augers: one with a 20 cm diameter and 50 cm length, and another with a 20 cm diameter and 100 cm length.

The four transects cover most sides of Horse Eye, with the exception of the eastern side, where access limitations prevented data collection. The transects were primarily distributed across the southern, western, and northern parts of the island. Two of the transects (Transect 1 and Transect 4) were positioned on the southern side of the island, which is oriented towards the modern-day coastline. The southern side's significance is increased by its exposure to coastal influences, which may have influenced sediment deposition.

4.3.1.2. The Transects

The table below (Table 4.3) summarizes the key details of each transect, including the number of boreholes completed, the number of samples taken, the elevation difference along the slope, and the distance and orientation of each transect.

Table 4.3 - Summary table of transects completed on Horse Eye during fieldwork in May 2023, including the number of boreholes completed and samples collected, the elevation difference, length, and orientation of each transect.

Transect #	Number of Boreholes	Number of Samples	Elevation Difference (m)	Transect Distance (m)	Orientation (Start to Finish)
Transect 1	9	48	7.7	140.3	180˚
Transect 2	7	36	5.6	269.3	272˚
Transect 3	3	15	3.9	127.8	11˚
Transect 4	6	54	2.9	105.1	179˚

The four transects completed during fieldwork were strategically positioned to capture the stratigraphic transition from on the island of Horse eye to the Pevensey Levels. Transect 3, located on the northern side, and Transect 2, situated on the western edge, provided valuable insights into the stratigraphy of these areas, with Transect 2 being the longest and covering the relatively gentle slopes on the western side. In contrast, Transects 1 and 4 were placed on the southern side of the island, which is oriented towards the ancient coastline of the Pevensey Levels embayment.

The transects revealed a range of elevation differences and orientations, capturing the diversity of stratigraphic transitions across the island. While Transects 1 and 4 provided insights into the southern slope's transitions, Transect 2 captured the gradual decline from the island's central high point to the western perimeter, and Transect 3 offered a perspective on the gentler slopes of the northern side.

Transect 1 is located on the southern side of Horse Eye (Figure 4.9A) and extends north-south with an orientation of 180˚. It starts near the center of the island and extends southwards toward the southern perimeter of the island. It measures 140.3 meters in length and includes nine boreholes, from which 48 sediment samples were collected. The elevation difference along this transect is approximately 7.7 meters, which is the largest of all transects. Transect 1 was critical in investigating the sediment distribution from the top to the bottom of the island. This transect captures the stratigraphic transition from the southern portion of the island into the Pevensey Levels.

Transect 2 is positioned on the western side of the island (Figure 4.9B), extending in an east-west direction with an orientation of 272˚. This transect is 269.3 meters long and consists of seven boreholes, yielding 36 sediment samples. It traverses from the central more elevated portion of the island towards the western perimeter of the island with an elevation difference along the transect of 5.6 meters. This transect captures the stratigraphic transition from the western portion of the island onto the Pevensey Levels.

Transect 3 is centrally located on the northern side of Horse Eye, extending in a north-south direction with an orientation of 11˚ (Figure 4.9C). It measures 127.8 meters in length, has an elevation difference of approximately 3.9 meters, and includes three boreholes, from which 15 sediment samples were collected. This transect starts from the central elevated portion of the island and extends northwards towards the northern perimeter of the island. This transect covers the transition from the northern portion of the island onto the Levels.

Transect 4 is centrally located on the southern side of Horse Eye (Figure 4.9D) approximately 200 meters to the east of Transect 1. It extends in a north-south direction in an orientation of 179˚. This transect is 105.1 meters long, has an elevation difference of 2.9 meters, and consists of 6 boreholes. Transect 4, despite being the shortest and having the smallest elevation difference, yielded the highest number of samples (n=54), which were pivotal for detailed laboratory analyses due to the significant findings along this transect. The strategic placement of these transects, particularly the focus on the southern side, allowed for a comprehensive understanding of the island's geomorphology, with Transect 4 emerging as a key area for further study due to its distinct sedimentary characteristics. It captures the stratigraphic transition from the southern portion of the island onto the levels. Due to significant findings along Transect 4, specifically at borehole HE23T4C4B, more detailed analyses were conducted on this transect. The comprehensive study of borehole HE23T4C4B is covered in the next section, where various laboratory analyses are discussed.

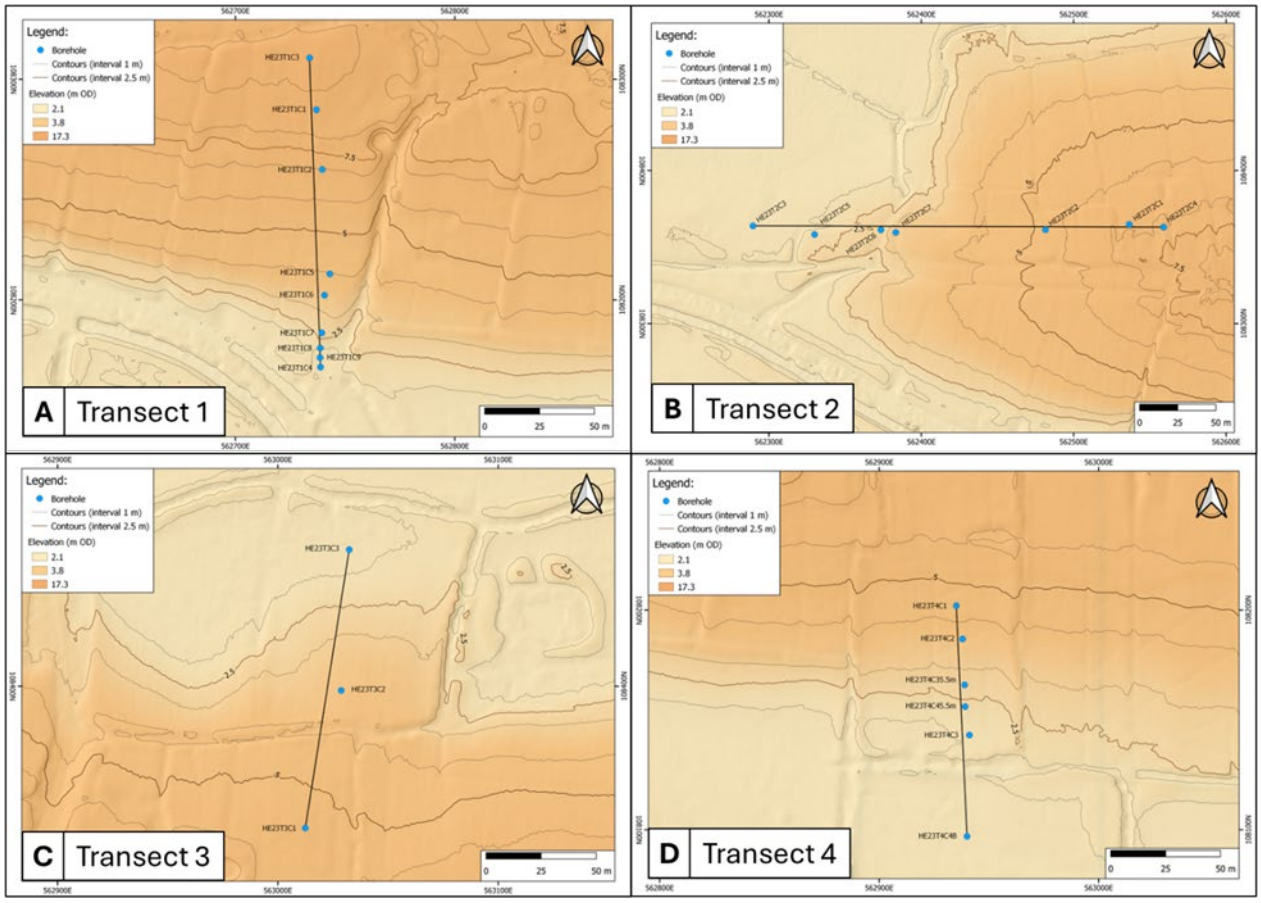


Figure 4.9 - Boreholes collected along four transects on Horse Eye during fieldwork in May 2023. (A) Transect 1, running north-south on the southern side of the island; (B) Transect 2, running east-west on the western portion; (C) Transect 3, running north-south in the central part of the island on the northern side; and (D) Transect 4, running north-south in the central part of the island on the southern side. Elevation is indicated in meters above Ordnance Datum (OD) with contour intervals of 1 and 2.5 meters. The maps include a two-meter resolution LiDAR hill shade digital terrain model (DTM) (UK Ordinance Survey, 2020).

4.3.2. Stratigraphy of Each Transect

The stratigraphic data, based on field observations from the four transects on Horse Eye, reveal similarities and differences in unit facies, thicknesses, lateral extent, and elevation. These patterns provide valuable insights into the stratigraphy of the island and the transition from the island to the surrounding Pevensey Levels. Across all transects, massive silty clay is the dominant facies, often accompanied by varying degrees of compaction, orange mottling, and organic material. These layers were consistently observed throughout all four transects, indicating that a significant portion of Horse Eye's

stratigraphy is composed of fine-grained silty clay with occasional orange mottling and organic material.

In Transect 1 (HE23T1), located on the southern side of the island, the stratigraphy on the island displays a gradual transition from an organic-rich topsoil to a more compacted, orange-mottled silty clay at greater depths. The upper layers generally consist of dark brown silty clay with high organic content and a high amount of roots, typically extending from 0 to 15 cm below the ground surface. This is followed by a more compact silty clay layer with orange mottling, generally found between 15 and 35 cm below the ground surface. The thickness of the silty clay layers varies along the transect, ranging from 20 to 35 cm in the more compacted sections. Lithological variations within these silty clay layers include differences in root content, organic material, and the degree of orange mottling, which is more prominent at greater depths. The stratigraphy also shows a lateral transition, with the southern boreholes (closer to the edge of the island) exhibiting a more pronounced presence of shell fragments at approximately 40 cm below the ground surface in HE23T1C4. This suggests a transition towards more marine-influenced sediment as the transect approaches the lower elevations at the edge of the island, where the island connects to the Pevensey Levels.

Transect 2 (HE23T2), located on the western side of the island, exhibits a more uniform stratigraphy with less variation compared to the other transects. The stratigraphy typically begins with a loose greyish-brown silty clay layer containing an abundance of roots, extending from 0 to about 9.5 cm below the ground surface. This is followed by a more compact silty clay layer with slight orange mottling, observed between approximately 9.5 and 16 cm. Below 16 cm, the stratigraphy generally consists of increasingly compact silty clay with less organic content and occasional small (~1 mm) manganese nodules. The orange mottling persists, though it becomes less prominent at greater depths. The thickness of the silty clay layers ranges from 9.5 to 16 cm, with minor variations in compaction and organic content. The uniformity in lithology across the transect suggests a stable depositional environment with minimal lateral variation in sediment composition. The shallower depth of the boreholes in this transect (compared to the other transects)

likely prevented the observation of deeper marine clays or significant transitions in lithology. The elevation of Transect 2 is relatively higher and more central on the island, which may explain the lack of marine clay influence and the absence of shell fragments.

Transect 3 (HE23T3), located on the northern side of the island, displayed a more variable stratigraphy with distinct changes in lithology and thickness along the transect. The uppermost layer, found typically between 0 and 8 cm below ground surface, consists of dark greyish-brown well-sorted silty clay and contained a significant amount of roots. As the transect moves northward towards the lower elevations near the edge of the island, the silty clay becomes more compacted and exhibits slight orange mottling (~3%) between 8 and 16.5 cm. At around 26.5 to 47 cm, the clay shows an increase in dark orange mottling (20-25%) and becomes highly plastic and dense, with manganese nodules noted at these depths. Below 47 cm, the stratigraphy generally consists of dense, compact silty clay with persistent orange mottling, extending to depths greater than 100 cm. The thickness of the silty clay layers varied considerably across the transect, ranging from 8 to 47 cm, with thicker layers found at lower elevations closer to the island's northern edge towards the Pevensey Levels. Lithological variations include the presence of manganese nodules, increased compaction, and changes in the degree of orange mottling. Shell fragments were observed at approximately 90 cm below ground surface in HE23T3C3, at the edge of the island and the Pevensey Levels. Thus, marking a transition towards more marine-influenced sediments as the transect approaches the northern edge of the island. Additionally, in borehole HE23T3C3, at approximately 100 cm, the presence of organic-rich black fibrous material similar to peat indicates a significant change in the depositional environment at the lower elevation at the edge of the island.

Transect 4 (HE23T4) exhibits the most complex stratigraphy among all transects, with significant variations in lithology, thickness, and lateral extent observed across the boreholes. The uppermost layers generally consists of dark greyish-brown silty clay, rich in organic material and roots, typically extending from 2 to 11 cm below ground surface. As the transect moves from the higher central parts of the island to the lower southern edge, a transition to greenish-grey silty clay with dark orange mottling (15%) is observed, typically

between 11 and 26 cm. Lenticular fine-grained sand laminations were noted within the silty clay layers, particularly between 26 and 50 cm, indicating periods of higher energy conditions that allowed for the deposition of sand within the predominantly silty clay matrix.

At greater depths, the stratigraphy exhibits more distinct facies changes, including the introduction of organic-rich peat layers and marine clay, and laminated fine sand. Two peat layers were identified: the first between 119 and 127 cm, characterized by black, fibrous material, and a large wood fragment (approximately 1 cm) at 124 – 125 cm, indicating an environment conducive to significant organic accumulation. The peat layer was underlain by a transition layer from peat into marine clay between 127 and 130.5 cm where peat mixed with marine clay, indicating a gradual shift from organic-rich conditions to more marine-dominated sedimentation. Following this transition, a layer of marine clay was observed, which included wood fragments and a small amount of sand.

A sharp boundary occurs at 165.5 cm, where the marine clay abruptly transitions into a grey silty clay with orange mottling, similar in composition to the upper silty clay observed above the first peat layer. This oxidized silty clay occurs from 165.5 to 173 cm and suggests a return to subaerial depositional conditions. Below this unit, there is a second peat layer between 173 to 180 cm. This layer is characterized by a very dry, fine fibrous texture, with no wood fragments, suggesting a period of significant organic accumulation in a low-energy environment.

Further below the second peat layer, the stratigraphy transitions back into marine clay, starting at approximately 180 cm and extending to 280 cm. Within this marine clay, there is approximately 1 to 2 mm fine sand laminations between 180 to 210 cm, indicating episodic higher energy conditions within the marine environment. Between 210 and 237 cm, the marine clay included shells, suggesting a marine environment with abundant biogenic material. From 237 to 280 cm, the marine clay becomes more uniform, lacking sand laminations or shells, but containing more manganese nodules, reflecting a more stable, lower-energy marine environment with reduced biogenic activity.

Given the detailed sequence of stratigraphic changes, including multiple transitions between terrestrial and marine environments, the presence of varied lithologies such as peat, marine clay with sand laminations or shell fragments, Transect 4 stands out as the most stratigraphically diverse section of the island. These characteristics necessitate a more detailed analysis, which will be discussed further in Section 4.3.4. This analysis will examine the stratigraphic complexity, illustrating the environmental changes over time as the transect moves towards the lower elevations near the southern edge of the island.

4.3.3. Summary of Stratigraphy Across Transects

The stratigraphic data collected from the four transects on Horse Eye reveal several key trends and differences that highlight the varied depositional environments across the island. One of the most consistent findings is the widespread presence of an upper silty clay with orange mottling across all transects, indicating that this lithology is a dominant and extensive facies of the island's stratigraphy. However, each transect also exhibits unique characteristics in terms of elevation differences, layer thicknesses, lateral extent, and specific lithological features, reflecting localized variations in sedimentation.

When comparing the stratigraphy across the four transects, several trends and differences become apparent. Transect 1, which has the highest elevation difference, captures a broad transition from the higher central areas of the island toward its southern edge connecting to the Pevensey Levels where marine influences become more apparent with the presence of shell fragments at greater depths. Similarly, Transect 3, located on the northern side, also shows shell fragments deeper in the stratigraphy, again indicating marine influence as the transect moves toward lower elevations near the island's edge. In contrast, Transect 2, positioned toward the west on the western portion of the island, has the shallowest boreholes and shows a more uniform stratigraphy, with no evidence of shell fragments or transitions to marine clay, likely due to limited depth.

Transect 4, despite having the smallest elevation difference and being the shortest of the transects, stands out due to its greater depth and extension off the island, where it reveals the most varied and complex stratigraphic sequence. This transect uniquely

contains two distinct peat layers and transitions between peat and marine clay- a combination of features not observed in the other transects. The presence of black fibrous organic-rich material, similar to peat, is also noted in both Transect 3 and Transect 4, further highlighting the differences in depositional environments across the island.

Overall, the stratigraphy suggests that the upper silty clay is predominantly found on the more elevated portions of the island, while transitions to marine clay and the presence of organic-rich layers, such as peat, are more common in the lower elevated areas, particularly near the island's edges. Transect 1, with its significant elevation change, captures a transition from terrestrial to marine influences, whereas Transect 2, due to its shallow depth, remains within the more uniform silty clay layers without significant transitions. Transect 4 provides the most detailed and varied stratigraphic record due to its depth, lateral extent off the island, and the presence of multiple transitions between terrestrial and marine environments.

The table below (Table 4.4) summarizes the key lithological features observed in selected boreholes from each transect. These boreholes were chosen to highlight significant stratigraphic transitions, such as changes in sediment type, the presence of organic layers, and the occurrence of shell fragments or peat. The lithological summary captures essential stratigraphic characteristics, including the predominance of silty clay, variations in organic content and compaction, and the identification of peat and marine clay in specific boreholes. These observations provide a foundation for understanding Horse Eye's stratigraphy and offer insights into the island's paleoenvironmental history.

While this summary provides a concise view of the stratigraphy across the transects, it is important to note that Transect 4 exhibited particularly complex stratigraphy, warranting a more detailed analysis. This will be explored further in Section 4.3.4. The following table serves as a foundational reference for understanding the sedimentological framework of Horse Eye, offering insights into the depositional environments and conditions that shaped the island.

Table 4.4 - Lithological summary of Selected Boreholes Across Transects Conducted on Horse Eye.

Transect	Borehole	Depth Below Ground Surface (cm)	Lithology	Description	Thickness (cm)
T1	HE23T1C1	0 – 15	Silty Clay	Dark brown, high organic content, roots present	15
T1	HE23T1C1	15 – 35	Silty clay with mottling	Light grey, orange mottling, compact	20
T1	HE23T1C1	35 – 50	Silty clay with shells	Light grey, shell fragments, increasing compaction with depth	15
T1	HE23T1C2	0 – 11	Silty clay	Medium grey-brown, roots present, some orange mottling	11
T1	HE23T1C2	11 – 18	Silty clay	Light grey, orange mottling, not compacted	7
T1	HE23T1C3	3 – 8	Silty clay	Medium grey-brown, lots of roots, not compacted	5
T1	HE23T1C3	8 – 15	Silty clay with sand	Not very compacted, orange mottling, some sand	7
T1	HE23T1C3	15 – 25	Silty clay with iron nodules	Gradual upper contact, few small roots, compacted, iron nodules	10
T2	HE23T2C1	0 – 9.5	Silty clay	Greyish brown, medium plasticity, lots of roots, not very compacted	9.5
T2	HE23T2C1	9.5 – 16	Silty clay	Increase of silt, light grey-brown, small amount of roots present, orange mottling	6.5
T2	HE23T2C1	0 – 7.5	Silt	Light buff brown, very dry, loose, no clay, well sorted	7.5
T2	HE23T2C1	7.5 – 13	Silt with clay	Darker buff brown, slightly compact, low plasticity	5.5
T2	HE23T2C1	8.5 – 18.5	Silt	Very dry, crumbly, no plasticity, loose, well sorted	10
T3	HE23T3C1	0 – 8	Silty clay	Dark greyish brown, well sorted, lots of roots, loose	8
T3	HE23T3C1	8 – 16.5	Silty clay with mottling	Dark greyish brown, compact, orange mottling (~3%)	8.5
T3	HE23T3C1	26.5 – 47	Silty clay with mottling	Dark greyish brown, compact, orange mottling (20-25%), dense, shell fragments	20.5

T3	HE23T3C3	0 – 8	Silty clay	Dark greyish brown, well sorted, lots of roots, loose	8
T3	HE23T3C3	8 – 16.5	Silty clay with mottling	Dark greyish brown, more compact, orange mottling (~3%)	8.5
T3	HE23T3C3	26.5 – 47	Silty clay with mottling	Dark greyish brown, high plasticity, dense, orange mottling (20-25%), shell fragments	20.5
T3	HE23T3C3	90 – 100	Silty clay with organic material	Dark greyish brown, dense, with black fibrous organic-rich material similar to peat	10
T4	HE23T4C4B	2 – 11	Silty clay with organics	Dark greyish brown, high organic content, loose, crumbly	9
T4	HE23T4C4B	11 – 26	Silty clay with mottling	Greenish grey, dark orange mottling (10-15%), dense	15
T4	HE23T4C4B	26 – 50	Clay with lenticular sand laminations	Greenish grey, orange mottling, very dense, small amount of f. sand	24
T4	HE23T4C4B	50 – 78	Clay	Greenish grey, dark orange mottling (20-30%), very compacted	28
T4	HE23T4C4B	78 – 119	Clay with silt	Greenish grey, dark orange mottling (30%), dense, small amount of silt (~5%)	41
T4	HE23T4C4B	119 – 127	Peat	Black fibrous peat, large wood fragment, sharp upper boundary	8
T4	HE23T4C4B	127 – 130.5	Clay with organic material	Dark greyish brown, high plasticity, high amount of organic material	3.5
T4	HE23T4C4B	130.5 – 133.5	Transition zone	Very dark greyish brown, very sticky and wet, high plasticity	3
T4	HE23T4C4B	133.5 – 165.5	Marine clay	Dark greenish grey, sticky, wet, less dense than transition zone	32
T4	HE23T4C4B	165.5 - 173	Peat	Black, very dry, fine fibrous, no wood	7.5

4.3.4. Detailed Stratigraphy of Transect 4

Transect 4 exhibits the most complex stratigraphy among all transects, with significant variations observed in different boreholes. This warranted a detailed analysis to capture the variations in the stratigraphy. What distinguishes Transect 4 from the other transects is the introduction of additional facies and units and a sedimentary structure that was not observed in the other transects. Specifically, core HE23T4C4B revealed unique characteristics, such as the presence of mostly horizontal sand laminations within the upper portion of the lower marine clay, which had not been seen in previous transects. These sand laminations differ from the lenticular sand laminations observed in the upper silty clay layers of other transects, identified in the cores as isolated lenses of sand, approximately 1-2 mm thick within a predominantly silty clay matrix. Additionally, Transect 4 is characterized by its low elevation; borehole HE23T4C4B, in particular, is the lowest among all boreholes across the transects and was located furthest from the center of the island. This borehole also extends the deepest into the Levels, reaching deeper stratigraphy, which is useful for reconstructing Horse Eye's paleoenvironments.

To better understand and visualize the variations in stratigraphy, the following lithofacies codes were developed based on field observations recorded during fieldwork. The codes categorize different sediment textures and attributes, including sedimentary structures, roots, mottling, and organic material, following the methodology of Farrell et al. (2012). Table 4.5 displays the lithofacies codes and their respective descriptions that were developed based on field observations.

Table 4.5 - Lithofacies Codes and Descriptions Identified in Transect 4 based upon field descriptions following Farrell et al. (2012).

Lithofacies Code	Description
$cZ_{rt\text{-}mot}$	Rooted, mottled, clayey silt
$(s)cZ_{rt}$	Rooted, slightly sandy, clayey silt
$(s)cZ_{mot}$	Mottled, slightly sandy, clayey silt
$(g)cZ_{mot}$	Mottled, slightly gravelly clayey silt

cZ_{mot}	Mottled, clayey silt
$(s)Z_{rt}$	Rooted, slightly sandy silt
$(g)cZ_{rt\text{-}mot}$	Rooted, mottled, slightly gravelly clayey silt
$zC_{rt\text{-}mot}$	Rooted, mottled, silty clay
zC_{mot}	Mottled silty clay
zC_{rt}	Rooted silty clay
$(g)zC_{mot}$	Mottled, slightly gravelly silty clay
$(s)zC_{mot}$	Mottled, slightly sandy silty clay
$zC_{mot}/(s)_{lam}$	Mottled, silty clay interlaminated with slightly sandy laminations
C_{mot}	Mottled clay
(s)zC	Slightly sandy silty clay
C_{org}	Clay with plant debris
C / S_{lam}	Interlaminated clay and sand, clay dominant
C	Clay
$zC_{mot}/Z_{l\text{-}lam}$	Interlaminations of mottled, silty clay and lenticularly laminated silt
$(z)C_{(mot)}$	Slightly mottled, slightly silty clay
(z)C	Slightly silty clay
$zC_{(rt)\text{-}mot}$	Slightly rooted, mottled, silty clay
$(s)zC_{(rt)\text{-}mot}$	Slightly rooted, mottled, slightly sandy silty clay
$C_{rt\text{-}mot} / S_{l\text{-}lam}$	Interlaminations of rooted, mottled clay and lenticularly laminated sand
P	Peat
Minerogenic Pan	Minerogenic Pan

After establishing the lithofacies codes, they were grouped into broader categories based on their primary characteristics, which include both lithology and associated sedimentary structures. The table below (Table 4.6) summarizes these groupings into three

main categories: clay, silt, and sand, with a couple of other unique units, such as peat and minerogenic pans, included under a separate “Other” category.

Table 4.6 - Groupings of Lithofacies Codes (following Farrell et al. (2012)) Identified in Transect 4.

Clay Group	Silt Group	Sand Group	Other
zC $_{rt\text{-}mot}$	cZ $_{rt\text{-}mot}$	C / S $_{lam}$	P (Peat)
zC $_{mot}$	(s)cZ $_{rt}$	C $_{rt\text{-}mot}$ / S $_{l\text{-}lam}$	Minerogenic Pan
zC $_{rt}$	(s)cZ $_{mot}$		
(g)zC $_{mot}$	(g)cZ $_{mot}$		
(s)zC $_{mot}$	cZ $_{mot}$		
zC $_{mot}$/(s) $_{lam}$	(s)Z $_{rt}$		
C $_{mot}$	(g)cZ $_{rt\text{-}mot}$		
(s)zC			
C $_{org}$			
C / S $_{lam}$			
zC $_{mot}$ /Z $_{l\text{-}lam}$			
(z)C $_{(mot)}$			
(z)C			
zC $_{(rt)\text{-}mot}$			
(s)zC $_{(rt)\text{-}mot}$			
C $_{rt\text{-}mot}$ / S $_{l\text{-}lam}$			

Following the groupings, a detailed cross-section was developed to visually represent the stratigraphic variations across Transect 4. This cross-section (Figure 4.10) uses lithofacies codes introduced earlier in Table 4.5 to categorize the various lithologies and sedimentary structures observed in the boreholes.

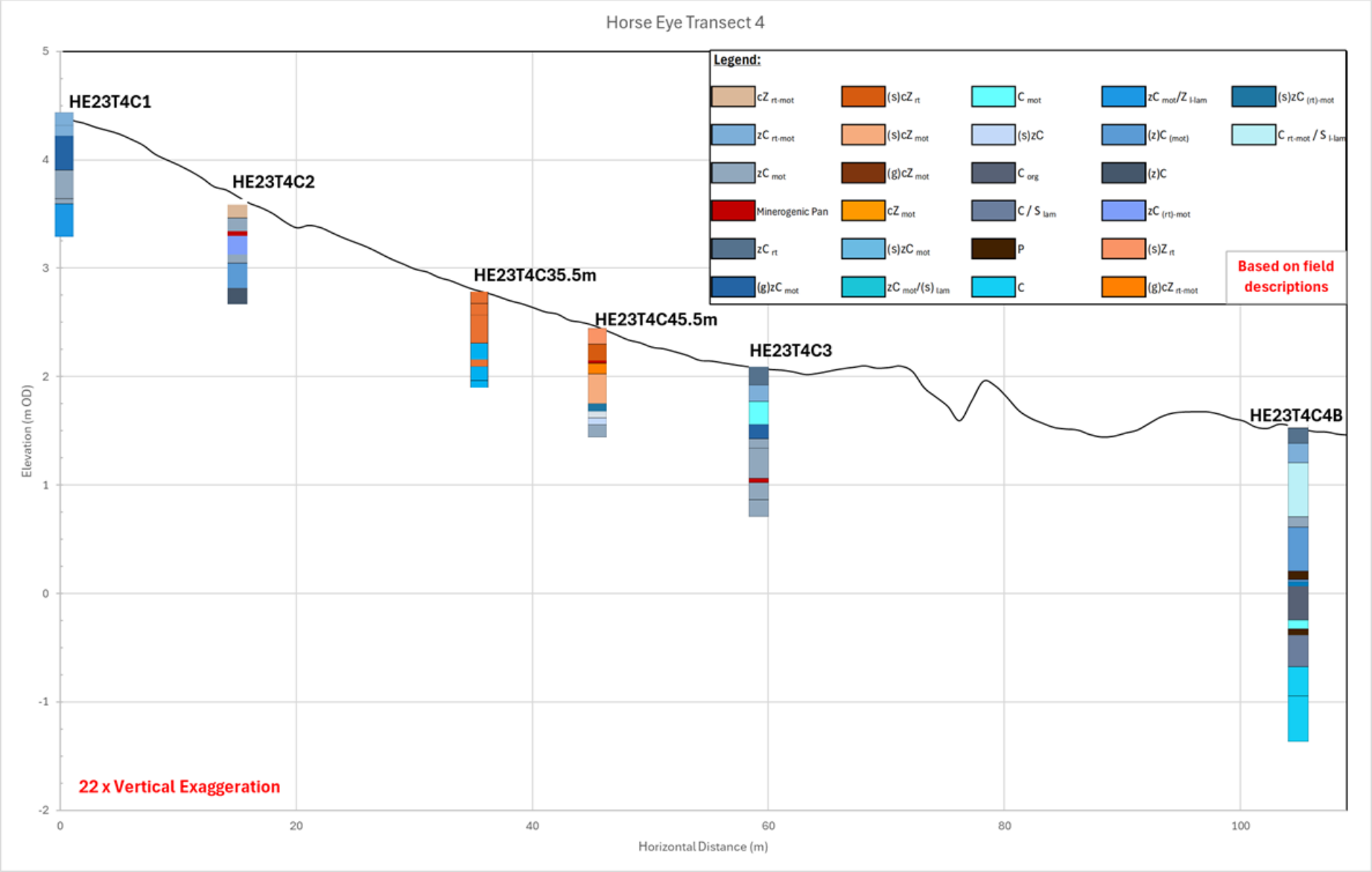


Figure 4.10 - A cross-section detailing the 26 lithofacies assigned to each borehole collected along the Transect 4 on Horse Eye, demonstrating the spatial facies distribution.

To further simplify and highlight the broader trends, a simplified cross-section (Figure 4.11) was created. This version distills the complex stratigraphy from field observations into five broader and more easily interpreted units: sand, silt, clay, peat, and minerogenic pans. The simplified cross-section provides a clear visualization of the general patterns in lithology, thickness, lateral extent, and elevation across Transect 4.

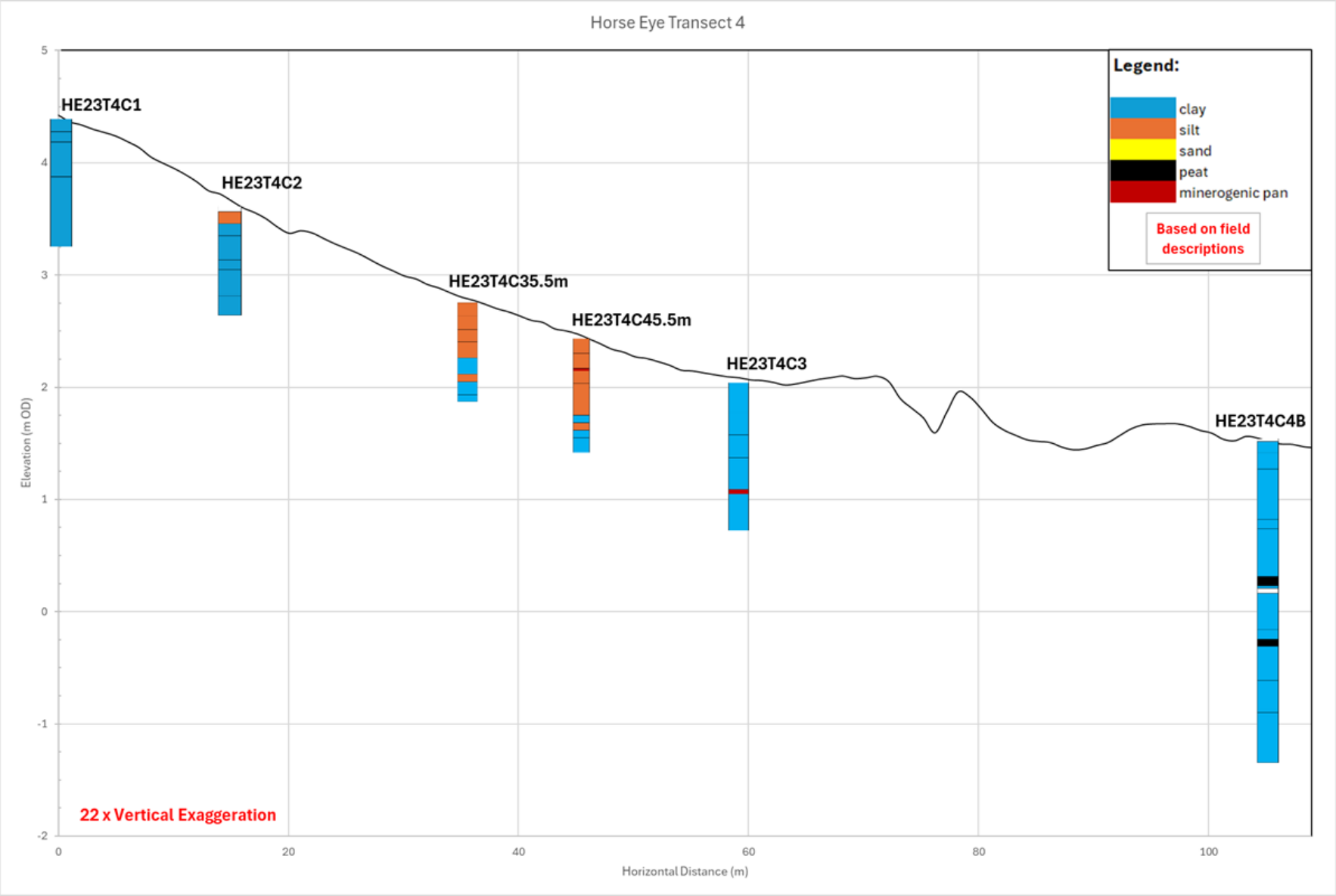


Figure 4.11 - A cross-section illustrating the simplified stratigraphic beds (silt, clay, peat, and minerogenic pan) identified in the boreholes along Transect 4 on Horse Eye.

The detailed cross-section (Figure 4.10) and simplified cross-section (Figure 4.11) reveal several key patterns for the stratigraphy of Transect 4, highlighting the lithological complexity and variations in thickness, lateral extent, and elevation changes across the transect.

In the uppermost layers, silty clay is a dominant facies across Transect 4, with thicknesses generally ranging from 11 to 26 cm. This layer is thickest in the higher-elevation boreholes, such as HE23T4C1 and HE23T4C2, which are located closer to the central part of the island, where the elevation is higher. In these boreholes, the silty clay reaches up to 26 cm in thickness, indicating stable, organic-rich depositional conditions typical of a more terrestrial environment. As the transect progresses toward lower elevations, particularly in borehole HE23T4C3, the thickness of the silty clay decreases to approximately 8 cm. This reduction in thickness corresponds with the transect moving toward the edge of the island and into areas where depositional conditions were more variable. As the silty clay layer thins, the stratigraphy begins to reveal more complex lithological changes, especially in the lower elevation boreholes such as HE23T4C4B. Here, the stratigraphy transitions from the upper silty clay, rich in roots and organic material, into a greenish-grey silty clay with dark orange mottling, typically observed between 11 and 26 cm below ground surface. This mottled silty clay indicates a shift in depositional conditions, potentially reflecting changes in the redox environment.

At greater depths, the lithological complexity increases, with the introduction of interbedded layers of peat, marine clay, and terrestrial clay, as well as an introduction of additional sedimentary structures. In borehole HE23T4C4B, a peat layer is encountered between 119 and 127 cm, characterized by black, fibrous material and a large wood fragment, suggesting a period of significant organic accumulation in a low-energy environment. Below this, the stratigraphy transitions to a mixed layer of peat and marine clay between 127 and 130.5 cm, marking a gradual shift from terrestrial to paludal and marine conditions. As the transect extends laterally towards the southern edge of the island and into the Pevensey Levels, the lower elevation boreholes, particularly HE23T4C4B, capture the most complex stratigraphy. Following the mixed peat-marine clay

transition layer, a distinct marine clay layer is observed, extending from approximately 130.5 cm to 165.5 cm. This layer includes a small amount of sand (15%) and wood fragments. The stratigraphy then shows a sharp boundary at 165.5 cm, transitioning into an orange-mottled clay, which persists until 173 cm. This abrupt change suggests a return to subaerial conditions.

Below the orange mottled clay, a second peat layer is present between 173 and 180 cm, characterized by its fine, fibrous texture, suggesting another period of organic accumulation. Following this, the stratigraphy transitions into the lower marine clay, extending from 180 cm down to 280 cm. This lower marine clay includes fine sand laminations between 180 and 210 cm, indicating fluctuating energy conditions. Further down, from 210 to 237 cm, the marine clay contains shell fragments, reflecting a marine environment rich in biogenic material. Finally, the deepest section, from 237 to 280 cm, is characterized by a more homogeneous marine clay, lacking sand laminations or shells but containing manganese nodules, indicating a stable, low-energy marine environment.

The patterns observed in the cross sections of Transect 4 reveal a complex interplay between lithology, thickness, lateral extent, and elevation. For instance, the variation in silty clay thickness, from thicker layers at higher elevations to thinner layers as the transect extends toward lower elevations, illustrates how depositional environments shifted across the island. These variations are further reflected in the transitions from terrestrial silty clay to marine clays, peat layers (paludal), and the inclusion of sand laminations and shell fragments at greater depths. The stratigraphy captured in Transect 4 thus records the dynamic processes of sedimentation, shaped by the changing elevations and lateral positions of the boreholes relative to the island.

This intricate stratigraphy not only highlights the complexity of the depositional environments but also provides valuable insights into Horse Eye's paleoenvironmental history. The detailed analysis of these transitions demonstrates how different environmental conditions influenced the sedimentation processes over time, offering a

clearer understanding of the dynamic nature of the region's sedimentary and paleoenvironmental history.

4.3.5. Laser Diffraction Grain Size Analysis

Laser Diffraction Grain Size analysis was conducted on sediment samples collected from six boreholes along Transect 4 at Horse Eye, which extends from the southern portion of the island into the Pevensey Levels. This transect was selected for its diverse stratigraphy, characterized by a variety of lithologies and sedimentary structures, particularly notable at borehole HE23T4C4B. The stratigraphy observed along Transect 4 includes transitions between orange-mottled silty clays, marine clays, and peat layers, reflecting a dynamic depositional environment influenced by both terrestrial and marine processes.

Observations during fieldwork recorded layers as silty clay, but Laser Diffraction grain size analysis revealed a tendency to classify these layers as clayey silt. This suggests that the field estimates tended to overestimate clay content and underestimate silt content, highlighting the challenges of visually estimating fine-grained sediment such as clay and silt in the field.

Across the six boreholes in this transect, 78 sediment samples were analyzed. A higher number of samples were analyzed in borehole HE23T4C4B. Sampling was done at a higher resolution, particularly in areas of interest such as near and encompassing sedimentary structures and contacts, as well as areas that exhibited higher amounts of sand. These samples reflect the grain size of the stratigraphy and how it changes vertically in the core and laterally along the transect. The detailed analysis of these samples provides insights into the depositional history of the area, illustrating the fluctuation between terrestrial and marine influences over time.

A grain size analysis at varying depths within each core along Transect 4 is presented, highlighting trends and patterns in grain size distribution. For each borehole, the corresponding figures include a grain size distribution bar chart, as well as their location in both map view and cross-sectional view. This additional spatial context helps to clarify each borehole's relative position and elevation, aiding the interpretation of stratigraphic data in multiple dimensions.

Eight samples were analyzed from borehole HE23T4C1, located at the highest elevation of this transect. Field observations initially recorded clay as the dominant grain size (as seen in the simplified cross-section in Figure 4.12B); however, laser diffraction analysis refined this description, revealing that silt is more accurately the dominant grain size. Both clay and silt are relatively fine grain sizes, both indicative of low-energy depositional environments. The grain size distribution, as shown in Figure 4.12A below, is characterized predominantly by silt, with percentages ranging from 69% to 86%. At the deepest sample (97 cm), the clay content is 25% and the silt content is 75%. As we move up the profile, the clay content increases, reaching its highest value of 31% at 88.75 cm, and then it decreases to 14% at the uppermost sample (23.5 cm). Results show sand is lacking throughout this borehole. The lack of sand and the clayey silt nature of the sediment throughout the profile suggests generally stable, low-energy depositional conditions. The accompanying map and cross-sectional views in Figure 4.12 provide spatial context, showing the borehole's location on the higher, central part of the island.

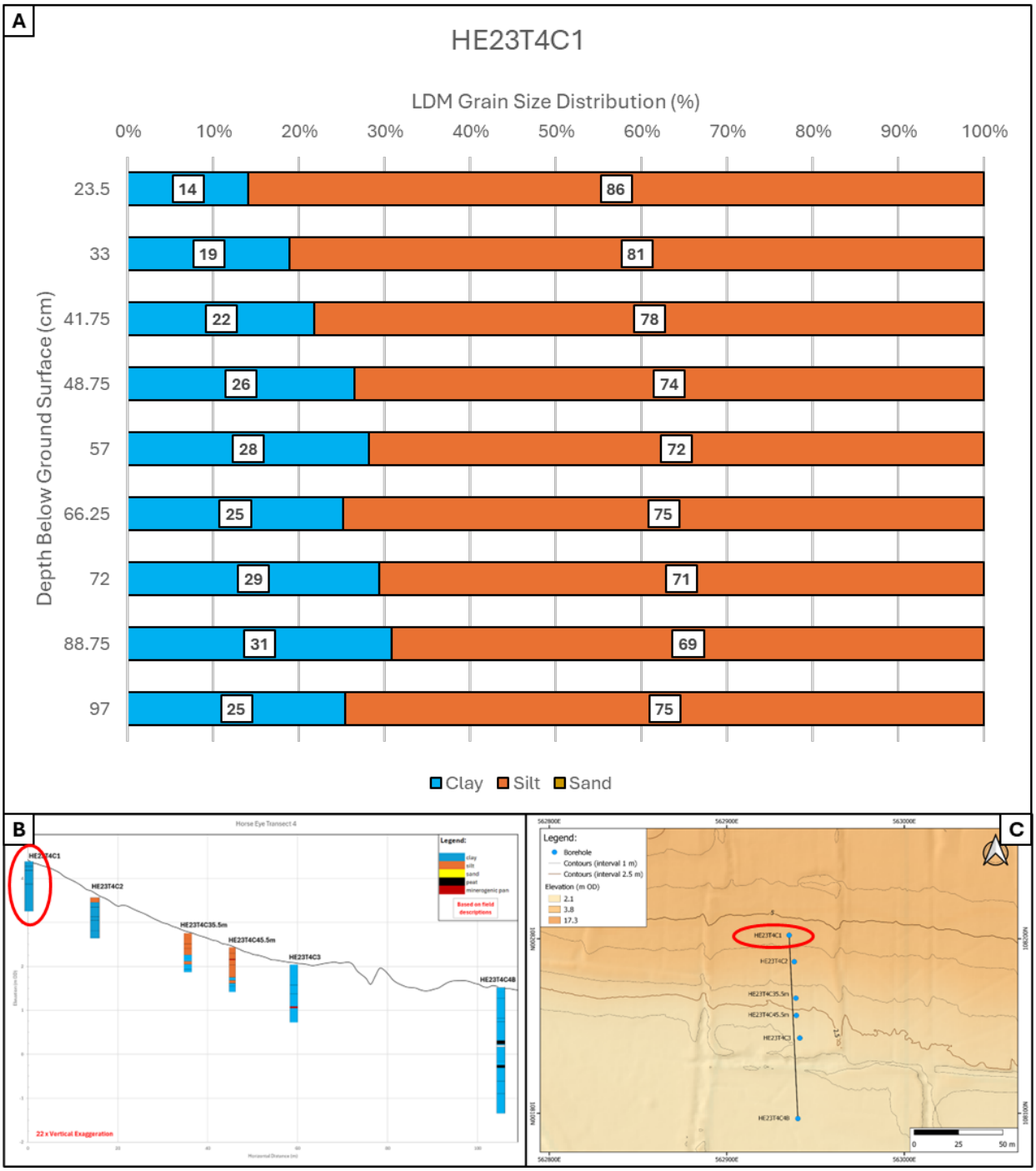


Figure 4.12 - Grain size distribution bar chart for borehole HE23T4C1 along Transect 4, showing the percentage of clay, silt, and sand at various depths below the ground surface. The figure also includes the simplified cross-section of Transect 4 based on field observations, as well as a map view of the transect, both of which highlight the location of borehole HE23T4C1 circled in red. The cross-section and map provide spatial context, illustrating the borehole's position.

Grain size analyses were also completed on seven samples from the second borehole (HE23T4C2) down the slope of Transect 4. This revealed a similar trend to HE23T4C1, with silt dominating at 69% to 90%. The clay content varies between 7% and 31%, and minimal sand is present only at the uppermost level, accounting for 3% at 23.5 cm (Figure 4.13A). The high percentage of silt (90%) and the presence of sand suggest a brief episode of higher energy conditions for the upper portion of the stratigraphy. The deepest sample (81.25 cm) is composed of 31% clay and 69% silt, with no sand present. Moving up the profile, the silt content increases slightly to 79% at 66.75 cm, while the clay content decreases to 21%. The clay content increases again to 30% at 56 cm, with 70% silt and sand is absent. However, closer to the surface, the clay content generally decreases while the silt content continues to increase. From 56 to 23.5 cm, the silt content remains the predominant grain size and increases with a decrease in depth (from 70% at 56 cm to 90% at 23.5 cm). The borehole's position on the slope of the island, transitioning towards the Pevensey Levels, may explain the greater variability in grain size when compared to HE23T4C1, as sediment supply and depositional energy may fluctuate more in transitional zones between higher and lower elevations.

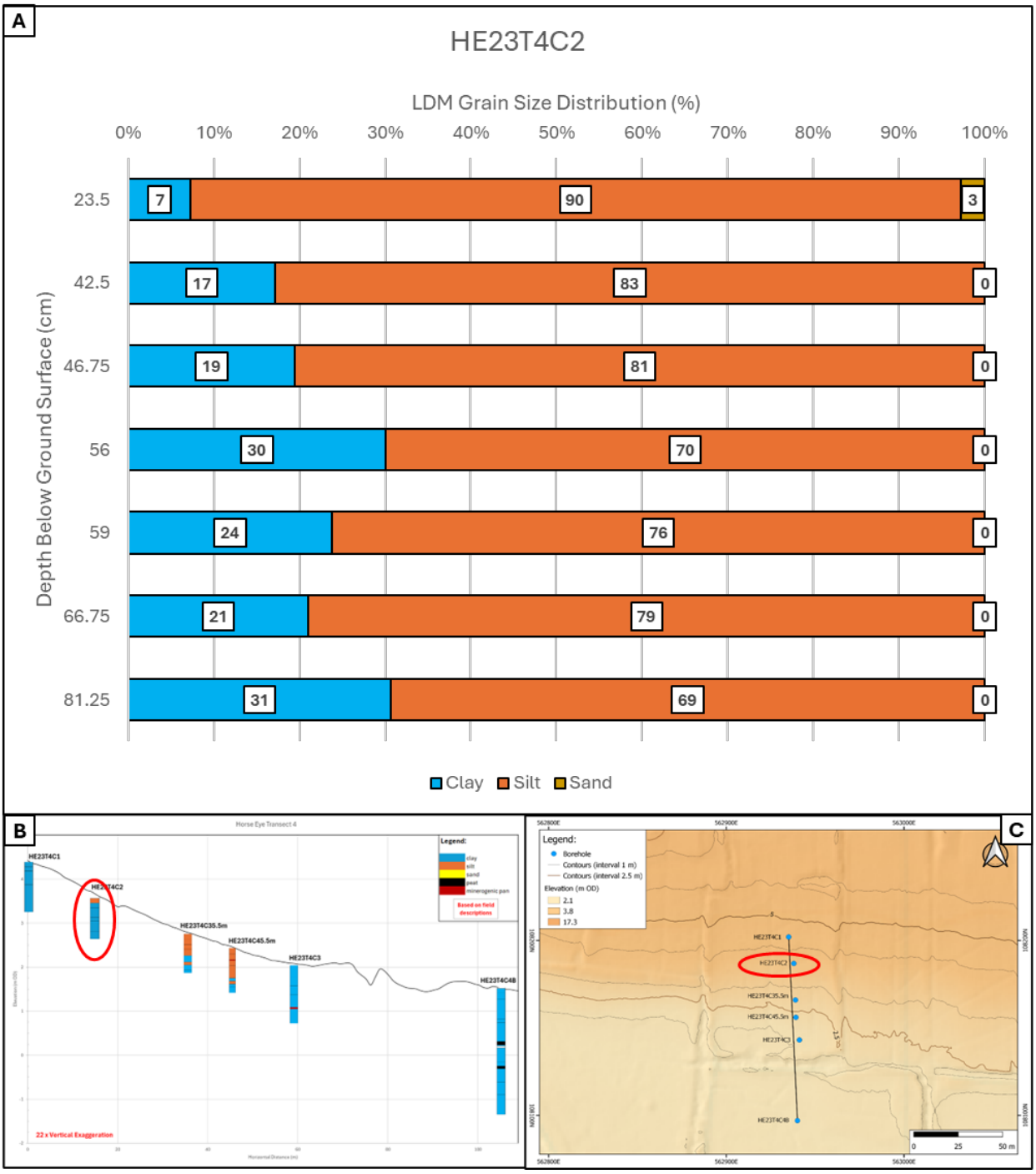


Figure 4.13 - (A) Grain size distribution bar chart for borehole HE23T4C2 along Transect 4, showing the percentage of clay, silt, and sand at various depths below the ground surface. The figure also includes (B) the simplified cross-section of Transect 4 based on field observations, and (C) a map view of the transect, both of which highlight the location of borehole HE23T4C2 circled in red. The cross-section and map provide spatial context, illustrating the borehole's position.

Four samples from the next borehole (HE23T4C35.5m) down the slope were also analyzed (Figure 4.14A). The deepest sample at 78 cm shows a grain-size distribution of 21.8% sand, 49.6% silt, and 28.6% clay. This suggests higher-energy depositional conditions towards the lower portion of the sediment core. As we move up the profile, the grain-size distribution becomes more consistent, with silt dominating (68-70%) and clay content ranging from 30% to 32%, while sand is absent in the upper three samples (51 cm, 61 cm, and 70 cm). These consistent grain-size proportions in the upper layers indicate a more stable, low-energy depositional environment.

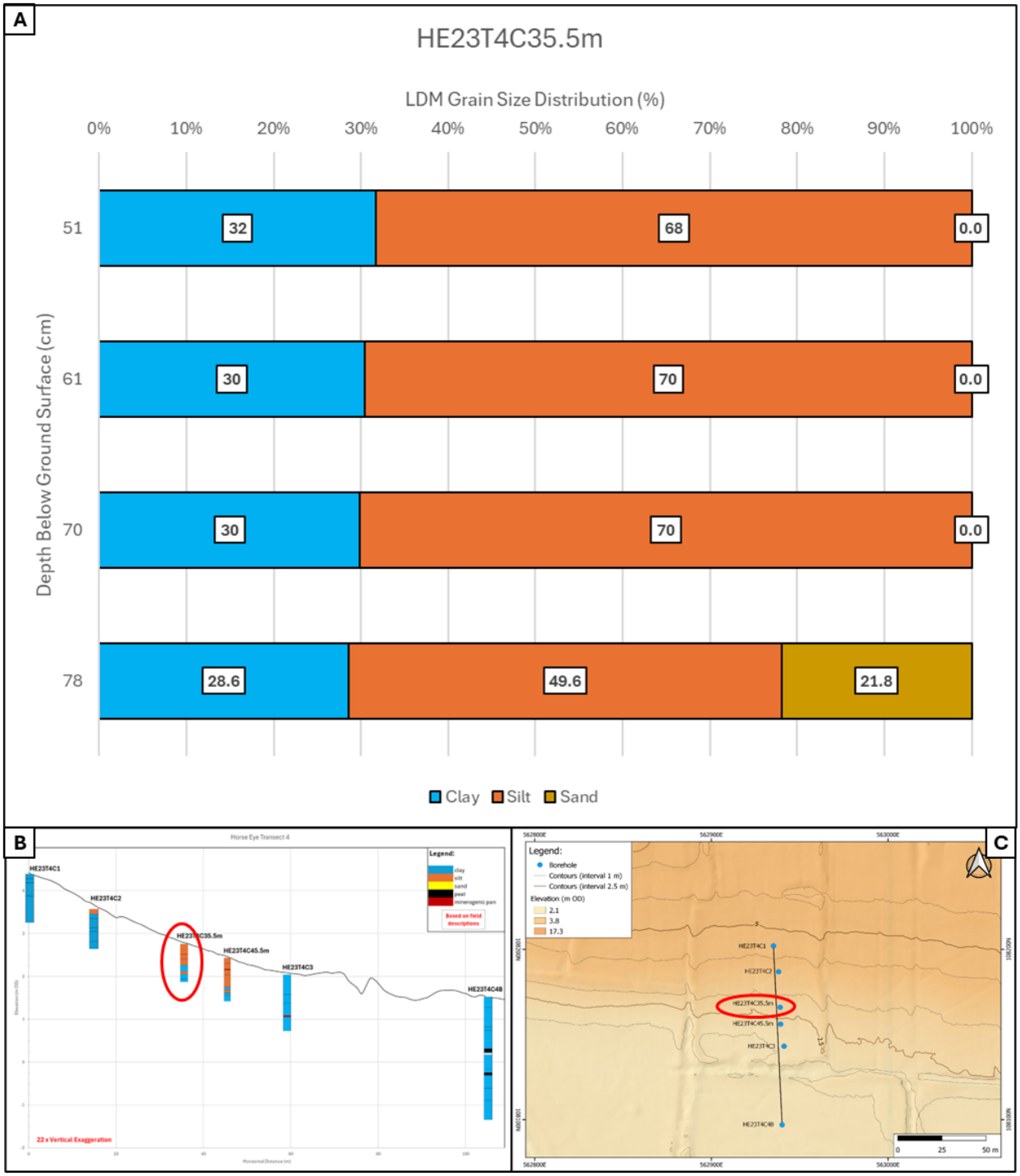


Figure 4.14 - (A) Grain size distribution bar chart for borehole HE23T4C35.5m along Transect 4, showing the percentage of clay, silt, and sand at various depths below the ground surface. The figure also includes(B) the simplified cross-section of Transect 4 based on field observations, and (C) a map view of the transect, both of which highlight the location of borehole HE23T4C35.5m circled in red. The cross-section and map provide spatial context, illustrating the borehole's position.

Five samples from borehole HE23T4C45.5m were analyzed. The grain-size distribution remains predominantly silt, ranging from 63% to 71%, with clay content varying between 29% and 37%. No sand was recorded at any depth in this borehole (Figure 4.15A). Starting from the deepest sample at 84.5 cm, the grain-size distribution consists of 34% clay and 66% silt. As we move up the profile, at 76 cm, the clay content remains similar but decreases to 30%, while the silt increases to 70%. At 70 cm, the clay continues to decrease to 29%, and the silt increases to 71%. An increase in clay content (37%) occurs at 64.5 cm, which may indicate natural variability from the overall trend of clay decreasing and silt increasing moving up in depth in the profile. The uppermost sample at 55.5 cm shows a return to a similar grain-size distribution to the lower portion of the core, with 30% clay and 70% silt.

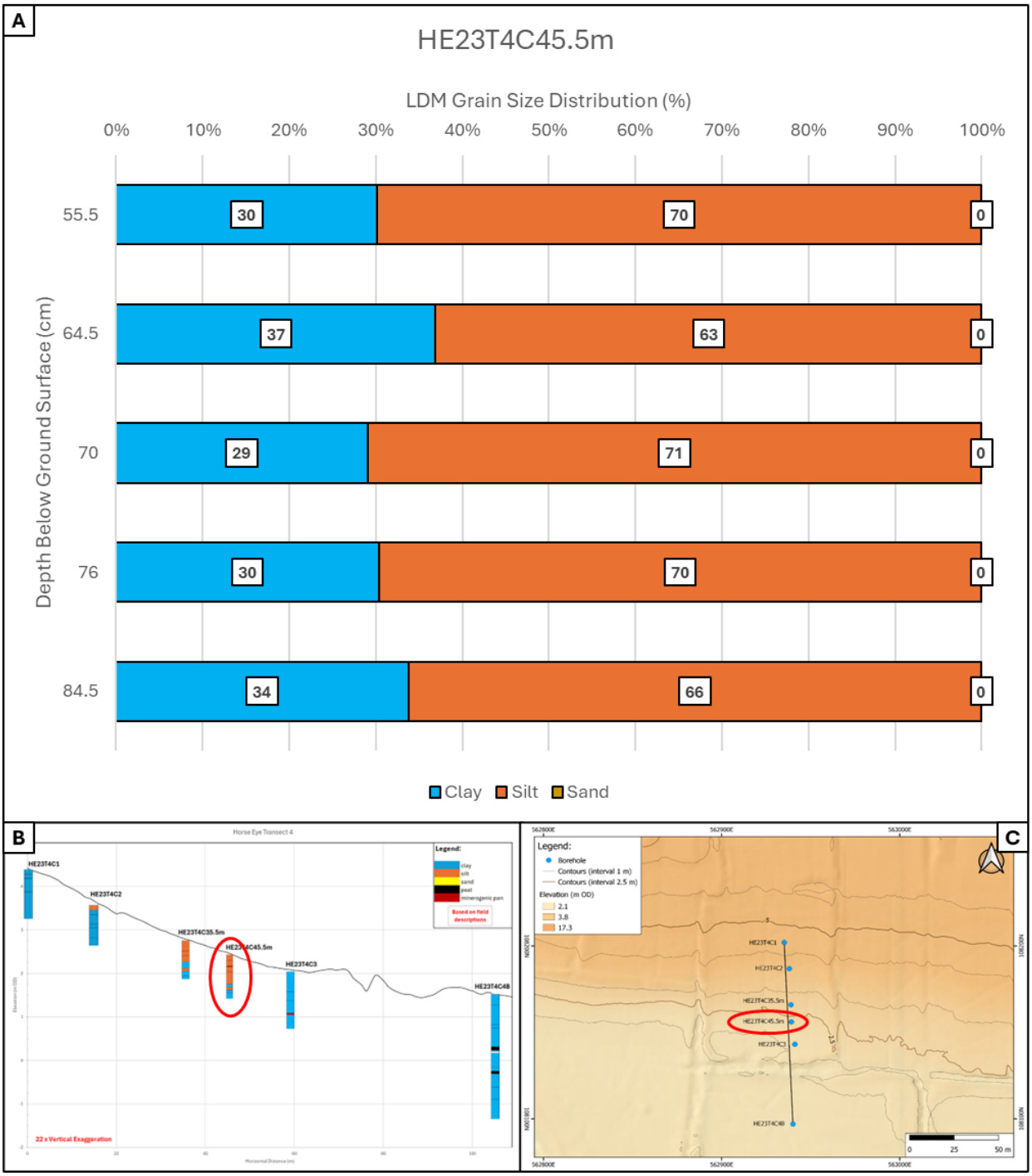


Figure 4.15 - (A) Grain size distribution bar chart for borehole HE23T4C45.5m along Transect 4, showing the percentage of clay, silt, and sand at various depths below the ground surface. The figure also includes (B) the simplified cross-section of Transect 4 based on field observations and (C) a map view of the transect, both of which highlight the location of borehole HE23T4C45.5m circled in red. The cross-section and map provide spatial context, illustrating the borehole's position.

Borehole HE23T4C3, which had seven samples analyzed, shows a fining-upward trend from base to middle, followed by relatively constant grain size, and one coarser sample at the top (Figure 4.16A). More specifically, starting from the deepest sample at 123 cm, the grain size distribution consists of 23% clay and 77% silt. Moving up the profile, clay content gradually increases to 27% at 107.5 cm and then to 32% at 98 cm. Between 98 cm and 43 cm, the clay content becomes relatively stable at around 30%, ranging between 32% and 29%, while the silt remains consistently high, ranging from 68% to 70%. However, at 35.5 cm, the clay percentage decreases to 19%, while the silt increases to 81%. No sand was recorded at any depth. This overall pattern suggests relatively stable depositional conditions with a slight increase in energy near the top, as indicated by the decrease in clay content and corresponding increase in silt.

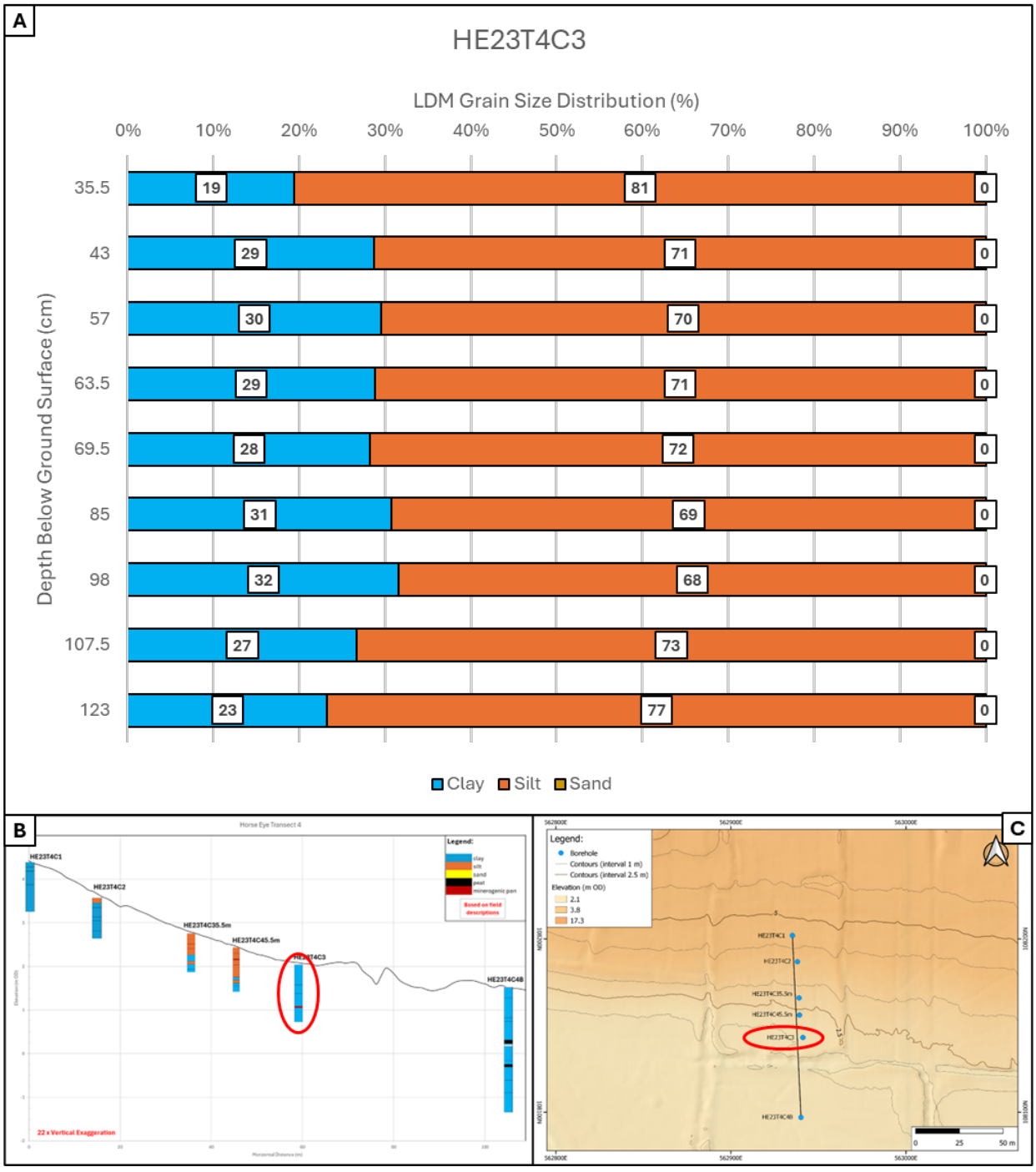


Figure 4.16 - (A) Grain size distribution bar chart for borehole HE23T4C3 along Transect 4, showing the percentage of clay, silt, and sand at various depths below the ground surface. The figure also includes (B) the simplified cross-section of Transect 4 based on field observations (C) and a map view of the transect, both of which highlight the location of borehole HE23T4C3 circled in red. The cross-section and map provide spatial context, illustrating the borehole's position.

Borehole HE23T4C4B, positioned at the southernmost end of Transect 4 and extending into the Pevensey Levels, is of particular interest due to its diverse facies, including sedimentary structures. Located at the lowest elevation within the transect, this borehole records a transition from sediment within the Levels to different sediment on the island. This borehole is significant because it records multiple depositional environments within a relatively small vertical profile (280 cm), showing transitions between high-energy events, likely marine incursions, and lower-energy terrestrial or paludal conditions. The presence of both marine and terrestrial influences reflected in sediment type, along with distinct sedimentary structures, makes the stratigraphy of HE23T4C4B important, offering valuable insight into the paleoenvironmental history of Horse Eye.

Forty-four sediment samples were analyzed from borehole HE23T4C4B, sampling was conducted at a higher resolution in particular areas around and including sediment structures and regions with higher sand content. The grain size distribution is shown in a bar chart in Figure 4.17A, this chart visually represents the proportions of sand, silt, and clay throughout the core.

Beginning from the base of the core, from 279 to 197.5 cm, the grain size distribution is dominated by clay and silt, with minimal sand content (only 11% in one sample at 279 cm). Clay percentages range from 24% to 33%, while silt content remains consistently high, fluctuating between 67% and 73%. These deeper layers represent a low-energy depositional environment, likely dominated by fine-grained marine sediments. The absence of significant sand and the consistent fine-grained sediment size suggest a stable, low-energy environment, possibly marine.

Between 197.5 and 186 cm, the grain size becomes more complex, with sand spikes occurring at 191 cm (29%) and 186.5 cm (37%), These peaks correspond to individual sand laminations observed after retrieving the core in the field, indicating brief episodes of higher-energy deposition. The intervening layers, where sand content drops to 0%, represent the matrix material between these laminations, which consists primarily of silty clay (silt ranging from 73% to 76%, and clay between 15% and 27%). This alternation

between sand and finer-grained material suggests fluctuating energy conditions, where episodes of higher-energy sand deposition are followed by more quiescent periods dominated by fine-grained sedimentation.

The lower peat layer was observed between 173 cm and 180 cm, and the upper peat layer was recorded between 127 and 119 cm, there was minimal detrital material in the peat layers, therefore no grain size analysis was completed. More information on these peat layers will be discussed in section 4.3.10 Geochronology Results. Between these two peat layers, the grain size returns to a predominantly silty clay, with minimal sand, reflecting a shift back toward lower-energy terrestrial deposition.

From 165 to 136, the grain size analysis shows a significant increase in sand content, with a range of 24% - 39%. The silt content ranges from 40% to 52%, and the clay content ranges from 26% to 20%. This suggests a higher energy depositional environment, where finer grain sizes dominate (silt and clay), but higher energy conditions allowed for the introduction of sand. Organic material is also interspersed within the sediment, indicating a mix of depositional processes that include both organic and sediment accumulation.

Between 136 cm and 86.5 cm, the grain size distribution is dominated by clayey silt, with clay content ranging between 24% and 30% and silt content fluctuating between 70% and 76%. No sand was recorded in this interval. This portion of the core likely represents a stable, low-energy depositional environment, as clay and silt are the dominant grain sizes.

From 74 cm to 40 cm, there are noticeable fluctuations in sand content, with peaks in the sand percentage ranging between 23% and 40%. However, it is important to note that these spikes are due to lenticular sand laminations that were observed in the field, these laminations were sampled and analysed within this interval. The surrounding matrix remains primarily composed of clayey silt, with a silt content of approximately 72-73%, and a clay content of approximately 27-28%. Lenticular sand laminations are isolated small lenses of sand in a muddy bed, these occur when sand becomes trapped in troughs in the mud as sand migrates across a muddy substrate (Prothero & Schwab, 2004). This

observation is important as these sand-rich spikes do not represent large, continuous sand layers, but rather isolated sand lenses within the predominantly fine-grained matrix.

Above 40 cm, there are smaller fluctuations in sand content, but they occur within the uppermost layers of the core, including the topsoil and subsoil. In these layers, the grain size distribution becomes more diverse, with sand content ranging between 40% and 16% between 40 and 25 cm, and 0% in the uppermost 20 cm. Clay percentages vary between 27% and 15%, and silt remains relatively high, ranging from 40% to 81%. These upper horizons reflect a combination of modern soil development processes and potential sediment reworking, leading to more variability in the grain size distribution.

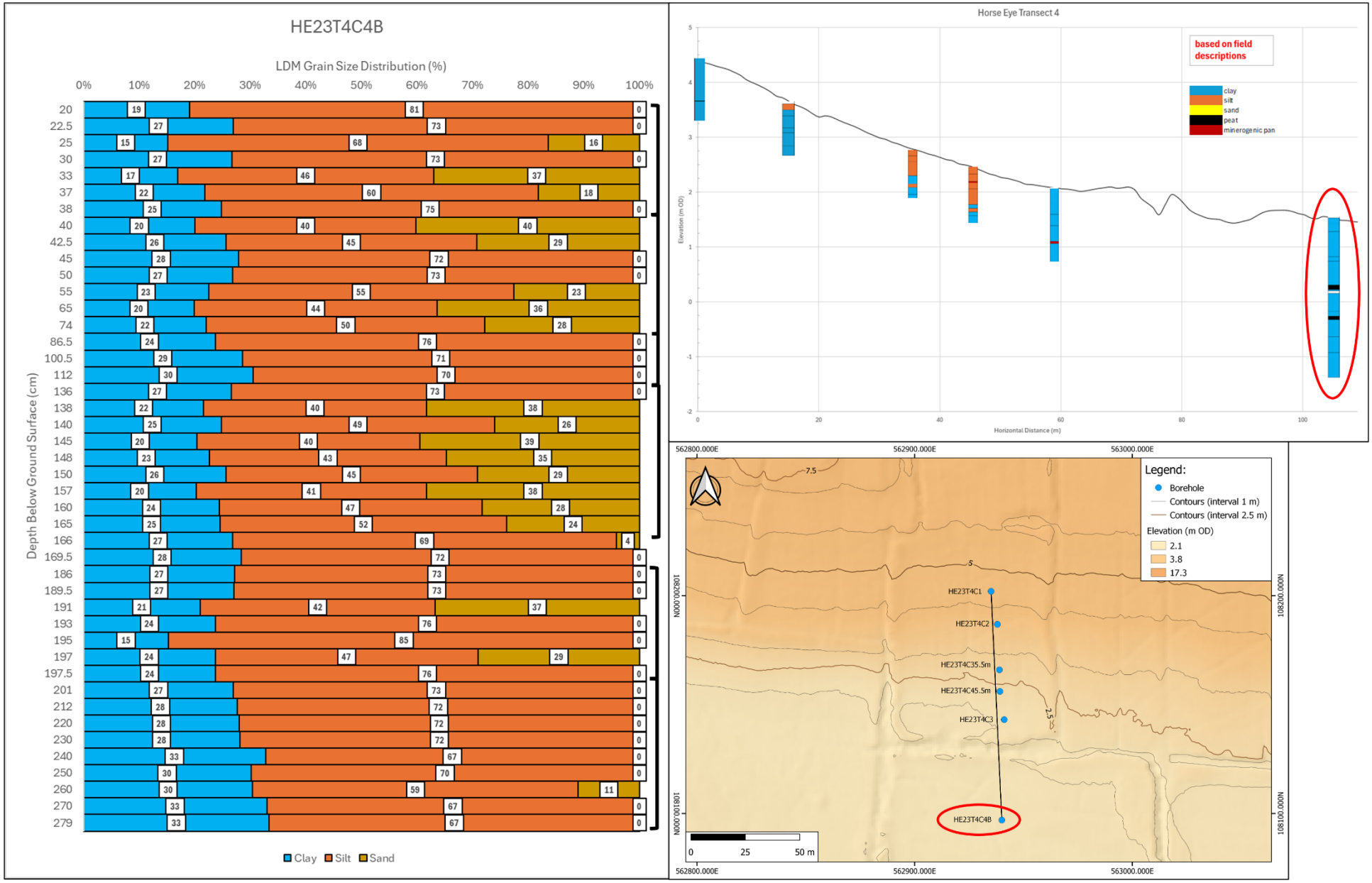


Figure 4.17 - (A) Grain size distribution bar chart for borehole HE23T4C4B along Transect 4, showing the percentage of clay, silt, and sand at various depths below the ground surface as well as brackets showing the divisions discussed in the text. The figure also includes the simplified cross-section of Transect 4 based on field observations (B) and a map view of the transect (C), both of which highlight the location of borehole HE23T4C4B circled in red. The cross-section and map provide spatial context, illustrating the borehole's position.

In addition to the grain size distribution bar chart, a more detailed breakdown of the sand, silt, and clay grain size distributions is shown for borehole HE23T4C4B in Figure 4.18. This analysis is presented through a series of line graphs that show the variability of sand, silt, and clay content downcore, alongside more specific sand and silt size classes. These charts illustrate the depth-dependent variability of each grain size fraction and help provide an understanding of the depositional environment recorded in borehole HE23T4C4B.

The first three charts (Figure's 4.18A, 4.18B, and 4.18C) show the distribution of sand, silt, and clay throughout borehole HE23T4C4B, from the base (279 cm) to the top of the borehole (20 cm). Unlike the bar charts shown above, these line graphs (with markers) offer a different perspective by plotting the grain size percentages in a down-profile format, making it easier to visualize the changes in grain size distribution across the entire core. By showing the location of each sample at its respective depth, these line graphs highlight trends and variations in sediment composition more clearly than the bar charts.

The sand content (Figure 4.18A) averages 13%, with a standard deviation of 15.7%. At the deepest layers, sand is minimal, peaking at 11% at 260 cm, indicating a predominantly low-energy depositional environment. Moving up the profile, sporadic spikes of sand appear, such as 28.9% at 197 cm and 36.7% at 191 cm, marking brief, high-energy depositional episodes. These fluctuations in sand content correspond to isolated sand laminations noted in the core while in the field. Above these laminations, the sand content returns to around 0% between 190 and 170 cm. Between 166 and 136 cm, there is a noticeable increase in sand content, ranging from 24% and 39%, suggesting a higher energy setting during deposition during this interval. However, above 136 cm, the sand content drops sharply, returning to 0% at 136 cm until 86.5 cm, indicating a return to lower-energy conditions dominated by finer-grained sediment (silt and clay). Above 86.5 cm, there is an apparent increase in sand content between 86.5 cm and 50 cm, ranging between 23% and 36%; However, it is important to note that the larger spacing between the samples in this section limits the ability to capture the fine details of the sand distribution, such as lenticular sand laminations. As previously mentioned, these laminations were recorded in the field, but their presence is not fully reflected in the grain size analysis due to

the broader spacing. The sand-rich appearance of this section may be misleading, as the sand exists within thin, isolated lenses (lenticular laminations) interspersed in the finer-grained matrix of clayey silt (or, mud). Without closely spaced samples, the graph may depict an averaged or mixed result, where the higher sand content reflects the blending of these laminations (approximately 2-3 mm thick) with the surrounding clayey silt matrix, rather than a continuous sand-rich layer. Above 40 cm, smaller fluctuations in sand content are observed, reaching 40% at 40 cm and 37% at 33 cm, before tapering off in the uppermost layers.

The silt content (Figure 4.18B), which dominates much of the profile, averages 62% with a standard deviation of 13.7%. At the base of the core (279 cm), silt accounts for 67% of the grain size distribution, indicative of a low-energy depositional environment. As we move upward, the silt content increases to roughly 72% until there is a noticeable fluctuation in silt content between 279 cm and 189.5 cm, with silt fluctuating between 42% (191 cm) and 89% (195 cm), coinciding with the presence of sand laminations. Between 189.5 cm and 169.5 cm, silt content continues to dominate accounting for roughly 72% of the grain size distribution. Between 166 and 136 cm, the silt content decreases significantly to roughly 45%, coinciding with an increase in sand content at this depth. From 136 cm to 86.5 cm, silt content stabilizes between 70% and 76%. Above 74 cm, however, silt content becomes more variable, reflecting the introduction of lenticular sand laminations, especially near 42 cm. Despite these fluctuations, silt remains the predominant grain size, with minor variations suggesting shifts between finer and coarser sedimentation episodes. In the upper 40 cm of the profile, the silt percentage drops slightly, ranging from 40% to 81%, with a more substantial variability reflecting the influence of modern surface processes and soil reworking.

The clay content (Figure 4.18C) averages 25%, with a standard deviation of 4.4%. At the deepest layers of the core (279 cm), clay makes up 32% of the grain size distribution. Moving up the profile, the clay content gradually decreases to roughly 27% at 201 cm. Above 201 cm, the clay content fluctuates slightly, dropping to 15% at 195 cm, coinciding with the presence of sand laminations. The clay content remains stable at around 27%

until 166 cm, where there is a noticeable drop in clay content. The percentage of clay fluctuates between 20% and 26% until 136 cm, coinciding with an increase in sand content at this depth. Above 136 cm, the clay content gradually increases to 30% at 112 cm, then gradually decreases to 20% at 65 cm, coinciding with the increase in sand at this depth. In the uppermost layers of the core, above 65 cm, the clay content decreases with substantial variability, ranging from 28% to 15%, indicating increased sand and silt dominance for the grain size distribution of the most recent sediment.

The sand fractions chart (Figure 4.18D) breaks down the sand content further into the two size classes that were recorded during the laser diffraction grain size analysis: very coarse sand (vCS, 1 – 2 mm) and coarse sand (CS, 62.5 μm–1 mm). This chart provides a more nuanced view of the sand deposition, offering insight into the energy of the depositional environment. At the base of the core (279 cm), sand content is minimal (generally 0%), and the sand fractions indicate no significant presence of very coarse or coarse sand until higher in the profile. Between 191 and 166 cm, which coincides with the presence of sand laminations identified earlier, the chart shows a clear increase in sand fractions, with the vCS and CS fractions contributing to the peaks in overall sand content observed. For example, at 191 cm, very coarse sand (vCS) contributes 37% of the grain size distribution, while the coarse sand (CS) contributes to 0% of the grain size distribution. This trend of vCS accounting for the percentage of sand observed continues until 25 cm, where the sand is composed of both vCS (4%) and CS (12.5%) fractions, totalling the 16.5% sand that was observed in the grain size distribution above (chart Figure 4.18A).

The silt fractions chart (Figure 4.18E) breaks down the silt fractions (2–62.5 μm) into five sub-classes: very fine silt (v.f, 2–4 μm), fine silt (f, 4–8 μm), medium silt (med, 8–16 μm), coarse silt (c, 16–31 μm), and very coarse silt (v.c, 31–62.5 μm). These subdivisions provide a more refined view of the energy conditions during deposition, as finer silt generally represents lower-energy conditions, while coarser silt indicates relatively higher energy during deposition. Down the profile of the core, a clear trend emerges: the v.f, f, and med silt fractions remain relatively stable, showing minimal fluctuations throughout the core. Conversely, most of the grain size fluctuations with depth are driven by variations in the

coarse (c) silt fraction. The coarse silt fraction shows notable peaks and troughs at several intervals, particularly in areas where sand laminations were noted in the field.

Lastly, Figure 4.18F illustrates the normalized fractions of very coarse sand (vCS, 1 – 2 mm) and coarse silt (cS, 16–31 μm) along the stratigraphic profile. Coarse sand proportions reflects shifts in depositional energy, where higher-energy conditions favour the deposition of very coarse sand, often linked to episodic events like storms or changing water flow dynamics. Conversely, lower depositional energy promoted the accumulation of finer sediment, particularly coarse silt fractions.

The grain size analysis conducted on the boreholes along Transect 4 through the laser diffraction method provides a detailed view of the depositional environments at Horse Eye. The results reveal a dynamic interaction between marine and terrestrial influences, with distinct grain size patterns corresponding to shifts in depositional energy conditions and depositional processes. Sand-rich laminations highlight episodic high-energy depositional events, such as storms or other brief increases in depositional energy, while clayey and silty layers reflect more stable, lower depositional energy conditions. Field observations combined with the laser diffraction analysis show the importance of high-resolution sampling, particularly in zones of interest, such as areas with sand laminations or sedimentary structures. The trends observed in core HE23T4C4B, including the relative proportions of very coarse sand and coarse silt fractions, further demonstrate the role of depositional energy in shaping the stratigraphic record. Overall, the grain size data offer insights into the depositional history of Horse Eye and the broader Pevensey Levels- aiding in the understanding of complex processes influencing these coastal landscapes.

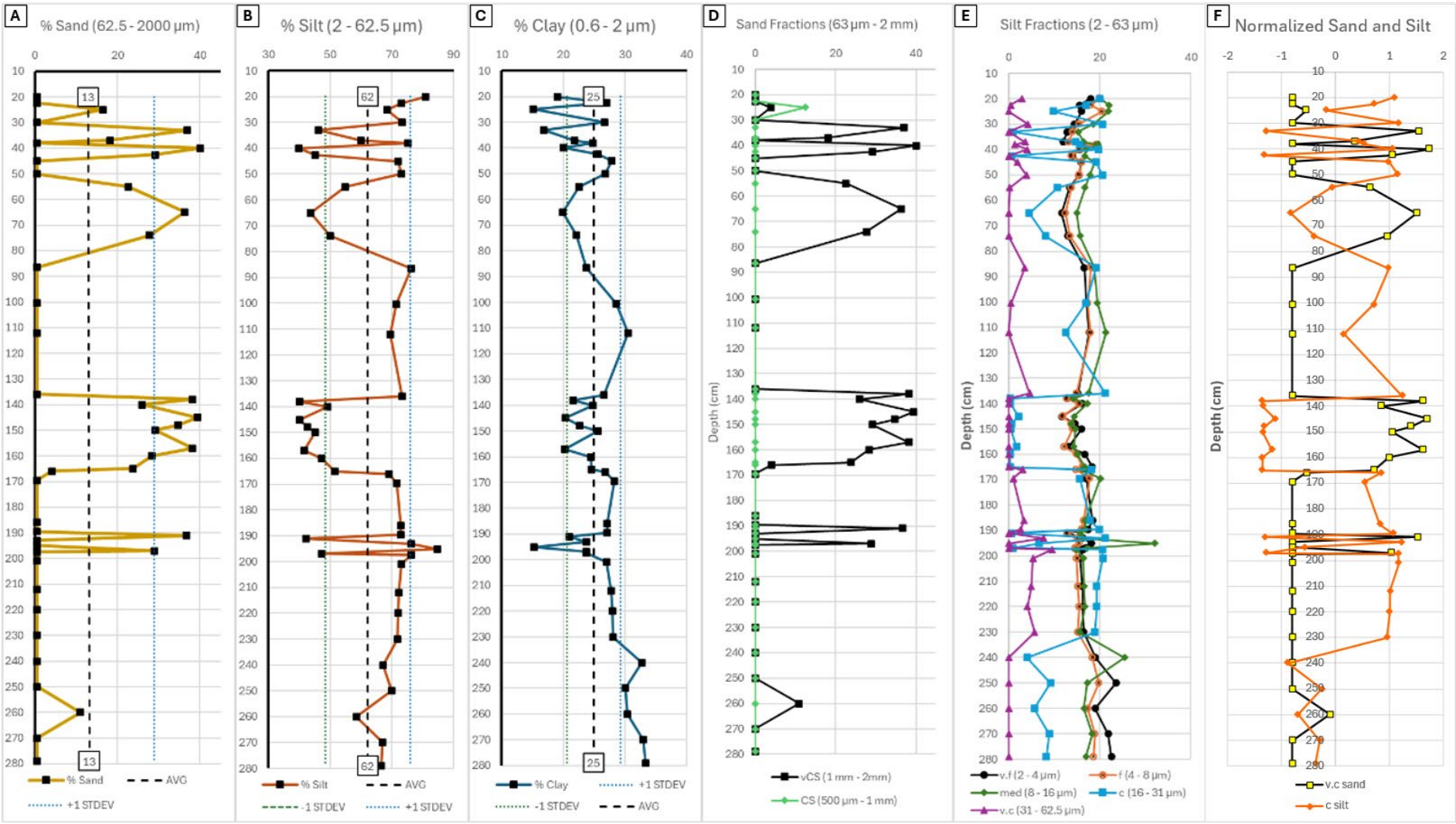


Figure 4.18 - Detailed grain size distribution analysis for borehole HE23T4C4B, showing six down-profile graphs. The first three graphs display the percentage of sand, silt, and clay at various depths below the ground surface, with their average values and standard deviations indicated. The sand fractions chart (D) breaks down the total sand percentage into very coarse sand (vCS, 1-2 mm) and coarse sand (CS, 500 µm - 1 mm), while the silt fractions chart (E) subdivides the total silt percentage into very fine (v.f, 2-4 µm), fine (f, 4-8 µm), medium (med, 8-16 µm), coarse (c, 16-31 µm), and very coarse (v.c, 31-62.5 µm) silt fractions. The final graph (F) depicts the normalized relationship between very coarse sand (vCS) and coarse silt (cS).

4.3.6. Portable X-ray Fluorescence (pXRF) Analysis

In this section, the results of the Portable X-ray Fluorescence (pXRF) analysis for both topsoil and peat layers from Horse Eye Transect 4 (Figures 4.19, 4.20, and 4.21) are presented and interpreted. These analyses provide the geochemical composition of the sediment samples at five different elevations along the transect. Geochemical composition may provide insights into depositional environments and sediment characteristics. Table 4.8 summarizes pXRF data for topsoil samples (0-10 cm) at three locations along Transect 4, while Table 4.9 presents pXRF data for both topsoil and deeper peat layer samples specifically from a single core, HE23T4C4B. Figure 4.21 visualizes the elemental composition of the samples in core HE23T4C4B taken within the topsoil, Upper Peat, and Lower Peat layers.

The pXRF data collected are grouped into seven elemental categories: Coarse Clastic, Fine Clastic, Redox, Carbonate, Proxy Organic, Heavy Metals/Pollutants, and Atmospheric Radioactive, to provide a clearer understanding of sedimentary textural and depositional history characteristics. As Davies et al. (2015) explain, these elements identified through pXRF can reflect the processes and environmental conditions under which they were deposited. Indicators of detrital inputs are represented by lithogenic elements such as aluminum (Al), silicon (Si), potassium (K), titanium (Ti), iron (Fe), rubidium (Rb), and zirconium (Zr), indicating the presence of minerogenic material that was transported and reflect erosion and runoff influences. Elements such as titanium, silicon, and zirconium represent coarse-grained clastic mineral deposition and are classified as Coarse Clastic, while elements like silicon, potassium, aluminum, and rubidium are associated with finer-grained deposition; these are grouped as Fine Clastic. Carbonate content, indicated by elements like calcium (Ca) and strontium (Sr), can reveal marine influence, and sulphur (S) serves as a Proxy Organic indicator, capturing organic-rich deposition. Redox-sensitive elements, including iron and manganese (Mn), suggest variations in oxygen availability linked to cycles of wetting and drying. Heavy Metals/Pollutants (e.g., Lead (Pb), zinc (Zn), and copper (Cu)) point to potential surface contamination, while atmospheric radioactive inputs are represented by thorium (Th).

Mapping these elemental categories allows for interpretations of both depositional and post-depositional processes, providing information about past environmental conditions (Davies et al., 2015). The elements which describe each elemental category are shown in Table 4.7 below.

Table 4.7 - Elemental categories and their associated elements identified through Portable X-ray Fluorescence (pXRF) analysis along Transect 4 on Horse Eye, after (Davies et al., 2015).

Elemental Category:	**Element(s):**
Coarse Clastic	Si, Ti, Zr
Fine Clastic	Rb, K, Al, Si
Redox	Fe, Mn, Cl
Carbonate	Ca, Sr
Proxy Organic	S
Heavy Metals/Pollutants	Pb, As, Zn, Cu, Cr, V, Sc, Nb
Atmospheric Radioactive	Th

4.3.6.1. Spatial and Elevation Relationships

Figure 4.19 provides a map view of Transect 4, showing the locations of the topsoil samples along the transect, which descends from the hilltop of the bedrock island toward lower elevations in the Levels. Figure 4.20 is a cross-sectional view which further illustrates Transect 4's profile, detailing the specific elevations at each sample. Topsoil samples were collected consistently from 0-10 cm depth, with elevations ranging from 4.3 m OD (HE23T4C1) to 1.48 m OD (HE23T4C4B). The pXRF data reveal notable correlations between elevation and sediment composition. Table 4.8 presents the pXRF data for topsoil samples (0-10 cm depth) from each of the locations: hilltop (4.3 m OD), mid-slope (2.4 m OD), and Levels (1.5 m OD).

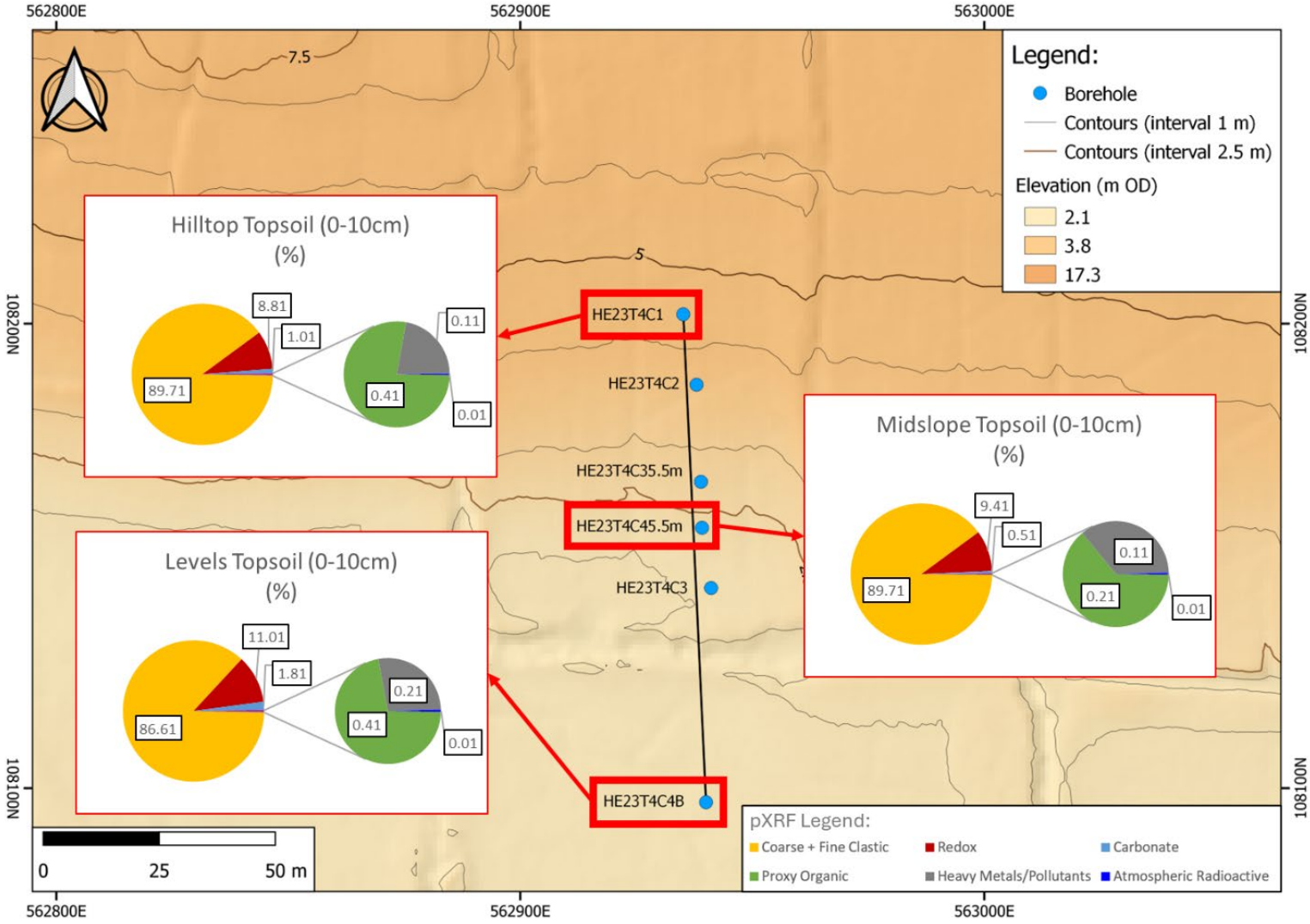


*Figure 4.19 - Map view of Horse Eye Transect 4 with sampling locations indicated along the topographic gradient from the hilltop of the bedrock island to the Levels. Each site along the transect is marked with its respective sampling depth and pie charts that display the relative proportions of each proxy (*Coarse + Fine Clastic, Redox, Carbonate, Proxy Organic, Heavy Metals/Pollutants, and Atmospheric Radioactive) at each location. This spatial overview provides context for understanding the relationship between a sample's spatial locations, elevation, and subsequent geochemical evaluation from the pXRF analyses.

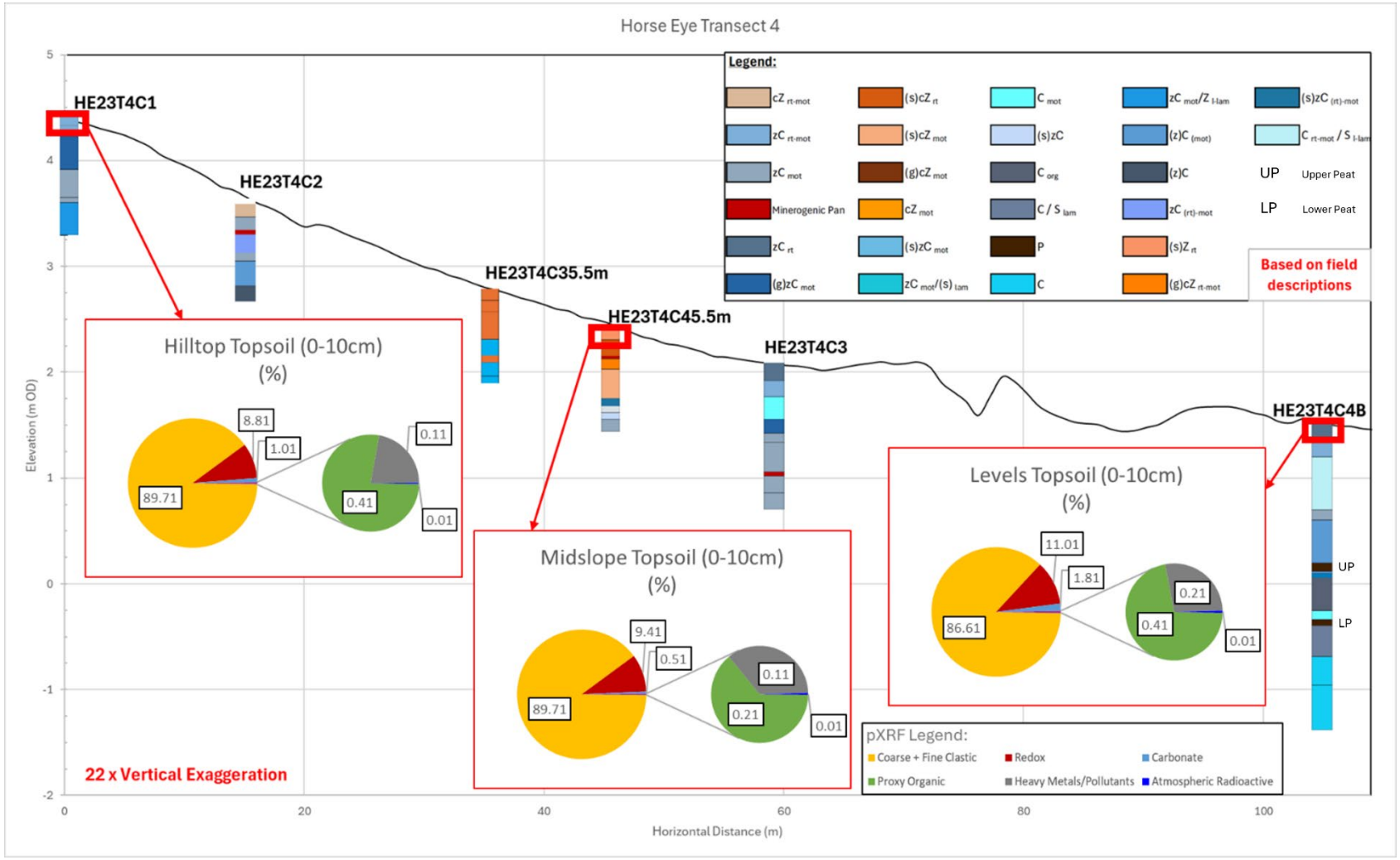


Figure 4.20 – Cross-section of Horse Eye Transect 4 showing the elevation profile and pXRF elemental composition of topsoil samples (0-10 cm depth) at the hilltop of Horse Eye, mid-slope of Horse Eye, and within the levels at the threshold of the bedrock island. Pie charts display the relative proportions of each proxy (Coarse + Fine Clastic, Redox, Carbonate, Proxy Organic, Heavy Metals/Pollutants, and Atmospheric Radioactive) at each location. The transect demonstrates the transition from higher to lower elevations (with a 22x Vertical Exaggeration) and associated geochemical variations in topsoil along the landscape.

For the Coarse + Fine Clastic category, which includes elements such as Silicon (Si), Titanium (Ti), and Zirconium (Zr) there is an increasing trend with decreasing elevation. The coarse + fine fraction rises from 135406.8 PPM at the hilltop to 145871.9 PPM in the levels at the transition from Horse Eye into the levels. Redox elements, represented by Iron (Fe), Manganese (Mn), and Chlorine (Cl), also increase with decreasing elevation, with values ranging from 13288.8 PPM at the hilltop to 18497 PPM at the levels. This trend suggests that reducing conditions are more prevalent in the lower-lying areas, likely due to increased water saturation.

Carbonate content, measured through elements like Calcium (Ca) and Strontium (Sr), displays a non-linear trend with elevation. Starting at 1573.9 PPM at the hilltop, carbonate content decreases to 833.2 PPM at the mid-slope, then peaks at 3103.4 PPM in the Levels. This pattern suggests that carbonate may accumulate more substantially in the lower portions of the landscape, though there is a notable decrease in content at the mid-slope location.

Proxy Organic content, represented by Sulphur (S), displays a similar pattern to carbonate content, with values dipping at the mid-slope before peaking at the Levels. Organic proxy values start at 560.4 PPM at the hilltop, decrease to 339.9 PPM at the mid-slope, and then rise to 666.1 PPM in the Levels. This trend suggests that organic matter, like carbonate, is more effectively preserved at both the hilltop and lower elevations.

The concentration of heavy metals and pollutants, which include elements such as Lead (Pb), As (As), and Zinc (Zn), increase with decreasing elevation. The Levels' topsoil has a value of 254.5 PPM, while the mid-slope and hilltop have lower concentrations at 188.6 PPM and 158.4 PPM, respectively. This trend suggests that heavy metals and pollutants may be more concentrated in surface layers at lower elevations, possibly due to runoff carrying these elements downslope, where they settle in lower-lying areas. Lastly, atmospheric radioactive content, represented by Thorium (Th), is only detectable in topsoil samples and increases with decreasing elevation in topsoil samples, peaking at 6.9 PPM at the Levels. The mid-slope has 3.3 PPM, while the hilltop decreases to 3 PPM. The presence

of atmospheric radioactive material only in the topsoil suggests that these elements are likely deposited by surfaces processes, such as atmospheric fallout, and accumulate in lower elevations where they are less subject to erosion.

Table 4.8 - Portable X-ray Fluorescence (pXRF) analysis of topsoil samples (0-10 cm) from Horse Eye Transect 4, showing elemental composition by proxy category (Coarse + Fine Clastic, Redox, Carbonate, Proxy Organic, Heavy Metals/Pollutants, and Atmospheric Radioactive) across varying elevations. The table highlights the relationship between elevation and elemental concentrations in the topsoil at hilltop, mid-slope, and in the Levels.

Sample	Lithocode	Depth (cm)	Elevation Range (m OD)	Coarse + Fine Clastic (PPM)	Redox (PPM)	Carbonate (PPM)	Proxy Organic (PPM)	Heavy Metals / Pollutants (PPM)	Atmospheric Radioactive (PPM)
HE23T4C1 Topsoil (Hilltop)	$zC_{rt\text{-}mot}$	0-10	4.3 – 4.2	135406.8	13288.8	1573.9	560.4	158.4	3
HE23T4C4 5.5m Topsoil (Mid Slope)	$(s)Z_{rt}$	0-10	2.4 – 2.3	138840.2	14496.4	833.2	339.9	188.6	3.3
HE23T4C4 B Topsoil (Levels)	zC_{rt}	0-10	1.48 - 1.38	145871.9	18497	3103.4	666.1	254.5	6.9

4.3.6.2. Depth and Composition Trends in Core HE23T4C4B

The pXRF analysis of core HE23T4C4B provides a detailed examination of elemental composition across different depths: the topsoil (0-10 cm), Upper Peat (120-130 cm), and Lower Peat (173-180 cm). This depth-focused analysis allows for an exploration of how geochemical trends shift between surface-rooted minerogenic layers and deeper, organic-

rich peat layers, revealing processes related to organic accumulation, sedimentary deposition, and reducing conditions.

As Davies et al. (2015) explains, the elements identified through pXRF can indicate the depositional environment and the conditions under which each layer was formed. Figure 4.21 below visually presents the pXRF data from core HE23T4C4B, illustrating the quantity of each geochemical proxy- Coarse + Fine Clastic, Redox, Carbonate, Proxy Organic, Heavy Metals/Pollutants, and Atmospheric Radioactive content- within the topsoil, Upper Peat, and Lower Peat layers. The visualization highlights the shifts in composition from the organic-rich, reducing environment in the peat layers to the mineral-dominated, oxidizing conditions in the topsoil.

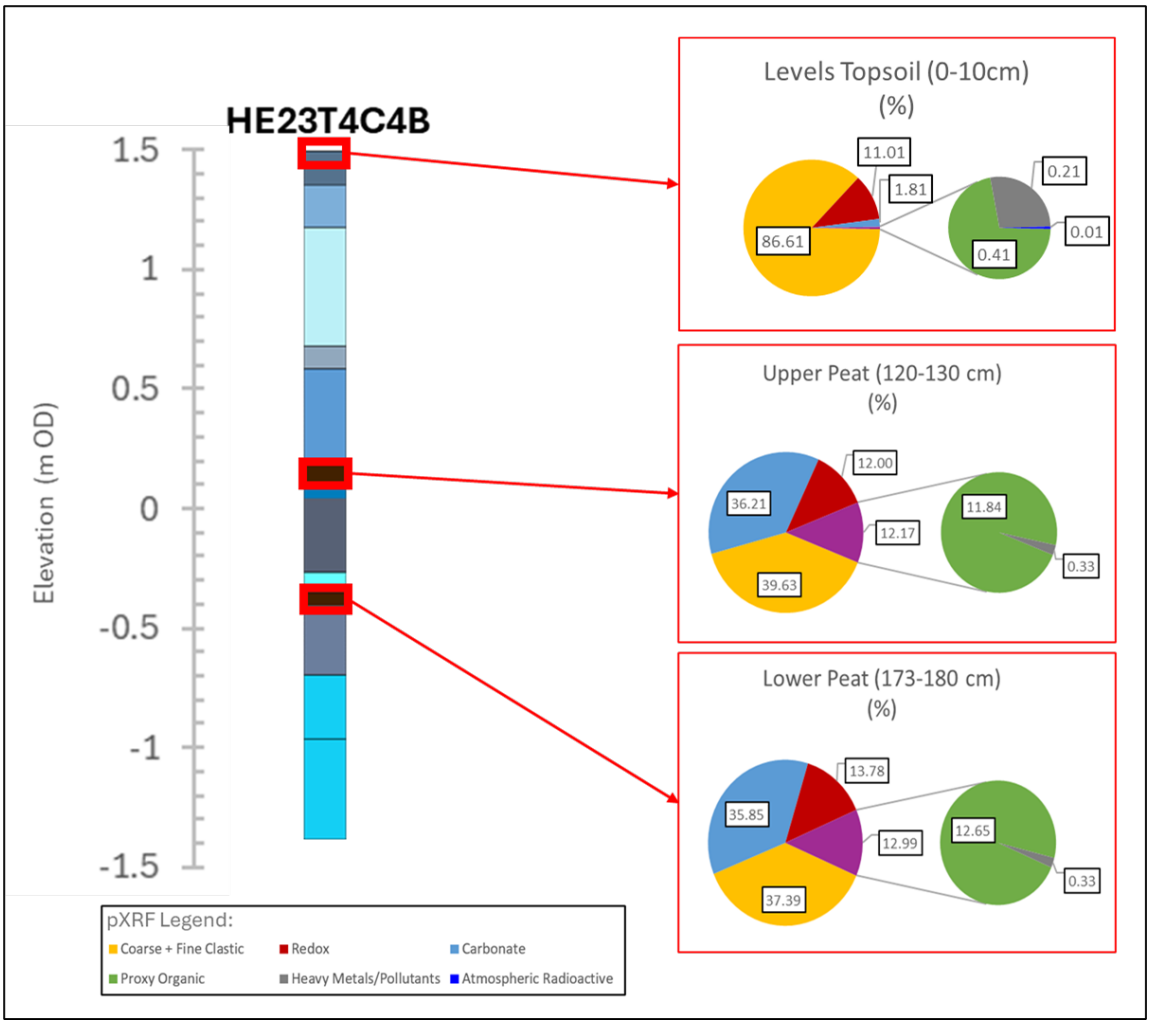


Figure 4.21 - pXRF analysis results for core HE23T4C4B, displaying the relative proportions of each geochemical proxy (Coarse + Fine Clastic, Redox, Carbonate, Proxy Organic, Heavy Metals/Pollutants, and Atmospheric Radioactive) across three depth intervals: topsoil (0-10 cm), Upper Peat (120-130 cm), and Lower Peat (173-180 cm).

The coarse + fine clastic category, which includes elements such as Ti, Si, and Zr, displays the most substantial increase from the deeper peat layers (Upper and Lower Peat) to the topsoil, reflecting the dominance of minerogenic material in the topsoil. In the Lower Peat, coarse + fine clastic content is at its lowest (10701.2 PPM), indicating limited clastic input in this organic-rich, reducing environment. Moving up to the Upper Peat, coarse + fine clastic content rises slightly to 12767.5 PPM, suggesting a gradual increase in minerogenic material as the depositional environment becomes slightly more mixed. The topsoil exhibits a drastic increase in in coarse + fine content, reaching 145871.9 PPM, reflecting a significant clastic input and surface exposure, likely due to ongoing mineral deposition.

This trend highlights a change in composition, with clastic material becoming predominant in the topsoil layer compared to peat layers.

Redox values, which indicate oxidation-reduction conditions, also increase significantly from the Lower Peat to the topsoil, suggesting a shift from stable, reducing conditions in the peat to oxidizing conditions at the surface. The Lower Peat has a redox content of 10261.2 PPM, indicating strong reducing conditions that favour organic matter preservation in this waterlogged layer. In the Upper Peat, redox values increase slightly to 11664.7 PPM, suggesting a transition toward slightly less stable conditions but still generally reducing. The topsoil shows the highest redox values at 18497 PPM, indicative of an oxidizing environment due to the surface exposure and oxygen availability that facilitate mineral oxidation and organic decomposition. This trend reveals a distinct environmental difference between the anaerobic peat layers and the aerated topsoil.

Carbonate content, represented by calcium and strontium, is the highest in the peat layers and decreases in the topsoil, indicating a difference in preservation conditions. The Lower Peat has the highest carbonate concentration at 3944.3 PPM, with the anaerobic, low-energy environment promoting stable carbonate preservation by minimizing dissolution and erosion processes. In the Upper Peat, carbonate content remains relatively high at 3864.7 PPM, though slightly lower, still benefiting from reduced leaching. In contrast, the topsoil exhibits a lower carbonate concentration at 3103.4 PPM, where exposure to dynamic, oxidizing conditions likely promotes carbonate loss due to organic matter decomposition and a related decrease in pH (Cochran et al., 2022; Jenkins & Hikida, 2011; Kibblewhite et al., 2015). This trend highlights the contrast between stable carbonate-preserving conditions in the peat layers and more variable conditions in the topsoil which lead to carbonate loss over time.

Proxy Organic content, represented by sulphur, provides a direct measure of organic material preservation, with values highest in the peat layers and significantly reduced in the topsoil. The Lower Peat shows high Proxy Organic values at 3621.2 PPM, reflecting substantial organic matter accumulation under reducing, waterlogged conditions. This

increases slightly in the Upper Peat to 3813.5 PPM, suggesting optimal organic preservation at this depth. However, in the topsoil, Proxy Organic content drops markedly to 666.1 PPM, consistent with increased biological activity, oxygen exposure, and decomposition processes that limit organic matter retention. This trend emphasizes the contrast between the organic-rich, anaerobic peat layers and the oxidizing surface layer, where organic content is diminished.

Heavy metals and pollutants, including elements like lead (Pb), zinc (Zn), and copper (Cu), show a pronounced difference between the topsoil and the peat layers, with higher concentrations in the topsoil. In the Lower Peat, heavy metal content is relatively low at 95.7 PPM, indicating minimal contamination in this deeper, organic-rich layer. The Upper Peat has a slightly higher concentration at 106.4 PPM, reflecting minor metal presence but still much lower than the topsoil. The topsoil exhibits the highest concentration of heavy metals and pollutants, at 254.5 PPM, likely due to surface contamination or recent environmental deposition. This distinct increase suggests that heavy metals tend to accumulate near the surface, with limited migration to the deeper layers, better preserving the lower peat from modern contamination.

Thorium (Th), the element representing atmospheric radioactive input, is only detected in the topsoil with a concentration of 6.9 PPM. The absence of measurable thorium in both the Upper and Lower Peat layers suggests that these layers have remained isolated from modern atmospheric deposition, retaining a composition indicative of older environmental conditions. The detection of Th solely in the topsoil implies surfaces processes such as atmospheric fallout are responsible for this input, with thorium unlikely to penetrate the organic-rich, protected peat layers below.

The pXRF analysis of core HE23T4C4B reveals distinct geochemical trends that align closely with variations in sediment composition and depth, from the minerogenic-rich topsoil to the organic-dominated peat layers. Table 4.9 provides a comprehensive overview of the elemental concentrations across each depth interval, highlighting the transitions in geochemical characteristics with depth. These patterns underscore the influence of

depositional and post-depositional conditions on elemental distributions within the core, reflecting shifts from surface-driven processes in the topsoil to stable, reducing conditions in the deeper peat layers.

Table 4.9 - Portable X-ray Fluorescence (pXRF) analysis of core HE23T4C4B, showing elemental concentrations across three depth intervals: Lower Peat (173 - 180 cm), Upper Peat (120 - 130 cm), and topsoil (0 - 10 cm). Each row provides the specific values for each geochemical proxy category: Coarse + Fine Clastic, Redox, Carbonate, Proxy Organic, Heavy Metals/Pollutants, and Atmospheric Radioactive, illustrating the changes in elemental composition with depth from the organic-rich peat layers to the mineral-dominated topsoil.

Sample	Lithocode	Depth (cm)	Elevation Range (m OD)	Coarse + Fine Clastic (PPM)	Redox (PPM)	Carbonate (PPM)	Proxy Organic (PPM)	Heavy Metals / Pollutants (PPM)	Atmospheric Radioactive (PPM)
HE23T4C4B Topsoil (Levels)	zC_{rt}	0-10	1.48 – 1.38	145871.9	18497	3103.4	666.1	254.5	6.9
HE23T4C4B Upper Peat (UP)	P	120-130	0.28 – 0.18	12767.5	11664.7	3864.7	3813.5	106.4	0
HE23T4C4B Lower Peat (LP)	P	173-180	(-0.24) – (-0.31)	10701.2	10261.2	3944.3	3621.2	95.7	0

Overall, the pXRF analysis reveals strong spatial and elevation-related trends across Horse Eye Transect 4, with decreasing elevation corresponding to increased organic matter, reducing conditions, and varying concentrations of clastic material and pollutants. These findings offer valuable insights into the transition from the mineral-rich, oxidizing environment of the topsoil to the organic, reducing conditions in the peat layers, highlighting how depth and elevation influence sediment composition. Together, these insights build a clearer picture of the environmental changes along the transect and emphasize the role of elevation in influencing depositional processes of sediment.

4.3.7. Loss on Ignition (LOI)

The Loss on Ignition (LOI) analysis for samples from Horse Eye Transect 4 provides insight into the moisture, organic, and carbonate content of sediment across different elevations and depths. This section first examines spatial and elevation trends across topsoil samples for Transect 4, then explores the depth- and composition-specific changes within a single core, HE23T4C4B, encompassing both topsoil and peat layers. It is important to note that the LOI samples are the same as those used in the portable X-ray Fluorescence (pXRF) analysis (Section 4.3.6 Portable X-ray Fluorescence (pXRF) Analysis), and thus the sample locations shown in the red boxes in the figures also apply here. For spatial and depth reference, refer to figures 4.19, 4.20, and 4.21 in Section 4.3.6.

4.3.7.1. Spatial and Elevation Relationships

Table 4.10 presents LOI data for topsoil samples (0-10 cm) collected at three elevations along Transect 4: hilltop (4.3 m OD), mid-slope (2.4 m OD), and the lowest elevation recorded within the Levels (1.48 m OD). This data provides insight into the comparison between moisture, organic, and carbonate content across a range of elevations, offering knowledge into how these properties vary along the landscape.

Table 4.10 - Loss on Ignition (LOI) data for topsoil samples (0-10 cm) collected from three elevations along Horse Eye Transect 4, including hilltop, mid-slope, and in the Pevensey Levels. The table displays elevation range, moisture, organic, and carbonate content.

Sample	Depth (cm)	Elevation Range (m OD)	Moisture content (%)	Organic content (%)	Carbonate content (CO3) (%)
HE23T4C1 Topsoil (Hilltop)	0-10	4.3 – 4.2	37.8	23.5	1.59
HE23T4C45.5m Topsoil (Mid Slope)	0-10	2.4 – 2.3	40.8	19.4	1.63
HE23T4C4B Topsoil (Levels)	0-10	1.48 - 1.38	33.4	19.9	2.01

Moisture content shows variability across the transect, with the mid-slope topsoil sample having the highest moisture content at 40.8%, followed by the hilltop at 37.8% and the lowest in the Levels at 33.4%. This demonstrates a pattern where mid-slope areas

retain more moisture compared to higher or lower elevations, consistent with findings by Tromp-van Meerveld & McDonnell (2006), who observed that mid-slope sections with deeper soils retained higher soil moisture due to greater water storage capacity. The lower moisture content at the hilltop may be due to its thin sediment cover when compared to sediment thickness observed mid-slope and within the levels. The thin sediment at the hilltop dries faster due to its thickness and greater exposure to wind and sun. In contrast, the low moisture content in the Levels may be influenced by current-day drainage infrastructure, which facilitates rapid water removal from low-lying areas through pumping stations positioned throughout the Levels. Together, these factors suggest that mid-slope topsoil samples accumulate runoff due to their intermediate topographic location and greater soil depth, while the hilltop and Levels samples experience reduced moisture retention for differing reasons.

Organic content also varies along the transect, with the hilltop showing the highest organic content at 23.5%, while the mid-slope and Levels samples are slightly lower at 19.4% and 19.9%, respectively. This trend indicates that organic matter in the topsoil decreases slightly as elevation decreases, which may be influenced by surface runoff or variations in vegetation cover across the transect, where the hilltop features denser and an increased amount of vegetation, such as thick grass, shrubs, bushes, and trees, while the mid-slope and Levels samples have sparse vegetation and are more exposed to the elements, including wind, rain, and surface runoff, which can erode or redistribute organic material and reduce its accumulation in the topsoil.

Carbonate content also varies with elevation. The highest carbonate content in the topsoil is found in the Levels (2.01%), with lower values at the mid-slope (1.63%) and hilltop (1.59%). This pattern indicates that carbonate content increases as elevation decreases. This variation is relatively small but measurable, with the Levels showing a carbonate content approximately 0.4% higher than the mid-slope and 0.42% higher than the hilltop. This increase in carbonate content at lower elevations compared to higher elevations may result from the accumulation of carbonate-rich material through runoff or

leaching processes from higher elevations, where carbonate is more easily transported downslope.

4.3.7.2. Depth and Composition Trends in Core HE23T4C4B

To explore LOI properties with depth and composition, Table 4.11 presents LOI data for a single core, HE23T4C4B, including samples from the topsoil (0-10 cm), Upper Peat (120-130 cm), and Lower Peat (173-180cm). This depth and composition focused analysis highlights the differences in moisture, organic, and carbonate content between the surface minerogenic topsoil and deeper, organic-rich peat layers.

Table 4.11 - Loss on Ignition (LOI) data for core HE23T4C4B, showing elevation range, moisture, organic, and carbonate content across three depth intervals: topsoil (0-10 cm), Upper Peat (120-130 cm), and Lower Peat (173-180 cm). This table illustrates depth-specific variations in LOI analysis, reflecting compositional differences between the minerogenic-rich topsoil and the organic-rich peat layers.

Sample	Depth (cm)	Elevation Range (m OD)	Moisture content (%)	Organic content (%)	Carbonate content (CO3) (%)
HE23T4C4B Topsoil (Levels)	0-10	1.48 – 1.38	33.4	19.9	2.01
HE23T4C4B Upper Peat (UP) 120-130	120-130	0.28 – 0.18	76.1	81.1	2.25
HE23T4C4B Lower Peat (LP) 173-180	173-180	(-0.24) – (-0.31)	69.5	59.0	2.22

The moisture content exhibits an increase in both depth and composition as the samples shift from minerogenic topsoil to organic-rich peat layers. The Lower Peat's (173-180 cm) moisture content is high at 69.5%, indicative of its dense, non-woody composition, which retains significant moisture under anaerobic conditions. Moving upward to the Upper Peat (120-130 cm), the moisture content rises further to 76.1%, reflecting the increased water retention capacity of woody peat, which has a more porous, fibrous structure. This fibrous composition allows woody peats to retain significantly more moisture compared to more decomposed, denser, non-woody peats, which exhibit lower water retention due to reduced porosity (Szajdak et al., 2011). The topsoil (0-10 cm), composed primarily of mineral material, has the lowest moisture content at 33.4%,

consistent with its exposure to surface drying and limited capacity for water retention. This trend suggests that both organic composition and depth-related anaerobic conditions in the peat layers significantly enhance moisture retention, with highest values in woody peat due to its structural porosity.

Organic content shows a distinct increase with depth as the sediment becomes more enriched in organic material. In the Lower Peat, organic content is substantial at 59%, reflecting conditions favorable for organic accumulation in a dense, non-woody matrix. The Upper Peat, which is woody and at a slightly shallower depth, exhibits the highest organic content at 81.1%. The topsoil has the lowest organic content at 19.9%, characteristic of its mixed composition with a greater proportion of minerals and exposure to oxidative conditions that promote organic decomposition. This progression from deep, organic-dense peat to the predominantly minerogenic topsoil highlights the role of both depth and composition in preserving organic matter, with woody peat providing the most conducive environment for organic retention.

Carbonate content remains relatively consistent across depths, with only small measurable differences observed between layers. The Lower Peat has a carbonate content of 2.22%, closely followed by the Upper Peat at 2.25%, indicating a difference of 0.03% in carbonate retention between both these organic-rich layers. In contrast, the topsoil has a lower carbonate content at 2.01%, reflecting a difference of 0.21% compared to the Upper Peat. This reduction of carbonate content in the topsoil may result from its dominantly minerogenic composition and exposure to leaching processes at the surface. Although these percentage differences are relatively small compared to variations in other proxies (e.g., organic content or moisture content), they suggest that carbonate content is generally stable down the profile for borehole HE23T4C4B. The increase in carbonate retention within the peat layers may be attributed to anaerobic conditions that help prevent carbonate dissolution. The consistency of carbonate content across these three layers highlights the limited impact of depth on carbonate distribution in this core, with composition likely playing a larger role in its stability.

In summary, the LOI analysis across Horse Eye Transect 4 reveals distinct patterns in moisture, organic, and carbonate content that vary with both elevation and depth, highlighting the influences of landscape position and sediment composition. Spatially, topsoil samples collected at varying elevations show trends in moisture and organic content that suggest mid-slope areas retain slightly more moisture, while organic content is slightly higher at the hilltop. When examined by depth in core HE23T4C4B, the organic-rich peat layers exhibit more moisture and organic matter retention, with the woody Upper Peat layer showing the highest values. Carbonate content remains relatively consistent across both spatial and depth profiles, with minor variations observed. Together, these results provide insight into how moisture, mineralogic composition, and organic matter vary across the landscape (elevation) and with depth in HE23T4C4B, characterizing the differences between sediment types such as organic-rich peat, topsoil, and minerogenic layers within Transect 4.

4.3.8. X-Ray Diffraction Analysis (XRD) of Core HE23T4C4B

The X-ray diffraction (XRD) analysis of core HE23T4C4B provides a detailed understanding of the mineralogical composition across various depths, focusing on major minerals such as quartz, calcite, and illite, alongside other trace minerals. This analysis aids in the interpretation of depositional processes, energy conditions, and environmental changes, and provenance. Figure 4.22 below illustrates the stratigraphic profile of core HE23T4C4B showing the lithologic units described in the field. The sampling depths where XRD analysis was performed are highlighted (30cm, 40cm, 65cm, 75cm, 95cm, 110cm, 148cm, 160cm, 190cm, 196cm, 215cm, and 235cm), giving a visual context to the cores sampling strategy.

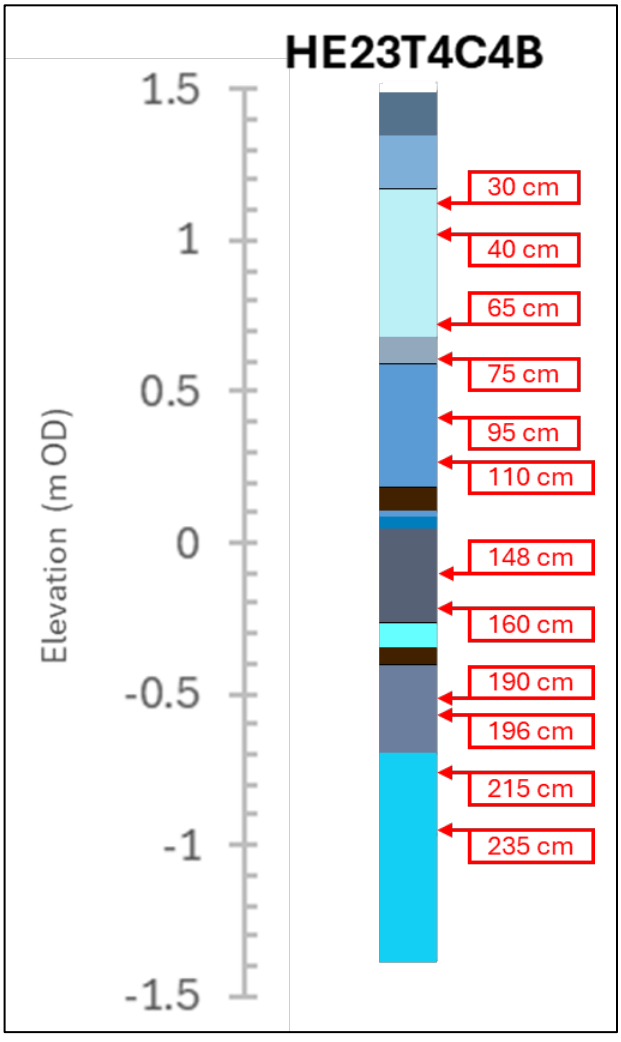


Figure 4.22 - Sampling depths of XRD analysis for core HE23T4C4B, providing context for the sampled locations, showing lithological units defined in the field.

Samples were collected at two intervals within each major stratigraphic unit, specifically targeting locations near intervals with increased sand content and intervals which observed sedimentary structures. These features served as key indicators of the boundaries and characteristics of major units. This approach provides a consistency check within each unit, enhancing data reliability and allowing for confirmation of observed trends. By sampling both shallow and deep intervals, this strategy captures shifts in mineral composition that may reflect changes in depositional environment, sediment source, and energy level. Table 4.12 summarizes the XRD results, presenting the mineral percentages at each sampled depth, which serves as a foundation for a detailed interpretation of mineralogical trends within the core. These trends can infer shifts in sedimentary processes, sediment origin, depositional environments, and potential climatic influences over time. This section delves into the observed patterns of quartz, calcite, illite, and other minerals observed through XRD analysis.

Table 4.12 - A summary table of the mineral percentages at each sampled depth, showing the variation of primary minerals (quartz, calcite, and illite) and trace minerals throughout core HE23T4C4B.

Depth (cm)	Quartz (%)	Calcite (%)	Illite (%)	Other Minerals (%)
30	62.8	-	-	Anorthoclase (35.8), Biotite (1.1), Montmorillonite (0.3)
40	80.1	17.4	-	Franklinite (1.1), Birnessite (0.7), Et2NH2 (0.3), Manganite (0.4)
65	74.3	24.1	-	Birnessite (1), Montmorillonite (0.6)
75	58.8	21.2	-	Biotite (20)
95	36.2	9.6	44	Kaolinite (10.2)
110	39.9	13.2	46.9	-
148	38.5	13.3	-	Muscovite (31.2), Albite (15.5), Orthoclase (1.5)
160	38.5	-	33.3	Albite (28.2)
190	45.2	17.1	37.7	-
196	47.5	15.1	-	Muscovite (26.2), Orthoclase (11.1)
215	47.4	20.1	-	Phengite (32.1), Alabandite (0.4)
235	38.1	6.4	54.1	Guidottiite (0.7), Biotite (0.6)

Quartz, calcite, and illite were selected for detailed analysis based on their implications in interpretating depositional conditions and energy levels. Quartz is often associated with high-energy depositional environments and serves as an indicator of such conditions in sedimentary deposits (Tucker, 2001). Calcite is commonly linked to marine or biogenic inputs, contributing to the interpretation of marine influence within sediment profiles (Flugel, 2010). Illite, a clay mineral, is typically indicative of low-energy depositional settings and can signal periods of reduced sediment transport (Chamley, 1989). Figure 4.23 displays the quartz, calcite, and illite distribution relative to depth, allowing for a comparative trend analysis.

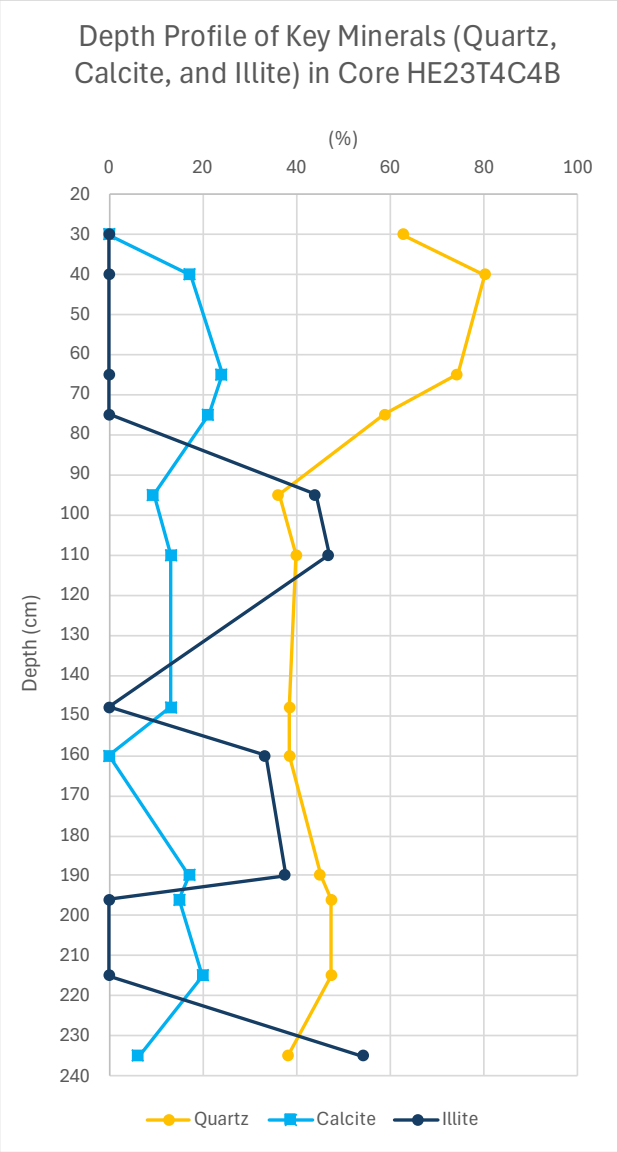


Figure 4.23 - A line graph showing the depth profile of quartz, calcite, and illite, allowing visualization of the mineral trends with increasing depth in the core.

Quartz is the dominant mineral across most sampled depths, ranging from 36.2% at 95 cm to 80.1% at 40 cm. The abundance of quartz peaks in the shallower depths, from 30 cm to 75 cm, averaging around 69%, reflecting potentially high-energy deposition, likely influenced by terrestrial or nearshore marine processes. Below 95 cm, the abundance of quartz displays lower and more stable concentrations in the deeper depths, with an average of approximately 41.4%, suggesting a shift to a relatively consistent, low-energy environment. This decrease aligns with finer-grained sediment deposition in deeper intervals (shown in Section 4.3.5. Laser Diffraction Grain Size Analysis), indicative of calmer, more stable depositional conditions.

Calcite exhibits a trend with depth, showing higher percentages in the upper depths (40-75 cm) with an average of 20.9%. The highest concentration of calcite is observed at 65 cm (24.1%), while the lowest concentration, excluding the absence of calcite at both 30 and 160 cm, is at 235 cm (6.4%). Below 75 cm, calcite concentrations remain relatively consistent down the profile, averaging 11.9% from 95 cm to 235 cm, though there are minor fluctuations. The steadiness suggests that calcite sources and depositional conditions were stable, with minor fluctuations, possibly reflecting a consistent level of marine input through the lower depths.

Illite displays variation with depth, primarily concentrated in the deeper part of the core with less or no concentration in the upper parts of the core. The highest percentage of illite is found at the deepest sampled interval, 235 cm (54.1%), while the shallowest sampled sections above 95 cm lack illite entirely. This absence in the upper depths suggests a distinct shift in depositional energy or sediment source in the shallower intervals. Illite concentrations are significant in intervals at 235 cm, 190 cm, 160 cm, 110 cm, and 95 cm, where it averages 43.2%, indicating low-energy depositional phases or indicating humid conditions. The minimum concentration is effectively 0% in the upper sections and within intervals in between the illite-rich layers, signifying periods where conditions did not favour its deposition.

To provide a more comprehensive view of the mineralogical composition, Figures 4.24 and 4.25 below illustrate the breakdown in percentage (%) of all minerals identified at each sampled depth. These pie charts offer insight into the relative abundance of primary minerals (quartz, calcite, and illite), as well as other minerals that were observed including those exceeding 10%.

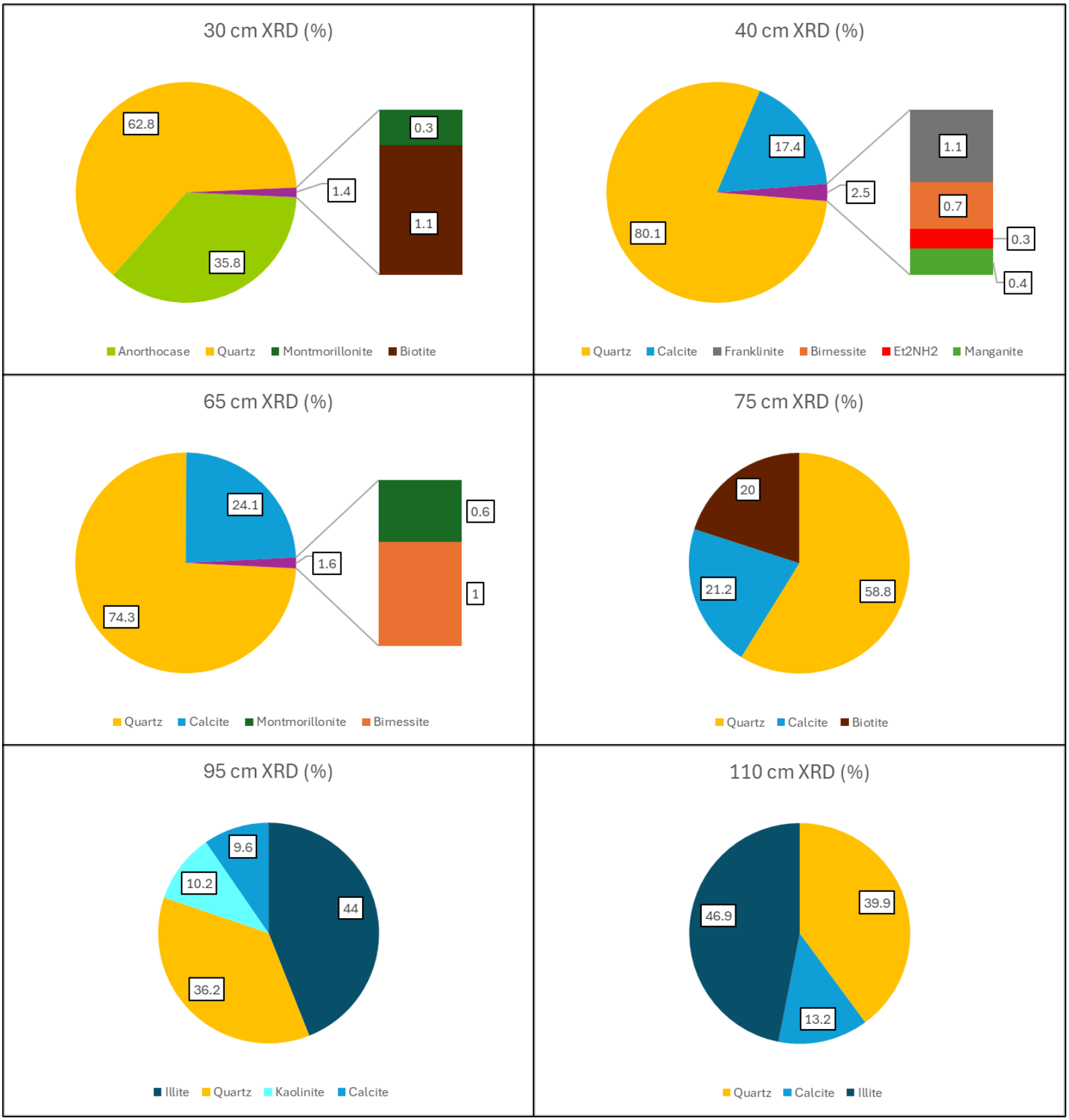


Figure 4.24 - XRD mineral composition pie charts for each sampled interval in core HE23T4C4B from 30 cm to 110 cm, showing the relative percentages of all identified minerals

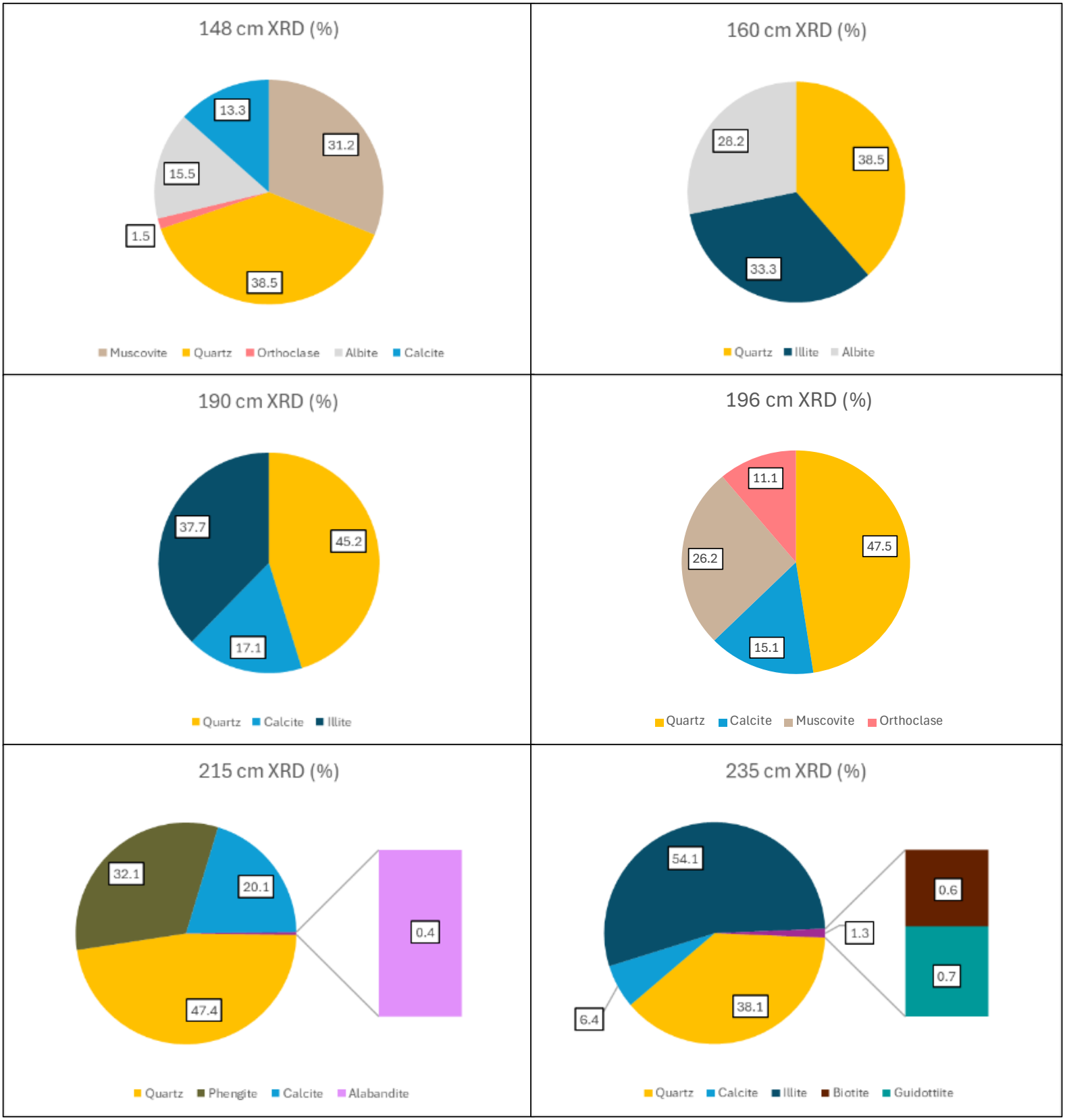


Figure 4.25 - XRD mineral composition pie charts for each sampled interval in core HE23T4C4B from 148 cm to 235 cm, showing the relative percentages of all identified minerals

In addition to quartz, calcite, and illite, several other minerals were identified, some of which were present in significant amounts. These include muscovite, kaolinite, albite, orthoclase, anorthoclase, biotite, and phengite, each contributing unique information regarding the depositional environment and sediment sources. Muscovite appears prominently at 148 cm and 196 cm, with a peak concentration of 31.2% at 148 cm, suggesting intervals of lower energy deposition where fine-grained mica could accumulate. Kaolinite, found primarily at 95 cm with a concentration of 10.2%, is often associated with intense weathering processes and potentially indicates an episode of sediment influx from a highly weathered terrestrial source, or an episode of weathering.

Albite, orthoclase, and anorthoclase, all feldspar minerals, were present at notable depths within the core. Albite peaks at 28.2% at 160 cm and is observed at 148 cm (15.5%), while orthoclase is recorded at 15.5% at 148 cm and 11.1% at 196 cm. Anorthoclase, with a significant concentration of 35.8% at 30 cm, is also a type of feldspar, often associated with igneous rock sources. The presence of these feldspars suggests episodes of sediment deposition from sources rich in feldspar, possibly transported from adjacent terrestrial areas or resulting from erosion of specific lithologies. Their abundance could also indicate periods of relatively high-energy conditions, as feldspars are typically more resistant to weathering and can withstand transport. Their abundance in these layers could indicate episodes of coarser, more resilient sediment influx.

Phengite and biotite, both mica minerals, contribute significantly to the mineral composition at various depths, with phengite reaching 31.2% at 215 cm and biotite recorded at multiple depths, including 20% at 75 cm and smaller amounts at 30 cm and 235 cm. The presence of these minerals may indicate low-energy depositional settings conducive to fine-grained mineral accumulation, with biotite's occurrence potentially suggesting episodic inputs from a weathered igneous or metamorphic source. The combination of phengite and biotite reflects shifts in sedimentary inputs that could indicate differing geologic sources influencing the depositional environment.

In addition to the major and significant secondary minerals observed, several trace minerals were identified in minimal amounts, including franklinite, montmorillonite, manganite, and guidottiite. Although these minerals each occur in low concentrations, often below 2%, their presence adds more information to the mineral profile of core HE23T4C4B. Trace amounts of montmorillonite (identified at 30 cm and 65 cm), a clay mineral, could suggest localized depositional conditions with limited weathering, while manganite (40 cm) and franklinite (40 cm and 65 cm), oxides of manganese and zinc, might indicate minor influences of geochemical conditions or mineral inputs from surrounding environments. Guidottiite (235 cm) is present only at the deepest sample, possibly reflecting unique geochemical conditions at this depth. These minerals are less indicative of broad depositional trends but may highlight occasional geochemical variations or brief environmental shifts within the sediment profile. While they do not significantly impact the overall mineralogical interpretation, acknowledging their presence adds compositional detail to the analysis of the core.

The XRD analysis of core HE23T4C4B reveals a mineralogical profile that reflects shifts in depositional environments, sediment sources, and energy conditions over time. The dominance of quartz in shallower intervals suggests relatively higher-energy conditions likely influenced by terrestrial or nearshore sources, while the consistent presence of calcite across depths implies a stable, ongoing marine influence. Illite's concentration in lower depths points to low-energy, fine-grained deposition, indicating more stable, reducing conditions. These phases of illite concentration typically align with higher percentages of silt and clay within the matrix. Additional minerals, including muscovite, kaolinite, albite, orthoclase, anorthoclase, biotite, and phengite, further highlight shifts in sediment inputs and episodic changes in environmental conditions. Trace minerals, though limited in concentration, provide additional detail to the core's mineral profile and hint at occasional geochemical fluctuations. Together, these mineralogical patterns provide a foundation for interpreting the paleoenvironmental conditions and the processes that shaped the stratigraphy of core HE23T4C4B. It is important to note, however, that potential errors may have influenced the results of the XRD analysis. Specifically, the collection of

small sediment samples for XRD analysis may have inadvertently included larger grains or sand grains from nearby laminations, particularly when distinguishing the finer matrix material in close proximity to coarser sediments. Additionally, the process of finely powdering the matrix material using a mortar and pestle could have introduced further contamination from crushed sand grains. These factors may have led to an overestimation of quartz content in some samples, skewing interpretations of depositional environments, particularly in intervals where quartz content was used to infer higher-energy depositional conditions. Recognizing these limitations is important for contextualizing results and interpretations.

4.3.9. Stratigraphic Units of Core HE23T4C4B

Core HE23T4C4B was selected to represent the broader depositional environment for Horse Eye because it displays a diverse range of facies and compositions, including variations in mineralogical and organic content, as observed in the field through descriptions and photographs. Other boreholes collected along Transect 4 on Horse Eye exhibited similar descriptions in their upper layers, primarily orange-mottled clayey silt, to those observed in the upper layers of HE23T4C4B. Given HE23T4C4B's greater depth and wider range of facies and compositions, it was considered the most suitable core to represent the broader depositional variability of Horse Eye. This core was divided into five primary stratigraphic units, which are further subdivided based on variations in sediment composition, texture, colour, and sedimentary structures. Laboratory proxies including pXRF, LOI, XRD, and laser diffraction grain size analysis were utilized with field observations and confirm stratigraphic boundaries. Differentiation of units and sub-units with similar field descriptions was achieved by integrating the results of these laboratory analyses. These analyses were used to identify unique compositional attributes. The units and sub-units which describe core HE23T4C4B are shown in Table 4.13, and the observed characteristics for each unit will be summarized in this section.

Table 4.13 - Stratigraphic units of core HE23T4C4B.

Unit	Sub-Unit	Depth (cm)	Depth (m OD)	Stratigraphic Description
5. Predominantly Terrestrial, Sandy clayey silt	5(d). Topsoil	0 – 26	1.48 – 1.22	**Sandy clayey silt** Brown sandy clayey silt with organic material and roots
	5(c). Upper Terrestrial	26 – 47	1.22 – 1.01	**Upper clayey sandy silt** Greenish grey clayey silt with orange mottling and lenticular laminations of coarse sand.
	5(b). Middle Terrestrial	47 – 86.5	1.01 – 0.615	**Lower Clayey sandy silt** Very stiff greenish grey clayey sandy silt with orange mottling
	5(a). Lower Terrestrial	86.5 – 119	0.615 – 0.29	**Upper mottled clayey silt** Stiff greenish grey clayey silt with orange mottling
4. Upper Peat	-	119 – 127	0.29 – 0.21	**Upper Peat** Partially decomposed very dark black fibrous woody peat with large wood fragments.
3. Transition Unit	3(b). Upper Marine-dominant	127 – 165.5	0.21 – (-0.175)	**Clayey sandy silt with organic material** Transitional mix of sticky clayey sandy silt with fibrous organic material and wood fragments, dark greenish grey in colour
	3(a). Lower Terrestrial-dominant	165.5 – 173	(-0.175) – (-0.25)	**Lower mottled clayey silt** Stiff greenish grey clayey silt with orange mottling
2. Lower Peat	-	173 – 180	(-0.25) – (-0.32)	**Lower Peat** Very dry fine fibrous dark brown peat layer
1. Predominantly Marine, Lower clayey silt	1(b). Upper Marine	180 – 201	(-0.32) – (-0.53)	**Clayey silt with sand laminations** Dark greenish grey, very sticky clayey silt matrix with distinct (~1-2mm) coarse sand laminations
	1(a). Lower Marine	201 – 280	(-0.53) – (-1.32)	**Clayey silt with shell fragments** Dense and sticky, homogenous clayey silt, greenish grey in colour with shell fragments and/or manganese nodules

Unit 1: Predominantly Marine

- Sub-Unit 1(a): Lower Marine (201–280 cm, -0.53 to -1.32 m OD)
  This basal unit consists of a dense and sticky, homogeneous clayey silt matrix with a greenish-grey colour (Munsell: 5GY 5/1) and a high plasticity. Shell fragments and/or manganese nodules (approximately 1 mm) are abundant within this layer, indicating an environment with stable, low-energy marine conditions. The presence of shell material suggests proximity to a shallow marine or intertidal setting, where fine sediments could settle without significant disturbance. Grain size analysis confirmed a dominance of fine silt with minimal sand, correlating with low-energy environments. XRD analysis revealed a moderate quartz concentration (approximately 43%) and a high illite concentration (approximately 54%), while a smaller concentration of calcite suggests limited biogenic inputs, supporting a prolonged deposition under calm marine conditions, with minimal terrestrial influence or depositional energy variations.
- Sub-Unit 1(b): Upper Marine (180–201 cm, -0.32 to -0.53 m OD)
  This sub-unit transitions to a dark greenish grey (Munsell: 5GY 4/1) very sticky clayey silt with a high plasticity, with distinct coarse sand lamination. These sand laminations are approximately 1-2 mm thick and are slightly inclined. These laminations, identified through field observations, and confirmed by grain size analysis, suggest episodic high-energy depositional events, such as storm surges or tidal influxes, which temporarily increased sediment transport and deposited coarser particles into the fine-grained marine matrix. XRD data show an increase in quartz, muscovite, and orthoclase, corresponding to the sandier intervals, while illite remains prevalent. These features indicate a shallowing phase, a shift toward a more proximal marine environment compared to unit 1a below, potentially moving towards a more dynamic nearshore environment as water depth decreased and energy conditions became more variable. This transition may reflect a regression of sea-level or progradation of the coastline, allowing coarser sediment to settle in areas previously dominated by finer marine deposits.

Unit 2: Lower Peat (173–180 cm, -0.25 to -0.32 m OD)

This unit comprises a very dark brown, fine fibrous peat layer, rich in organic material but does lack any visible wood fragments. The high organic content identified through LOI indicates a marshy or paludal environment, marking a phase of terrestrialization within the predominantly marine sequence. The peats fine, fibrous texture and well-humified nature, supported by pXRF results indicating elevated calcium, potentially from biogenic sources, suggests moderate to high decomposition (Szajdak et al., 2011).

Unit 3: Transition Unit (127–173 cm, 0.21 to -0.25 m OD)

This unit is characterized by a transition between marine and terrestrial influences, divided into two sub-units that reflect shifts in the depositional environment:

- Sub-Unit 3(a): Lower Terrestrial-Dominant (165.5–173 cm, -0.175 to -0.25 m OD)
  This sub-unit consists of a stiff greenish grey (Munsell: 5GY 5/1) clayey silt with orange mottling (Munsell: 10YR 6/6). The orange mottling indicates fluctuating groundwater conditions and intermittent oxidation. Grain size analysis confirmed the dominance of finer silt and clay fractions. This layer marks a shift from primarily marine to more terrestrial conditions within the transition unit.
- Sub-Unit 3(b): Upper Marine-Dominant (127–165.5 cm, 0.21 to -0.175 m OD)
  This sub-unit is a dark greenish grey (Munsell: 5GY 4/1) clayey sandy silt with organic material wood fragments interspersed display a mixture of marine and terrestrial characteristics. Grain size analysis revealed an increased sand content relative to Sub-Unit 3(a), alongside organic matter. XRD data displayed an increase in albite and muscovite, aligning with an increase in grain size, as well as an abundance of illite and calcite, aligning with nearshore marine conditions. The sticky consistency and high plasticity suggest lower-energy, nearshore marine conditions, with organic material and fine wood fragments indicating occasional terrestrial input. The presence of both marine and terrestrial sediments reflects a transitional depositional phase.

Unit 4: Upper Peat (119–127 cm, 0.29 to 0.21 m OD)

This unit is comprised of a dry, very dark black peat, moderately to highly decomposed, with a fine fibrous texture and visible wood fragments. The level of decomposition, confirmed by LOI, which indicated high organic content consistent with moderate to high decomposition observed in the field. pXRF results indicated elevated calcium and phosphorus concentrations, consistent with biogenic accumulation. The high level of decomposition suggests a moderate to high humification, indicating a well-developed peat layer with reduced moisture. This layer indicates a marshy or peat-forming depositional environment, likely indicating organic accumulation within a stable terrestrial environment.

Unit 5: Predominantly Terrestrial (0–119 cm, 1.48 to 0.29 m OD)

This unit transitions to a more consistent terrestrial environment, with sub-units reflecting variations in sediment composition and colour due to exposure and soil formation processes:

- Sub-Unit 5(a): Lower Terrestrial (86.5–119 cm, 0.615 to 0.29 m OD)
  This upper mottled clayey silt is stiff and is characterized by a greenish grey (Munsell: 5GY 5/1) colour with orange mottling (Munsell: 10YR 6/6), this orange mottling indicates variations in groundwater saturation. Grain size analysis showed silt and clay as the predominant grain size fractions, and XRD identified the primary minerals in this unit as quartz, illite, calcite, and kaolinite. The fine grain size and the abundance of clay minerals within the sediment indicates slower drainage, consistent with redox processes which align with a stable terrestrial depositional environment.
- Sub-Unit 5(b): Middle Terrestrial (47–86.5 cm, 1.01 to 0.615 m OD)
  This sub-unit consists of lower clayey sandy silt, it is very stiff, greenish grey (Munsell: 5GY 5/1) in colour with orange mottling (Munsell: 10YR 6/6). Grain size analysis shows a predominance of silt with the addition of coarse sand, this allows for slightly better drainage and the development of orange mottles during periods of drying and exposure to oxygen.

- Sub-Unit 5(c): Upper Terrestrial (26–47 cm, 1.22–1.01 m OD)

  The upper terrestrial layer is composed of a very stiff greenish grey (Munsell: 5GY 5/1) clayey sandy silt with orange (Munsell: 10YR 6/6) mottle, distinguished by lenticular laminations of coarse sand interspersed. These lenticular laminations suggest episodic high-energy depositional events, such as stormwater influx or fluvial processes impacting a terrestrial depositional environment. Grain size analysis confirmed the sand-rich nature of these lenticular laminations, while XRD indicated mixed mineralogical composition. The orange mottling reflects oxidation during periods of exposure and drying, indicative of a dynamic near-surface depositional environment.
- Sub-Unit 5(d): Topsoil (0–26 cm, 1.48–1.22 m OD)

  This layer consists of a dark greyish brown (Munsell: 10YR 4/3) sandy clayey silt with organic material and rootlets. It represents the modern ground surface, where active soil formation processes, such as organic material have accumulated, as well as root activity. LOI confirmed high organic content, and pXRF analysis revealed nutrient accumulation through an increase in phosphorus and potassium, linked with organic matter breakdown and nutrient cycling, consistent with modern biological activity within a stabilized terrestrial environment.

The stratigraphic units and sub-units of core HE23T4C4B were defined using a combination of field observations and laboratory analyses, including pXRF, LOI, XRD, and grain size analysis. Key indicators such as sediment colour, texture, and sedimentary structures provided the initial framework for unit designation, while laboratory proxies enhanced and reinforced the unit division and interpretation.

Grain size analysis was fundamental in differentiating unit boundaries and correcting the initial percentages of sand, silt, and clay which were estimated in the field. This analysis highlighted shifts from fine clayey silt in low-energy marine conditions to sandier compositions associated with higher-energy depositional influences. XRD data provided mineralogical context, linking variations in quartz, calcite, illite, feldspars, and mica minerals to depositional settings and potential sediment provenance. LOI identified

organic content, particularly in peat layers and in the topsoil, confirming stages of terrestrialization and levels of decomposition. pXRF analysis complemented this by highlighting elevated calcium and phosphorus levels, which are associated with biogenic activity and nutrient cycling (Louhisuo et al., 2024).

Units with similar stratigraphic descriptions, such as the upper and lower clayey silts in Unit 5, were distinguished through specific features additional to their composition. For instance, the presence of lenticular sand laminations in sub-unit 5(c) indicated a contrast with the finer-grained, stable conditions in sub-unit 5(a). This differentiation was achieved through the combined application of grain size analysis, field observations of sedimentary structures, and mineralogical analysis through XRD. The integration of these methods provided a detailed record of environmental transitions and sedimentary processes. Each unit reflects a unique phase in the fluctuation between marine and terrestrial depositional processes, with sub-units capturing a finer scale of variability. This multi-proxy approach outlines the complexity of the depositional history of Horse Eye.

4.3.10. Geochronology Results

This section presents the geochronologic results from the AMS C^{14} age dating conducted on HE23T4C4B, as well as their corresponding age-depth modelling results. Radiocarbon ages were obtained on two primary peat layers within the core (Upper Peat – Unit 4, 119 – 127 cm; and Lower Peat – Unit 2, 173 – 180 cm) as well as an additional third peat sample collected from a nearby core (approximately 1 m west of HE23T4C4B) at 90 cm depth, which was included as an optional data point in certain age-depth model scenarios. The detrital sediment in this nearby core was not sampled or described in the field, this nearby core posed only as an optional additional age date for age-depth models.

Radiocarbon age dating was performed at the 14Chrono Centre for Climate, Queen's University Belfast, calibrated to calendar years (±BP) using the IntCal20 calibration curve (Reimer et al., 2020). To provide additional verification and detail, the calibrated ages for each sample were processed using OxCal version 4.4 (Bronk Ramsey, 2001, 2017) with the IntCal20 calibration curve. This step provided a cross-reference of chronological quality and improved calendric date output (2σ [95.4%] and 1σ [68.2%] precision). The calibrated probability distributions for the three samples are presented in Figure 4.26, showing the range of calibrated ages and associated probabilities. These distributions serve as a foundational input for the subsequent Bayesian age-depth models.

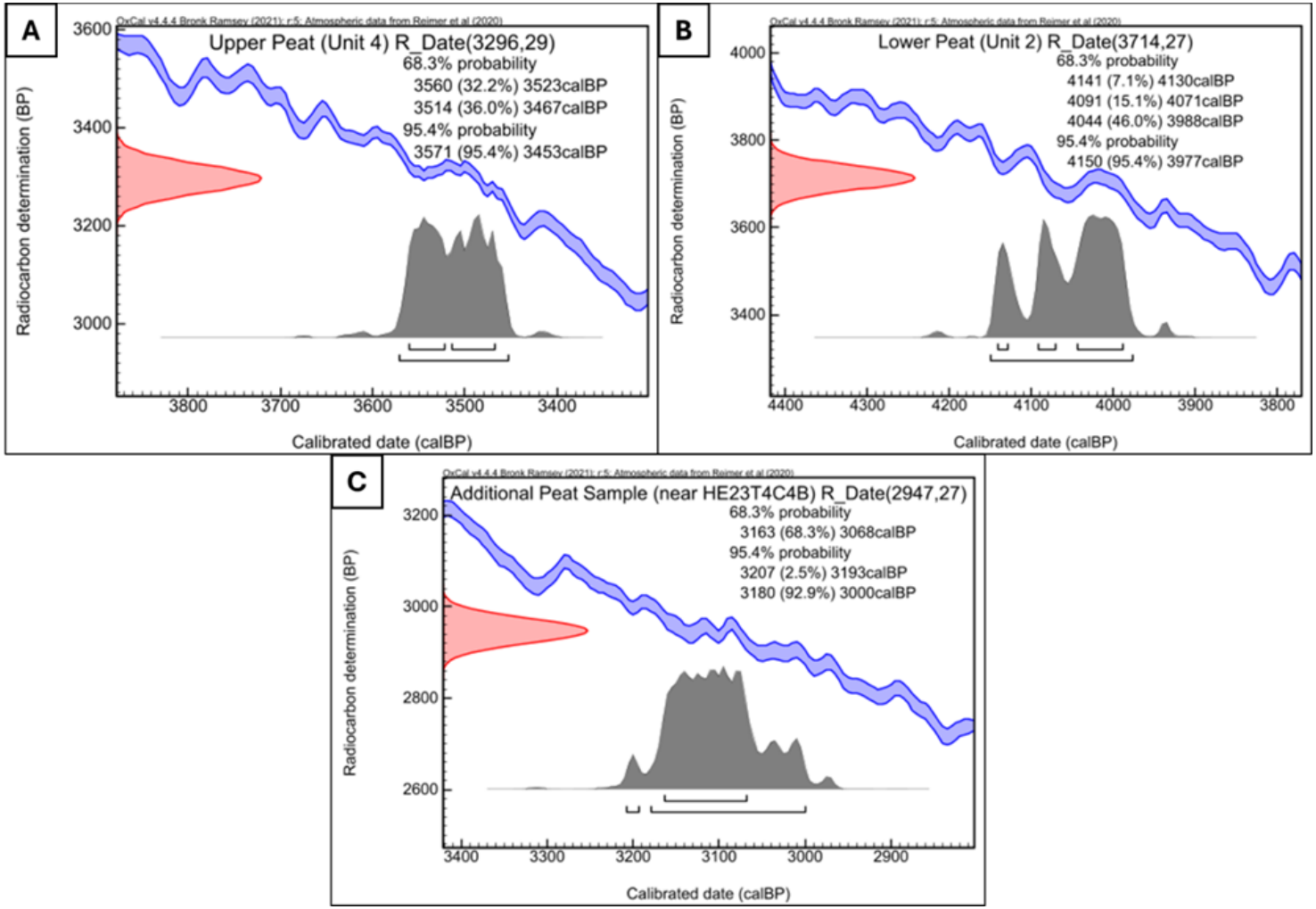


Figure 4.26 - Combined calibrated radiocarbon age distributions for samples collected on Horse Eye, (A) Upper Peat (Unit 4) in core HE23T4C4B, (B) Lower Peat (Unit 2) in core HE23T4C4B, and (C) an additional peat sample collected nearby core HE23T4C4B. Calibrated using OxCal v4.4 (Bronk Ramsey, 2001, 2017) and the IntCal20 calibration curve (Reimer et al., 2020).

Age-depth models were constructed using Bacon (rbacon) v.3.3.1 (Blaauw, 2010) within R version 4.4.1 (R Core Team, 2024), employing Bayesian statistical methods to account for uncertainties and segment-based linear deposition rates. The uncalibrated conventional radiocarbon results and their corresponding calibrated dates (cal BP) from OxCal are presented below in Table 4.14.

Table 4.14 - Summary table of samples from Horse Eye that were processed at 14Chrono Centre for Climate, the Environment and Chronology at Queen's University Belfast. The stratigraphy, depth, material, laboratory reference, uncalibrated and calibrated dates for each sample are summarized.

Stratigraphy	Depth (cm)	Material	Lab Ref	Uncalibrated Result BP	IntCal20 Calibrated Date (2σ 95.4%) (cal BP)
Upper Peat (Unit 4)	120-126	Wood and Peat	UBA-52882	3296 ± 29	3453-3471
Lower Peat (Unit 2)	180	Peat	UBA-52887	3714 ± 27	3977-4150
Additional Peat Sample (near HE23T4C4B)	90	Peat	UBA-52880	2947 ± 27	3000-3193

To interpret the implications of varying assumptions on the age-depth relationships within HE23T4C4B, four scenarios (A, B, C, and D) were developed and explored. The age-depth models created for core HE23T4C4B are based on a different combination of assumptions:

- **Top age = 0 BP (present day) or not:** Scenarios A and B assume the top of the core represents the present day (0 BP), reflecting a direct connection to modern terrestrial deposition. Conversely, Scenarios C and D do not include this assumption, allowing for the potential that the surface may not reflect modern deposition rates.

- **Inclusion of Third Peat Sample:** Scenarios B and C incorporate the third peat sample from a nearby core, based on its proximity and stratigraphic similarity, while Scenarios A and D exclude it.

Each scenario assumes deposition rates are roughly constant within segments but vary between segments. Segments are placed in between samples that were age dated. The third peat sample was considered a useful addition for scenarios B and C due to its proximity and stratigraphic context, offering a potentially more robust age-depth framework. However, its exclusion in scenarios A and D avoids potential biases from lateral variability in deposition between two different cores at a distance. Each scenario was analyzed in terms of minimum, maximum, median, and mean calibrated age ranges for the five primary units within core HE23T4C4B. These results, constructed using Bacon (rbacon) v.3.3.1 (Blaauw, 2010), are summarized in Table 4.15.

Table 4.15 provides a summary of the calibrated age ranges (BP) for each scenario; the differences between the scenarios reveal the influence of specific assumptions on the results. The assumption that the top of the core represents the present day (Scenarios A and B) anchors the surface of the age-depth model to 0 BP, which stretches the age-depth relationship, resulting in older maximum ages for the deeper units when compared to Scenarios C and D, which do not make this assumption. This assumption also impacts the modelled age of Unit 5 (uppermost unit), as anchoring the surface to 0 BP forces the model to interpolate a younger age for this unit, reflecting a slower rate of deposition between the surface and base of Unit 5. For example, in Unit 1, Scenario A (modern deposition assumed) produces a maximum age of 4902 cal. BP, while Scenario D (no modern deposition assumed) produces a maximum age of 4462 cal. BP. This effect reflects a slower, more continuous rate of deposition when modern deposition is assumed.

The inclusion of the additional data point from a nearby core (Scenarios B and C) distinctly impacts the age ranges. For example, when comparing Scenarios A and B (both assuming a modern top age), the third data point in Scenario B reduces the maximum age for Unit 1 from 4902 cal. BP (Scenario A) to 4906 cal. BP (Scenario B). Similarly, in Unit 3,

the additional data point narrows the calibrated range from 3321-4339 cal. BP in Scenario A to 3459-4316 cal. BP in Scenario B, indicating a more refined interpolation. A similar effect is observed between Scenarios C and D, where neither assumes modern deposition. In Unit 1, Scenario D has a maximum age of 4462 cal. BP, where the inclusion of the third data point in Scenario C increases the maximum age to 4464 cal. BP. Additionally, in Unit 3, Scenario D produces a wider range of 3444-4133 cal. BP, compared to the more refined range of 3429-4134 cal BP in Scenario C. The third data point acts as a constraint in the middle of the profile, which can reduce variability between units.

These comparisons show how the assumptions about modern deposition and the inclusion of an additional data point influence the results. The assumption of a modern top age (Scenarios A and B) results in older maximum ages for the basal units due to the extended depositional timeline, while excluding this assumption (Scenarios C and D) produces younger maximum ages, reflecting potentially different surface conditions. Similarly, the inclusion of the third data point in Scenarios B and C narrows the age ranges and provides a more refined interpolation by constraining the model mid-profile, where Scenarios A and D rely solely on data from HE23T4C4B, resulting in broader age ranges that reflect greater variability. Together, these differences emphasize the sensitivity of age-depth models to input assumptions, highlighting the trade-offs between precision and consistency.

Table 4.15 - Summary table of calibrated age ranges (cal BP) for each stratigraphic unit across age-depth model scenarios A, B, C, and D.

Age-depth Scenario	Unit	Minimum Age Range (cal BP)	Maximum Age Range (cal BP)	Median Age Range (cal BP)	Mean Age Range (cal BP)
A	Unit 5	(-70) - (3085)	(-69) - (3574)	(-69) - (3381)	(-69) - (3369)
A	Unit 4	(3128) - (3302)	(3594) - (3720)	(3407) - (3538)	(3397) - (3537)
A	Unit 3	(3321) - (3884)	(3735) - (4339)	(3550) - (4041)	(3549) - (4057)
A	Unit 2	(3895) - (3979)	(4351) - (4418)	(4051) - (4116)	(4067) - (4134)
A	Unit 1	(3989) - (4223)	(4427) - (4902)	(4128) - (4487)	(4145) - (4510)
B	Unit 5	(-70) - (3334)	(-69) - (3647)	(-69) - (3456)	(-69) - (3463)
B	Unit 4	(3351) - (3449)	(3658) - (3734)	(3469) - (3557)	(3476) - (3566)
B	Unit 3	(3459) - (3896)	(3746) - (4316)	(3568) - (4052)	(3577) - (4065)
B	Unit 2	(3907) - (3990)	(4326) - (4387)	(4063) - (4123)	(4075) - (4140)
B	Unit 1	(4000) - (4229)	(4399) - (4906)	(4134) - (4497)	(4151) - (4516)
C	Unit 5	(1792) - (3325)	(2553) - (3565)	(2227) - (3446)	(2216) - (3445)
C	Unit 4	(3335) - (3421)	(3576) - (3643)	(3457) - (3530)	(3456) - (3531)
C	Unit 3	(3429) - (3840)	(3651) - (4134)	(3540) - (3978)	(3541) - (3981)
C	Unit 2	(3849) - (3920)	(4141) - (4205)	(3987) - (4042)	(3991) - (4049)
C	Unit 1	(3931) - (4075)	(4216) - (4464)	(4052) - (4243)	(4059) - (4250)
D	Unit 5	(1790) - (3327)	(2608) - (3613)	(2255) - (3464)	(2240) - (3464)
D	Unit 4	(3341) - (3434)	(3621) - (3680)	(3474) - (3544)	(3475) - (3546)
D	Unit 3	(3444) - (3847)	(3687) - (4133)	(3554) - (3980)	(3556) - (3983)
D	Unit 2	(3858) - (3925)	(4142) - (4200)	(3989) - (4044)	(3993) - (4050)
D	Unit 1	(3933) - (4083)	(4210) - (4462)	(4053) - (4245)	(4059) - (4252)

The scenarios were designed to evaluate the influence of varying assumptions on the age-depth relationships, particularly with respect to the inclusion of the third peat sample and the interpretation of the core's uppermost layer as representing the modern day. Each scenario provides insight into the depositional history and stratigraphic context of core HE23T4C4B, emphasizing different combinations of chronological and depositional assumptions. The following outlines the specific details of each scenario, accompanied by their respective age-depth models (rbacon), and discussing the implications of these assumptions.

Scenario A: Top = 0 (present day), Two peat samples- excluding third peat sample

Scenario A assumes the top of core HE23T4C4B represents 0 BP, reflecting a direct link to modern terrestrial deposition. The model includes only the two peat samples collected from HE23T4C4B, excluding the third peat sample from the nearby core. This exclusion eliminates the potential bias that might arise from lateral variability of stratigraphy. Figure 4.27 shows the resulting age-depth model, with illustrates the interpolation between age-dated segments and the extrapolation beyond them.

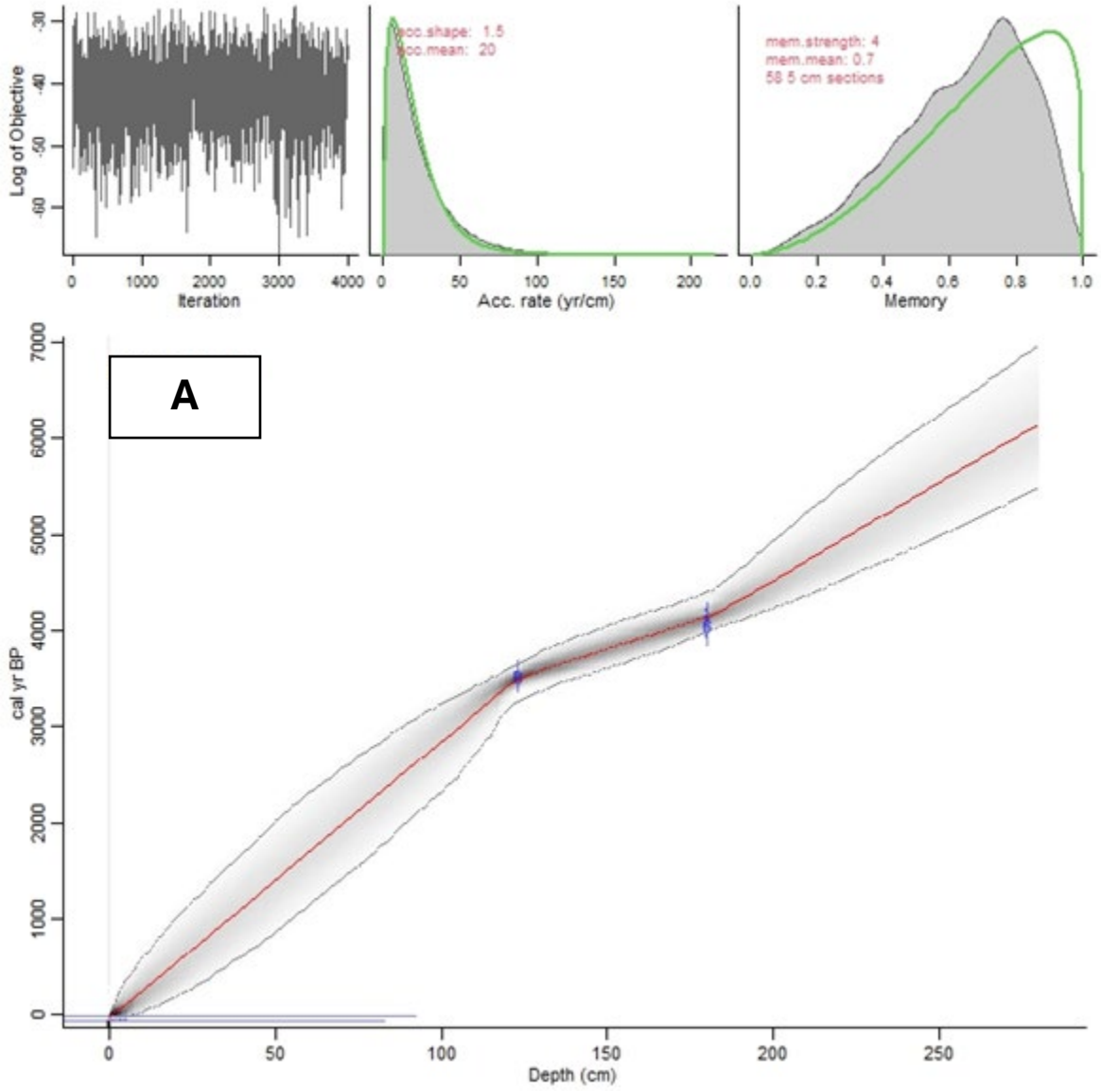


Figure 4.27 - Age-depth model for Scenario A. Modelled age (cal BP).

Scenario B: Top = 0, Three Peat Samples

Scenario B builds on scenario A by including the third peat sample from the nearby core, providing additional chronological data to enhance the model's resolution (Figure 4.28). The inclusion of this sample increases the number of segments within the model, allowing for potentially more detailed interpolation between dated points and improved extrapolation toward the basal and uppermost layers. The assumption of a modern-day surface remains consistent with Scenario A, providing a direct comparison of how the addition of the third nearby peat sample influences the age-depth relationship.

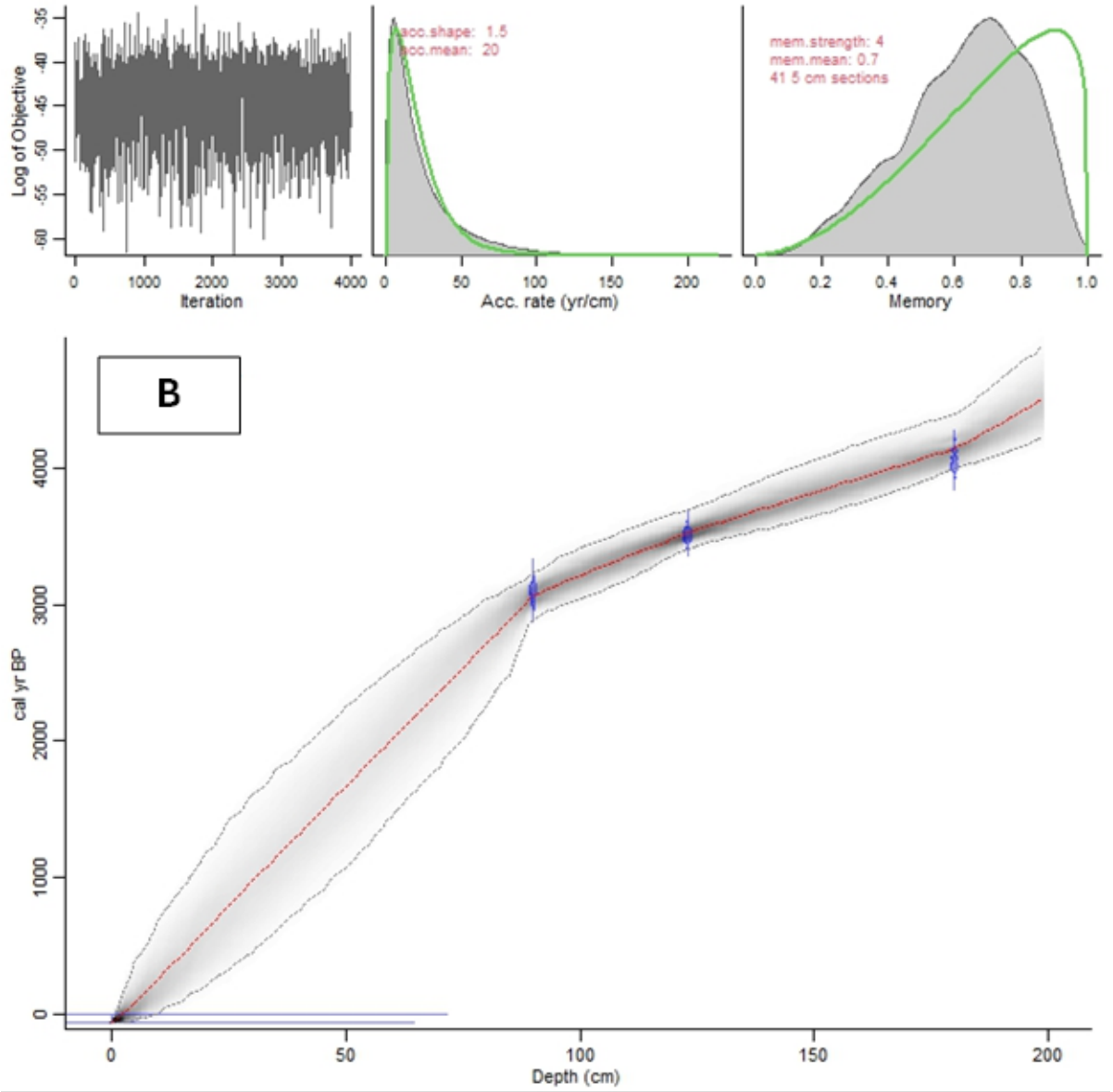


Figure 4.28 - Age-depth model for Scenario B. Modelled age (cal BP).

Scenario C: Top ≠ 0, Three Peat Samples

Scenario C assumes that the uppermost layer of core HE23T4C4B does not represent the modern day, removing the assumption of 0 BP for the surface. The model incorporates the third peat sample from the nearby core, which provides an additional data point for interpolation (Figure 4.29). By removing the modern surface assumption, Scenario C allows for alternative interpretations of the uppermost segment's age, which could reflect erosion, historical erosion, hiatuses in deposition, or slower deposition rates.

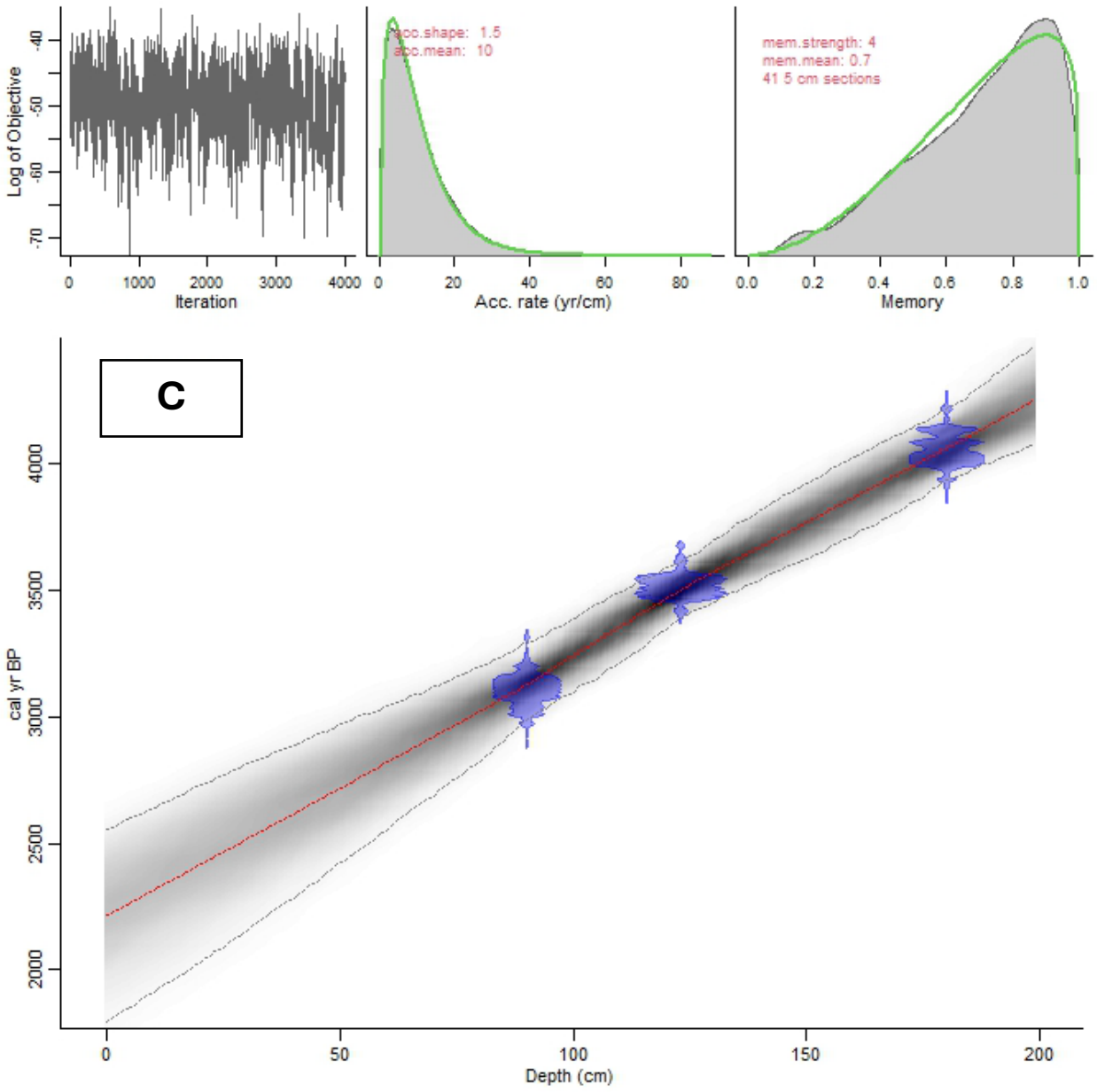


Figure 4.29 - Age-depth model for Scenario C. Modelled age (cal BP).

Scenario D: Top ≠ 0, Two Peat Samples

Scenario D (Figure 4.30) is the most conservative approach, excluding the third peat sample and not assuming the uppermost layer reflects the present day (0 BP). This configuration reduces the potential bias introduced by the additional peat sample and allows the model to operate independently of assumptions regarding modern deposition. The resulting age-depth model highlights a simplified chronology, providing a baseline for comparison against the other scenarios.

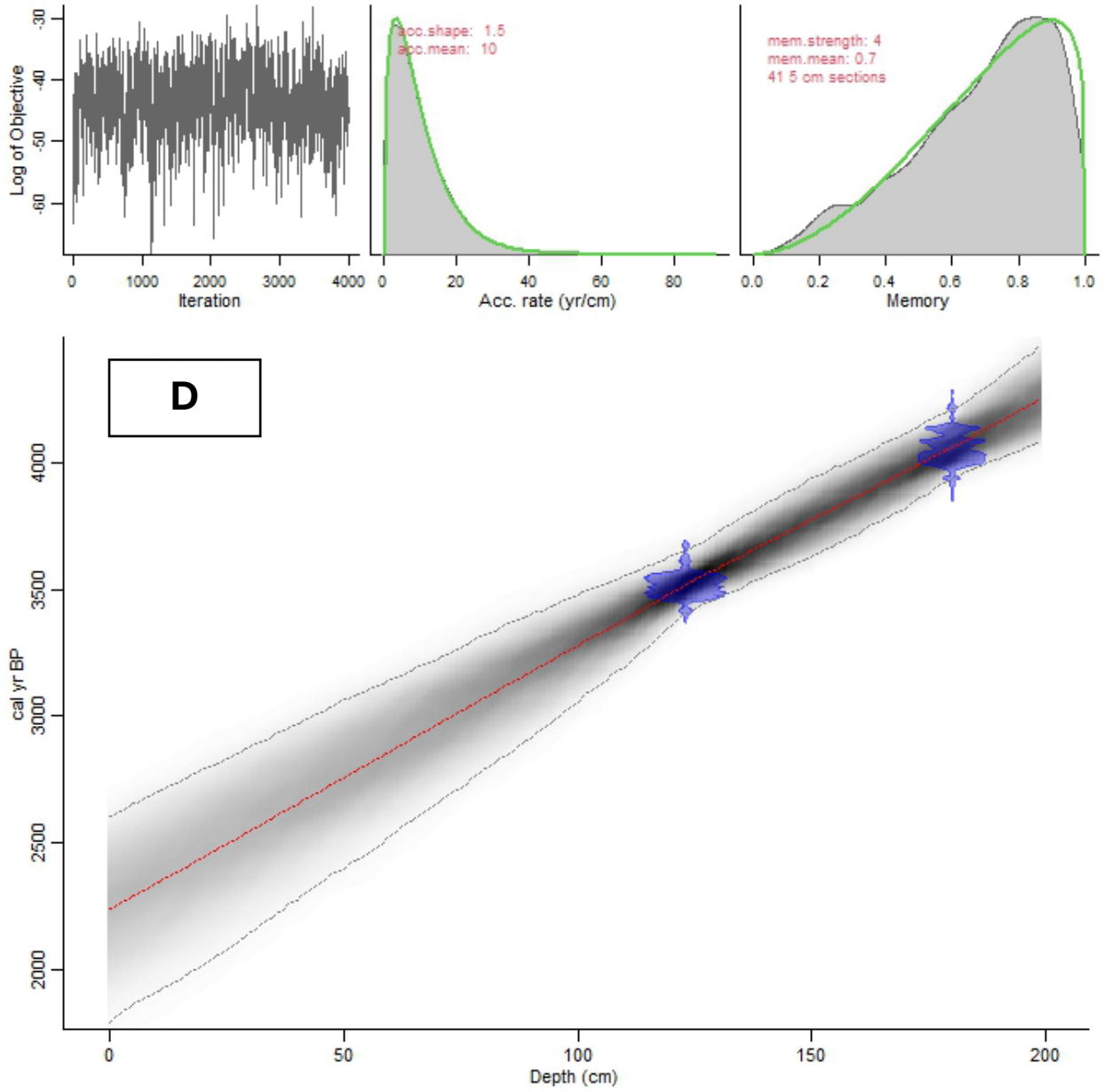


Figure 4.30 - Age-depth model for Scenario D. Modelled age (cal BP).

Among the four scenarios that were developed, scenario A was selected as the most fitting for interpreting the depositional history of core HE23T4C4B. This decision was based on its balance between chronological restraints and minimizing uncertainties introduced by incorporating external data points. By creating an age-depth model with data derived directly from core HE23T4C4B, Scenario A provides a focused and internally consistent approach to reconstructing the stratigraphic and depositional history of the site.

One of the primary reasons for selecting Scenario A is its reliance solely on the radiocarbon-dated peat layers within core HE23T4C4B. While the third peat sample from a nearby core was considered for inclusion, it was ultimately excluded to avoid potential biases associated with lateral variability. Including this third peat sample in Scenario B narrows the age ranges interpolated between dated depths. For example, in Unit 3 (Table 4.15), the calibrated age range is reduced from 3321-4339 cal. BP in Scenario A to 3459-4316 cal. BP in Scenario B. However, this refinement introduces a potential inconsistency, as the third peat sample was not observed in core HE23T4C4B and could reflect differences in depositional history or stratigraphy between cores. Excluding the third peat sample ensures that the age-depth model reflects only the stratigraphic and chronological data linked directly to the core, eliminating uncertainties related to lateral stratigraphic variability. This approach also aligns with the methodology used for other laboratory analyses, such as laser diffraction grain size analysis, pXRF, LOI, and XRD, all of which were conducted exclusively on material from core HE23T4C4B. By relying solely on data from a single core, Scenario A prioritizes consistency over interpolation precision, offering a more realistic representation of the stratigraphy within HE23T4C4B while avoiding uncertainties introduced by external data points.

Another key factor is the assumption that the uppermost layer of the core represents modern-day deposition (0 BP). This assumption is supported by stratigraphic evidence, particularly the characteristics of the topsoil (Unit 5, sub-unit 5[d]). The dark greyish-brown sandy clayey silt with organic material and rootlets is consistent with modern terrestrial soil formation processes, such as nutrient cycling and active biological activity, as confirmed by LOI and pXRF analyses. These features suggest that the surface

layer reflects relatively recent deposition and organic accumulation, making it reasonable to assume that it corresponds to modern conditions. Including 0 BP at the top of the age-depth model provides an anchor for the chronological framework, ensuring consistency and clarity when interpreting the depositional history. By limiting assumptions and focusing on directly observed data, this model provides high-resolution chronological information while maintaining methodological consistency. The average minimum, maximum, median, and mean ages for each stratigraphic unit under scenario A are summarized in Table 4.16.

Table 4.16 - Summary of average age ranges (cal BP) for Scenario A across the stratigraphic units for core HE23T4C4B.

Scenario A:						
Unit	**Depth (cm)**	**Depth (m OD)**	**Average Minimum Age (cal BP)**	**Average Maximum Age (cal BP)**	**Average Median Age (cal BP)**	**Average Mean Age (cal BP)**
Unit 5 – Predominantly Terrestrial, Sandy clayey silt	0 – 119	1.48 – 0.29	1187.2	2106.6	1637.8	1638.9
Unit 4 – Upper Peat	119 – 127	0.29 – 0.21	3221.8	3655	3478.4	3472.6
Unit 3 – Transition Unit	127 – 173	0.21 – (-0.25)	3598.9	4063.5	3798.7	3807.3
Unit 2 – Lower Peat	173 – 180	(-0.25) – (-0.32)	3936.1	4385.4	4083.3	4100.1
Unit 1 – Predominantly Marine, Lower clayey silt	180 – 280	(-0.32) – (-1.32)	4105.4	4648.3	4305.3	4324.9

Additionally, scenario A age-depth model, illustrated in Figure 4.31, highlights the connection between the stratigraphic units and their modelled ages. Figure 4.31 emphasizes the integration of the radiocarbon-dated peat layers (labelled with blue boxes) with interpolated and extrapolated segments (labelled with grey boxes), demonstrating a coherent chronological progression from Unit 1 (Predominantly Marine) through Unit 5 (Predominantly Terrestrial).

Scenario A was selected because it achieves a balance between chronological precision and analytical consistency. By focusing exclusively on data from core HE23T4C4B and assuming 0 BP at the top of the core, scenario A provides the clearest and most reliable framework for understanding the depositional history and environmental changes recorded within the core and extends to approximately 6000 BP as shown in Figure 4.27. Its alignment with stratigraphic observations and laboratory data makes it the most appropriate choice for interpreting the stratigraphy and paleoenvironmental transitions of Horse Eye.

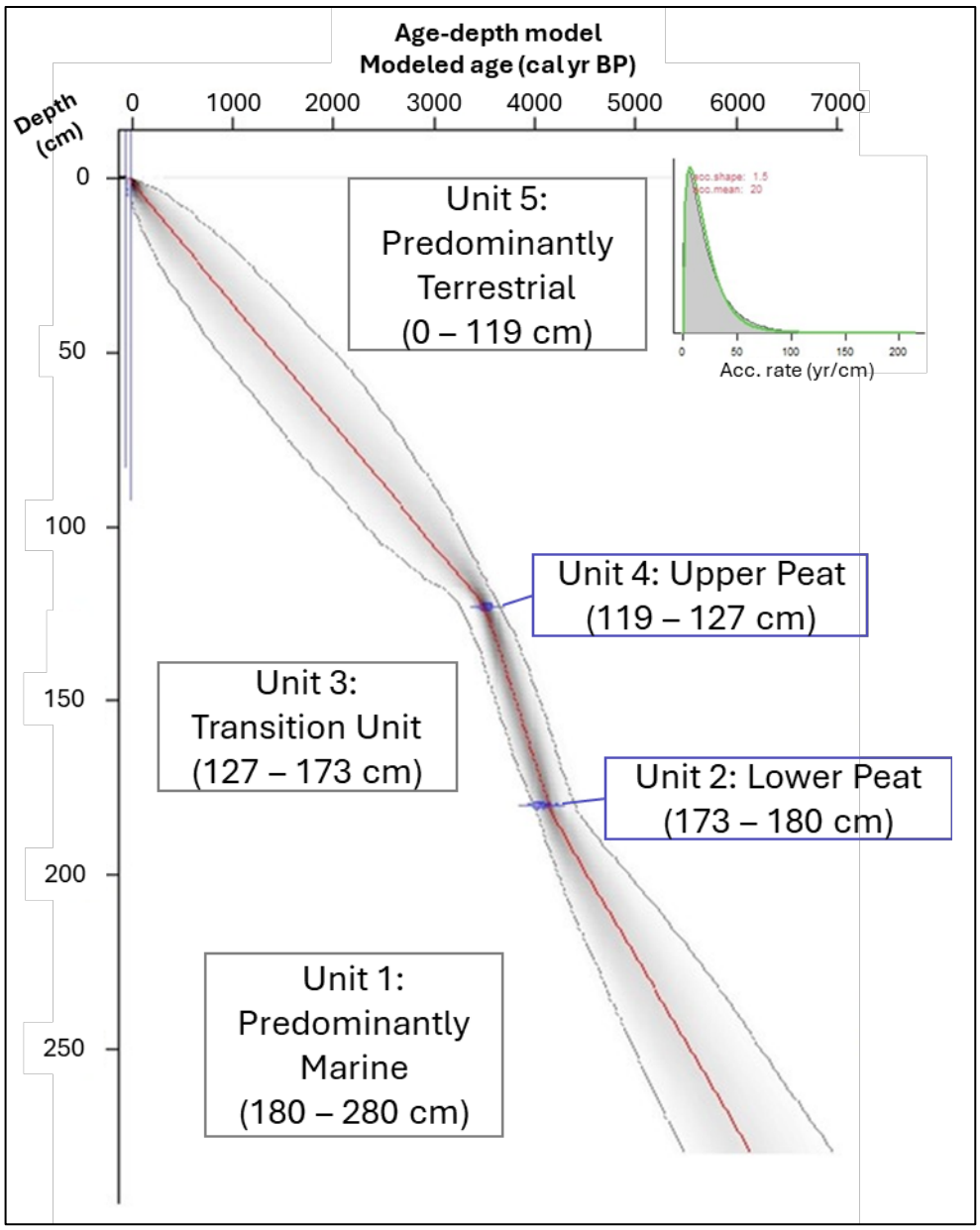


Figure 4.31 - Age-depth model for Scenario A, showing modeled ages (cal BP), labeling each segment as a stratigraphic unit, with the blue labels aligning with age-dated peat samples in the core HE23T4C4B.

In summary, four age-depth modeling scenarios were developed based upon the geochronologic results that were collected for core HE23T4C4B and from a nearby core. These scenarios were developed to explore the varying assumptions on the depositional history of core HE23T4C4B. Scenario A was ultimately selected as the most fitting framework due to its balance between chronological precision and analytical consistency. By limiting the model to radiocarbon-dated peat layers directly within the core and

assuming 0 BP for the surface, scenario A avoids potential biases introduced by external data points, such as the third peat sample from a nearby core. This approach aligns with stratigraphic evidence, including the characteristics of the modern topsoil, and provides a temporal anchor for interpreting depositional and environmental transitions. The resulting age model describes five stratigraphic units, each corresponding to distinct depositional phases. This progression highlights shifts in depositional conditions form predominantly marine influences in Unit 1 to predominantly terrestrial environments in Unit 5. While the upper and lower peat layers envelop the transitional phase, highlighting periods of organic accumulation amidst changes in depositional energy and sediment supply. The model demonstrates a steady rate of deposition within each segment defined by radiocarbon-dated peat layers, with variability in deposition rates between segments reflecting shifts in environmental conditions. This age framework provides context for the stratigraphic units defined in Section 4.3.9, serving as a foundation for reconstructing the environmental conditions and depositional history of Horse Eye.

Chapter 5: Reconstructing the Depositional History in the Pevensey Levels (Horse Eye and North Eye)

5.1.0. Introduction

The stratigraphic and sedimentological analyses conducted on Horse Eye and North Eye reveal a detailed narrative of the depositional evolution of the Pevensey Levels over the last 6000 years, spanning part of the Holocene epoch and encompassing transitions between marine, terrestrial, and transitional depositional environments. Figure 5.1 illustrates the topographic and spatial context of Horse Eye and North Eye, including their dimensions and elevation. Horse Eye is an elongated island, approximately 1.8 km in length and 0.6 km in width at its widest point (with an area of approximately 0.23 km^2), with a maximum elevation of approximately 9 meters OD. North Eye has a smaller area (approximately 0.21 km^2), is also elongated but is smaller, roughly 0.9 km in length and 0.5 km in width, reaching a lower maximum elevation of approximately 7 meters OD. Horse Eye, larger in size (approximately 0.02 km^2) and with a higher elevation (~2 meters) has a thicker sediment cover when compared to North Eye, which has exposed bedrock (Tunbridge Wells Sand Formation) observed in the eastern part of North Eye. The combined topographic and surface characteristics of these islands establish the context for understanding subsurface variability.

The land use history and surface characteristics of both islands further highlight their distinctions. North Eye contains archaeological evidence of a medieval chapel and records of a historic settlement, indicating significant human activity during the medieval period. Today, North Eye is used for grazing, with no modern structures, only archaeological deposits remain, and is sparsely vegetated with grasses. Horse Eye, on the other hand, has a documented history of human settlement back to the Medieval period, with one household and one plough team, as noted in Section 2.7.0. There is currently one household on Horse Eye, but the surrounding area is primarily used for grazing. Its higher elevations are characterized by shrubbery and trees marking field boundaries, whereas the lower areas are covered by grasses and are dominated by grazing. The differences in

vegetation and land use between Horse Eye and North Eye highlight their different historical settlements and modern adaptations. While both islands are now primarily used for grazing, the archaeological evidence of a medieval chapel and settlement at North Eye indicates significant human activity in the past.

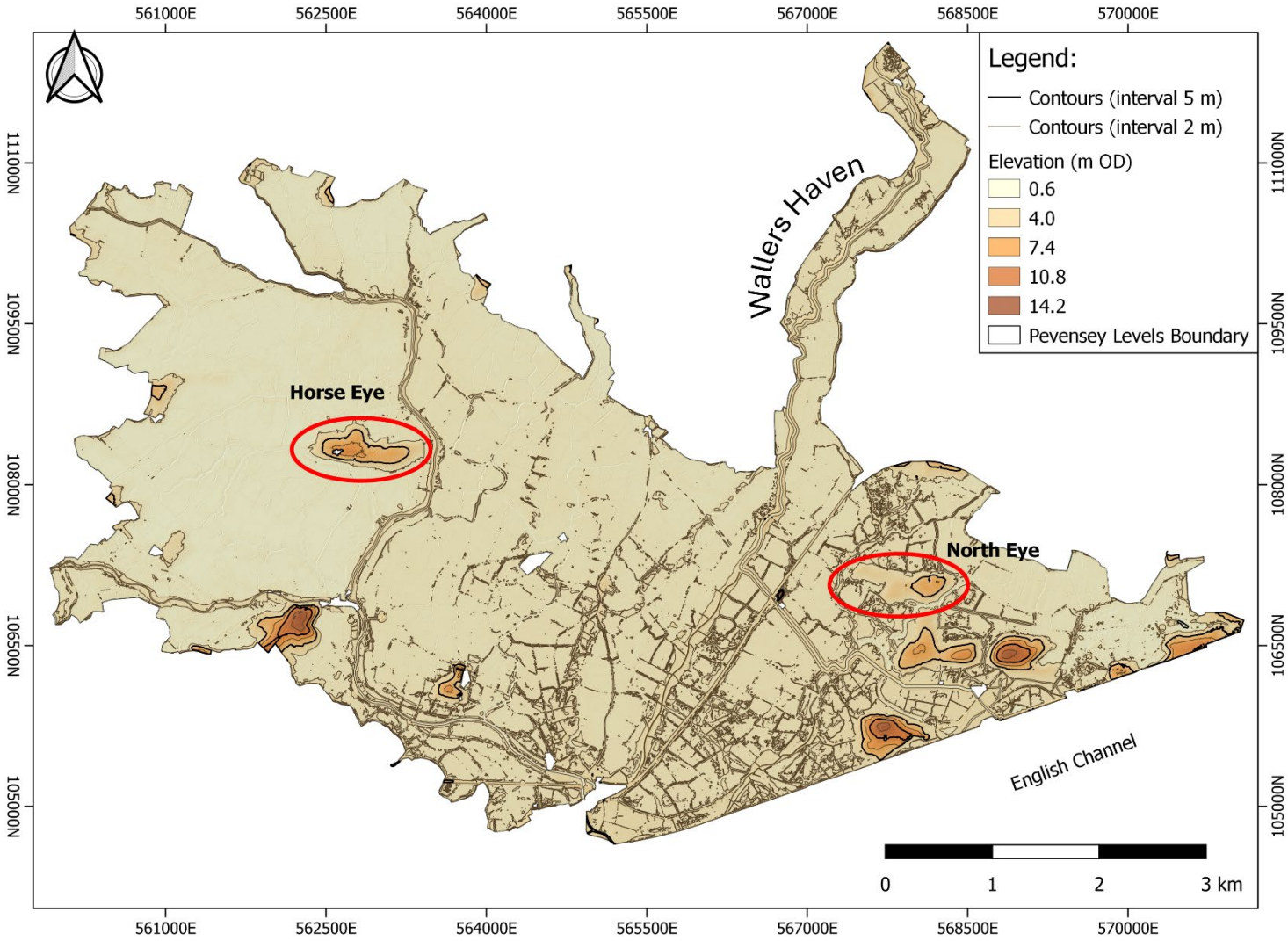


Figure 5.1 - Topographic map of the Pevensey Levels showing the locations of Horse Eye and North Eye, providing spatial context while highlighting the relative locations and elevations of the two bedrock islands. Contour intervals highlight elevation changes, with Horse Eye and North Eye outlined in red.

This chapter explores the depositional sequences comprising Horse Eye and North Eye (shown in Figure 5.1), comparing and contrasting the stratigraphic units cored in the field to regional studies, such as Champness (2009), Jennings & Smyth (1990), Waller & Kirby (2020), and Jones (2002), to provide a context for understanding the dynamic processes influencing this landscape. The Horse Eye sedimentary sequence, particularly core HE23T4C4B, provides a detailed view into shifts in depositional environments, linked to climatic events, and potential anthropogenic influences. The subsequent sections of this chapter will focus on the stratigraphic sequences, depositional environments, and processes that helped form the sediment layers covering the islands and contributing to the shape of the "islands" we see today. This chapter also integrates field observations and laboratory analyses among the two islands to create a stratigraphic framework of the Pevensey Levels.

5.2.0. Synthesis of Stratigraphy of Horse Eye and North Eye: Building on Regional Context

The stratigraphic and sedimentologic analyses from Horse Eye and North Eye offer a detailed understanding of the depositional history of the Pevensey Levels. This section integrates stratigraphic findings from this project with another study conducted on North Eye (Champness, 2009) and a regional study on the Pevensey Levels (Jones, 2002), to establish a broader stratigraphic framework. Figure 5.2 provides the location of the transects conducted at North Eye (both from Champness (2009) and this study), illustrating the locations of boreholes from the North Eye transect conducted in this study alongside the boreholes and conducted along the transect conducted in Champness' (2009) archaeological report where both transects are parallel and separated by approximately 110 meters. The shorter transect collected in this thesis focuses on the northwest edge of the island, while Champness' (2009) transect extends across the island along its long axis.

Both North Eye and Horse Eye exhibit a broadly consistent stratigraphic sequence that transitions from predominantly marine silty clays at the base and lowest edge of the islands to overlying transitional units containing minerogenic material and organics and/or peat layers extending up into the sides of the islands and finally to overlying predominantly terrestrial clayey silts covering all units and overtop the islands. This sequence generally aligns with Champness's (2009) stratigraphic findings at North Eye and with the stratigraphic framework established by Jones (2002) across the Pevensey Levels. Please refer to Figure 5.3 when referencing the stratigraphic findings of Champness (2009).

The correspondence of units recorded by Champness (2009) and Jones (2002) and those recorded in this thesis are described below. At the base of Champness' cores, bluish-grey silts and clays were recorded, corresponding to Unit 1 (predominantly marine clayey silts) identified at North Eye and Horse Eye in this study, as well as the basal marine units described by Jones (2002). Similarly, Champness's thick wood peat layer (radiocarbon dated to approximately 3490 BP) corresponds to Unit 4 (lower peat) from Horse Eye; they are both situated at a similar elevation of approximately 0 m OD and date

to a similar time range (as discussed in section 4.3.10: Geochronology Results), aligning with Jones' identification of upper and lower peat layers. However, while distinct peat layers were identified at Horse Eye in core HE23T4C4B, such as Unit 2 (upper peat) and Unit 4 (lower peat), the cores collected from North Eye during this study did not contain well-developed peat layers. Instead, organic material was observed dispersed within the lower clayey silt (North Eye Unit 10). Champness's earlier work, in contrast, documented substantial peat deposits at North Eye, including the radiocarbon-dated wood peat layer. Above these layers, Champness (2009) recorded terrestrial clays and silts, corresponding to the predominantly terrestrial clayey silts (Unit 5) identified at both Horse Eye and North Eye in this study and the upper terrestrial units described in the regional framework established by Jones (2002).

The basal predominantly marine units (Unit 1) at both sites record mid-Holocene low-energy depositional conditions interspersed with episodic higher-energy depositional events, evidenced by shell fragments and sand laminations. At Horse Eye, the clayey silt sequence reflects low-energy marine depositional settings consistent with tidal or lagoonal depositional environments. In contrast, the basal sequence at North Eye includes more frequent sand laminations, suggesting periodic higher-energy depositional events likely tied to fluvial or marginal marine influences.

The transitional sediments (Unit 3) at both sites indicate shifts between marine, paludal, and terrestrial depositional environments. North Eye's mottled silts and interlaminated sands highlight fluctuating depositional energy conditions, likely driven by fluvial inputs and marine regression. Organic material interspersed within these sediments reflects phases of reduced marine influence and increased terrestrial deposition. Notably, Unit 10 at North Eye, while lacking distinct peat layers, aligns with Unit 3b at Horse Eye but shows less evidence of organic accumulation. Champness (2009), however, identified peat layers in their transect at North Eye (Figure 5.2 and Figure 5.3), highlighting localized variability in peat formation at North Eye within the Pevensey Levels.

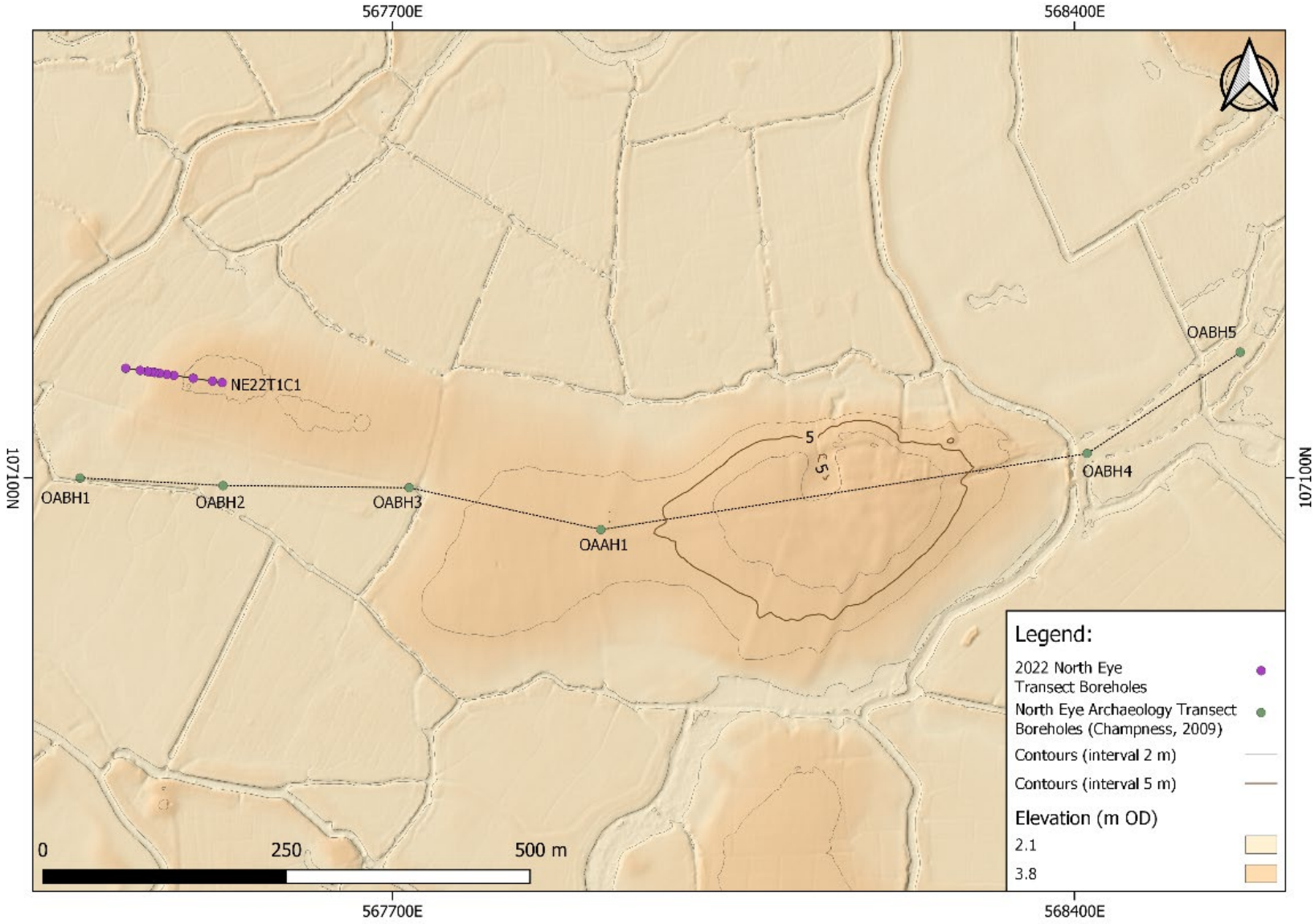


Figure 5.2 - Topographic map of North Eye showing the locations of boreholes from Fieldwork 2022 transect and Champness' (2009) transect, with 2 m and 5 m contours.

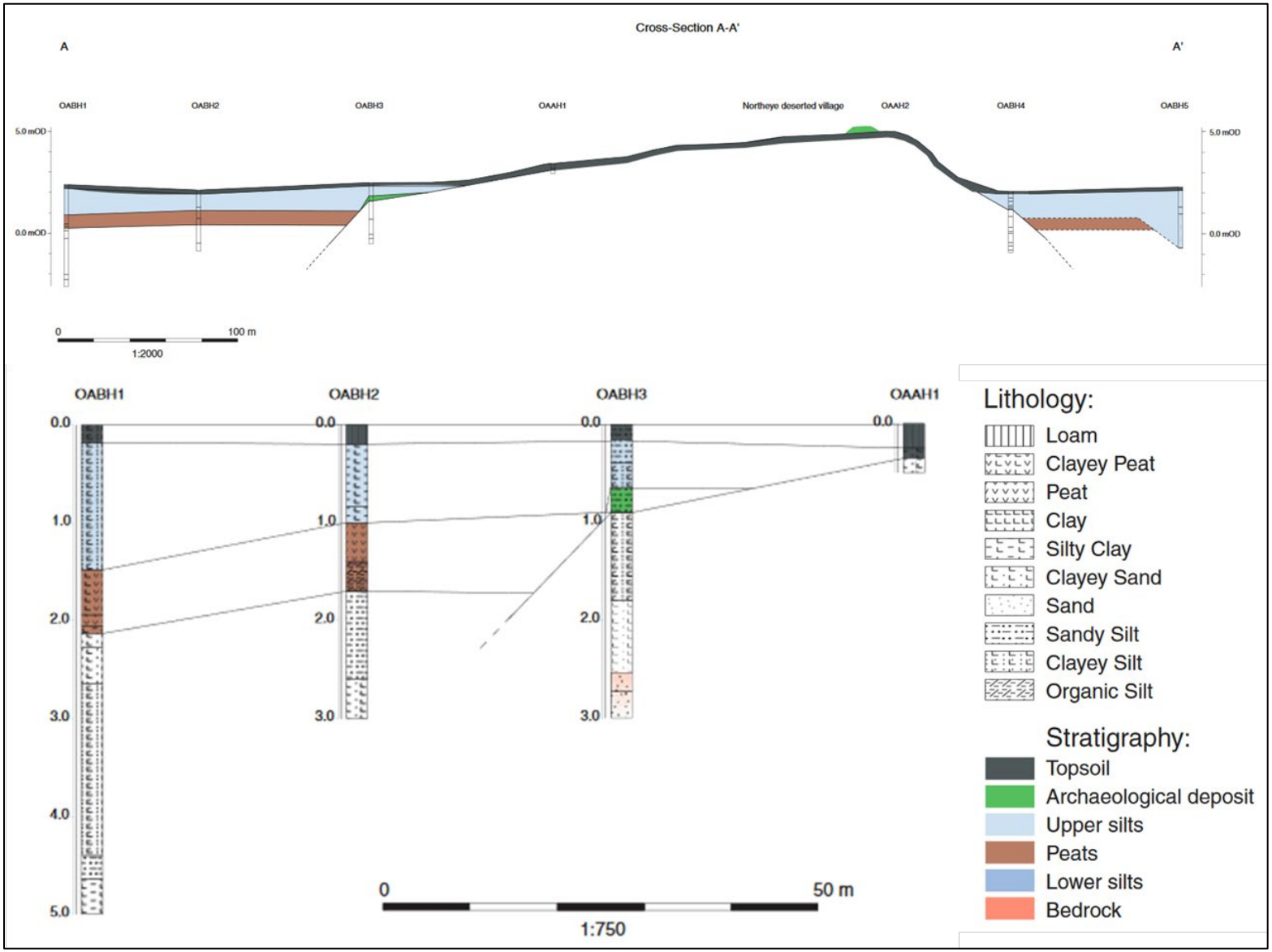


Figure 5.3 - Full cross-section (top) of North Eye, and detailed cross section of the western side of the bedrock island (bottom) (modified from Champness (2009)).

Following the comparison of units between this thesis and Champness (2009) and Jones (2002), Figures 5.4 and 5.5 present the lateral and vertical distribution of stratigraphic units along the transect at North Eye and Transect 4 at Horse Eye, respectively. These cross-sections provide a visual representation of how the general stratigraphic framework identified at Horse Eye (Predominantly Marine, Peat (if applicable), Transition, and Predominantly Terrestrial) applies to both islands. At Horse Eye, peat layers (Units 4 and 2) are well-developed, particularly in core HE23T4C4B, while at North Eye, distinct peat layers were not identified in this study, aligning instead with organic material mixed into a minerogenic matrix in North Eye's Unit 10. Another key difference between the Horse Eye and North Eye cross-sections is the greater development of transitional units at North Eye (Pink in Figure 5.4), where these transitional units are more laterally and vertically extensive. These observations highlight variations in depositional environments and hydrological conditions across the two islands.

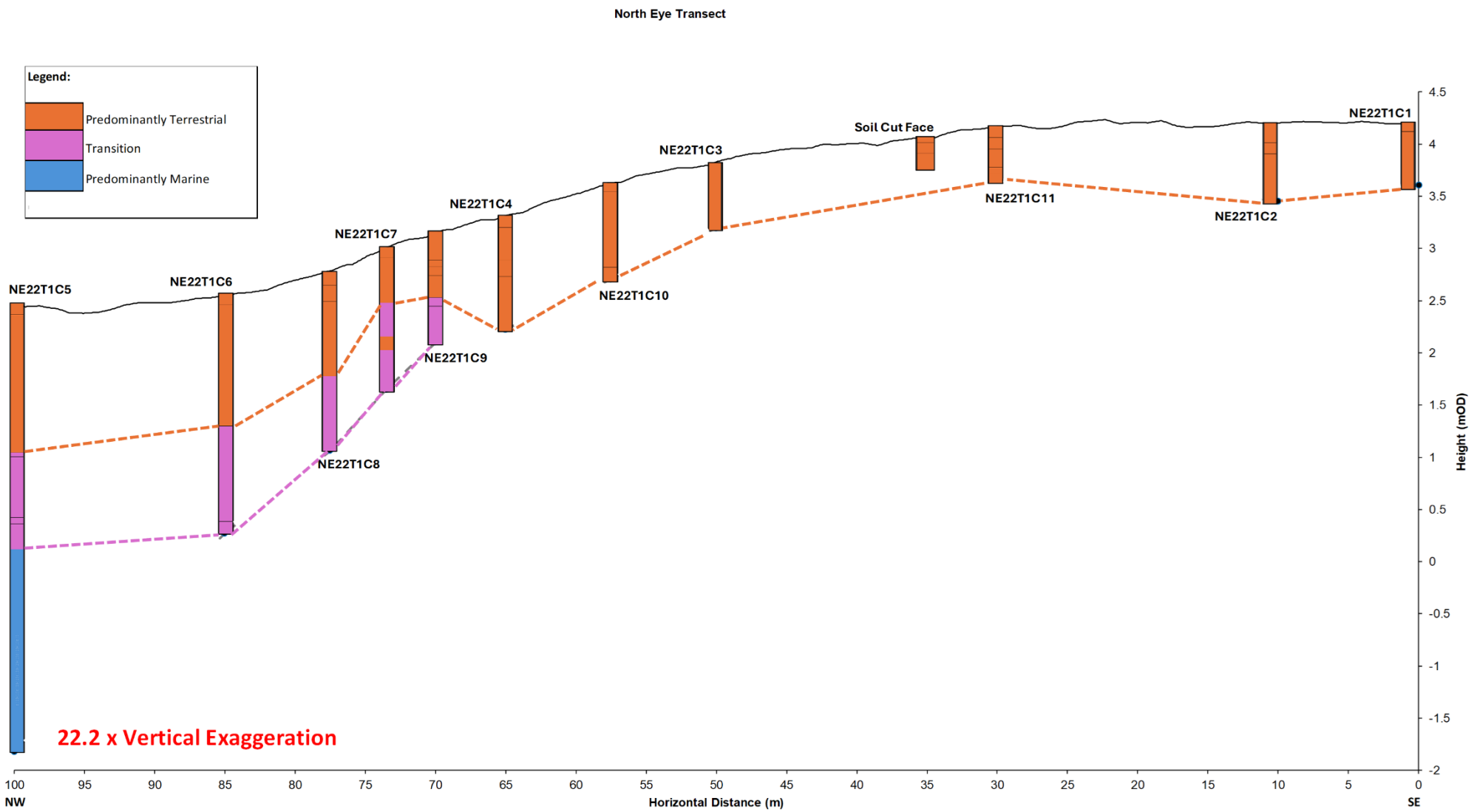


Figure 5.4 - Cross-section of North Eye transect, showing stratigraphic units and assumed bedrock contact. This cross-section illustrates stratigraphic units defined at Horse Eye, predominantly terrestrial, transitional, and predominantly marine. Elevation (m OD) is indicated on the y-axis, with 22.2x vertical exaggeration.

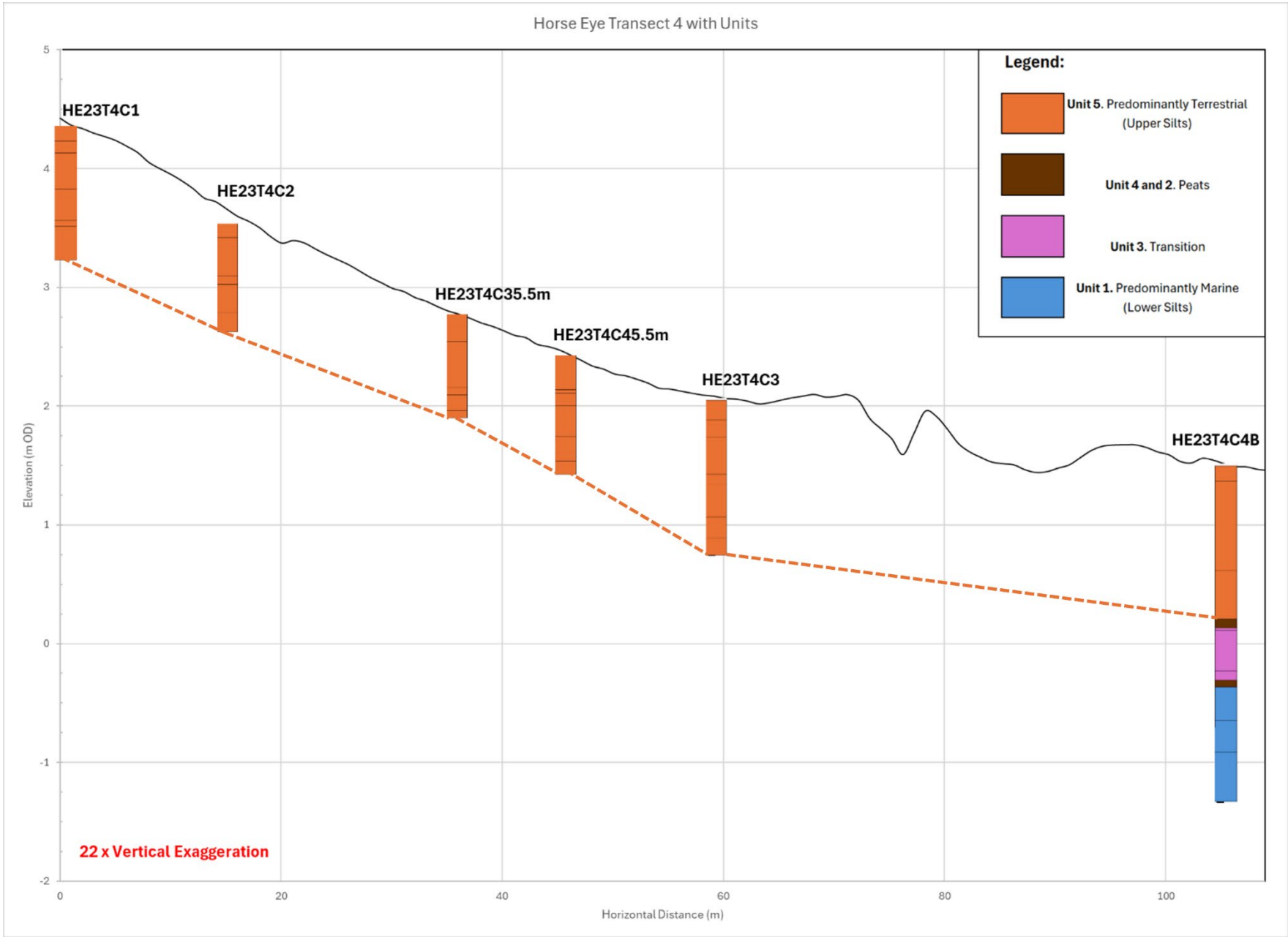


Figure 5.5 - Cross-section of Transect 4 at Horse Eye, showing the stratigraphic units defined at Horse Eye. Elevation (m OD) is indicated on the y-axis with 22x vertical exaggeration. Stratigraphic units include predominantly marine, peat, transitional, and predominantly terrestrial. The figure demonstrates spatial variability in stratigraphy and elevation across the transect.

One of the most notable differences in the stratigraphy observed between Horse Eye and North Eye is the presence of sand-dominated units at North Eye, which were not observed at Horse Eye. The term “sand-dominated” refers to sediment where sand-sized particles (63 μm to 2 mm) constitute more than 50% of the material, making sand the most abundant grain size fraction within this unit. At Horse Eye, sand was primarily observed in parallel or lenticular laminations within a clayey silt matrix in Units 1 and 5. At North Eye, a distinct sand-dominated unit (Unit 6) was identified, consisting of up to 56% sand as measured by the Laser Diffraction Method (LDM). The sand in Unit 6 is clean, light beige/grey in colour, fine-grained, and visually consistent with the Tunbridge Wells Sand Formation (TWS) based on its grain size and colour, aligning with documented descriptions of TWS in southeastern England. Additionally, the bedrock geology at North Eye was mapped by the BGS as TWS and supports this interpretation. Figure 5.6 shows a photograph of an exposure of bedrock on the eastern portion of North Eye, showing the light buff-brown/grey sandstone consistent with the TWS formation, the location of this exposure is shown in Figure 5.7. In contrast, Horse Eye’s bedrock geology is mapped as the Weald Clay Formation (WC), a predominantly fine-grained and clay-rich unit. This formation lacks significant sand-sized sediment, which may explain the absence of sand-dominated units in the stratigraphy of Horse Eye. The sand observed at Horse Eye was primarily as parallel or lenticular laminations within a clayey silt matrix in Units 1b and 5c rather than forming a distinct, thick unit of sand as at North Eye.

These similarities across marine, peat/transitional, and terrestrial units indicate a shared depositional history of the area shaped by marine transgressions, terrestrial influences, and peat accumulation during the late Holocene. The presence of a sand-dominated unit at North Eye, in contrast to sand observed as only laminations at Horse Eye, highlights site-specific differences likely driven by variations in sediment sources, such as the proximity to the English Channel or the Wallers Haven, as well as the influence of local bedrock geology. The variability in the occurrence and thickness of peat layers, particularly at North Eye, provides an example of the localized hydrological and depositional conditions influencing stratigraphy across the Pevensey Levels.



Figure 5.6 - Photograph of Tunbridge Wells Sand Formation (TWS) bedrock exposed on the eastern portion of North Eye.

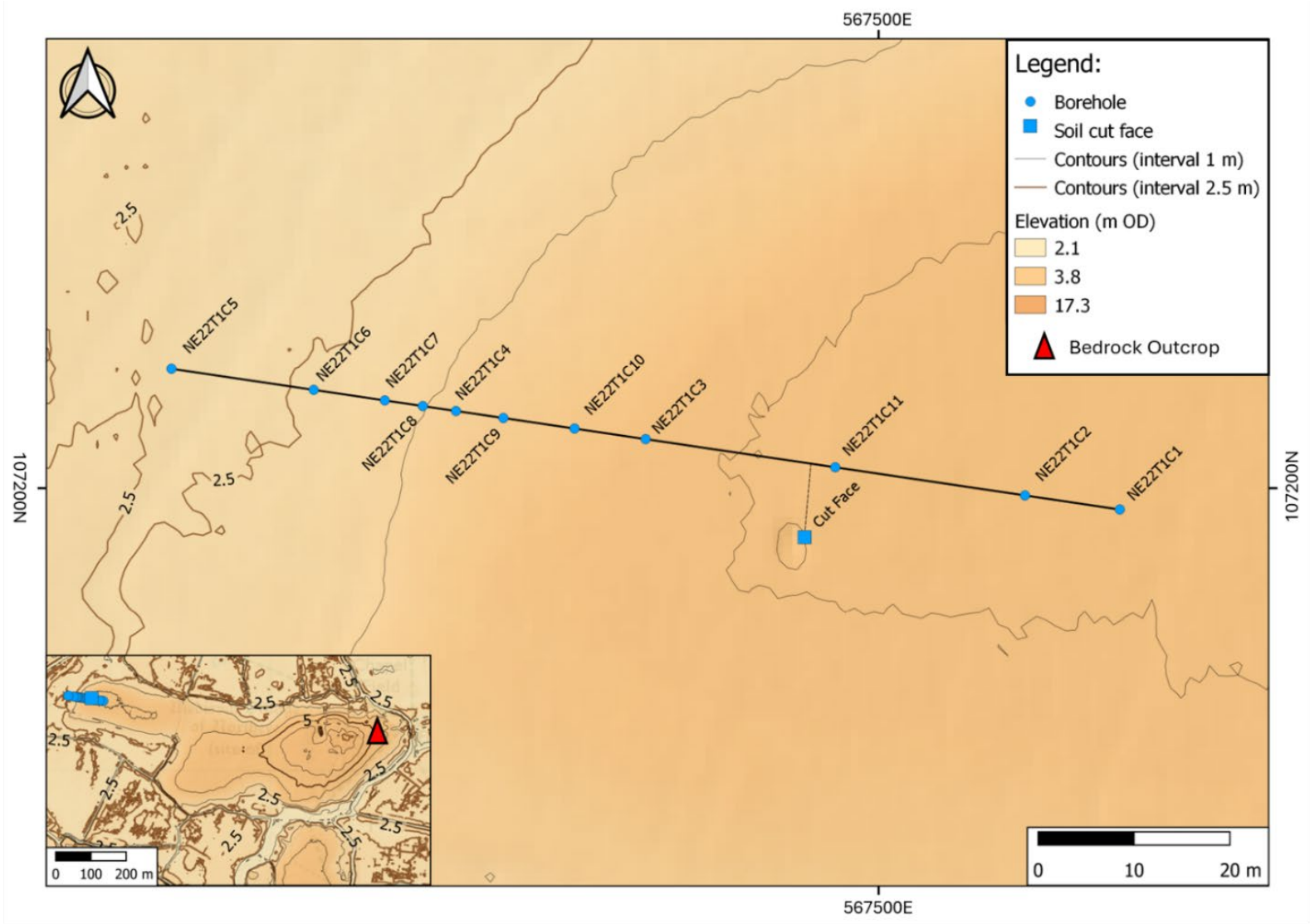


Figure 5.7 - Topographic map showing boreholes collected along 2022 North Eye transect, with 1- and 2-meter interval contours. Inset map shows the entire bedrock island of North Eye with a red triangle indicating the location of the TWS bedrock exposure (Figure 5.6).

The sand-dominated Unit 6 at North Eye may reflect localized depositional conditions influenced by its proximity to sediment sources. North Eye's location, closer to the English Channel (~1.6 km) and the Wallers Haven fluvial system (~1.4 km), potentially facilitated the erosion of the TWS bedrock or the transport and deposition of sand during high-energy deposition events, such as marine transgressions or storm surges. The Wallers Haven flows over Holocene alluvium but could provide a path for transporting sand-sized sediment under higher depositional energy conditions. In contrast, Horse Eye's location (~6.5 km from the English Channel and ~3.8 km from the Wallers Haven) likely reduced its exposure to such depositional processes, resulting in a stratigraphic sequence where sand is confined to laminations rather than forming a distinct unit. Sediment thickness and bedrock contact further distinguish the sites. At North Eye, Champness (2009) reported that bedrock was encountered at approximately 2 m OD at the edge of the island and 3.5 m OD at the island's center. In contrast, sediment at the edge of Horse Eye extended to approximately -1.5 m OD without encountering bedrock, suggesting a significantly thicker sediment cover at Horse Eye. These differences in sediment cover, combined with proximity to sediment sources, elevation, and bedrock lithology, show localized factors shaping the stratigraphy of each island. These geomorphological contrasts further emphasize the shared yet distinct depositional environments of North Eye and Horse Eye. While both islands experienced similar large-scale environmental changes over the Late Holocene, their distinct elevations, bedrock compositions, and proximity to sediment sources have influenced their stratigraphy.

Building on the stratigraphic similarities and contrasts identified between North Eye and Horse Eye, comparisons with regional studies provide further insights into the depositional processes influencing the Pevensey Levels. The results at North Eye are consistent with those observed in the nearby Romney Marsh. Grant & Waller (2010) highlight the role of climatic variability in driving sedimentation patterns, which can be seen in the peat accumulation and transitional sedimentation observed at Horse Eye. These processes parallel those described in the organic-rich units at North Eye.

Additionally, Evans et al. (2001) discuss the role of tidal channel dynamics in shaping late Holocene sedimentation, emphasizing the formation of high-energy depositional sequences, such as the sand-dominated Unit 6 at North Eye. Similarly, Long et al. (2006) described the influence of coastal barriers, such as the Dungeness Foreland, in controlling back-barrier sedimentation. A comparable barrier at the mouth of the Pevensey Levels embayment may have controlled marine inflow, influencing sediment transport and deposition inland within the Levels, including sand-dominated sequences like those at North Eye.

In conclusion, the integration of stratigraphic findings from Horse Eye and North Eye with insights from regional studies highlight the interaction of environmental, hydrological, topographical, and geological factors shaping the Pevensey Levels. While shared depositional processes- such as marine transgressions, terrestrial influences, development of peat layers, and transitional phases- are evident across the region, site-specific characteristics, including proximity to sediment sources, local bedrock geology, and elevation, have resulted in distinct variations in the stratigraphy of each island.

5.3.0. Climatic and Anthropogenic Influences

The stratigraphy of the Pevensey Levels, as observed in Horse Eye core HE23T4C4B, provides an opportunity to investigate potential connections between depositional processes and external drivers, including global climatic phases and regional human activities. Stratigraphic units were age-dated using AMS radiocarbon age dating (as discussed in section 4.3.10: Geochronology Results) with interpolated ages for the non-peat units providing a temporal framework. This framework enables comparisons with global climatic records, such as $\delta^{18}O$ data from the NGRIP ice core (Andersen et al., 2004), and historical accounts of land use and modification within the Pevensey Levels (Moore, 2020). The aim is to assess whether local stratigraphic changes correspond with major climatic phases, and/or align with anthropogenic influences during the late Holocene.

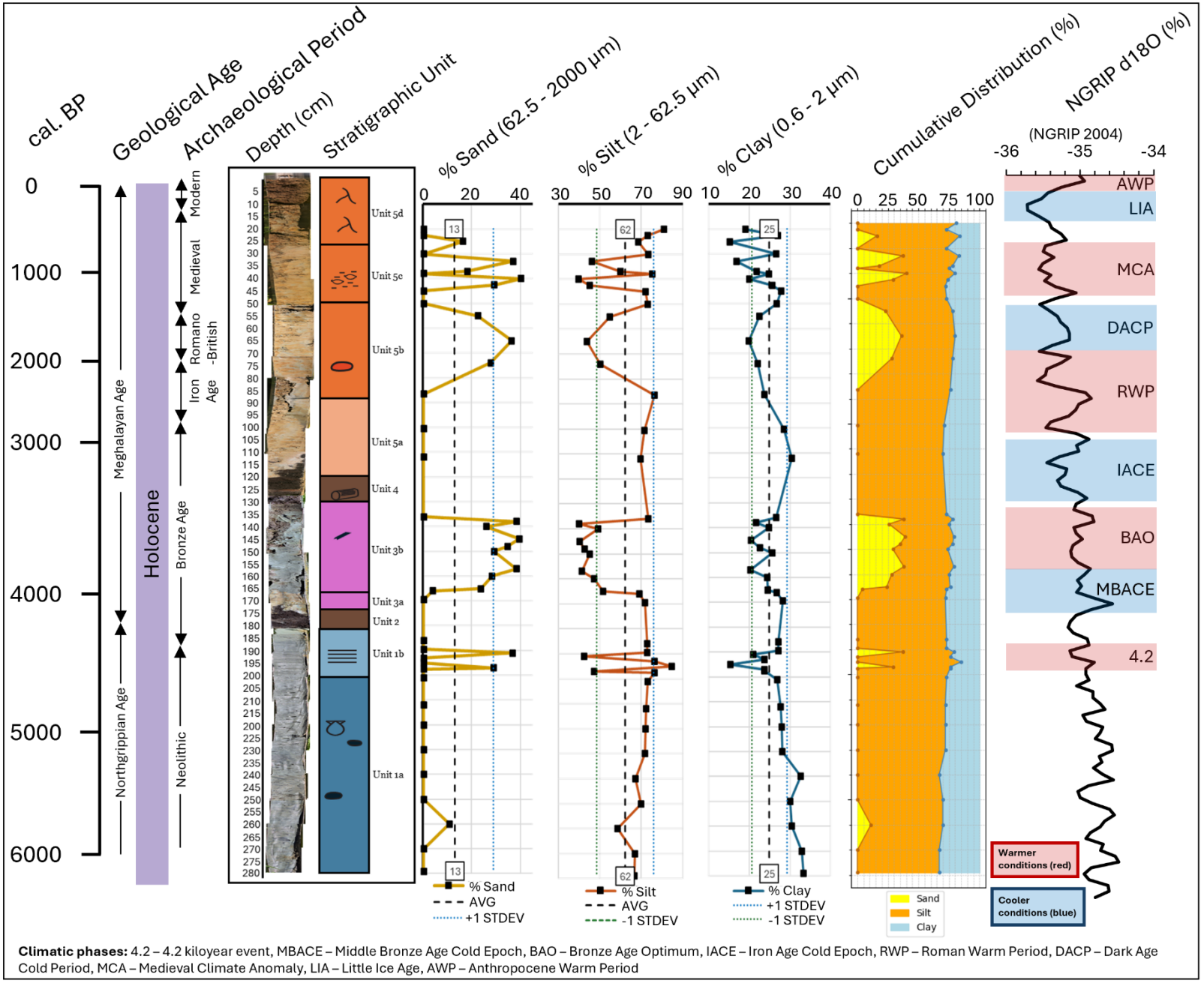
The potential connections between stratigraphic units, such as increases in grain size and differences in mineralogy, and global climatic phases are examined in greater detail in Section 5.3.1, focusing on climatic variability. Potential indicators of anthropogenic activity, such as localized increases in sand content and lenticular laminations, are discussed in Section 5.3.2, with consideration of how they correspond temporally to periods of documented land use changes, including medieval drainage and reclamation efforts. While direct evidence of human modification is absent in the sedimentary record, the temporal and contextual alignment suggests that these features could reflect anthropogenic influences on sediment transport and deposition.

5.3.1. Climatic Variability in Part of the Holocene

The Holocene epoch has been marked by several global climatic phases, such as the 4.2 ka event, a globally recognized climatic anomaly associated with widespread aridification in some regions and wetter conditions in others, including parts of northwest Europe (Walker et al., 2018), the Bronze Age Optimum (BAO), and the Medieval Climate Anomaly (MCA), which are recognized for their environmental impacts on depositional systems. This section investigates whether the stratigraphic and mineralogic data (from XRD) from Horse Eye core HE23T4C4B corresponds in timing with $\delta^{18}O$ records from the

NGRIP ice core (Andersen et al., 2004), a globally recognized proxy for climate variability. The validity of applying NGRIP data to the Pevensey Levels is supported by Hudson et al. (2023), which used NGRIP data to interpret climatic influences in Yorkshire, UK. Despite Yorkshire being approximately 400 km north of the Pevensey Levels, both regions are subject to similar North Atlantic weather systems and share comparable paleoclimate conditions during the late Holocene, making the application of NGRIP data plausible for investigating if it corresponds to other data at this site. These comparisons aim to assess the correspondence between global climatic events and local depositional responses, particularly in the context of low-lying, hydrologically sensitive environments such as the Pevensey Levels.

The stratigraphic units in core HE23T4C4B identified through multiproxy analyses (Section 4.3.9.) and established age model (Section 4.3.10.) show some correspondence, broadly to global climatic phases, such as the 4.2 ka event, the Bronze Age Optimum (BAO), and the Medieval Climate Anomaly (MCA). Figure 5.8, which integrates stratigraphic data, grain size distributions, $\delta^{18}O$ records from the NGRIP ice core, and radiocarbon-based chronology, serves as the primary framework for evaluating these correspondences. This figure provides an overview of stratigraphic units and their temporal alignment with recognized global climatic phases, enabling a comparative analysis between global trends and potential local sedimentary responses. For instance, Unit 2 (lower peat), radiocarbon dated to 3977-4150 cal BP, aligns temporally with the 4.2 ka event. This unit represents a prolonged depositional environment conducive to peat formation, characterized by reduced depositional energy conditions and sustained organic accumulation in waterlogged conditions. In contrast, Unit 1b, below Unit 2, contains higher-energy sand laminations, suggesting episodic higher-energy depositional shifts immediately preceding this event.



Climatic phases: 4.2 – 4.2 kiloyear event, MBACE – Middle Bronze Age Cold Epoch, BAO – Bronze Age Optimum, IACE – Iron Age Cold Epoch, RWP – Roman Warm Period, DACP – Dark Age Cold Period, MCA – Medieval Climate Anomaly, LIA – Little Ice Age, AWP – Anthropocene Warm Period

Figure 5.8 - Holocene stratigraphic and climatic context of core HE23T4T4B from Horse Eye. Displayed are the stratigraphic units defined, grain size distributions (% sand, % silt, % clay), cumulative grain size distribution (%), and $\delta^{18}O$ records from the NGRIP ice core (NGRIP 2004- Andersen et al. (2004)) to interpret depositional and climatic variability. Climatic phases (e.g., 4.2 kiloyear event, Middle Bronze Age Cold Epoch (MBACE), Bronze Age Optimum (BAO), Roman Warm Period (RWP), Dark Age Cold Period (DACP), Medieval Climate Anomaly (MCA), Little Ice Age (LIA), and Anthropocene Warm Period (AWP)) are shown to provide chronological context. Calibrated radiocarbon dates (cal. BP) are provided alongside archaeological and geological ages for reference.

The comparison of $\delta^{18}O$ data from the NGRIP ice core with the average sand percentages (averaged in 50-year intervals in cal. BP to match age intervals of NGRIP data) in core HE23T4C4B (shown in Figure 5.9) reveals a weak negative correlation (-0.33). This negative correlation suggests that higher sand percentages generally coincide with higher $\delta^{18}O$ values, which are typically associated with warmer periods globally. Warmer conditions can be linked to increased depositional energy, which can mobilize and transport sand-sized particles. However, the weakness of the correlation implies that global climatic trends do not solely drive this relationship. Instead, local factors, such as fluvial and tidal activity and sediment transport, may play a role in the deposition of sediment in the Pevensey Levels.

The NGRIP $\delta^{18}O$ data also exhibit a slight cooling trend from approximately 6 ka to the Little Ice Age in the 19th century, with noticeable cold-warm cyclicity superimposed on this broader trend. These cycles reflect shorter-term climatic variability, which may have contributed to fluctuations in depositional energy and sediment transport during warmer intervals. Despite this variability, periods with higher $\delta^{18}O$ values correspond broadly to increased sand deposition, highlighting a general connection between global climatic phases and localized sedimentary processes.

If the correlation were strong, it would suggest a consistent and direct relationship between $\delta^{18}O$ values and sand deposition, with warmer periods leading to higher sand content due to increased depositional energy. However, the weak correlation observed here indicates that, while warmer conditions broadly align with increased sand deposition, localized geomorphological and hydrological controls significantly influence sedimentary processes. The negative direction of the correlation is still meaningful: it aligns warmer conditions with an increase in sand deposition, potentially due to increased sediment transport during higher-energy depositional phases. The weak strength of the correlation highlights that local geomorphological and hydrodynamic controls, such as the influence of the topography of the bedrock islands on sediment trapping, variations in tidal activity, fluvial discharge, and proximity to sediment sources like the Wallers Haven and the English Channel, play significant roles in shaping the depositional environment. For example, the

elevation difference or pre-depositional slope of the bedrock islands could create areas where sediment is more likely to accumulate and be preserved, rather than be transported away. These localized factors impact the response of the Pevensey Levels to global climatic trends. To illustrate this correspondence, Figure 5.9 provides a graphical representation of the alignment of the percentage of sand with $\delta^{18}O$ data as a global proxy for climatic variability.

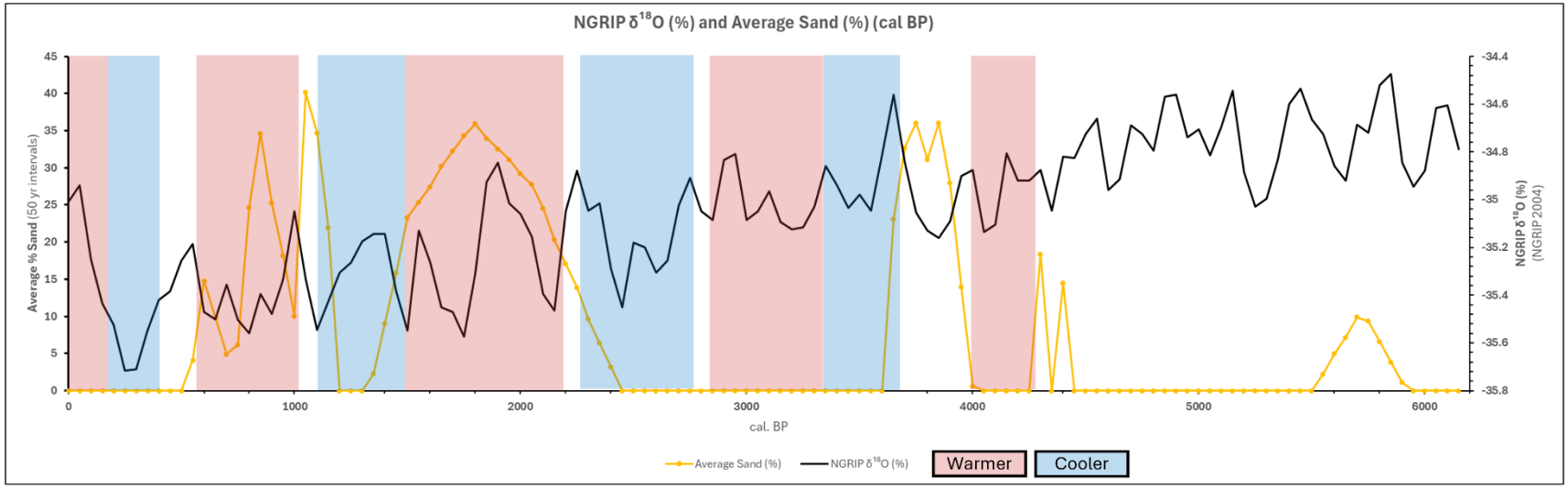


Figure 5.9 – A plot showing $\delta^{18}O$ data (%) from the NGRIP ice core (50-yr intervals) (Andersen et al., 2004), a global proxy for climate variability, warmer periods are indicated in pink and cooler periods are indicated in blue, alongside averaged sand percentages(50-yr intervals) derived from core HE23T4C4B at Horse Eye, both plotted against calibrated years before present (cal BP) on the x-axis. Average % Sand is plotted on the primary y-axis, $\delta^{18}O$ data is plotted on the secondary y-axis.

The mineralogical data from XRD analysis completed on HE23T4C4B complements the observation of higher sand content aligning weakly with warmer periods by linking mineralogical shifts to an increase in sand percentage (Figure 5.10). Units with increased sand content, such as Unit 1b, 3b, and portions of 5c, exhibit a notable enrichment of mica and feldspar minerals. This increase in mica and feldspar minerals suggest that high-energy depositional conditions, driven by local hydrodynamics, facilitated the input and deposition of these minerals alongside coarser sediment. For example, the mica content, often associated with fluvial or marginal-marine depositional environments, points to episodic sediment transport and deposition during periods of heightened hydrological activity. The presence of feldspar minerals, which are typically more angular and less resistant to weathering when compared to quartz, are often associated with less mature sediment derived from nearby terrestrial sources, such as eroded uplands or reworked coastal sediment. The co-occurrence of feldspar and mica with coarser grains could indicate periods of increased depositional energy, such as storm events, or enhanced tidal flows, that were capable of mobilizing and transporting these heavier and plate-shaped minerals.

Unit 5c (Horse Eye core HE23T4C4B) aligns with a later climatic phase, the MCA, during which warmer conditions and shifts in depositional energy likely influenced sediment transport. The lenticular laminations observed in this unit are indicative of mixed-energy depositional environments, where alternating high- and low-energy conditions result in the interbedding of sand and mud layers. As detailed in Dalrymple (1992), lenticular bedding is typical of intertidal settings, particularly within mixed and mud flats, where deposition from suspension during slack water is interrupted by erosion or reworking during tidal currents of storm-driven wave activity. This bedding pattern reflects an environment dominated by tidal dynamics, with fluctuating energy conditions capable of periodically transporting coarser-grained material into predominantly mud-dominated areas. Such depositional conditions suggest that tidal processes, potentially amplified by episodic storm activity, played a significant role in shaping this unit. The increase in feldspar minerals within Unit 5c provides another example of climatic variability aligning

with localized depositional processes, such as the reworking of terrestrial sediment. This integration of mineralogical evidence with grain size shows how geomorphological factors, such as proximity to sediment sources, fluvial discharge, and tidal energy, combine with climatic influences to shape the depositional environments within the Pevensey Levels.

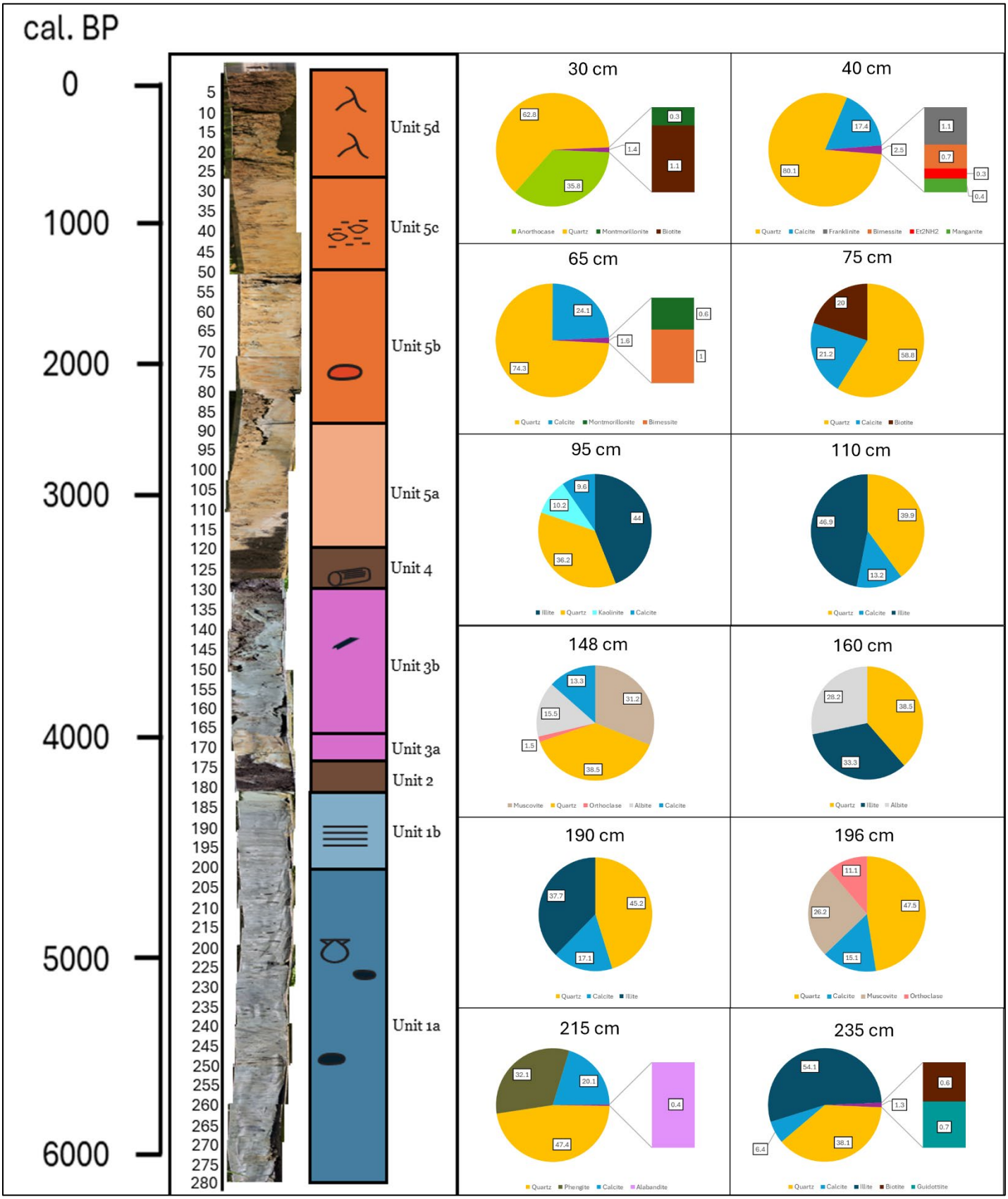


Figure 5.10 - Stratigraphic profile and mineralogical composition of core HE23T4C4B. The stratigraphic units (left) span the Holocene, showing transitions between marine, paludal, and terrestrial environments. The pie charts (right) display XRD-derived mineral compositions at selected depths, refer to figures 4.24 and 4.25 for a larger legend for the XRD pie charts.

This section has shown how the stratigraphy and mineralogical data from core HE23T4C4B correspond in timing with global climatic phases, as indicated by $\delta^{18}O$ data from NGRIP. While a weak negative correlation (-0.33) was observed between sand percentages and $\delta^{18}O$ values, the alignment suggests warmer periods coincide with increased sand deposition, driven by higher-energy depositional processes. However, this relationship is not solely dictated by global climatic trends; local geomorphological and hydrodynamic factors, such as fluvial activity, tidal dynamics, and proximity to sediment sources, modify the deposition of sediment within the Pevensey Levels. Figures 5.8, 5.9, and 5.10 collectively display how integrating stratigraphic, mineralogical, and climatic proxies can be corresponded and can provide information on how global and local influences impact depositional environments in the Pevensey Levels during the late Holocene.

5.3.2. Anthropogenic Contributions

The Pevensey Levels contain a preserved stratigraphic record that reflects not only natural climatic and hydrodynamic processes but also the influence of human activities, during the late Holocene. While deeper and older stratigraphic units primarily reflect natural deposition, shallower and younger units generally align temporally with archaeological periods characterized by significant human activity. This section investigates whether features in the stratigraphy, such as increased sand content and lenticular laminations, may serve as potential indicators of human modification. However, it is important to note that direct evidence of human modification, such as artifacts or man-made structures, has not been identified within the stratigraphy examined in this thesis. Instead, increased sand content and lenticular laminations are interpreted as potential indicators of human modification, based on their temporal alignment with periods of documented human modification and activity in the region.

The transition between Units 3a and 3b at Horse Eye (seen in Figure 5.8), characterized by an increase in grain size, aligns temporally with the Bronze Age, a period associated with the establishment of settlement networks and early land modification along the Sussex Coast (Yates, 2007). This period saw the development of rudimentary drainage systems and land use changes to support agricultural expansion. Where there is no direct evidence in the sedimentary record linking Unit 3b to human activities, the temporal correspondence and increased sand content may suggest that anthropogenic activity on the island during this time may have increased erosion and sediment transport. Pollen analyses from nearby regions, including the Brede-Pett Levels (Waller, 1998) and Romney Marsh (Waller et al., 1998), indicate significant deforestation and agricultural expansion during the Bronze Age, which likely contributed to increased soil erosion during the Bronze Age, which likely contributed to increased soil erosion and sediment transport into lowland or embayed areas such as the Pevensey Levels. These findings support the interpretation that increased sand content in Unit 3b could reflect sediment mobilization driven by land-use changes in the surrounding hinterlands.

Unit 5c (Figure 5.8), characterized by lenticular laminations composed of coarse sand, aligns temporally with the Medieval Climate Anomaly (MCA) and historically documented human efforts to modify the Pevensey Levels landscape during the Medieval period. During this period, regional authorities, such as Battle Abbey, heavily invested in land drainage and reclamation projects, which included constructing drainage systems and embankments to manage water levels (Moore, 2020). These modifications likely altered hydrologic conditions, impacting sediment transport and deposition. Pollen data from the Rother Valley and Pett Levels (Timpany et al., 2021) show reduced tree cover and increasing evidence of arable and pastoral activity during this period, reflecting a heavily modified landscape. These paleoenvironmental records provide additional context for understanding how human land use in surrounding areas may have contributed to increased sediment input into the Pevensey Levels, particularly during land reclamation efforts.

The increased sand content within lenticular laminations observed in Unit 5c could represent localized disturbances caused by these reclamation efforts, although these features may also have natural origins through potential storm activity, tidal surges, or increased fluvial discharge, which may have been linked to the warming climate. Temporally, Unit 5c aligns with a time of significant human intervention in the Pevensey Levels, when medieval drainage networks were developed to alter tidal flow and expand arable land. Such activities are documented as having influenced sedimentation in nearby regions, such as the Romney Marsh (Waller & Kirby, 2020) by impacting sediment transport pathways and depositional patterns. Similarly, the palaeoecological record from Romney Marsh highlights an open landscape during the Medieval period, characterized by increased erosion and sediment transport, supporting the interpretation that anthropogenic modifications in the areas surrounding the Pevensey Levels likely influenced the sedimentary record. The similarities in timing and depositional characteristics between Unit 5c and other anthropogenically modified coastal wetlands nearby suggest that human activity could have played a role in shaping the stratigraphy during the Medieval period.

Overall, the stratigraphy at Horse Eye and North Eye are interpreted to reflect a product of both natural processes and anthropogenic activities. While deeper and older stratigraphic units primarily reflect natural processes, the shallower and younger units align temporally with periods of documented human activity described by Moore (2020) in the Pevensey Levels. The integration of paleoenvironmental and palaeoecological records from nearby regions, such as the Romney Marsh, Brede-Pett Level, and Rother Valley, highlights a regional pattern of deforestation, soil erosion, and land-use changes that likely influenced sedimentation within the Pevensey Levels. This alignment suggests that features such as increased sand content and lenticular laminations in units 3b and 5c could correspond to anthropogenic modifications, such as drainage or reclamation efforts, rather than purely natural processes. Although direct evidence of human activity is absent, the multiproxy data combined with historical documentation provide a compelling framework for interpreting potential human influence on sediment transport and deposition, likely contributing to the stratigraphy preserved in the Pevensey Levels during the late Holocene.

5.4.0. Summary of Data Compilation

This chapter integrated stratigraphic, sedimentological, and mineralogical data to reconstruct the depositional history of the Pevensey Levels. Using multiple proxies, the findings provide information into paleoenvironmental changes influenced by climatic variability, hydrodynamic processes, and potential anthropogenic activities during the late Holocene.

The depositional sequences are interpreted to reflect an environmental change in the Pevensey Levels. Horse Eye is characterized by well-defined peat layers, indicative of prolonged low depositional energy and waterlogged conditions, as well as sand lamentations below the peat layers suggestive of episodic high depositional energy. These high-energy depositional events are interpreted as responses to localized shifts in hydrology, potentially influenced by climatic and/or anthropogenic factors, such the warmer climate during the BAO and MCA climatic events, storm surges, or drainage modifications in the landscape. North Eye's stratigraphy exhibited sand-dominated units with thinner sediment cover when compared to Horse Eye, likely reflecting both the influence of bedrock topography, bedrock geology (Tunbridge Wells Sand Formation), greater proximity to sediment sources or sediment transport sources, and depositional processes across the Pevensey Levels as a whole. The variability in sediment cover, combined with differences in stratigraphic sequences, highlights the influence of localized geomorphological and hydrological factors in shaping the depositional environments of each island.

Both islands contribute to a broader understanding of the stratigraphic variability across the Pevensey Levels, aligning with regional patterns described by Jones (2002) and Champness (2009). Comparisons with nearby sites, such as the Romney Marsh, Brede-Pett Level, and Rother Valley, further emphasize the interconnected nature of these low-lying or embayed marshland systems and their sensitivity to environmental and anthropogenic influences. Pollen studies in these regions highlight widespread deforestation, increased erosion, and the expansion of arable and pastoral activities, which

likely contributed to sediment transport into the Pevensey Levels and influenced their stratigraphic record. These regional connections provide context for understanding the depositional evolution of the Pevensey Levels.

The integration of findings from both Horse Eye and North Eye highlight how stratigraphic units across the Pevensey Levels collectively encapsulate transitions from marine to paludal to terrestrial environments. These transitions reflect a region-wide paleoenvironmental evolution rather than site-specific changes as they align across the Levels (Jones, 2002) and at both islands, as well as a broad temporal correspondence with global climatic phases. The presence of organic-rich peats within the stratigraphic sequences at both islands supports a reconstruction of prolonged waterlogged conditions during periods of reduced depositional energy. Conversely, the intermittent presence of sand at both sites highlights their sensitivity to episodic higher depositional energy conditions, such as storms or changes in tidal dynamics. The sand-dominated units at North Eye, particularly, demonstrate the potential influence of nearby sediment sources, such as the Wallers Haven and the English Channel, during periods of increased depositional energy.

By situating the findings within a regional and temporal context, this chapter highlights how the Pevensey Levels' stratigraphy encapsulates the paleoenvironmental change over the late Holocene. The comparison with nearby lowland systems further illustrates the role of regional environmental and anthropogenic processes in shaping sedimentary records. The two islands highlight the coastal systems and local to regional influences, offering insight into their dynamic evolution.

Chapter 6: Conclusions & Opportunities for Future Research

6.1.0. Thesis Contributions

This thesis presents a stratigraphic framework and paleoenvironmental reconstruction of the Pevensey Levels, focusing on the depositional history and paleoenvironmental transitions of Horse Eye and North Eye. By integrating field observations, sedimentological analyses, geochemical data, mineralogical data, and geochronological data, this thesis enhances the understanding of the Pevensey Levels coastal system in the middle and late Holocene.

This study addresses several knowledge gaps in the depositional history of the Pevensey Levels by examining potential connections between stratigraphy and climatic, hydrologic, and anthropogenic influences, building on the regional, foundational work of Jones (2002). Jones' (2002) study provided a stratigraphic framework of the Pevensey Levels, whose transect extended longitudinally through the Pevensey Levels roughly northwest-southeast and produced a multiproxy dataset, including sea-level index points and biostratigraphic proxies such as pollen, foraminifera, and diatoms, to reconstruct paleoenvironments in the Levels. This thesis advances Jones' (2002) regional work focusing on the bedrock-cored islands in the Levels to capture the preserved stratigraphic transition from the Pevensey Levels onto the islands, as well as integrating additional proxies, such as elemental analyses (pXRF) and mineralogical analyses (XRD), with radiocarbon age dating to identify connections between stratigraphy and climatic phases and/or anthropogenic activities. The overall depositional sequence across both islands follows a consistent pattern: marine-dominated silty clays transition to organic-rich peat layers within a transition zone and culminate in terrestrial silty clays, with the addition of sand in the upper stratigraphy of North Eye. This aligns with the findings of Jones (2002), while establishing links between these stratigraphic units and specific climatic phases, such as the 4.2 ka event and the MCA, but also suggested a relation between anthropogenic activity and the preserved stratigraphic record.

The stratigraphic analyses revealed localized variability in depositional environments. For example, the presence of sand-dominated units and episodic higher-energy depositional influences at North Eye, likely reflects its greater proximity to dynamic sediment sources, including the English Channel and the Wallers Haven in combination with thin sediment cover overlying the Tunbridge Wells Sand Formation, the bedrock geology of North Eye, that is partially exposed today. In contrast, Horse Eye is characterized by thicker sediment cover, a dominance of waterlogged conditions, and more continuous peat layers indicative of prolonged lower-energy conditions during the late Holocene. The findings highlight the importance of local geological and geomorphological factors, such as bedrock composition, elevation or topography, and proximity to sediment inputs, in determining depositional patterns and processes.

High-energy depositional events, shown through sedimentary structures such as sand laminations and lenticular sand laminations, reflect dynamic depositional processes, likely driven by potential storm activity, tidal surges, or increased fluvial discharge. These transitions could result from storms transporting sediment inland during higher-energy marine incursions, tidal fluctuations redistributing sediment along coastal margins, or heightened fluvial discharge during periods of increased precipitation. These higher-energy depositional events are often associated with major climatic phases, including the globally recognized 4.2 ka event, which corresponds to shifts in the stratigraphy observed at both Horse Eye and North Eye. Both islands exhibit similar depositional environments to these climatic drivers, with transitions to waterlogged conditions conducive to peat formation followed by higher-energy and terrestrial depositional conditions. The consistent stratigraphic response across the Pevensey Levels indicates a response to regional climatic processes within the context of localized geomorphological controls.

Anthropogenic influences, particularly during the Medieval period, are interpreted in the stratigraphy through features such as lenticular laminations and increased sand content in Unit 5c (Horse Eye Core HE23T4C4B). These features temporally align with documented land drainage and reclamation efforts, which likely modified hydrology and sediment transport dynamics. While direct evidence of human activity, such as artifacts, is

absent at Horse Eye, the sedimentary structures and increase in grain size align with historical documents, providing a framework for interpreting anthropogenic impacts on sediment transport and deposition. Further, the study of stratigraphic sequences at North Eye was inspired by the works of Champness (2009), who documented similar stratigraphic sequences and peat layers at this site- however, this thesis used multiple proxies and went into more detail than Champness' (2009) study. Together, these studies highlight the role of human and natural factors in shaping the stratigraphy and paleoenvironmental evolution of the Pevensey Levels.

By integrating findings from nearby lowland systems such as the Romney Marsh, the Brede-Pett Level, and Somerset Levels, this thesis establishes a broader regional context for interpreting the smaller-scale stratigraphic changes identified at Horse Eye and North Eye. Palaeoecological studies from these comparable sites highlight similar anthropogenic influences, including deforestation, expansion of agriculture, and drainage modifications during the Medieval period, which align with the stratigraphic responses observed in the Pevensey Levels. For instance, sedimentary changes in the Romney Marsh area reflect heightened erosion and sediment transport tied to human land use, while peat layers and transition zones in the Brede-Pett Level provide parallels to the depositional sequences identified at Horse Eye. These comparisons reinforce the interpretation that localized geomorphological and hydrological processes at Horse Eye and North Eye were embedded within broader regional patterns of environmental and anthropogenic change.

Situating these findings within a regional framework and drawing comparisons with adjacent systems, such as the Romney Marsh and the Somerset Levels, which have similar coastal-lagoonal characteristics and depositional histories, contextualizes the Pevensey Levels within a broader narrative of coastal environmental evolution and also contributes new insights that can inform future studies in this area. The data and interpretations presented in this thesis- such as the identification of high-energy depositional events, variability in peat accumulation, and anthropogenic influences- add new details to the broader understanding of the Pevensey Levels' coastal development. These findings highlight how such systems respond to climatic shifts and human interventions, offering a

framework that can be applied to similar embayments. In doing so, this thesis provides a foundation for both comparative studies and targeted investigations, providing information for paleoenvironmental research in low-lying coastal landscapes.

6.2.0. Future Research Directions

This thesis establishes a stratigraphic framework to reconstruct the paleoenvironmental history in the Pevensey Levels. Suggested avenues for further research are included below:

- Identify the provenance of mica and feldspar minerals. Determining the origin of the mica and feldspar minerals associated with increased grain size could help clarify the source and transport mechanisms of the sediment during higher-energy depositional phases.
- Expand the stratigraphic framework to additional bedrock islands, namely South Eye, Rickney, and Chilley in the Pevensey Levels (Figure 1.5). This could help refine the stratigraphic framework of the Levels and determine whether similar depositional processes and anthropogenic influences occurred across the Pevensey Levels.
- Obtain deeper cores (or more cores in certain areas) and geophysical methods to investigate the bedrock inside the Pevensey Levels and the origin of these topographically elevated areas in a Holocene-filled embayment.
- Further investigate and integrate archeological and historical records, examining human land use and activities in the Pevensey Levels and nearby similar coastal embayments. This might help better interpret and identify human-related components and differentiate natural and anthropogenic influences in these depositional environments and sedimentation.
- Increase the stratigraphic detail at Horse Eye and North Eye. Expanding the current stratigraphic framework to other parts of Horse Eye and North Eye would enhance the understanding of sediment covering these bedrock-

cored islands. For instance, deeper coring techniques, such as Geoprobe, could provide better insight into sediment thickness and stratigraphy at depths difficult to reach with a gouge auger. Targeting unstudied areas of these islands could reveal new sedimentary features, such as other high-energy sand units, or additional peat layers, this can be used to refine interpretations in this thesis.

- Add proxies to better understand the paleoenvironment. Incorporating biological proxies such as pollen, diatoms, and foraminifera, particularly in the peat units, could provide detailed reconstructions of vegetation, hydrology, and environmental conditions during key climatic phases and/or archaeological periods. Jones (2002) utilized pollen, diatoms, and foraminifera to reconstruct paleoenvironments in the Pevensey Levels, providing a framework for future studies that integrate similar proxies to expand paleoenvironmental reconstructions.
- Test the feasibility of using optically stimulated luminescence (OSL) to determine the age of sand units or laminations.
- Conduct hydrological modeling. Simulating groundwater and surface-water flow, sediment transport, and flooding dynamics in the Pevensey Levels would offer insight into hydrological processes and their effects on the stratigraphy.

References:

Allen, J. R. L. (1990). The Severn Estuary in southwest Britain: Its retreat under marine transgression, and fine-sediment regime. *Sedimentary Geology*, *66*(1), 13–28. https://doi.org/10.1016/0037-0738(90)90003-C

Andersen, K. K., Azuma, N., Barnola, J.-M., Bigler, M., Biscaye, P., Caillon, N., Chappellaz, J., Clausen, H. B., Dahl-Jensen, D., Fischer, H., Flückiger, J., Fritzsche, D., Fujii, Y., Goto-Azuma, K., Grønvold, K., Gundestrup, N. S., Hansson, M., Huber, C., Hvidberg, C. S., … North Greenland Ice Core Project members. (2004). High-resolution record of Northern Hemisphere climate extending into the last interglacial period. *Nature*, *431*(7005), 147–151. https://doi.org/10.1038/nature02805

Arthur, R. G. (2002). *English-Old Norse Dictionary*.

Ballard, A. (1910). The Sussex Coast Line. In *Sussex Archaeological Collections* (Vol. 6).

Bensharada, M., Telford, R., Stern, B., & Gaffney, V. (2022). Loss on ignition vs. thermogravimetric analysis: A comparative study to determine organic matter and carbonate content in sediments. *Journal of Paleolimnology*, *67*(2), 191–197. https://doi.org/10.1007/s10933-021-00209-6

Blaauw, M. (2010). Methods and code for 'classical' age-modelling of radiocarbon sequences. *Quaternary Geochronology*, *5*(5), 512–518. https://doi.org/10.1016/j.quageo.2010.01.002

Blott, S. J., & Pye, K. (2001). GRADISTAT: A grain size distribution and statistics package for the analysis of unconsolidated sediments. *Earth Surface Processes and Landforms*, *26*(11), 1237–1248. https://doi.org/10.1002/esp.261

Boggs, S. (2012). *Principles of sedimentology and stratigraphy* (5th ed.). Pearson Prentice Hall.

Bronk Ramsey, C. (2001). Development of the Radiocarbon Calibration Program. *Radiocarbon*, *43*(2A), 355–363. https://doi.org/10.1017/S0033822200038212

Bronk Ramsey, C. (2009). Bayesian Analysis of Radiocarbon Dates. *Radiocarbon*, *51*(1), 337–360. https://doi.org/10.1017/S0033822200033865

Bronk Ramsey, C. (2017). Methods for Summarizing Radiocarbon Datasets. *Radiocarbon*, *59*(6), 1809–1833. https://doi.org/10.1017/RDC.2017.108

Büntgen, U., Tegel, W., Nicolussi, K., McCormick, M., Frank, D., Trouet, V., Kaplan, J. O., Herzig, F., Heussner, K.-U., Wanner, H., Luterbacher, J., & Esper, J. (2011). 2500 Years of European Climate Variability and Human Susceptibility. *Science*, *331*(6017), 578–582. https://doi.org/10.1126/science.1197175

Cameron, K. (1961). *English place-names*. Batsford.

Chamley, H. (1989). *Clay Sedimentology*. Springer. https://doi.org/10.1007/978-3-642-85916-8

Champness, C. (2009). *Northeye, Pevensey Levels, East Sussex, Geoarchaeological Assessment Report* (p. 46). Oxford Archaeology. https://library.oxfordarchaeology.com/doc/342

Cochran, J. K., Landman, N. H., Jakubowicz, M., Brezina, J., Naujokaityte, J., Rashkova, A., Garb, M. P., & Larson, N. L. (2022). Geochemistry of Cold Hydrocarbon Seeps: An Overview. In A. Kaim, J. K. Cochran, & N. H. Landman (Eds.), *Ancient Hydrocarbon Seeps* (pp. 3–45). Springer International Publishing. https://doi.org/10.1007/978-3-031-05623-9_1

Dalrymple, R. W. (1992). Tidal depositional systems. In *Facies Models* (Vol. 62, pp. 201–232). Geological Association of Canada. https://doi.org/10.1306/D4267A69-2B26-11D7-8648000102C1865D

Davies, S. J., Lamb, H. F., & Roberts, S. J. (2015). Micro-XRF Core Scanning in Palaeolimnology: Recent Developments. In I. W. Croudace & R. G. Rothwell (Eds.), *Micro-XRF Studies of Sediment Cores: Applications of a non-destructive tool for the environmental sciences* (pp. 189–226). Springer Netherlands. https://doi.org/10.1007/978-94-017-9849-5_7

Degeai, J.-P., Devillers, B., Dezileau, L., Oueslati, H., & Bony, G. (2015). Major storm periods and climate forcing in the Western Mediterranean during the Late Holocene. *Quaternary Science Reviews*, *129*, 37–56. https://doi.org/10.1016/j.quascirev.2015.10.009

Di Stefano, C., Ferro, V., & Mirabile, S. (2010). Comparison between grain-size analyses using laser diffraction and sedimentation methods. *Biosystems Engineering*, *106*(2), 205–215. https://doi.org/10.1016/j.biosystemseng.2010.03.013

Drew, K. L. (2021). *Interpreting and extrapolating late Holocene stratigraphic multi-proxy data in Pevensey Levels, on the south coast of East Sussex, United Kingdom*. University of Waterloo.

Engelhart, S. E., Horton, B. P., & Kemp, A. C. (2011). Holocene Sea Level Changes Along the United States' Atlantic Coast. *Oceanography*, *24*(2), 70–79.

Environments of Change. (2023, June 21). Environments of Change. https://www.medieval-environment.com

Evans, J. R., Kirby, J. R., & Long, A. J. (2001). The litho- and biostratigraphy of a late Holocene tidal channel in Romney Marsh, southern England. *Proceedings of the Geologists' Association*, *112*(2), 111–130. https://doi.org/10.1016/S0016-7878(01)80021-3

Farrell, K. M., Harris, W. B., Mallinson, D. J., Culver, S. J., Riggs, S. R., Pierson, J., Self-Trail, J. M., & Lautier, J. C. (2012). Standardizing Texture and Facies Codes for A Process-Based Classification of Clastic Sediment and Rock. *Journal of Sedimentary Research*, *82*(6), 364–378. https://doi.org/10.2110/jsr.2012.30

Flugel, E. (with Munnecke, A.). (2010). *Microfacies of carbonate rocks: Analysis, interpretation and application* (2nd ed.). Springer. https://doi.org/10.1007/978-3-642-03796-2

FRITSCH. (2009). *Laser Particle Sizer "Analysette 22" MicroTec plus Operating Instructions*. https://www.yumpu.com/en/document/read/23274287/laser-particle-sizer-analysette-22-microtec-plus-pdf-john-morris-

Grant, M., & Waller, M. P. (2010). *Holocene Fire Histories from the edge of Romney Marsh* (pp. 53–73).

Green, C. (with Creswell, M.). (2021). *Shaping of the English Landscape: An Atlas of Archaeology from the Bronze Age to Domesday Book*. Archaeopress Publishing Ltd.

Haslett, S., Davies, P., & Strawbridge, F. (1998). Reconstructing Holocene sea-level change in the Severn Estuary and Somerset Levels: The foraminifera connection. *Archaeology in the Severn Estuary*, *8*, 29–40.

Haslett, S. K., Davies, P., Curr, R. H. F., Davies, C. F. C., Kennington, K., King, C. P., & Margetts, A. J. (1998). Evaluating late-Holocene relative sea-level change in the Somerset Levels, southwest Britain. *The Holocene*, *8*(2), 197–207. https://doi.org/10.1191/095968398669499299

Hewitt, C. M. (2018). Mapping the Pevensey Area Back to 1066: The Historical Environmental Evidence. *Cartographica*, *53*(2), 75–85. https://doi.org/10.3138/cart.53.2.2017-0001

Higham, N. J., Ryan, M. J., & Manchester Centre for Anglo-Saxon Studies. (2011). *Place-names, language and the Anglo-Saxon landscape*. Boydell.

Hudson, S. M., Waddington, C., Pears, B., Ellis, N., Parker, L., Hamilton, D., Alsos, I. G., Hughes, P., & Brown, A. (2023). Lateglacial and Early Holocene palaeoenvironmental change and human activity at Killerby Quarry, North Yorkshire, UK. *Journal of Quaternary Science*, *38*(3), 403–422. https://doi.org/10.1002/jqs.3488

Jenkins, R. G., & Hikida, Y. (2011). Carbonate Sediments Microbially Induced by Anaerobic Oxidation of Methane in Hydrocarbon-Seeps. In V. Tewari & J. Seckbach (Eds.),

STROMATOLITES: Interaction of Microbes with Sediments (pp. 591–605). Springer Netherlands. https://doi.org/10.1007/978-94-007-0397-1_26

Jennings, S., & Smyth, C. (1987). Coastal sedimentation in East Sussex during the Holocene. *Progress in Oceanography*, *18*(1), 205–241. https://doi.org/10.1016/0079-6611(87)90034-6

Jennings, S., & Smyth, C. (1990). Holocene evolution of the gravel coastline of East Sussex. *Proceedings of the Geologists' Association*, *101*(3), 213–224. https://doi.org/10.1016/S0016-7878(08)80006-5

Jones, S. L. (2002). *Sea-level changes in south east England and northern France* [Ph.D., Queen Mary University of London]. http://qmro.qmul.ac.uk/xmlui/handle/123456789/28591

Kibblewhite, M., Tóth, G., & Hermann, T. (2015). Predicting the preservation of cultural artefacts and buried materials in soil. *Science of The Total Environment*, *529*, 249–263. https://doi.org/10.1016/j.scitotenv.2015.04.036

Long, A. J., Waller, M. P., & Plater, A. J. (2006). Coastal resilience and late Holocene tidal inlet history: The evolution of Dungeness Foreland and the Romney Marsh depositional complex (U.K.). *Geomorphology*, *82*(3–4), 309–330. https://doi.org/10.1016/j.geomorph.2006.05.010

Louhisuo, A., Yli-Halla, M., Termonen, M., Kykkänen, S., Järvenranta, K., & Virkajärvi, P. (2024). Long-term changes in soil phosphorus in response to fertilizer application and negative phosphorus balance under grass rotation in mineral soils in Nordic

conditions. *Soil Use and Management*, *40*(1), e13013. https://doi.org/10.1111/sum.13013

Makvandi, S., Cauzid, J., Tarantola, A., Melfos, V., & Voudouris, P. (2023, August 31). *XRD clustering and quantitative analysis as a fingerprinting technique to study ore deposits*.

Miall, A. D. (2022). *Facies Models* (N. P. James & R. W. Dalrymple, Eds.). Springer International Publishing. https://doi.org/10.1007/978-3-030-87536-7_4

Moore, A. (2020). *Brief Historical and Geographical Context for Pevensey Levels*.

Moore, A. (2021). *Manorial Regulation and Negotiation in a Late Medieval Environment: Land and Community at Herstmonceux, 1308-1440* [Doctoral Thesis, University of Waterloo]. https://uwspace.uwaterloo.ca/handle/10012/17776

Mu, Y., Saffarzadeh, A., & Shimaoka, T. (2017). Influence of ignition process on mineral phase transformation in municipal solid waste incineration (MSWI) fly ash: Implications for estimating loss-on-ignition (LOI). *Waste Management*, *59*, 222–228. https://doi.org/10.1016/j.wasman.2016.09.028

Newell, A. J., & Peacock, D. C. P. (2023). The Isle of Wedmore relay ramp: How fault evolution created King Alfred's historic landmark. *Proceedings of the Geologists' Association*, *134*(3), 314–321. https://doi.org/10.1016/j.pgeola.2023.04.001

Papuga, K., Kaszubkiewicz, J., Kawałko, D., & Kreimeyer, M. (2022). Effect of Organic Matter Removal by Hydrogen Peroxide on the Determination of Soil Particle Size Distribution Using the Dynamometer Method. *Agriculture*, *12*(2), Article 2. https://doi.org/10.3390/agriculture12020226

Pears, B., Brown, A. G., Toms, P. S., Wood, J., Sanderson, D., & Jones, R. (2020). A sub-centennial-scale optically stimulated luminescence chronostratigraphy and late Holocene flood history from a temperate river confluence. *Geology*, *48*(8), 819–825. https://doi.org/10.1130/G47079.1

Pennington, B. T., Hamdan, M. A., Pears, B. R., & Sameh, H. I. (2019). Aridification of the Egyptian Sahara 5000–4000 cal BP revealed from x-ray fluorescence analysis of Nile Delta sediments at Kom al-Ahmer/Kom Wasit. *Quaternary International*, *514*, 108–118. https://doi.org/10.1016/j.quaint.2019.01.015

Pevensey Levels | Ramsar Sites Information Service. (1999). https://rsis.ramsar.org/ris/973

Povinec, P. P., Litherland, A. E., & Reden, K. F. von. (2009). Developments in Radiocarbon Technologies: From the Libby Counter to Compound-Specific AMS Analyses. *Radiocarbon*, *51*(1), 45–78. https://doi.org/10.1017/S0033822200033701

Prothero, D. R., & Schwab, F. L. (2004). *Sedimentary geology: An introduction to sedimentary rocks and stratigraphy* (2nd ed.). W.H. Freeman.

Reimer, P. J., Austin, W. E. N., Bard, E., Bayliss, A., Blackwell, P. G., Bronk Ramsey, C., Butzin, M., Cheng, H., Edwards, R. L., Friedrich, M., Grootes, P. M., Guilderson, T. P., Hajdas, I., Heaton, T. J., Hogg, A. G., Hughen, K. A., Kromer, B., Manning, S. W., Muscheler, R., … Talamo, S. (2020). *The Intcal20 Northern Hemisphere radiocarbon age calibration curve (0-55 cal kBP)*. https://hdl.handle.net/1912/26524

Rippon, S., Aalbersberg, G., Allen, J. R. L., Allen, S., Cameron, N., Gleed-Owen, C., Davis, P., Hamilton-Dyer, S., Haslett, S., Heathcote, J., Jones, J., Margetts, A., Richards, D., Shiel, N., Smith, D., Smith, J., Timby, J., Tinsley, H., & Williams, H. (2000). The

Romano-British Exploitation of Coastal Wetlands: Survey and Excavation on the North Somerset Levels, 1993–7. *Britannia*, *31*, 69–200. https://doi.org/10.2307/526920

Roberts, H. M., & Plater, A. J. (2007). Reconstruction of Holocene foreland progradation using optically stimulated luminescence (OSL) dating: An example from Dungeness, UK. *The Holocene*, *17*(4), 495–505. https://doi.org/10.1177/0959683607077034

Szajdak, L. W., Szatyłowicz, J., & Kõlli, R. (2011). Peats and Peatlands, Physical Properties. In J. Gliński, J. Horabik, & J. Lipiec (Eds.), *Encyclopedia of Agrophysics* (pp. 551–555). Springer Netherlands. https://doi.org/10.1007/978-90-481-3585-1_221

Timpany, S., Arnold, A., Howard, R., Dunbar, E., Reimer, P., Smith, D., Tyers, C., & Marshall, P. (2021). *Pett Level, Rother, East Sussex: Palaeoecological investigation of the 'submerged forest' and intertidal peat*.

Tromp-van Meerveld, H. J., & McDonnell, J. J. (2006). On the interrelations between topography, soil depth, soil moisture, transpiration rates and species distribution at the hillslope scale. *Advances in Water Resources*, *29*(2), 293–310. https://doi.org/10.1016/j.advwatres.2005.02.016

Tucker, M. E. (2001). *Sedimentary petrology: An introduction to the origin of sedimentary rocks* (3rd ed.). Blackwell Science.

Walker, M., Head, M. J., Berkelhammer, M., Björck, S., Cheng, H., Cwynar, L., Fisher, D., Gkinis, V., Long, A., Lowe, J., Newnham, R., Rasmussen, S. O., & Weiss, H. (2018). Formal ratification of the subdivision of the Holocene Series/Epoch (Quaternary System/Period): Two new Global Boundary Stratotype Sections and Points (GSSPs)

and three new stages/subseries. *Episodes Journal of International Geoscience*, *41*(4), 213–223. https://doi.org/10.18814/epiiugs/2018/018016

Waller, M. P. (1998). An Investigation into the Palynological Properties of Fen Peat through Multiple Pollen Profiles from South-Eastern England. *Journal of Archaeological Science*, *25*(7), 631–642. https://doi.org/10.1006/jasc.1997.0222

Waller, M. P., Burrin, P. J., & Marlow, A. D. (1998). Flandrian sedimentation and palaeoenvironments in Pett Level, the Brede and Lower Rother valleys and Walland Marsh. *Oxford University Committee for Archaeology*, *Monograph No. 24*(3–29). https://www.researchgate.net/publication/261830383_Waller_MP_Burrin_PJ_Marlow_AD_1988_Flandrian_sedimentation_and_palaeoenvironments_in_Pett_Level_the_Brede_and_Lower_Rother_valleys_and_Walland_Marsh_In_Eddison_J_Green_CP_eds_Romney_Marsh_Evolution_Oc

Waller, M. P., & Kirby, J. (2020). Coastal peat-beds and peatlands of the southern North Sea: Their past, present and future. *Biological Reviews*, *96*(2), 408–432. https://doi.org/10.1111/brv.12662

Waller, M. P., & Marlow, A. D. (1994). Flandrian vegetational history of south-eastern England. Stratigraphy of the Brede valley and pollen data from Brede Bridge. *New Phytologist*, *126*(2), 369–392. https://doi.org/10.1111/j.1469-8137.1994.tb03956.x

Wang, Z. (2020). Review of real-time three-dimensional shape measurement techniques. *Measurement*, *156*, 107624. https://doi.org/10.1016/j.measurement.2020.107624

Wen, B., Aydin, A., & Duzgoren-Aydin, N. (2002). A Comparative Study of Particle Size Analyses by Sieve-Hydrometer and Laser Diffraction Methods. *Geotechnical Testing Journal*, *25*(4), 1–9. https://doi.org/10.1520/GTJ11289J

Appendix A – North Eye Field Notes

TQ 568088
106883

Monday May 23rd, 2022

11:00AM North Eye
long shallow transect

NE22T1C1 0m:
50cm long
no compaction or rodding

1. Topsoil 0 - 7.5cm
   Light – medium brown
   Fairly friable
   Organic, lots of roots
   Sandy silt 40/60

2. **Clayey sandy silt** 7.5 – 27 cm
   20/20/60
   Light – grey brown
   *orange mottling
   More compacted
   Less roots than 1.

3. **Iron Pan** 27 – 33.5 cm
   More dense / compact
   Large dark iron spheroid
   brown/black
   *sesquioxide **sandy clayey silt**
   25/30/45

4. 34 – 46 cm
   Sharp upper boundary
   Sandy clayey silt -> much more clay
   - Light grey-brown

- Orange mottling
- Fairly compacted

Very little to no roots “E horizon”

15 / 35-40 / 45
concentrated near #5
gradual boundary @ bottom to next unit
few iron nodules

5. 46 – 49 cm
   Transition to next unit
6. Uniform: 49 – 55 cm
   ➔ **Sand** very clean well sorted
   ➔ Light grey/white fine grained
   ➔ Loose / moderately compacted

7. 55 – 60 cm
   Iron pan 2
   Sand, orange mottling
   Dark brown iron pan
   Sharp boundary to upper layer
   Very oxidized

NE22T1C2 10m:

1. **Topsoil**: 0 – 7.5cm

---

2. **Clayey Sandy Silt**: 7.5 – 18.5 cm

---

4. **Unit 4** 18.5 – 29cm

---

5. **Transition** 29 - 36 cm

---

6. Sample taken 36 – 39 cm

Same nice clean sand
TWS

---

6. A) 39 – 75 cm

- More orange mottling
- Some more clay

Otherwise, the same as 6

NE22T1C3 50m 34m dug section

1. 0 – 13.5 cm
Topsoil

---

2. **Clayey sandy silt**
13.5 – 27 cm

---

4. 27 cm – 42.5 cm

---

7. **Transition** with nodule
42.5 – 49 cm

---

8. 49 – 55 cm
very fine clay, some silt
very compacted
light grey, orange brown mottling
gradational boundary above and below

sample taken

7.A
less nodules 55 - 60 cm

NE22T1C4: 70m

0 – 10 cm
1. Topsoil

---

10 – 25 cm:
2. Subsoil

---

25 – 39 cm:
4

---

39 – 48.5 cm
5

48.5 – 52.5 cm
7 little bit darker grey

52.5 – 59 cm
8

---

59 – 85 cm
8A highly compacted heterogeneous
silty clay darker grey
lots of orange/brown mottling

---

87 – 100 cm
8 orange mottling
dry

NE22T1C5 100m:

0 – 9.5 cm

1

Topsoil

Thicker grass, tussocks,
flat ground
marsh vegetation

9.5 – 19 cm

Clay-silt subsoil

dark grey

transition zone to clay

2.A crumbly fine grained – clay

small # of roots

---

19 – 75 cm

8 A **clay silt** 70/30

darker grey w/ brown / orange mottling

---

75 – 139 cm:

8 A cont.

Extra oxidization + mottling

Some sand ~15% discontinuous

---

139 – 143.5 cm

Intermediate, sand content, transition layer

9 lost orange mottling

increasing sand content w/ depth

Clayey sand

143.5 – 177.5 cm

10. **Clayey sand**

Laminated clay + very to fine grained sand

Darker grey 1mm

Lots more orange and brown mottling

Mottling and sand interbedded

10.A 177.5 – 190 cm

Increased sand content / # laminations
orange mottling

10.B 190 – 201 cm

More blue grey
~~lack~~ of mottling
none no sand

---

11. 201 – 206 cm

Dark grey blue silty clay
20% silt 80% clay

Manganese content/ nodules

- Heavily gleyed

Nearly no orange
same mineralogy as **10.B**

Lamination locations:

142 cm ½ cm thick lam's
143 – 160 cm interbedded
mottling + sand

163 cm, 167 cm, 172 cm
3cm long 2 cm long 3 cm long

179 – 189 cm
grading upwards U-channel?
amount & thickness

190 – 198 cm
interbedded ½ cm long
laminations of sand

202 – 207 cm 11 cont.

---

207 – 232 cm
transition **12**

Increase in sand content

Darker grey very fine sand

With 2 – 3 mm sand laminations @ 210cm, 222cm, 229cm

Interlaminated

---

232 – 268 cm sample plant

: 245 – 250

13 (246 – 249 cm) (237 – 244 cm)
1 mm laminations of black in the dark grey

DARK grey, nearly black in colour, some lighter grey spots

Silty clay
20/80

13.A 268 – 276 cm
manganese nodules
increase in some sand,
very black interlamination

---

13 276 – 301 cm

@ 294 more manganese nodules

---

314 -> 380 cm lighter grey
silty clay **SHELLS**

14 >380 lost core
Sample taken

---

390 – 405 cm 14

---

405 – 428 cm bedrock 428?

NE22T1C6 85m:

0 – 9 cm:

1

---

9 – 23 cm:

2 A subsoil, more compact

---

23 – 125 cm:

8 A very small amounts of sand
less / no roots mottling
more clayey



Increasing depth -> increasing mm lamination of v.f sand

Packets of sand lams + clay ~60cm
Repeating & alternating

red mottling & some manganese

---

10 125 – 160 cm

---

10 A 160 – 185 cm 163 – 167 organics
increased sand lams

---

10 C organics 185 – 218 cm

Black flecks

Same as 10 B, more blue grey, more clay %
BUT organics organic wisps

207 & 214 organic layers

---

218 – 228 cm much more compact

12 30 / 70 lighter grey
clayey silt gradual colour change

SAMPLE TAKEN

NE22T1C7 77.5m:

1 Topsoil 0 – 11 cm

---

2 Subsoil 11 – 19 cm

---

4. A 19 – 29 cm **sandy clayey silt**
increase in orange mottling than **4**

---

4 29 – 45 cm

---

8 45 – 66 cm:

increase sand packet @ 58 – 59 cm

---

10 66 – 89 cm:

☆ Large sand pack? @ 66 – 67 cm at the contact

Sand horizon
Organized sand in small laminae (1mm) with depth
no pattern, not packets

Increase in mottling

Pocket of sand 80 – 85 cm

Many 1 – 2 mm continuous laminae

85 – 89 cm clay packet, some sand, less.

10. A increased sand lams 89 – 105 cm:

Increase in 1 – 2 mm sand lams

94 – 100: oxidized heavily, same comp, increase in sand lams

100 – 105: less oxidized, more sand lams

---

6. A 105 – 121 cm

Sharp boundary to sand.

uniform, well sorted v.f. to f sand

Manganese nodules @ upper contact!

Saturated sand @ 105 ~ 120

White / light grey has brown colouration

---

13 Sharp upper boundary 121 – 147 cm

Clayey sandy silt heavily oxidized (137 – 141 cm)

Light grey with much less clay, more silt, w/ sand

10/30/60-70 large manganese nodule @ 139 cm mark

---

13. A 147 – 171 cm:

Coarsening up

more clay than 13

Clay packets @ : 147 – 150 cm

161 – 164 cm

167 – 169 cm

Slightly oxidized packets in-between

Large ferrous nodule @ 155 cm mark

NE22T1C8 73.5 m

1 0 – 10 cm:
topsoil, very dark lots of roots

---

2 subsoil, more terrestrial & less clayey 10 – 23 cm 0

100

Slight orange mottling terrestrial
clayey

subsoil

subsoil

---

4 A 23 – 43 cm: sandy clayey silt

Increase in orange mottling
very little to no roots deep orange packets between silty packets

43 – 69 cm: sandy clayey silt
increase in sand nodules with depth

Silty packets: 53 – 58 deep rootlets

☆Sand coarser medium grains visible @ 65 – 69 marks☆

69 – 80 cm dark orange mottling

4. A cont.
increase in sand w/ depth
slight hints of lams near 74
patches of dark orange mottling

---

80 – 83 cm silty clay

Finer comp. clayey silt

10. A increase in clay comp.☆

83 – 91 cm

@90 break in core,
sand contact
white v.f to f sand

86 – 88 some small sand lams

91 – 99 cm 99 – 108 cm
rest of sand

~~108 – 125 cm:~~

Clayey lams in **clayey silt**

Concentrations:
113cm 118cm 129cm

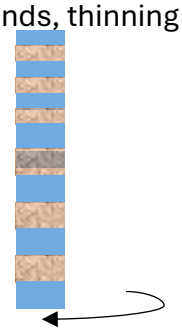
2 – 3 cm thick **silty clay** in **clayey silt**

Orange sand packets
109 – 112
114 – 117
118 – 123

Pattern:
silty clay | silty sand | silty clay | ...

End -> 133 cm

Silty clay band @ 127 – 128.5
sharp boundaries
thicker bands, thinning upwards



Just below slope break

NE22T1C9 65m:

1	0 – 8 cm	topsoil	
2	8 – 26 cm	subsoil terrestrial subsoil orange mottling	
3	28 – 32 cm	iron pan	*massive* iron chunk taken
2	32 – 45 cm	cont.	
3	42 – 44 cm iron pan, small pebble		
	45 – 60 cm:	moderately compacted medium brown	
	Clayey sandy silt 5 – 10 / 20 / 70		
3	iron pan	56 – 60 cm	
14	60 – 67 cm dark brown/grey Some orange mottling hints of organic ↑ small rootlets @ contact		
Buried Topsoil			
	~~SHARP Contact~~		

Similar silty clay ↑clay%

10 ?? very compact

67 – 78cm – 83

78 – 83 cm transition from dirty clay to clays from 78 to 83
darker grey

10A increased sand content

83 – 91.5 cm

Clayey sandy silt

---

10 91.5 – 105 cm

Increase clay ↑

silty clay orange mottling

NE22T1C10 57.5m:

1 0 – 7.5 cm topsoil

2 7.5 – 20 cm subsoil, terrestrial

4 20 – 36 cm **sandy clayey silt** with iron nodules @ 28 – 30 cm
iron-rich

8 ? 36 – 60 cm

clayey silt light brown / grey
very compacted clay / silt
20 / 80

Light orange mottling

slightly

gradational boundary

Slightly more more

8 ? grain size relatively the same, colour change gradually changed

Some orange mottling

60 – 72 cm

72 – 76 cm: light grey sharp upper & lower boundary

fine sized sand

Sand present, mostly silt

76 – 89.5 cm: well sorted coarser, medium sand

Iron staining

Some smaller clay mixing / inter laminations

Dark red / orange / brown colour iron staining @ 77 cm mark

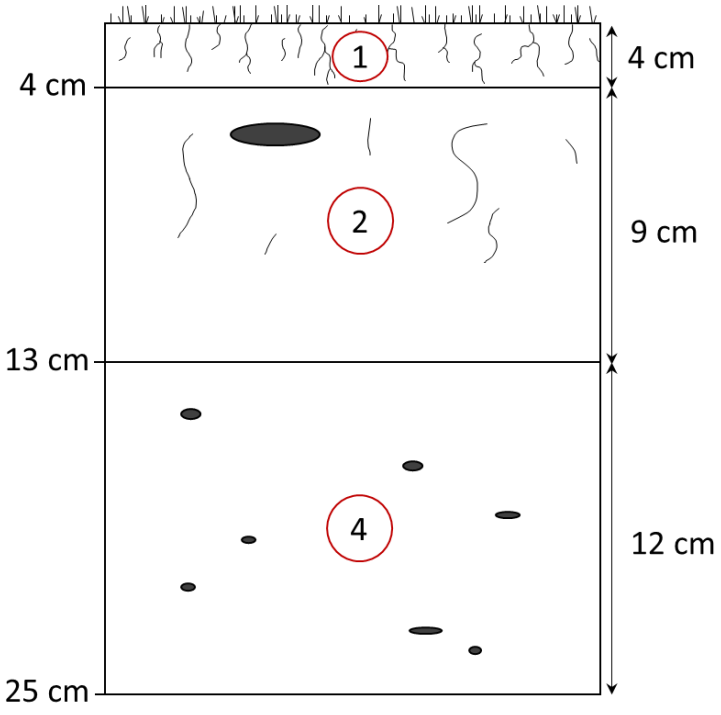
Fine grained: 82 & 86 clay layers

Impenetrable below 92 cm

87 cm – 92cm:

White band @ 89 – 90

CONTACT @ 92 very hard, dense


1
2
4
4 cm
4 cm
9 cm
13 cm
12 cm
25 cm

NE22T1C11 30m:

0 – 10 cm: (1)
topsoil

---

10 – 21.5 cm: (2) less roots

Subsoil

21.5 – 39 cm:

(4)

Transition zone 39 – 44 cm

Nodule-heavy ◯ 5 grades up orange mottling
iron spot @ 41.5

---

(6) v.f grained sand light beige

Less mottling

45 – 50 cm

Appendix B – Horse Eye Field Notes

Tuesday May 9th

Day 1: Cloudy, overcast, some sun

¬¬Transect running: 178˚ South

HE23T1C1: 0 m

6 – 13 cm (compacted? Does not start at 0 cm)

Subsoil, lots of roots

Medium grey brown

Silty clay

35 / 65 medium plasticity

Loose, not compacted

13 – 24 cm

Same medium grey brown

Slight orange mottling ~20 -24 cm

Less roots, but still some roots present, smaller roots

* Wetter clay (closer to ground surface, is this from rain?)

Gradual subtle upper boundary

Similar matrix to previous

Silty clay with granules

30 / 70 ~<5% granules: 1.5mm, larger pebble “med pebble” @ 20 cm

Increase in pebbles lower in depth in the unit

24 – 37 cm *dryer clay*

Sharp upper boundary

Light brown grey, lots of orange. Predominantly orange

Very dry and crumbly, very compacted compared to previous units

Silty clay – 40 / 60 , maybe 45 / 55 ?

Looks like clay but crumbles when dried out

Darker grey lamination ~ 1mm thick

Dark grey ~ 1mm nodules / granules ? and dark orange / brown (Iron?) nodules / granules closer to bottom of unit, ~ 33 cm and up

36.5 – 41 cm (**36.5 – 52 cm)

Gradational upper boundary

Light blue grey matrix with orange mottling, less orange than previous

Drier than first unit

Increase in darker grey (manganese?) nodules ~ 1 mm – 1.5 mm

** small white flecks starting @ 38 cm

Iron nodules (?) (dark orange / brown granules) missing.

Silty clay

30 / 70

**continued to 52 cm

With orange nodules re-appearing @ 50 cm

Could not get any deeper past 52 cm

HE23T1C2 25 m

5 – 11 cm (compacted? Does not start at 0 cm)

Medium grey brown

Disturbed soil, lots of roots and grass

Silty clay, very wet, medium to high plasticity

30 / 70

11 – 18 cm

Same colour with some orange mottling @ 14 – 17 cm

Loose, not compact

Some roots, but not as much as previous unit, smaller roots

Subsoil

Silty clay

30 / 70

18 – 29.5 cm

Grey-brown with lots of orange mottling

Sandy silty clay with granules and nodules?

5 / 20 / 75 mostly clay but can feel grit from sand? Or small clasts / nodules?

Gradational upper boundary

Matrix is same as previous

29.5 – 41.5 cm

Grey brown matrix, similar colour to previous unit

Gradational upper boundary for matrix, but abrupt addition of small very dark black granules in clusters <1mm

(is this carbon? Organic? Manganese? No purple / blue hue though)

Slightly larger, 1.5 mm granules NOT dark black slightly brown, maybe iron?

Matrix is silty clay- mostly clay, 30 / 70

** black granule clusters crumble when compressed with fingers **

Some, very few orange iron nodules, with some orange mottling

41.5 – 51 cm (**41.5 – 56 cm)

Starts off similar grey brown, but becomes lighter, more like beige as you get lower, near ~ 46 cm

A lot more orange than previous units

More compact

Gradational upper boundary, but abrupt orange increase

More crumbly (very crumbly), less wet, shiny when scraped, like unit 3 in C1

Clayey silt, less clay than previous

45 / 55 low to medium plasticity

Black nodules / granules present again, but less clustered

Cored deeper, previous unit continues to ~56 cm

56 – 67 cm

Compacted

Gradual upper contact, gradual colour change to a light brown / tan

Slight increase in plasticity, more medium plasticity

Black nodules / granules still present, ~5% distribution, mostly 1 mm

Some larger- pebble sized @ 62 cm

Silty clay, very compacted

30 / 70

Slight increase in red colour further down

67 – 80 cm

Decrease in black nodules / granules further down

INCREASE in red colour, more visibly red than orange

With very small amount of greenish blue grey mottling / mixing

Very compacted

Silty clay – 20 / 80

Very smooth when squished, with some granules.

Gradual upper contact

80 – 88 cm

TRANSITION ZONE

Silty clay – 20 / 80 with very little of black nodules from earlier

Mixing the colours from upper and lower units (red and greenish – blue – grey)

From more red to more greenish grey

Gradual boundaries / mixing of units

88 – 100 cm

Silty clay

20 / 80

Very little black nodules

Mixture of greenish grey & bright red mottling

NO nodules at bottom of core

Gradual contact with transition zone above

Smooth / shiny clay like earlier

Wednesday May 10th

Day 2: sunny, with rain patches

Negative before 0 m

X -------- 0m ----------25 m

176˚ South

HE23T1C3 -25 m

3 – 8 cm

Medium grey brown

Similar if not the same uppermost unit from yesterday

Loose, lots of roots

Silty clay – 35 / 65

Medium to high plasticity

Same as 1, top / subsoil

8 – 15 cm

Gradual upper contact

Same medium grey brown, lightens slightly overall near bottom, loose- not compacted

Introduction of some orange mottling

Loose

Silty clay with <1% v.f. sand grains

40 / 60

Slightly more silty, med to low plasticity than above

Some roots, less than above, smaller thinner roots

15 – 25 cm

Gradual upper contact

Very few small roots present

Slightly more compact

Lots of orange mottling

With dark orange brown hard granules <1 mm clusters forming @ mottling

Very little black wispy streaks present

Silty clay – 35 / 65 with orange brown crumbly granules

Light grey brown transitions lighter more into of a grey- grey brown @ bottom

Medium to high plasticity with some grit from orange nodules / granules

25 -53 cm

More compact and lighter colour, more grey, with light brown undertones

A lot more orange mottling concentrated

Gradual colour change in matrix upper contact, but more abrupt introduction of more orange & compaction is more sharply introduced

Low plasticity, clayey silt – 35 / 65 with orange granules / pebbles (~1mm)

Much more crumbly

~ 1 – 3% black wisps / dots

* cored deeper, unit continues to 53 cm, originally 43 cm

53 – 64 cm -> 79.5 cm (53 – 79.5 cm)

Similar grey colour matrix

Matrix is much more dry and crumbly

Much more orange crumbly granules

Very compact / dense

Matrix gradual upper boundary, but increase in orange granules is abrupt.

Black flecks / granules smearing / spreading black residue to nearby matrix

Low plasticity

Clayey silt with orange granules

10-15 / 20 / 65

Cored deeper, continues to 79.5, but gradually gets slightly more wet further down

79.5 – 91 cm

Medium plasticity, more wet and compact

Silty clay – 35 / 65

Very gradual upper boundary, slow transition above

Mostly grey with some orange mottling and smearing

Black flecks and smearing present @ 89 cm

91 – 96 cm (91 – 100 cm)

Same silty clay matrix- 35 / 65

Wet

91 – 93 cm light brown / tan SILT package ***

Mixed in with silt package, ½ ½ sharp contact between silty clay matrix and silt package

Bottom is mixture of same silty clay and silt package

Cored deeper, continues to 100 cm

But an introduction of more orange mottling, predominantly orange & grey mixed together, compacted, wet, silt (tan) is still present, mixed in with clear contacts

Orange / brown spots is silt packages mixed into silty clay

Abundance of ~1.5 mm 1 mm

Dark brown / prupley nodules / granules @ 98 cm, very compact group of nodules

Gradual upper contact

Some brown 1.5 – 2 mm granules mixed in

Bit crumbly, falls apart easily @ bottom portion of core, last 3 cm

Friday May 12

Day 3: cold, cloudy, rainy.

Starting @ 25 m = 0 m

167˚ South towards #5 flag, C4 @ 50 m in that direction from flag #5

174˚ South towards End flag, +42.5 m from #5 flag in direction.

HE23T1C4 ~117.5 m

4 - 9 cm: topsoil

Darker brown than usual cores above

Grass / litter, A layer, @ top, lots of roots

Silty clay, 35 / 65

Dark brown, medium plasticity, loose

** rain fall makes true comp and colour more difficult to determine **

---

9 – 14 cm: subsoil

Same dark brown

Same silty clay, 35 / 65

Less roots, smaller roots

Upper contact gradual

Slightly more compact

---

14 – 19.5 cm

Gradual upper boundary

Transition zone from darker top & subsoil, to lighter grey brown silty clay with much more visible silt

~ 40 / 60 – 45 / 55

Small roots present, tapers @ bottom

19.5 – 25 cm:

Same unit as before, more light grey brown

Silty clay 40 / 60 – 45 / 55

Gradual slanted contact, colour change.

Less small roots

---

25 – 36 cm: (43.5 cm)

Clayey silt, lots of silt seen in hand lens.

30 / 70 – 35 / 65

Light grey brown with orange mottling + smearing.

Gradual upper contact

Black (organic?) flecks concentrated @ 33 cm.

SHELL fragments @ 33 cm with slightly more orange near bottom

“Very dark grey brown”

Medium to high plasticity.

Cored deeper. Continues to 43.5. More shells, less orange mottling

Same grey brown

Clayey silt 35 / 65 – 40 / 60 with orange mixed in

*** more shells @ 39 – 42 cm ***

43.5 – 54.5 cm

Gradual matrix upper boundary, increase in orange mottling, same dark grey brown, abrupt increase of more orange for upper boundary.

Clayey silt 40 / 60 – 45 / 55

Medium plasticity (no rain)

HE23T1C5: (75 m)

2 – 6 cm:

Medium to low plasticity

Clayey silt 40 / 60

Greyish brown, lots of roots, A zone, litter, modified ground

Loose.

---

6 – 17 cm:

Clayey silt 20 / 80, loose

Lots of silt, can see silt in hand lens.

Low to medium-low plasticity

Less roots still present, smaller roots

Lighter grey, “brownish grey” with orange mottling <5%

Orange mottling near bottom of unit

Gradual upper contact

---

17 – 34 cm:

Increase in orange mottling and orange mottled silt.

Matrix is light grey silty clay 30 / 70

Medium to high plasticity

Matrix gradual upper contact, abrupt orange increase

Lots of black / grey granules & pebbles present, one 0.5 pebble? Piece of wood that is very angular and layered, fossil?

Very little amount of small roots.

More compact

Small amount of red rusty granules ~1 mm

---

34 – 49.5 cm:

Very compact

Small laminations <~1 mm of light brownish yellow / orange, and light grey wispy laminations

Silty clay 35 / 65 – 40 / 60

Predominantly yellow / orange with some bright orange mottling, some dark wisps / laminations, predominantly purple/grey, gradual upper boundary

Cored deeper, continued to 105 cm

Orange and grey inter lamination continue, mixture of both colours

Very compacted and dense

Struck water table, bottom very wet & fell out.

Composition gets more clayey nearing bottom, very wet

Silty clay 25 / 75 – 30 / 70 ish

Some manganese nodules / granules @ 82 cm

Gradually gets wetter and more clayey further down, no visible upper contact.

Monday May 15th

Sunny and hot

175˚ South starting at C5 (75 m) + 10 m = 85 m

HE23T1C6 85 m

3 – 8 cm

Medium to low plasticity

A zone, litter, lots of roots, modified ground, loose

Clayey silt 15 / 85

Dark grey brown

---

8 – 19 cm

Low plasticity

Gradual upper boundary

Dark grey brown with orange mottling

Crumbly, less roots but still have some present, smaller roots

Silt with clay 90 / 10

Loose and crumbly

---

19 – 30.5 cm

Lighter grey brown with orange mottling & ~ 1mm laminations / streaks

Slightly more clay than above, more compact, with some grit

Clayey silt 20 / 80

Low / medium plasticity

Drier, lots of orange streaking & some granules

Firm and dry, minimal amount of small roots

Gradual upper boundary

30.5 – 40.5 cm:

More clay, gradual matrix upper boundary, abrupt increase of orange mottling & streaks

Silty clay 35 / 65

30 – 40 % orange

Large pebble @ 36 – 37 cm (2 cm x 0.5 cm)

More compact at bottom with some black granules @ bottom

Firm

40.5 – 59.5 cm: (40.5 – 81 cm)

Increase in light orange mottle smearing laminations (~1mm) ~50%

Much more firm, very dense, increase in clay

Medium plasticity

Silty clay, 30 / 70

Gradual upper boundary

Cored deeper to 81 cm

Same unit

30 / 70 grey / light yellow orange

HE23T1C7 100 m

0 – 9 cm:

Litter, top soil, A-zone, lots of roots

Low to medium plasticity

Dark grey brown

Clayey silt 20 / 80

---

9 – 22 cm:

Loose, flakey, platy

Grey with orange mottling (3 – 5%)

Medium plasticity

Clayey silt 25 / 75

Still darker grey

Slightly more compacted

Gradual upper boundary

---

22 – 30 cm

Gradual upper boundary, more compacted

Dark grey, increase in orange mottling

Clayey silt 35 / 65

---

30 – 36 cm:

Silty clay 30 / 70

Increase of clay

Some colour

More clay, medium plasticity

---

36 – 43 cm

More compact

Medium to high plasticity

Silty clay 25 / 75 – 20 / 80

More orange

Some black smearing / streaks

Cored deeper

43 – 60 cm missing

60 – 71 cm:

Low to medium plasticity

dark grey with lots of dark orange rusty mottling (~5%)

silty clay with some orange grit 20 / 80 compact

---

71 – 79 cm

Medium plasticity

Light grey with ~ 5 – 8 % orange mottling / smearing

Gradual upper boundary

---

79 – 107.5 cm:

Abrupt increase in orange / yellow colour, upper contact

Medium to high plasticity

More wet and compacted, firm @ dense

Clay with silt 85 / 15

Mostly yellow / orange

Some grey mottling / smearing

Tuesday May 16

Sunny & hot

Starting @ 100 m going 168˚ South, going 7.5 m from 100 m = 107.5 m

---

HE23T1C8 (107.5)

2.5 – 7 cm:

Clayey silt 30 / 70

Medium to low plasticity, holds shape but still a bit crumbly

Lots of roots, litter zone, modified ground, dark brown

---

7 – 17 cm:

Dark grey brown

Clayey silt 30 / 70

Holds shape but still falls apart – medium plasticity

Some light brown mottling

Gradual upper boundary

---

17 – 42 cm:

Clayey silt w/ v.f sand (<5%)

30 / 70 25 / 70 / 5

Lighter grey brown with <5% orange mottling

More silty @ top near 20 cm, more clayey @ bottom of unit near ~40 cm

Gradual increase in clay ~25% -> ~35% fining downward

Orange mottling decreases near bottom but still present, some dark brown mottling / smearing

---

~~42 – 51 cm:~~ 42 – 59 cm:

Clayey silt 25-30 / 65-70

Low plasticity – medium/low plasticity

Still similar clayey silt matrix

SAND package @ 45 – 48 cm

v.f sand -> light yellow brown

medium light grey silty clay matrix

sandy clayey silt 15 / 25 / 60

@ 51 cm, 1.5 cm pebble

Cored deeper -> 80 cm

Same unit continues to 59 cm

Same clayey silt matrix, but there is an increase of sand, clayey sandy silt 10 / 30 / 60

Orange mottling, medium to low plasticity, and v.f sand package @ 56 – 59 cm

---

59 – 80 cm:

Increase in clay content, medium plasticity, holds ~2mm rolls moderately well

Increase in rusty brown mottling -> v.f sand

rusty brown mottle is v.f sand in packet @ 69 – 72 cm

light buff brown v.f sand packets in laminations and mottles @ 61 – 68 cm

overall, increase in clay, and sand packets still present

overall: clayey sandy silt

sandy clayey silt

15 sand / 30 clay / 55 silt

Red sand laminations

Light grey matrix

Weird white hard granules? fossils? @ 69

Gradual upper boundary

Dark grey steaks ~1mm

HE23T1C9 113.5 m –> 13.5 m from C7 (4th flag from bottom)

2 – 7 cm:

Topsoil, litter zone, A zone, lots of roots

Dark brown, modified soil, more wet, loose

Medium plasticity

Silty clay 35 / 65

---

7 – 16.5 cm:

Med to med-high plasticity

Loose, less small roots

Some orange mottling

Less wet, slightly more compact

Silty clay 35 / 65

Same as @ end core

Gradual upper boundary

16.5 – 32 cm:

Silty clay 30 / 70

Dark grey brown

SHELLS, small fragments near 24 – 32 cm

Some orange mottling, <2%

Chert granules & pebbles

Some small roots @ top

Very little amount

Gradual upper boundary

Firm, more compact, dense

Medium plasticity

Wednesday May 17

Sunny & hot

Resuming from C9, cored deeper.

CONT. HE23T1C9:

Continued last unit from yesterday

32 – 43 cm:

Still orange mottling & shell fragments present (38 – 43 cm)

Mottling & shell fragments present, fewer nearing bottom, but still present

Very little small roots

Cored deeper and brought up soil @ 33 – 35 cm

& hit lots of chert pebbles

HE23T2C1: 0m

0 – 9.5 cm:

Top soil, modified ground, lots of roots, litter zone (A zone)

Greyish brown

Silty clay 40 / 60

Medium plasticity

Substantial silt in hand lens

Loose but not crumbly

9.5 – 16 cm:

Matrix continues, slightly more silt, silty clay 40 / 60 – 42 / 58 ish

Same brownish grey, BUT introduction of orange mottling ~2% - 5%

Still some small roots present, not as much

Gradual upper boundary

---

16 – 27 cm:

Lighter grey brown than before 2 top layers

BUT increase in rusty orange / brown mottling ~5-7 %, and some orange brown granules, that can be crushed in fingers

Very small # of roots near top

Silty clay 40 / 60

Medium low plasticity

Black nodule again ~3mm @ 25.5 cm depth

Moderately well sorted, slightly more compact than above

---

27 – 34.5 cm:

Much more light in colour, with lighter yellow / orange mottling / streaks, no roots

More compact than above units

Much more dry & crumbly than other units, very dry and dense

Light orange / yellow smearing / streak / laminations ~2 mm

Clayey silt 20-25 / 80-75

Gradual upper boundary

Well sorted, low to medium low plasticity

Cored deeper, same unit until 45.5 cm

Feels like clay, but is very crumbly

Cored deeper to 66.5 cm, same dry unit, hard, dry, crumbly

Low plasticity, same colours

Thursday May 18th

Sun and cloud

265˚ West from HE23T2C1 @ 53.5 m west from C1

HE23T2C2 53.5 m

2 – 7.5 cm:

Pretty wet / moist

Dark greyish brown, medium to medium high plasticity

Well sorted, lots of roots, A zone, litter, modified soil, topsoil

Silty clay 30 / 70

7.5 – 12.5 cm:

Same dark grey brown, orange mottling ~1%

Well sorted, less roots, smaller roots, gradual upper boundary, loose, still moist, bit crumbly

Silty clay 30 / 70

12.5 – 23 cm:

Silty clay 35 / 65

Medium to med-high, more medium, plasticity

Little bit lighter grey brown than 2 top units, increase in orange mottling, ~5%

Small roots present

More firm / compact

---

23 – 28.5 cm:

Transition layer from above lighter greyish brown with orange mottling, to light grey with orange mottling below.

Matrix is gradual for upper and lower boundary, BUT abrupt increase in orange mottling ~30 – 35%

Slightly more firm than above unit

Small pebbles present (1.5 mm), medium plasticity

clayey silt 35 / 65

28.5 – ~~36 cm~~: -> 45 cm

Light grey with orange mottling ~10 %

Small pebbles present, very small % of small roots near top, and orange smearing / laminations???

Medium to medium-low plasticity

MATRIX: silty clay 35 / 65 pretty platy

Orange mottle: more silty? More grainy, either silty or mineralization & oxidation

Very firm and dense

31.5 – 34 black specks / granules – manganese?

Cored deeper, same unit ends @ 45 cm

More manganese @ 37, 38 cm, 42 – 44 cm

Small pebbles (chert pebbles) @ 40 – 43 cm, large pebble @ 41 cm

Silty clay 35 / 65

Light grey with orange mottling ~25 % orange brown

Moderate sorting, matrix is well sorted

Low to medium plasticity

Cored deeper, Unit continues to 53 cm

Iron / rusty nodules @ 50 cm

46 – 48 cm & 51 – 53 cm manganese packets

Cored deeper, 53 until 83 cm

53 – 64.5 cm: Iron Pan

Iron pan with manganese nodules, very crumbly

No matrix

64.5 – 71 cm: Transition Unit

½ iron pan & manganese

½ lower silty clay (medium plasticity)

---

71 – 83 cm:

Medium plasticity, light grey with orange brown smeared lower half @ 77.5 (same composition)

Silty clay 25 / 75

Well sorted, manganese nodule @ 75 cm & smaller ~1mm manganese nodules dispersed heterogeneously

Very firm & dense, compacted

Friday May 19, overcast & sun

HE23T2C3 (End ? m)

6 – 14.5 cm: lots of roots, litter, loose, A-zone

Very dark grey brown

Medium to medium-high plasticity

Silty clay 40 / 60 well sorted

Lots of visible silt, modified ground

14.5 – 24 cm:

Small roots, small amount still present

Greyish brown, lighter with slight orange mottling ~1%

Silty clay 35 / 65 visible silt. Lots

Gradual upper boundary , well sorted

Medium – med-high plasticity

Slightly more compact than last unit

---

24 – 39 cm:

Small amount of small roots in top portion of unit (24 – 30 cm) present

Manganese nodules @ 29 cm, & cluster @ 33 cm

Some iron nodules

Orange mottling ~ 5 – 10 %

More compacted and dense than earlier units

Very small shell fragments (~2mm) @ 29 cm

Light brown grey, lighter than above with orange mottling

Gradual upper boundary

Not well sorted, but not poorly sorted

Silty clay 35-40 / 65-60

Cored deeper:

39 – 53: same unit, less manganese

Same properties, silty clay, but slightly more wet, medium plasticity

Manganese nodules still present, **no** shell fragments

Silty clay 35-40 / 65-60

Slight increase in orange mottling – 10-15% moderate sorting

cored deeper: to 108 cm

same unit until ~ 65 cm then becomes more wet & clay

lots of orange/iron mottling at bottom

A little bit of SAND at bottom (between v.f. sand and silt)

~ 65 – 108 cm:

More wet, slightly higher plasticity, med to high plasticity

Silty clay, 25-30 / 75-70

Less manganese nodules

Compact, light grey with 30% orange mottling / smearing

Lots of orange @ bottom

Shells? -> ~1.8m elevation

TQ 62324 08368

Top -> TQ 62534 08365

Monday May 22

Cloudy, overcast

274˚W towards C1, 105 m.

-105 m from C1

HE23T2C4 -105m terrestrial top soil

0 – 7.5 cm: Topsoil, Litter, A zone

Lots of roots, very dry, very loose & crumbly, no clay

None to v. low plasticity

Silt 100% with lots of roots

Light buff brown, light grey well sorted

7.5 – 13 cm: MISSING CORE

---

13 – 19.5 cm:

Slightly darker buff brown

Some orange mottling, <1%

Very dry, very crumbly, but slightly compact.

Low plasticity

Well sorted < 5% clay ~95↑% silt

Silt with clay

Still some small roots missing

Upper boundary.

19.5 – 27.5 cm:

Low plasticity, can't hold much shape

< 0.5 cm scarce small roots

Very dry, much more compact

Much more orange mottling ~3%

Silt with slightly more clay, but still very silt heavy

5-7.5 / 95-92.5
clay / silt

Transitions to increase in clay and lighter colour near bottom of unit, similar colour to darker buff brown

---

27.5 – 35.5 cm

Light grey brown with light yellow hue

Medium to low-medium plasticity, lots of orange mottling and staining 10-15%

Very compact and dense

Some iron nodules & some black staining / smearing

Silty clay 40 / 60

Gradual upper transition

35.5 – 41 cm

Gradual upper boundary

Gradual increase in clay % as you increase in depth

Silty clay 35 / 65 medium plasticity

Light grey matrix with ~30% light yellow orange mottle / streaking & dark red brown mottle ~3%

Very compact, very dense

Some iron nodules

Well sorted

---

41 – 47.5 cm:

Very dense & compact, same colouring as above

More clay

Silty clay 30 / 70

A lot more orange ~40 – 45%, ~3% dark red brown mottle

Well sorted, more moist

Gradual upper boundary

---

156 m from C2 @ 269˚ W

Total of 209.5m from 0m mark

HE23T2C5:

A lot of compaction?

8.5 – 18.5 cm: no plasticity

Very dry & crumbly, very brittle

Lots of roots very loose,

Litter, A-zone, modified soil

SILT dark grey brown
100

18.5 – 24 cm: gradual upper contact

Transition zone, from dry, loose & crumbly to dry & compact,

Same dark grayish brown

Very stiff & crumbly, compact

Well sorted, no plasticity

Some small roots still present

SILT 100% subsoil -ish

---

24 – 33 cm: **charcoal??**

Very dense & compact

Dark brown

Some small roots @ top

Low plasticity, can mold into shape but falls apart

Bright red orange mark / smear @ 27.5 cm

Gradual upper contact w/ transition layer

Silt with very minimal clay to help hold shape

Silt with clay <5 / >95

---

33 – 43 cm:

Gradual upper boundary

Very dense & compact, stiff

Dark brown, scarce small roots

Low-medium plasticity

Well sorted clay & silt
~50 / ~50

Slightly more clay heavy, moist

Some orange mottling ~1%

Some black marks, w/ larger black chunks ~2mm, charcoal??? Plant material??

➔ Rare presence of v.f. sand

---

43 – 50 cm:

Same matrix -> clay & silt 50 / 50

Dark grey brown

Increase in sand packets

~5% sand, v.f. sand

Very dense & compact

Black chunks still present

Medium plasticity, well sorted matrix w/ sand lams & packets

Cored deeper

50 – 68.5 cm:

Med plasticity silty clay 40 / 60

Greyish brown, lighter near bottom, continuation of upper unit.

(43 – 68.5) compact,

Well sorted some sand packets ~3-5%

68.5 – 76 cm:

Transition unit from before with black pieces to incorporating

Orange mottling ~3%

Silty clay 40 / 60 compacted

Black @ 75cm

---

76 – 89 cm:

More moist, silty clay 30 / 70

More clay lighter colour, grey brown

Medium to high plasticity,

Increase in orange mottling ~10% @ top of unit, ~20% near bottom of unit

Very compact & firm

(look @ Anna notes)

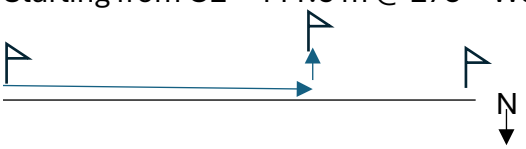
ANNA NOTES:

Greyish brown

More moist, more clay %, silty clay 30 / 70

Tuesday May 23 Sunny, windy

Starting from C2 + 111.5 m @ 278 ˚ West and + 2.1 m @ 170 ˚ South



HE23T2C6 (165m total)

Compaction
7.5 – 13 cm: Top soil, modified ground, litter (A) zone

Less compact, more loose, crumbly

Silty clay 40/60

Dark greyish brown lots of roots

Medium to medium-high plasticity

Well sorted fairly moist

---

13 – 21.5 cm: subsoil

Dark greyish brown

Silty clay 40/60

Slightly more compact

Still lots of roots, small roots

< 1% orange mottle

Gradual upper boundary well sorted medium plasticity

Small twig @ 15 cm

21.5 – 33.5 cm: (21.5 – 48.5 cm)

Silty clay 35 / 65 matrix

Dark orange mottle is more coarse ~10 – 15%

More mottle near bottom

Medium plasticity, more compacted, very compacted and dense

small granules poorly sorted (2mm large)

~ 1mm large black chunck @ 29.5 cm

Cored deeper to 40 cm:

Same unit continues to 40 cm

Medium plasticity, silty clay 35 / 65

Poorly sorted, matrix with nodules & granules

& mottling abrupt introduction of manganese nodules @ 34 cm ~1mm large

Brownish grey matrix with ~20% brown orange mottle & ~3% manganese nodules

Very compact & dense,

No roots,

Matrix: gradual upper boundary

Cored deeper to 66 cm:

Same recent unit continues to 48.5 cm: 40 – 48.5 cm:

Still very compact & dense, very dry

Mixture of older colours (from above) with brownish grey,

Orange mottling, still has manganese nodules

Medium plasticity

More well sorted, mottle is no longer coarser

Silty clay 35 / 65

More stiff and dry

Chalk-like white granules, not as much iron nodules

48.5 – 55 cm:

Transition unit

Colour transitions between browinish grey mixes in light grey orange mottle present (~20-25%)

Shiny when scraped

Increase of white mottling / chalk granules (~3-5%)

Light grey matrix from greyish brown -> very compact while more lighter in grey

---

55 – 66 cm:

Very compact / dense

Matrix – light grey, very dry, can mold, but very crumbly

Increase in white mottling / granules

Still have black chunks / manganese nodules

Well sorted – medium plasticity (feels like low plasticity because it is dry)

Lots of colour mixing, light/dark orange mottling, light/dark grey

Iron/manganese smearing

Very dry

Silty clay 25-30 / 75-70

Smears easily

➔ Orange decreases further down to ~20%

very firm, also shiny when scraped

medium plasticity

very platy

silty clay (20-30 / 80-70)

gradual upper boundary with transition zone/unit

orange mottling forms 1 mm streaks / laminations

white chunks range in size from 1 – 3 mm – they are heterogeneously distributed

white chunks have visible very small grains- gritty

well sorted

HE23T2C7

Same direction: + 102 m (from C2) @ 278 ˚ West and + 2.5 m @ 170 ˚ South



12 – 16.5 cm:

Dark greyish brown

Loose and crumbly

Very dry, top soil lots of roots

A-zone, modified ground

Silt 100, well sorted.

16.5 – 24 cm:

dark greyish brown very dry

still crumbly subsoil

still some roots, small roots 1% orange mottling

slightly compact but mostly loose

silt 100

gradual upper contact, well sorted

---

24 – 33 cm:

Dark greyish brown w/ ~10% orange mottling

Very compact & dense and dry

Shiny when scraped

Clayey

Silty clay 35/65

Gradual upper contact

Well sorted

Some small roots @ top of unit

Wednesday May 24th 2023

Sunny day, John accompanying us

New Transect, @ 0 m

HE23T3C1:

0 – 8 cm: zC $_{rt\text{-}org}$

Topsoil lots of roots

Well sorted

Dark greyish brown

Litter A-zone

Silty clay 35/65 medium plasticity

Loose, dry, & crumbly

---

8 – 16.5 cm: subsoil, roots visible zC $_{rt\text{-}mot}$

Medium – low plasticity

Orange mottling ~3%

Dark greyish brown matrix, slightly lighter than top unit

Slightly more compact than above

Slightly more silt than above

Silty clay 40/60

16.5 – 35 cm: zC $_{rt\text{-}mot}$

Light greyish brown with dark orange mottling (~20-25%)

Increase in clay % from 2nd unit

Silty clay 25 / 75 Medium plasticity

More compact, less roots than above

Medium sized pebble @ 24 – 25 cm ~1cm in size (long-axis)

Gradational upper boundary well sorted

---

35 – 45.5 cm: zC $_{rt\text{-}mot}$

Medium-high plasticity

More clay – silty clay 10-15 / 90-85

Light grey with dark orange mottle ~25%

Dense, pretty dry very little amount of roots

Gradational upper boundary

Manganese nodule (40-44 cm)

Well sorted

cored deeper to 77 cm

45.5 – 72 cm: zC $_{mot}$

Continuation of previous unit (silty clay 10-15 / 90-85)

Light grey with dark orange mottle (~5–10%)

Dense, medium-high plasticity

Little amount of roots

Damp

---

72 – 77 cm: (new unit) (72 – 110 cm) (z)C $_{mot}$

Damp / sticky, very moist

High plasticity clay with very minimal silt < 3 / ~97

Abrupt / sharp contact @ ~72 cm

Dark orange mottle (40-45%) with black smearing (manganese) (~5%)

Matrix – light grey

Still very dense but less than above

Compact

cored deeper to 110 cm

previous unit continues down

much more manganese near bottom

orange mottle relatively the same, iron nodules

not a drastic change

HE23T3C2 ? m

[soil horizon: 0 - 33 cm, 3 sub-units within
natural ground 33 – 43 cm]

0 – 33 cm:

(3 sub units)

0 – 6 cm: lots of silt and organics Z $_{rt-org}$

A horizon litter @ top

(clayey silt 25 / 75 ? insinuated - was not written)

Greyish brown

Lots of roots, mostly roots, silt and organic material

Loose, Dry

---

6 – 23 cm: $cZ_{rt\text{-}mot}$

Less roots

Compacted a bit, dry

Low plasticity

Very crumbly, same clay

Slight increase in clay

Clayey – silt 25 / 75

Matrix the same, but intro of orange mottle (10%)

---

23 – 33 cm: $(g)zC_{mot}$

some medium pebbles (~ 1 cm large) @ 24 – 29 cm range near bottom of soil horizon

pebbles ~ 1 cm long axis

same greyish brown matrix but increase in orange mottling (~20%)

less roots, dry, slightly more compact

silty clay 40 / 60

increase in clay further down in unit

---

33 – 43 cm: (33 – 87 cm) $(z)C_{mot}$

Clay, < 3% silt

Moisture content increased near bottom of unit

High plasticity

Yellowish brown matrix with light grey mottle ~5% and red mottle 5%

Manganese nodules (1mm) ~3%

Dense and compact

Cored deeper to 87, same unit.

43 – 87 cm:

Continuation of same unit, yellowish brown matrix

Very platy, high plasticity

Mainly clay

Manganese nodules (0.5 – 1 mm) ~3%

Grey mottle 5%, red mottle %

Dense and compact

HE23T3C3

? m

0 – 13 cm: $Z_{rt\text{-}org}$

Dark grey brown matrix, silt and roots

Lots of roots

A-horizon, silt and organic material and roots

Loose material

---

13 – 28 cm: $zC_{rt\text{-}org}$

Gradual upper contact

Abrupt lower contact, middle is gradational

Mixture of upper and lower

Transition unit

Medium plasticity

Clay w/ organics, medium roots

Dark orange mottling ~5%

---

28 – 43 cm: (28 – 58 cm) (z)C $_{mot}$

Roots

Grey matrix with dark orange mottling (20%)

High plasticity

Moisture similar to 1st core

Clay, almost 100%

Low roots

Very dense / compact

Cored deeper to 58 cm

Relatively the same unit

Grey matrix with dark orange mottling (20-25%)

High plasticity

Clay

Iron and manganese nodules 1-2%

Broken shell (1 mm) @ ~52 cm

White granule at ~49.5 cm

Dense and compact

Cored deeper to 112 cm

58 – 98 cm: C_{mot}

SHELL fragment at 91 cm

Grey matrix with dark orange mottling

Many shells

High plasticity

Comp: Clay and shells

High density and compacted

Manganese nodules, mottling 10%

Shells size ~ 1mm

---

98 – 109 cm: $C_{org\text{-}mot}$

Dense and compacted

Organics

Grey matrix with dark orange mottling, w/ very dark grey / black organics

High plasticity

Clay with silt (5-10% silt)

1 cm organic pocket (99 – 100 cm)

Shiny organics

ABRUPT introduction of organics

---

109 – 112 cm: $C_{org\text{-}mot}$ / $(s)_{l\text{-}lam}$

SAND

Yellowish brown matrix clay w/ sand packets

(visible but not incorporated)

Dense / compact

Organics (5%)

Cored deeper to 143 cm

continuation of previous unit

manganese nodules scattered throughout ~3%

water table

very wet and saturated, hit around organics

high plasticity

clay w/ sand *[estimation after reading notes: ~95-90 clay ~5-10 sand]*

saturated

yellowish brown w/ orange mottling (5%)

very dense and compact

Thursday May 25th

(with John & Ben)

HE23T4C1 0 m

0 – 52 cm – 4 units subdivided into 2 units total

0 – 10 cm: zC $_{rt\text{-}mot\text{-}org}$

Dark greyish brown with minimal orange mottle (< 3%)

Low / medium-low plasticity

Lots of roots

A-horizon, litter, loose / crumbly

Illuviated Zone (10 – 18 cm)*
(shallow Illuviation) (flushed / clean)

* similar to 3m elevation at 35.5 m distance and unit 58 – 63 organics (soil?), 63 – 75 (Illuviated)
(deep ILL)

---

10 – 18 cm: zC $_{mot}$

Dark grey with min dark orange mottle (< 3%)

Silty clay 25-30 / 75-70

Medium plasticity

Slightly more compact, but not very

---

18 – 46 cm: (g)zC $_{mot}$

Grey matrix with dark orange mottle (15 – 20%)

Medium plasticity

~ 32 – 35 cm -> iron pan (1 cm large iron nodule @ 30 cm)

Manganese

Grey transitions to yellowish – brown grey, still medium plasticity

---

46 – 52 cm: (46 – 70 cm) zC $_{mot}$

Grey with dark orange mottle (10-15%)

Medium – high plasticity

Silty clay 10 / 90

Increased density / compaction

Bottom unit *
matrix – orange then becomes mixed in w/ grey after iron pan – more dense / compact

cored deeper to 74 cm

52 – 70 cm:

Continuation of previous unit-

Grey w/ dark orange mottle (15%), manganese (3 – 5%)

Medium plasticity

Silty clay 10 / 90

Dense / compacted / dry -> factor of weathering

---

70 – 74 cm: zC $_{mot}$

Brownish yellow matrix with bright orange mottle (~10%)

Very dense / compact

Medium plasticity

Silty clay 10 / 90

Slightly more visible silt

Much drier than previous unit

Gradual upper boundary

Upper half of first unit slightly less compacted -> indicated in a separate sample

---

Cored deeper to 101 cm

74 – 101 cm: $zC_{mot}/Z_{l\text{-}lam}$ lenticularly laminated mottled silty clay with silt, silty clay dominant

Fairly similar to previous unit (continued)

Yellowish brown w/ some light grey mixing in (~15 %)

Bright orange mottle (10%) and ~10 % manganese nodules

Medium plasticity

Silty clay 10 / 90

Small isolated silt packets @ ~95 cm

More silt towards the bottom

Very dense / compact

HE23T4C2 14 m from C1 @ 171˚ South

4 – 14 cm: $cZ_{rt\text{-}mot\text{-}org}$

Darker greyish brown, A-zone, silt with some clay

Loose, primarily roots, silt, some clay

60 plant material / 30 silt / 10 clay

---

14 – 23 cm: zC $_{mot}$

Greyish brown

Med - med-low plasticity

Silty clay 10-15 / 90-85

Loose, slightly more compact

~10% dark orange mottling

Iron pan separates unit from top of next unit

---

23 – 42.5 cm: zC $_{(rt)\text{-}mot}$

Greyish brown w/ iron pan and ~34 cm transitions to a lighter greyish brown w/ increase of orange mottling

Med plasticity

Silty-clay 10 / 90

Small amount of small roots

Iron pan (23 – 27 cm)

Increases in density cont. w/ rest of units

Iron pan -> iron nodules (1.5 mm in size) (30 – 40% orange mottling & granules)

~15 % orange mottling @ top- lower = ~30 % orange mottling

42.5 – 51 cm: zC $_{mot}$

Light greyish brown w/ orange mottling

As unit increases in depth less mottling

Dense & compact

Med plasticity

Silty clay 10 / 90

Manganese nodules 3%

Orange mottling 20%

---

51 – 60 cm: (51 – 73.5 cm) (z)C $_{(mot)}$

Transitions from light greyish brown to light grey

Med – high plasticity

Silty clay 5 / 95

Mostly clay

Most compact / dense of all units

Gradual increases from 51 – 55 cm orange mottling ~5%

From 55 – 60 mottling disappears and becomes orange mixed in w/ light greyish brown matrix

cored deeper to 89 cm

60 – 73.5 cm:

Light grey mixed w/ light orangish brown (not mottling)

Some reddish mottling < 3%

Med plasticity

Dense / compact

Dense and dry at top

Brownish yellow silty clay 5-10 / 95-90 up to 73.5 cm

cont. of previous unit

73.5 – 89 cm: (z)C

Med-high plasticity

Still fairly dry but more moist than above unit

Silty clay 5 / 95

Gets a glean when scraped*

@ 85.5 cm small amount of evaporates

Very dense / compact

Gradual upper boundary, gradual colour change – yellowish brown w/ light grey mixed in (~30% yellowish brown)

@ 82 cm yellowish brown decreases to ~15% same location where evaporates are (82 – 89 cm)

HE23T4C3 59 m from C1 @ 171˚ S

2 – 15.5 cm: $zC_{rt\text{-}org}$

Dark greyish brown

Lots of roots, topsoil

Silty clay 20 / 80

Med plasticity

Loose / crumbly

Abrupt boundary 11 cm

Slight orange mottling 1% @ 10 – 15.5 cm – more friable

15.5 – 26.5 cm: zC $_{rt\text{-}mot}$

Greyish brown w/ orange mottling (10%)

Roots (less than above)

Silty clay 10 / 90

Slightly more compact

26.5 – 47 cm: C $_{mot}$

Greyish brown w/ dark orange mottling (20-25%)

Moist, high plasticity

Clay 100

More dense / compact

Manganese granule @ 37cm + other nodules

Cored deeper to 72 cm

47 – 60 cm: (g)zC $_{mot}$

Greyish brown w/ dark orange mottling (15%)

Silty clay 10 / 90

Dense & compact

Manganese nodules (55-60 cm) 5%, 1mm size nodules

60 – 67 cm: zC $_{mot}$

Greyish brown w/ dark orange mottling (30%)

Med plasticity

Silty clay 10 / 90

Moist, dense / compact

---

67 – 72 cm: (67 – 96 cm) zC $_{mot}$

Greyish brown w/ dark orange mottling (15-20%)

Slightly more moist than above unit

Med plasticity

Silty clay 10 / 90

Dense / compact

cored deeper to 95 cm

cont. of previous unit until 95 cm

evaporite at 83 – 84 (close up photo)

** An X on one side of core sample indicates the bottom **

cored deeper to 115 cm

unit cont. to 96 cm

96 – 100 cm:

Manganese pan

Greyish brown, primarily dark grey w/ some orange mottling (10%)

Clay w/ manganese

Much more moist than lower unit

Sharp upper and lower boundary

---

100 – 115 cm: zC_{mot}

Light grey w/ dark orange mottling (45%)

Med plasticity

Silty-clay 15-20 / 85-80

Dense / compact

Much drier than above unit

Cored deeper to 131 cm

115 – 131 cm: zC_{mot}

Colour: cont. of previous unit

Med-high plasticity

Dense / compact

More moist than previous unit

Evaporate (120 – 127 cm) (8-10%) small, (< 1mm)

Silty clay 10 / 90

Manganese nodules heterogeneously dispersed (~5%)

Friday May 26th **(B) ? m @ 171˚ S**

HE23T4C4B

2 – 11 cm: zC $_{rt\text{-}org}$

Litter zone, lots of roots

Dark greyish brown

Med plasticity

High organics (less degraded)

Fresh, top soil

Loose / crumbly

Silty clay & organics ***2-9 cm Ben has sample***

---

11 – 26 cm: zC $_{rt\text{-}mot}$

Greenish grey w/ dark orange mottling (10 – 15%)

Dense / compact

Med plasticity, more moist than previous unit

Fresh organics, less roots & smaller roots

Silty clay 5 / 95, slightly darker than 3rd

---

26 – 50 cm: (26 – 70 cm) C $_{rt\text{-}mot}$ / S $_{l\text{-}lam}$

Greenish grey w/ dark orange mottling (20%)

Med plasticity

Most dense of all previous units

Very little amount of small roots

Clay

~5% manganese- v.f sand packets heterogeneously dispersed (42 cm down)

Cored deeper to 78 cm

Cont. of previous unit

---

50 – 70 cm:

Greenish grey w/ dark orange mottling (20%)

Med plasticity

Clay w/ small amount of roots near the top (< 5%)

Very dense / compact

~1% manganese (~ 59 – 64 cm) but dispersed

---

70 – 78 cm: zC $_{mot}$

Greenish grey w/ dark orange mottling (30%)

More stiff

Med plasticity- slightly more moist than above unit

Clay w/ small amount of grains near bottom of unit – (<5%) (Iron?)

Very dense / compact

cored deeper to 127 cm

*** hit water table @ 65 – 75 cm ***

78 – 119 cm: (z)C $_{mot}$

Greenish grey w/ dark orange mottling 30%

Med plasticity

Very dense / compact but initially saturated

Clay w/ small amount of silt (<5%)

Small amount of manganese (94 – 99 cm) (<3%)

---

119 - 127 cm:

PEAT (120 – 126 cm) (estimated ~2000 – 2500 yrs old)

Large wood fragment @ 124 – 125 cm

Sharp boundary at 119 introducing peat from above clay

Fibrous material – black peat

Cored deeper to 180 cm

Clay began ~ 130 cm in previous sample as well (Ben's sample)

127 – 130.5 cm:

Base of peat

Sharp boundary – black top

130.5 – 133.5 cm:

Transition zone

Sharp boundary

Organic content in marine clay

Very dark greyish brown

High plasticity

133.5 – 165.5 cm: C_{org}

Sharp boundary

Dark greenish grey

Very sticky and wet

Clay

High plasticity

Water, very saturated

Less dense than previous clay

*marine clay

Wood fragments (143 – 148 cm)

165.5 – 173 cm: C_{mot}

Sharp boundary

Greenish grey w/ dark orange mottling (~25%) *similar to units above peat

Med-high plasticity

Clay

Movement from higher ground down (terrestrial)

Very dense / compact

Not saturated

---

173 – 180 cm:

Sharp upper boundary

PEAT, black

Very dry, fine, fibrous

No wood

cored deeper to 280 cm

(3 units total)

180 – 210 cm: C / S_{lam}

Dark greenish grey

High plasticity, very sticky

v.f sand laminations (1-2 mm) inclined but but not all majority horizontal

[episodic moderately higher energy condition]

mostly clay

dense / compact

No bioturbation

---

210 – 237 cm: C

Dark greenish grey

High plasticity

Very sticky

Dense / compact

Slightly more manganese (5%), sporadic nodules

Clay

Shells (possibly Bithynia?)  212, 216.5, 221 – 225.5, 225, 235 – 236 (large)

---

237 – 280 cm: C

Greenish grey

High plasticity, very sticky

Manganese nodules (increased from previous unit) (10-15%)

w/ some 1mm nodules @ 250 cm

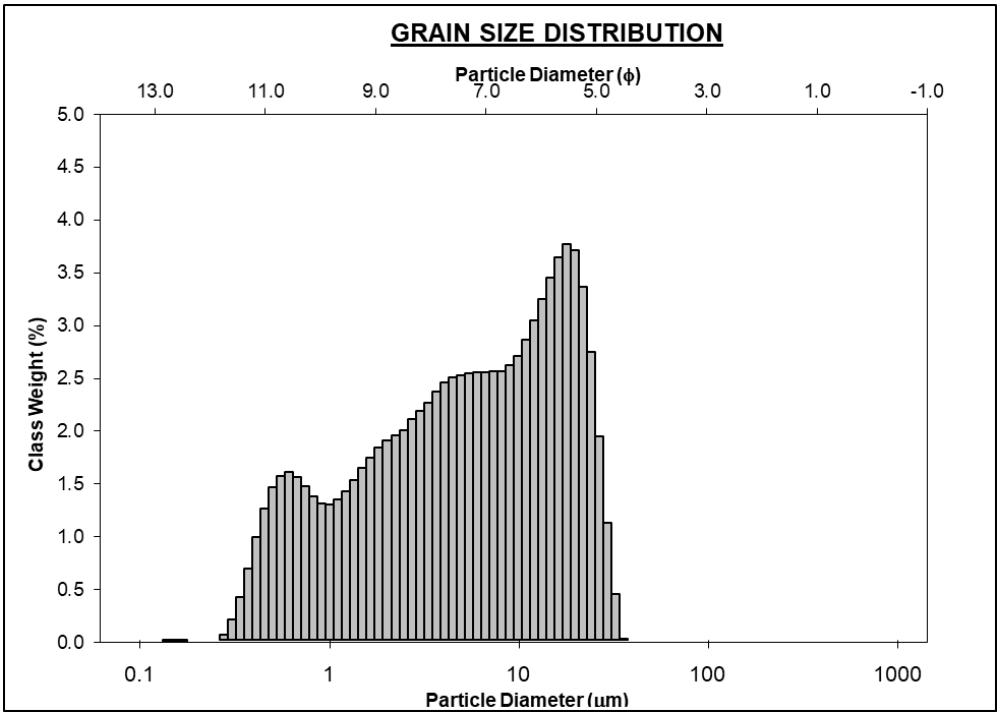
NO shells

Increase in manganese density @ 265 – 268 cm (~30%)

Clay (marine)

Appendix C – GRADISTAT grain size distribution output (phi)

22.5 cm



SAMPLE STATISTICS

SAMPLE IDENTITY: **HE23T4C4B 22.5 cm** ANALYST & DATE: K Drew,

SAMPLE TYPE: Bimodal, Poorly Sorted TEXTURAL GROUP: Mud

SEDIMENT NAME: Medium Silt

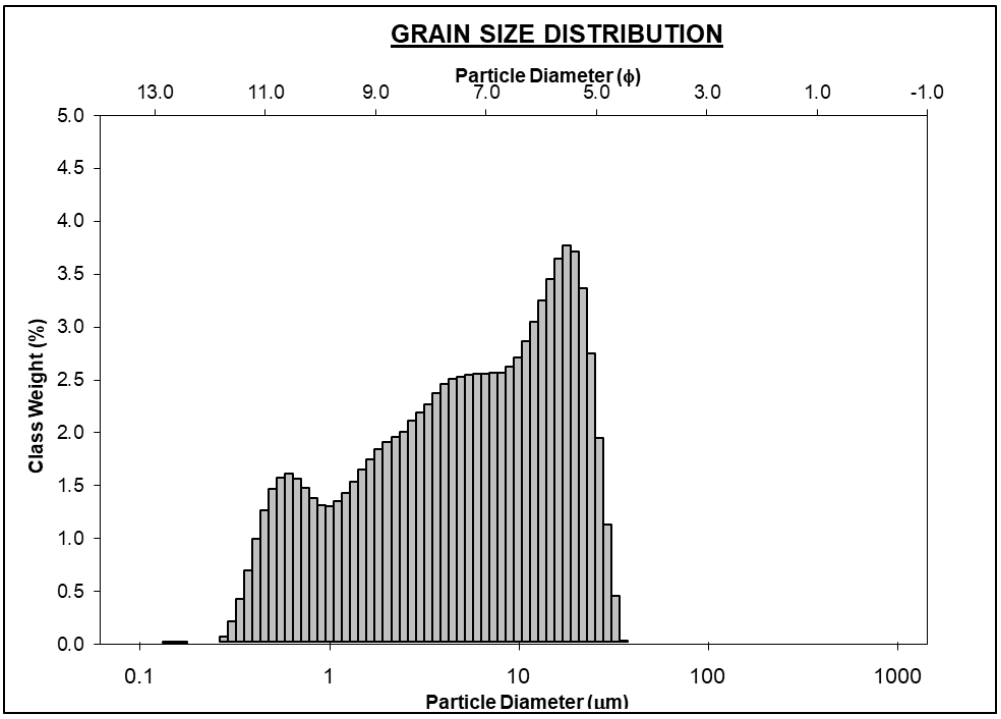
	µm	ϕ
MODE 1:	18.03	5.796
MODE 2:	0.615	10.67
MODE 3:		
D_{10}:	0.719	5.589
MEDIAN or D_{50}:	5.689	7.458
D_{90}:	20.77	10.44
(D_{90} / D_{10}):	28.90	1.868
(D_{90} - D_{10}):	20.05	4.853
(D_{75} / D_{25}):	7.225	1.462
(D_{75} - D_{25}):	11.96	2.853

GRAIN SIZE DISTRIBUTION

GRAVEL: 0.0%	COARSE SAND: 0.0%
SAND: 0.0%	MEDIUM SAND: 0.0%
MUD: 100.0%	FINE SAND: 0.0%
	V FINE SAND: 0.0%
V COARSE GRAVEL: 0.0%	V COARSE SILT: 0.4%
COARSE GRAVEL: 0.0%	COARSE SILT: 20.4%
MEDIUM GRAVEL: 0.0%	MEDIUM SILT: 20.9%
FINE GRAVEL: 0.0%	FINE SILT: 17.9%
V FINE GRAVEL: 0.0%	V FINE SILT: 15.0%
V COARSE SAND: 0.0%	CLAY: 25.3%

	METHOD OF MOMENTS			FOLK & WARD METHOD		
	Arithmetic µm	Geometric µm	Logarithmic ϕ	Geometric µm	Logarithmic ϕ	Description
MEAN ($\bar{x}$):	8.547	4.784	7.707	4.820	7.697	Fine Silt
SORTING (σ):	7.866	3.385	1.759	3.574	1.837	Poorly Sorted
SKEWNESS (Sk):	0.937	-0.422	0.422	-0.211	0.211	Fine Skewed
KURTOSIS (K):	2.872	2.077	2.077	0.794	0.794	Platykurtic

25 cm



SAMPLE STATISTICS

SAMPLE IDENTITY: **HE23T4C4B 25 cm** ANALYST & DATE: K Drew,

SAMPLE TYPE: Polymodal, Very Poorly Sorted TEXTURAL GROUP: Sandy Mud

SEDIMENT NAME: Coarse Sandy Medium Silt

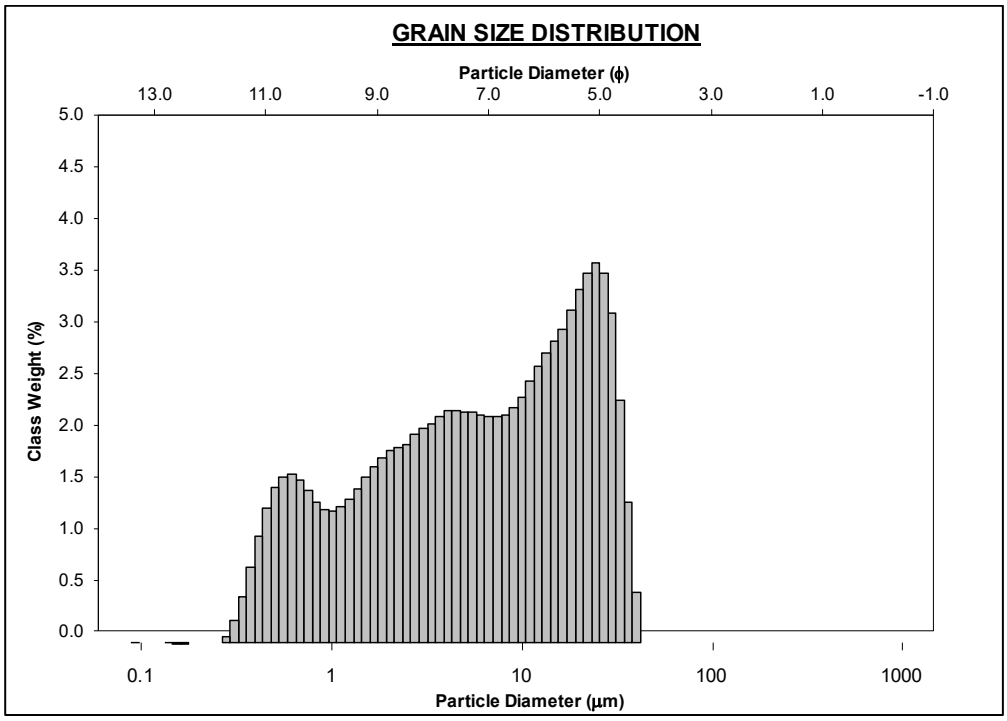
	µm	ϕ
MODE 1:	959.9	0.061
MODE 2:	16.32	5.939
MODE 3:	7.370	7.086
D_{10}:	1.517	0.115
MEDIAN or D_{50}:	8.075	6.952
D_{90}:	923.3	9.365
(D_{90} / D_{10}):	608.7	81.36
(D_{90} - D_{10}):	921.8	9.250
(D_{75} / D_{25}):	5.309	1.414
(D_{75} - D_{25}):	14.46	2.408

GRAIN SIZE DISTRIBUTION

GRAVEL: 0.0%	COARSE SAND: 12.0%
SAND: 16.4%	MEDIUM SAND: 0.0%
MUD: 83.6%	FINE SAND: 0.0%
	V FINE SAND: 0.0%
V COARSE GRAVEL: 0.0%	V COARSE SILT: 0.0%
COARSE GRAVEL: 0.0%	COARSE SILT: 13.1%
MEDIUM GRAVEL: 0.0%	MEDIUM SILT: 21.5%
FINE GRAVEL: 0.0%	FINE SILT: 20.1%
V FINE GRAVEL: 0.0%	V FINE SILT: 15.2%
V COARSE SAND: 4.5%	CLAY: 13.6%

	METHOD OF MOMENTS			FOLK & WARD METHOD		
	Arithmetic	Geometric	Logarithmic	Geometric	Logarithmic	Description
	µm	µm	ϕ	µm	ϕ	
MEAN ($\bar{x}$):	162.7	12.61	6.309	24.20	5.369	Coarse Silt
SORTING (σ):	350.4	8.336	3.059	12.69	3.666	Very Poorly Sorted
SKEWNESS (Sk):	1.845	1.059	-1.059	0.460	-0.460	Very Coarse Skewed
KURTOSIS (K):	4.469	3.220	3.220	1.739	1.739	Very Leptokurtic

30 cm



SAMPLE STATISTICS

SAMPLE IDENTITY: **HE23T4C4B 30 cm**

ANALYST & DATE: K Drew,

SAMPLE TYPE: Trimodal, Poorly Sorted

TEXTURAL GROUP: Mud

SEDIMENT NAME: Coarse Silt

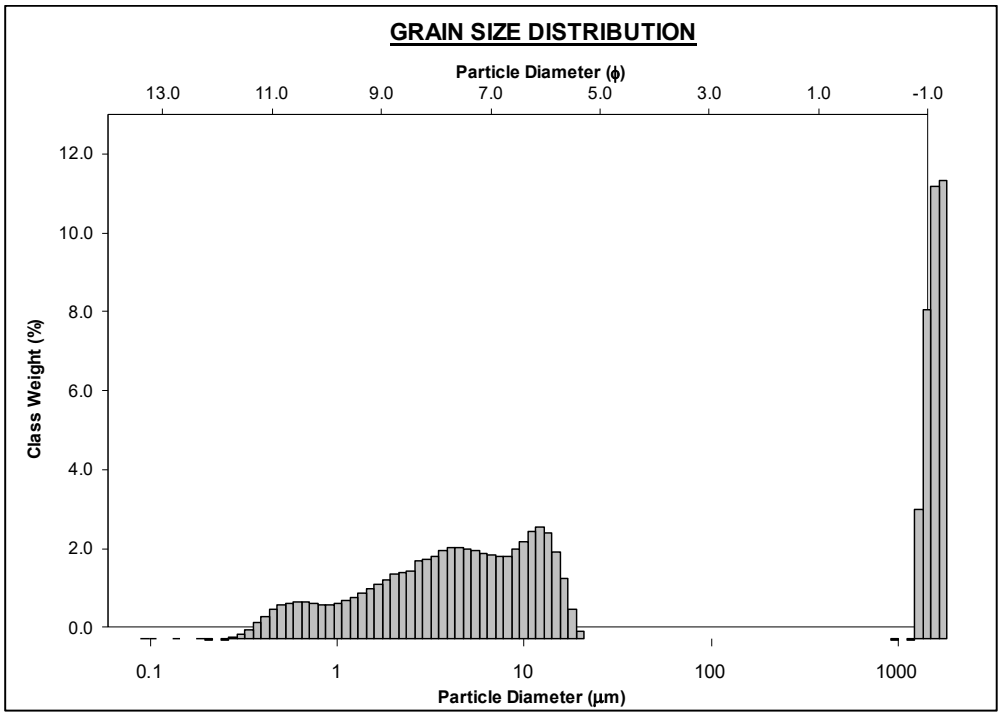
	µm	ϕ
MODE 1:	24.29	5.365
MODE 2:	4.484	7.803
MODE 3:	0.615	10.67
D_{10}:	0.708	5.255
MEDIAN or D_{50}:	6.342	7.301
D_{90}:	26.18	10.46
(D_{90} / D_{10}):	36.99	1.991
(D_{90} - D_{10}):	25.47	5.209
(D_{75} / D_{25}):	8.753	1.533
(D_{75} - D_{25}):	15.09	3.130

GRAIN SIZE DISTRIBUTION

GRAVEL: 0.0%	COARSE SAND: 0.0%
SAND: 0.0%	MEDIUM SAND: 0.0%
MUD: 100.0%	FINE SAND: 0.0%
	V FINE SAND: 0.0%
V COARSE GRAVEL: 0.0%	V COARSE SILT: 4.1%
COARSE GRAVEL: 0.0%	COARSE SILT: 23.6%
MEDIUM GRAVEL: 0.0%	MEDIUM SILT: 17.8%
FINE GRAVEL: 0.0%	FINE SILT: 15.5%
V FINE GRAVEL: 0.0%	V FINE SILT: 14.1%
V COARSE SAND: 0.0%	CLAY: 25.1%

	METHOD OF MOMENTS			FOLK & WARD METHOD		
	Arithmetic µm	Geometric µm	Logarithmic ϕ	Geometric µm	Logarithmic ϕ	Description
MEAN ($\bar{x}$):	10.31	5.333	7.551	5.372	7.540	Fine Silt
SORTING (σ):	9.974	3.704	1.889	3.927	1.973	Poorly Sorted
SKEWNESS (Sk):	0.952	-0.386	0.386	-0.198	0.198	Fine Skewed
KURTOSIS (K):	2.816	1.998	1.998	0.769	0.769	Platykurtic

33 cm



SAMPLE STATISTICS

SAMPLE IDENTITY: **HE23T4C4B 33 cm** ANALYST & DATE: K Drew,

SAMPLE TYPE: Trimodal, Extremely Poorly Sorted TEXTURAL GROUP: Sandy Mud

SEDIMENT NAME: Very Coarse Sandy Medium Silt

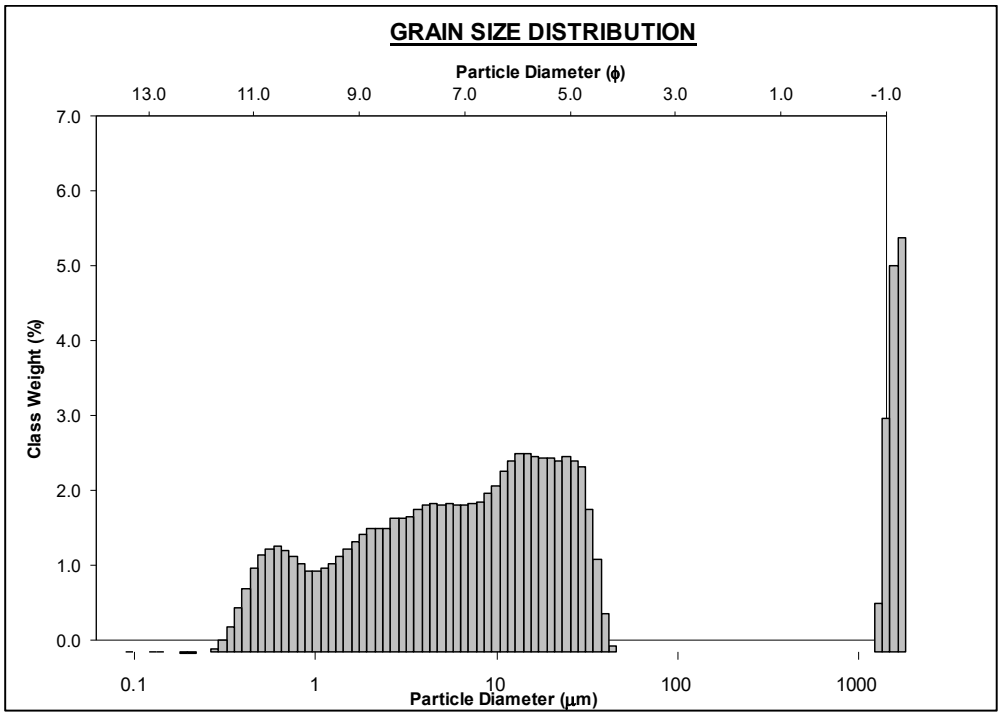
	µm	ϕ
MODE 1:	1742.4	-0.799
MODE 2:	12.11	6.369
MODE 3:	4.484	7.803
D_{10}:	1.251	-0.853
MEDIAN or D_{50}:	11.37	6.459
D_{90}:	1806.3	9.643
(D_{90} / D_{10}):	1443.8	-11.304
(D_{90} - D_{10}):	1805.0	10.50
(D_{75} / D_{25}):	456.9	-12.620
(D_{75} - D_{25}):	1564.3	8.836

GRAIN SIZE DISTRIBUTION

GRAVEL: 0.0%	COARSE SAND: 0.0%
SAND: 40.3%	MEDIUM SAND: 0.0%
MUD: 59.7%	FINE SAND: 0.0%
	V FINE SAND: 0.0%
V COARSE GRAVEL: 0.0%	V COARSE SILT: 0.0%
COARSE GRAVEL: 0.0%	COARSE SILT: 2.2%
MEDIUM GRAVEL: 0.0%	MEDIUM SILT: 15.7%
FINE GRAVEL: 0.0%	FINE SILT: 14.1%
V FINE GRAVEL: 0.0%	V FINE SILT: 12.2%
V COARSE SAND: 40.3%	CLAY: 15.4%

	METHOD OF MOMENTS			FOLK & WARD METHOD		
	Arithmetic	Geometric	Logarithmic	Geometric	Logarithmic	Description
	µm	µm	ϕ	µm	ϕ	
MEAN ($\bar{x}$):	500.2	22.70	4.596	34.04	4.877	Very Coarse Silt
SORTING (σ):	732.5	20.25	4.349	17.09	4.095	Extremely Poorly Sorted
SKEWNESS (Sk):	0.830	0.524	-0.185	0.377	-0.377	Very Coarse Skewed
KURTOSIS (K):	1.744	1.609	1.326	0.510	0.510	Very Platykurtic

37 cm



SAMPLE STATISTICS

SAMPLE IDENTITY: **HE23T4C4B 37 cm** ANALYST & DATE: K Drew,

SAMPLE TYPE: Polymodal, Extremely Poorly Sorted TEXTURAL GROUP: Sandy Mud

SEDIMENT NAME: Very Coarse Sandy Coarse Silt

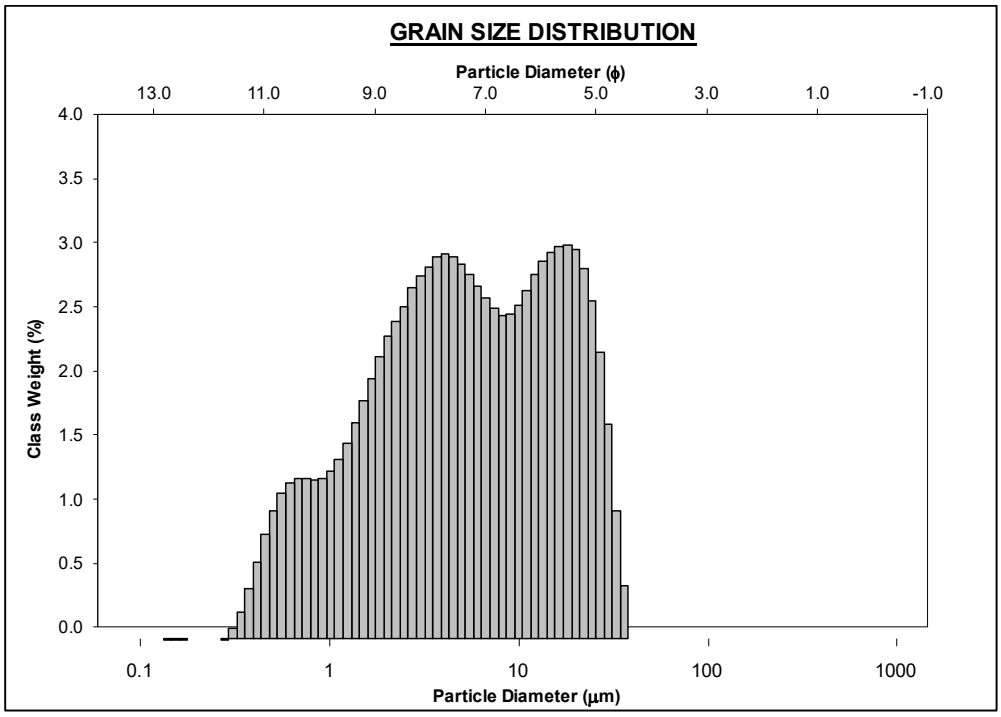
	μm	ϕ
MODE 1:	14.78	6.082
MODE 2:	5.470	7.516
MODE 3:	4.484	7.803
D_{10}:	0.828	-0.718
MEDIAN or D_{50}:	9.843	6.667
D_{90}:	1644.7	10.24
(D_{90} / D_{10}):	1985.3	-14.261
(D_{90} - D_{10}):	1643.9	10.96
(D_{75} / D_{25}):	10.49	1.652
(D_{75} - D_{25}):	24.62	3.391

GRAIN SIZE DISTRIBUTION

GRAVEL: 0.0%	COARSE SAND: 0.0%
SAND: 18.2%	MEDIUM SAND: 0.0%
MUD: 81.8%	FINE SAND: 0.0%
	V FINE SAND: 0.0%
V COARSE GRAVEL: 0.0%	V COARSE SILT: 3.5%
COARSE GRAVEL: 0.0%	COARSE SILT: 17.1%
MEDIUM GRAVEL: 0.0%	MEDIUM SILT: 15.8%
FINE GRAVEL: 0.0%	FINE SILT: 13.2%
V FINE GRAVEL: 0.0%	V FINE SILT: 11.7%
V COARSE SAND: 18.2%	CLAY: 20.5%

	METHOD OF MOMENTS			FOLK & WARD METHOD		
	Arithmetic	Geometric	Logarithmic	Geometric	Logarithmic	Description
	μm	μm	ϕ	μm	ϕ	
MEAN ($\bar{x}$):	228.8	10.69	6.111	27.18	5.201	Coarse Silt
SORTING (σ):	549.9	10.41	3.549	19.14	4.259	Extremely Poorly Sorted
SKEWNESS (Sk):	2.131	0.997	-0.804	0.366	-0.366	Very Coarse Skewed
KURTOSIS (K):	5.606	3.282	2.682	1.408	1.408	Leptokurtic

38 cm



SAMPLE STATISTICS

SAMPLE IDENTITY: **HE23T4C4B 38 cm**

ANALYST & DATE: K Drew,

SAMPLE TYPE: Trimodal, Poorly Sorted

TEXTURAL GROUP: Mud

SEDIMENT NAME: Fine Silt

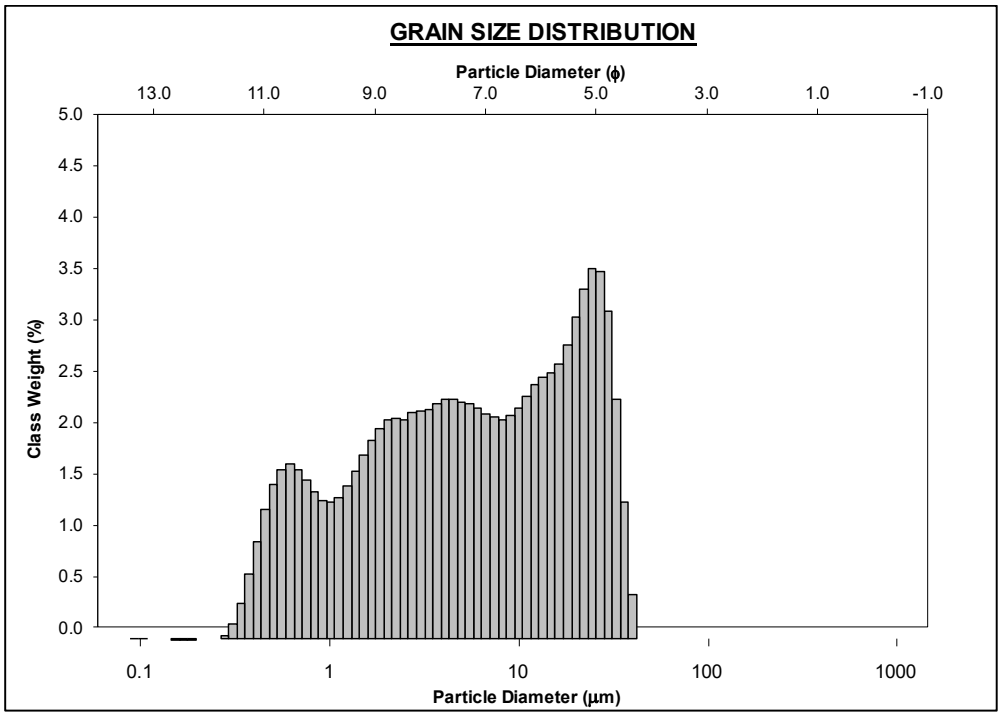
	μm	ϕ
MODE 1:	18.03	5.796
MODE 2:	4.060	7.946
MODE 3:	0.750	10.38
D_{10}:	0.927	5.539
MEDIAN or D_{50}:	5.178	7.593
D_{90}:	21.50	10.08
(D_{90} / D_{10}):	23.20	1.819
(D_{90} - D_{10}):	20.57	4.536
(D_{75} / D_{25}):	6.112	1.418
(D_{75} - D_{25}):	10.97	2.612

GRAIN SIZE DISTRIBUTION

GRAVEL: 0.0%	COARSE SAND: 0.0%
SAND: 0.0%	MEDIUM SAND: 0.0%
MUD: 100.0%	FINE SAND: 0.0%
	V FINE SAND: 0.0%
V COARSE GRAVEL: 0.0%	V COARSE SILT: 1.4%
COARSE GRAVEL: 0.0%	COARSE SILT: 18.4%
MEDIUM GRAVEL: 0.0%	MEDIUM SILT: 19.1%
FINE GRAVEL: 0.0%	FINE SILT: 19.6%
V FINE GRAVEL: 0.0%	V FINE SILT: 18.8%
V COARSE SAND: 0.0%	CLAY: 22.8%

	METHOD OF MOMENTS			FOLK & WARD METHOD		
	Arithmetic	Geometric	Logarithmic	Geometric	Logarithmic	Description
	μm	μm	ϕ	μm	ϕ	
MEAN ($\bar{x}$):	8.518	4.909	7.670	5.038	7.633	Fine Silt
SORTING (σ):	8.207	3.153	1.657	3.315	1.729	Poorly Sorted
SKEWNESS (Sk):	1.189	-0.292	0.292	-0.085	0.085	Symmetrical
KURTOSIS (K):	3.551	2.167	2.167	0.844	0.844	Platykurtic

40 cm



SAMPLE STATISTICS

SAMPLE IDENTITY: **HE23T4C4B 40 cm**

ANALYST & DATE: K Drew,

SAMPLE TYPE: Polymodal, Poorly Sorted

TEXTURAL GROUP: Mud

SEDIMENT NAME: Coarse Silt

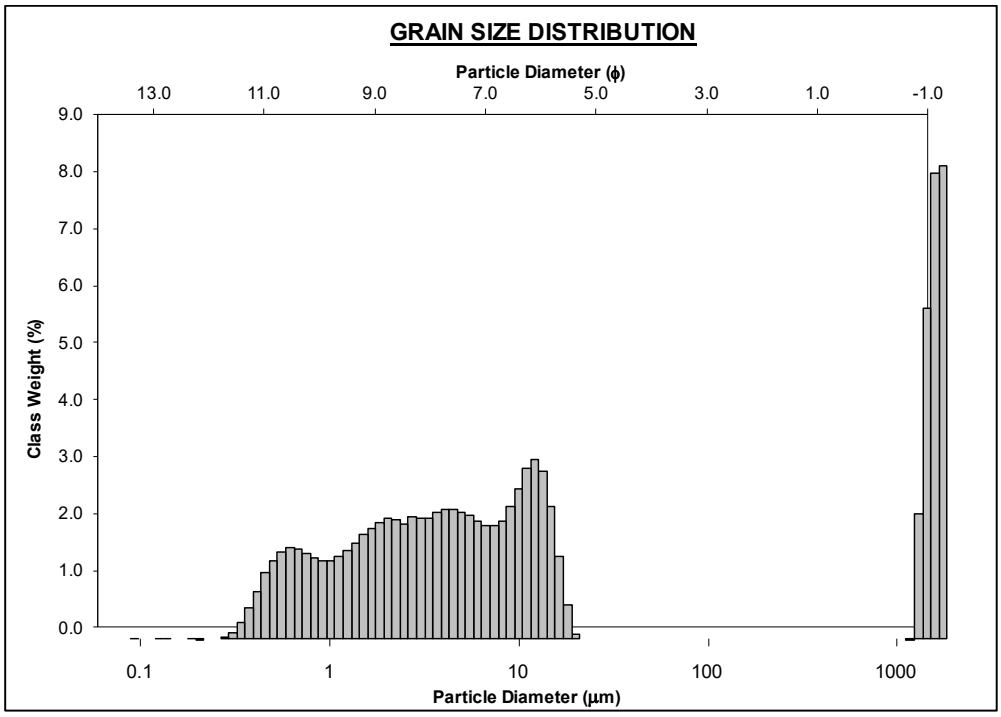
	µm	ϕ
MODE 1:	24.29	5.365
MODE 2:	4.484	7.803
MODE 3:	2.237	8.806
D_{10}:	0.719	5.259
MEDIAN or D_{50}:	5.650	7.468
D_{90}:	26.11	10.44
(D_{90} / D_{10}):	36.31	1.985
(D_{90} - D_{10}):	25.39	5.182
(D_{75} / D_{25}):	8.852	1.531
(D_{75} - D_{25}):	14.55	3.146

GRAIN SIZE DISTRIBUTION

GRAVEL: 0.0%	COARSE SAND: 0.0%
SAND: 0.0%	MEDIUM SAND: 0.0%
MUD: 100.0%	FINE SAND: 0.0%
	V FINE SAND: 0.0%
V COARSE GRAVEL: 0.0%	V COARSE SILT: 4.0%
COARSE GRAVEL: 0.0%	COARSE SILT: 22.3%
MEDIUM GRAVEL: 0.0%	MEDIUM SILT: 16.5%
FINE GRAVEL: 0.0%	FINE SILT: 15.8%
V FINE GRAVEL: 0.0%	V FINE SILT: 15.3%
V COARSE SAND: 0.0%	CLAY: 26.1%

	METHOD OF MOMENTS			FOLK & WARD METHOD		
	Arithmetic µm	Geometric µm	Logarithmic ϕ	Geometric µm	Logarithmic ϕ	Description
MEAN ($\bar{x}$):	9.952	5.089	7.618	5.152	7.601	Fine Silt
SORTING (σ):	9.955	3.667	1.875	3.905	1.965	Poorly Sorted
SKEWNESS (Sk):	1.022	-0.294	0.294	-0.131	0.131	Fine Skewed
KURTOSIS (K):	2.916	1.944	1.944	0.759	0.759	Platykurtic

42.5 cm



SAMPLE STATISTICS

SAMPLE IDENTITY: **HE23T4C4B 42.5 cm** ANALYST & DATE: K Drew,

SAMPLE TYPE: Polymodal, Extremely Poorly Sorted TEXTURAL GROUP: Sandy Mud

SEDIMENT NAME: Very Coarse Sandy Mud

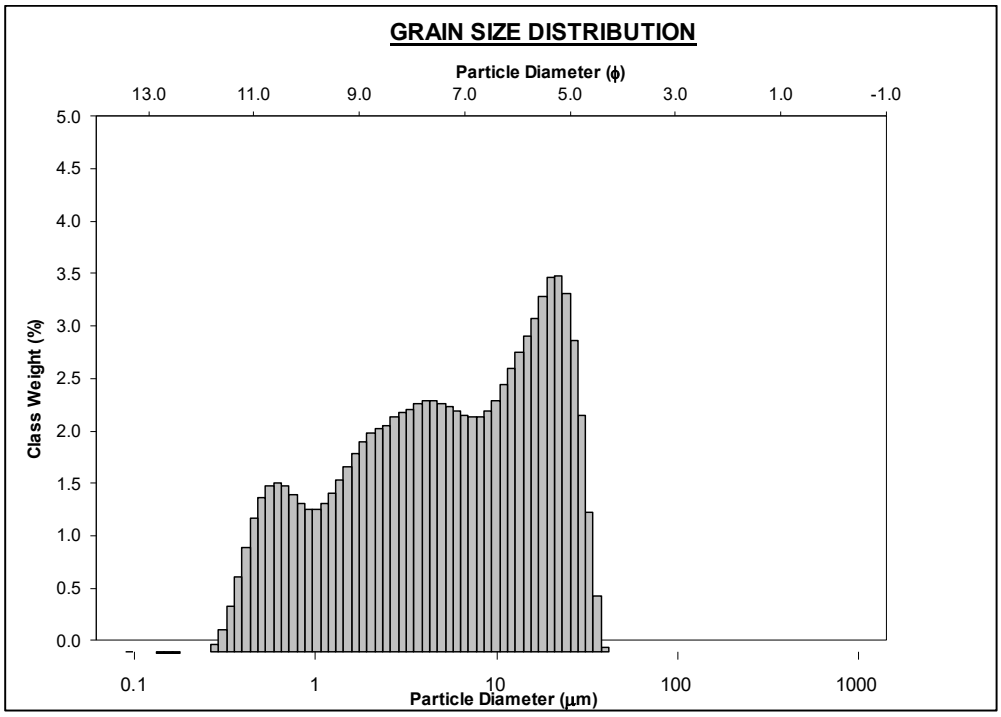
	µm	ϕ
MODE 1:	12.11	6.369
MODE 2:	4.484	7.803
MODE 3:	2.728	8.519
D_{10}:	0.794	-0.804
MEDIAN or D_{50}:	7.136	7.131
D_{90}:	1745.5	10.30
(D_{90} / D_{10}):	2198.7	-12.816
(D_{90} - D_{10}):	1744.7	11.10
(D_{75} / D_{25}):	685.2	-17.904
(D_{75} - D_{25}):	1410.5	9.420

GRAIN SIZE DISTRIBUTION

GRAVEL: 0.0%	COARSE SAND: 0.0%
SAND: 29.2%	MEDIUM SAND: 0.0%
MUD: 70.8%	FINE SAND: 0.0%
	V FINE SAND: 0.0%
V COARSE GRAVEL: 0.0%	V COARSE SILT: 0.0%
COARSE GRAVEL: 0.0%	COARSE SILT: 1.9%
MEDIUM GRAVEL: 0.0%	MEDIUM SILT: 17.1%
FINE GRAVEL: 0.0%	FINE SILT: 13.9%
V FINE GRAVEL: 0.0%	V FINE SILT: 13.8%
V COARSE SAND: 29.2%	CLAY: 23.9%

	METHOD OF MOMENTS			FOLK & WARD METHOD		
	Arithmetic	Geometric	Logarithmic	Geometric	Logarithmic	Description
	µm	µm	ϕ	µm	ϕ	
MEAN ($\bar{x}$):	363.5	12.24	5.719	24.28	5.364	Coarse Silt
SORTING (σ):	662.4	16.56	4.211	20.05	4.326	Extremely Poorly Sorted
SKEWNESS (Sk):	1.330	0.899	-0.603	0.437	-0.437	Very Coarse Skewed
KURTOSIS (K):	2.828	2.313	1.774	0.499	0.499	Very Platykurtic

45 cm



SAMPLE STATISTICS

SAMPLE IDENTITY: **HE23T4C4B 45 cm**

ANALYST & DATE: K Drew,

SAMPLE TYPE: Trimodal, Poorly Sorted

TEXTURAL GROUP: Mud

SEDIMENT NAME: Coarse Silt

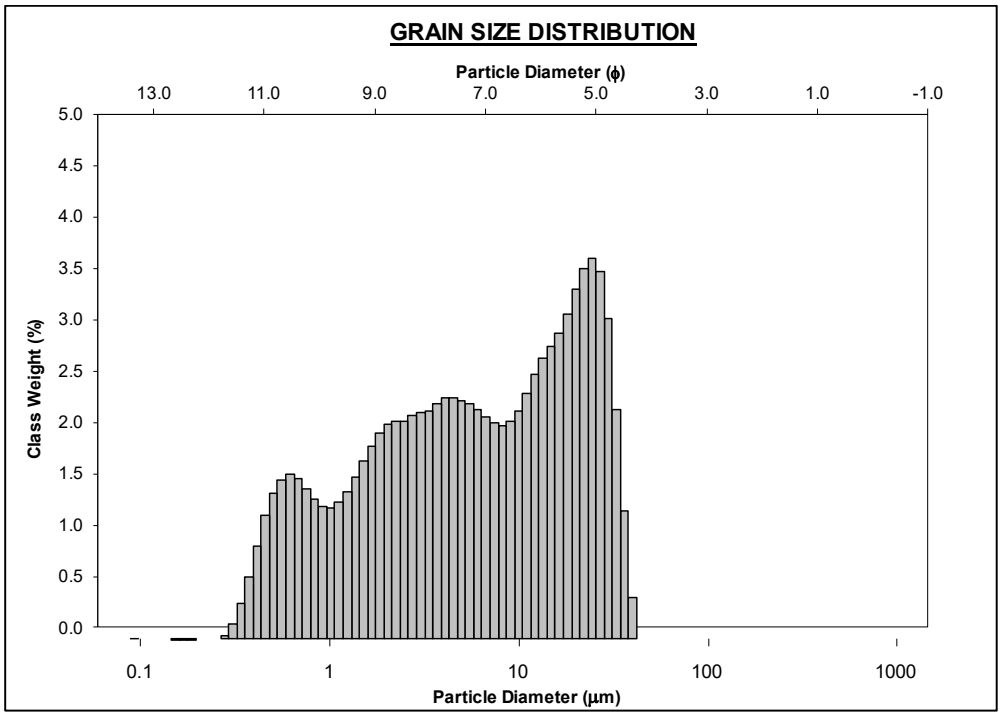
	μm	ϕ
MODE 1:	21.99	5.509
MODE 2:	4.060	7.946
MODE 3:	0.615	10.67
D_{10}:	0.715	5.414
MEDIAN or D_{50}:	5.529	7.499
D_{90}:	23.45	10.45
(D_{90} / D_{10}):	32.81	1.930
(D_{90} - D_{10}):	22.73	5.036
(D_{75} / D_{25}):	8.192	1.502
(D_{75} - D_{25}):	13.29	3.034

GRAIN SIZE DISTRIBUTION

GRAVEL: 0.0%	COARSE SAND: 0.0%
SAND: 0.0%	MEDIUM SAND: 0.0%
MUD: 100.0%	FINE SAND: 0.0%
	V FINE SAND: 0.0%
V COARSE GRAVEL: 0.0%	V COARSE SILT: 1.8%
COARSE GRAVEL: 0.0%	COARSE SILT: 22.2%
MEDIUM GRAVEL: 0.0%	MEDIUM SILT: 18.1%
FINE GRAVEL: 0.0%	FINE SILT: 16.2%
V FINE GRAVEL: 0.0%	V FINE SILT: 15.6%
V COARSE SAND: 0.0%	CLAY: 26.1%

	METHOD OF MOMENTS			FOLK & WARD METHOD		
	Arithmetic	Geometric	Logarithmic	Geometric	Logarithmic	Description
	μm	μm	ϕ	μm	ϕ	
MEAN ($\bar{x}$):	9.221	4.885	7.678	4.928	7.665	Fine Silt
SORTING (σ):	8.963	3.553	1.829	3.761	1.911	Poorly Sorted
SKEWNESS (Sk):	1.004	-0.336	0.336	-0.155	0.155	Fine Skewed
KURTOSIS (K):	2.954	1.991	1.991	0.771	0.771	Platykurtic

50 cm



SAMPLE STATISTICS

SAMPLE IDENTITY: **HE23T4C4B 50 cm**

ANALYST & DATE: K Drew,

SAMPLE TYPE: Trimodal, Poorly Sorted

TEXTURAL GROUP: Mud

SEDIMENT NAME: Coarse Silt

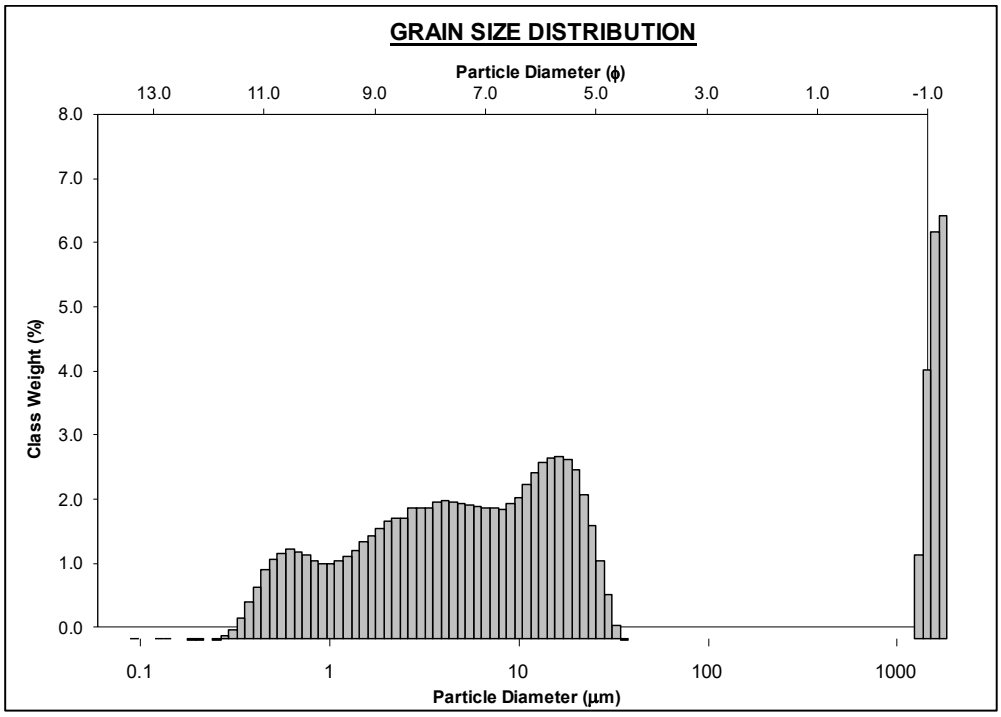
	µm	ϕ
MODE 1:	24.29	5.365
MODE 2:	4.484	7.803
MODE 3:	0.615	10.67
D_{10}:	0.745	5.271
MEDIAN or D_{50}:	5.958	7.391
D_{90}:	25.90	10.39
(D_{90} / D_{10}):	34.78	1.971
(D_{90} - D_{10}):	25.16	5.120
(D_{75} / D_{25}):	8.607	1.527
(D_{75} - D_{25}):	14.86	3.106

GRAIN SIZE DISTRIBUTION

GRAVEL: 0.0%	COARSE SAND: 0.0%
SAND: 0.0%	MEDIUM SAND: 0.0%
MUD: 100.0%	FINE SAND: 0.0%
	V FINE SAND: 0.0%
V COARSE GRAVEL: 0.0%	V COARSE SILT: 3.8%
COARSE GRAVEL: 0.0%	COARSE SILT: 23.4%
MEDIUM GRAVEL: 0.0%	MEDIUM SILT: 16.9%
FINE GRAVEL: 0.0%	FINE SILT: 15.7%
V FINE GRAVEL: 0.0%	V FINE SILT: 15.2%
V COARSE SAND: 0.0%	CLAY: 25.0%

	METHOD OF MOMENTS			FOLK & WARD METHOD		
	Arithmetic	Geometric	Logarithmic	Geometric	Logarithmic	Description
	µm	µm	ϕ	µm	ϕ	
MEAN ($\bar{x}$):	10.13	5.275	7.567	5.347	7.547	Fine Silt
SORTING (σ):	9.879	3.630	1.860	3.831	1.938	Poorly Sorted
SKEWNESS (Sk):	0.970	-0.340	0.340	-0.153	0.153	Fine Skewed
KURTOSIS (K):	2.830	1.979	1.979	0.765	0.765	Platykurtic

55 cm



SAMPLE STATISTICS

SAMPLE IDENTITY: **HE23T4C4B 55 cm** ANALYST & DATE: K Drew,

SAMPLE TYPE: Polymodal, Extremely Poorly Sorted TEXTURAL GROUP: Sandy Mud

SEDIMENT NAME: Very Coarse Sandy Medium Silt

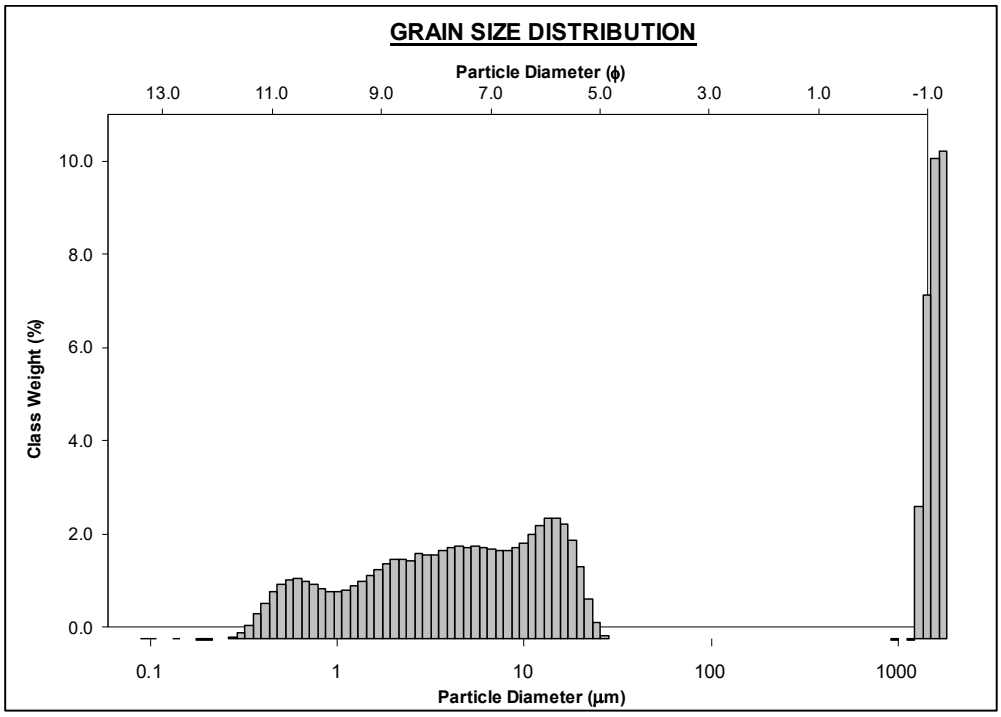
	µm	ϕ
MODE 1:	16.32	5.939
MODE 2:	4.060	7.946
MODE 3:	3.014	8.376
D_{10}:	0.848	-0.760
MEDIAN or D_{50}:	8.699	6.845
D_{90}:	1694.0	10.20
(D_{90} / D_{10}):	1997.7	-13.418
(D_{90} - D_{10}):	1693.2	10.96
(D_{75} / D_{25}):	10.22	1.630
(D_{75} - D_{25}):	22.52	3.354

GRAIN SIZE DISTRIBUTION

GRAVEL: 0.0%	COARSE SAND: 0.0%
SAND: 22.6%	MEDIUM SAND: 0.0%
MUD: 77.4%	FINE SAND: 0.0%
	V FINE SAND: 0.0%
V COARSE GRAVEL: 0.0%	V COARSE SILT: 0.2%
COARSE GRAVEL: 0.0%	COARSE SILT: 13.2%
MEDIUM GRAVEL: 0.0%	MEDIUM SILT: 16.0%
FINE GRAVEL: 0.0%	FINE SILT: 13.8%
V FINE GRAVEL: 0.0%	V FINE SILT: 13.1%
V COARSE SAND: 22.6%	CLAY: 21.0%

	METHOD OF MOMENTS			FOLK & WARD METHOD		
	Arithmetic µm	Geometric µm	Logarithmic ϕ	Geometric µm	Logarithmic ϕ	Description
MEAN ($\bar{x}$):	282.0	11.27	5.955	26.60	5.233	Coarse Silt
SORTING (σ):	600.8	12.49	3.813	19.46	4.282	Extremely Poorly Sorted
SKEWNESS (Sk):	1.754	0.994	-0.751	0.401	-0.401	Very Coarse Skewed
KURTOSIS (K):	4.139	2.889	2.282	1.419	1.419	Leptokurtic

65 cm



SAMPLE STATISTICS

SAMPLE IDENTITY: **HE23T4C4B 65 cm** ANALYST & DATE: K Drew,

SAMPLE TYPE: Polymodal, Extremely Poorly Sorted TEXTURAL GROUP: Sandy Mud

SEDIMENT NAME: Very Coarse Sandy Medium Silt

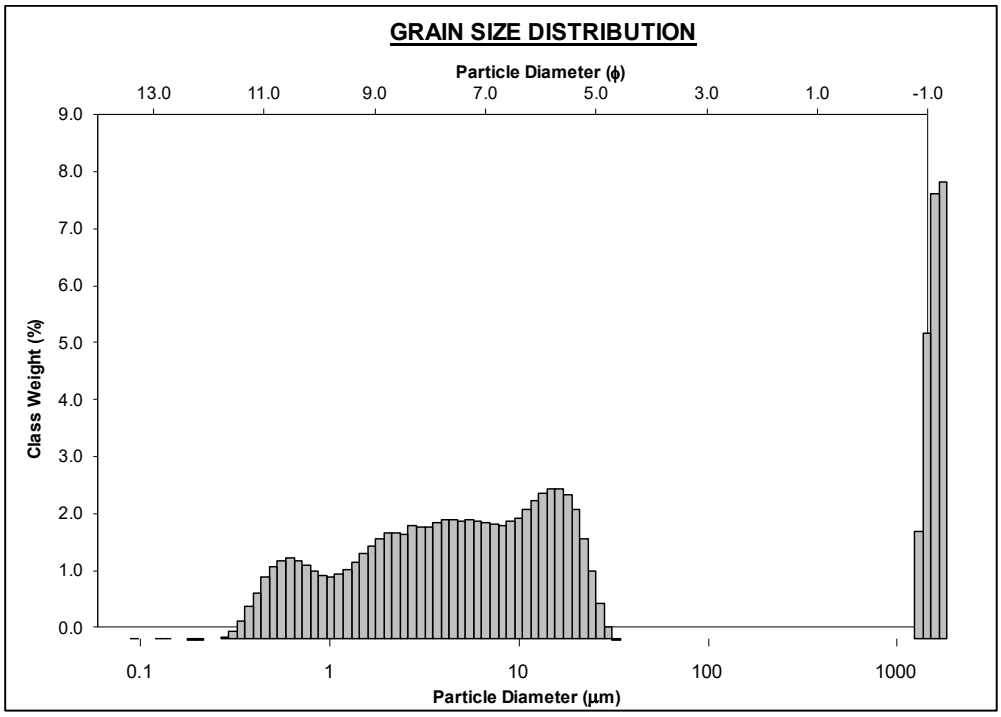
	µm	ϕ
MODE 1:	14.78	6.082
MODE 2:	5.470	7.516
MODE 3:	4.484	7.803
D_{10}:	0.944	-0.839
MEDIAN or D_{50}:	11.59	6.430
D_{90}:	1789.4	10.05
(D_{90} / D_{10}):	1896.0	-11.971
(D_{90} - D_{10}):	1788.4	10.89
(D_{75} / D_{25}):	525.0	-13.712
(D_{75} - D_{25}):	1527.8	9.036

GRAIN SIZE DISTRIBUTION

GRAVEL: 0.0%	COARSE SAND: 0.0%
SAND: 36.4%	MEDIUM SAND: 0.0%
MUD: 63.6%	FINE SAND: 0.0%
	V FINE SAND: 0.0%
V COARSE GRAVEL: 0.0%	V COARSE SILT: 0.0%
COARSE GRAVEL: 0.0%	COARSE SILT: 6.6%
MEDIUM GRAVEL: 0.0%	MEDIUM SILT: 14.4%
FINE GRAVEL: 0.0%	FINE SILT: 12.5%
V FINE GRAVEL: 0.0%	V FINE SILT: 11.4%
V COARSE SAND: 36.4%	CLAY: 18.6%

	METHOD OF MOMENTS			FOLK & WARD METHOD		
	Arithmetic	Geometric	Logarithmic	Geometric	Logarithmic	Description
	µm	µm	ϕ	µm	ϕ	
MEAN ($\bar{x}$):	451.9	19.04	4.929	31.72	4.979	Very Coarse Silt
SORTING (σ):	711.2	19.10	4.317	18.50	4.209	Extremely Poorly Sorted
SKEWNESS (Sk):	0.993	0.602	-0.282	0.337	-0.337	Very Coarse Skewed
KURTOSIS (K):	2.040	1.786	1.449	0.511	0.511	Very Platykurtic

74 cm



SAMPLE STATISTICS

SAMPLE IDENTITY: **HE23T4C4B 74 cm** ANALYST & DATE: K Drew,

SAMPLE TYPE: Polymodal, Extremely Poorly Sorted TEXTURAL GROUP: Sandy Mud

SEDIMENT NAME: Very Coarse Sandy Medium Silt

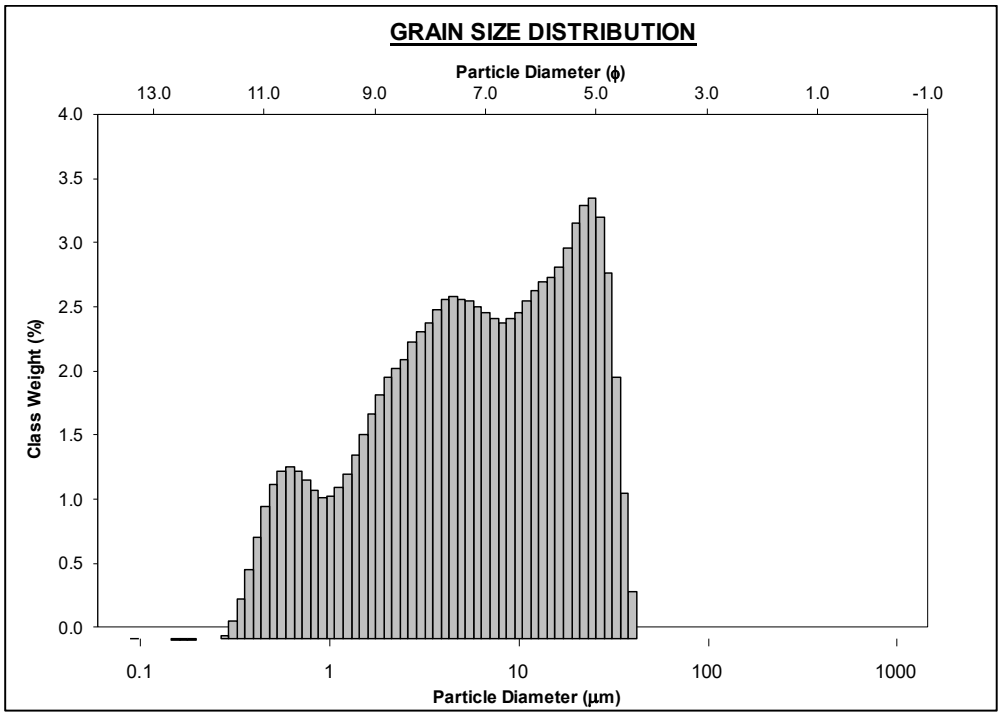
	µm	ϕ
MODE 1:	4.484	7.803
MODE 2:	5.470	7.516
MODE 3:	2.728	8.519
D_{10}:	0.852	-0.797
MEDIAN or D_{50}:	9.237	6.758
D_{90}:	1737.6	10.20
(D_{90} / D_{10}):	2038.6	-12.791
(D_{90} - D_{10}):	1736.8	10.99
(D_{75} / D_{25}):	551.9	-18.423
(D_{75} - D_{25}):	1381.6	9.108

GRAIN SIZE DISTRIBUTION

GRAVEL: 0.0%	COARSE SAND: 0.0%
SAND: 27.8%	MEDIUM SAND: 0.0%
MUD: 72.2%	FINE SAND: 0.0%
	V FINE SAND: 0.0%
V COARSE GRAVEL: 0.0%	V COARSE SILT: 0.0%
COARSE GRAVEL: 0.0%	COARSE SILT: 10.4%
MEDIUM GRAVEL: 0.0%	MEDIUM SILT: 15.0%
FINE GRAVEL: 0.0%	FINE SILT: 13.5%
V FINE GRAVEL: 0.0%	V FINE SILT: 12.7%
V COARSE SAND: 27.8%	CLAY: 20.6%

	METHOD OF MOMENTS			FOLK & WARD METHOD		
	Arithmetic	Geometric	Logarithmic	Geometric	Logarithmic	Description
	µm	µm	ϕ	µm	ϕ	
MEAN ($\bar{x}$):	346.2	13.46	5.604	27.80	5.169	Coarse Silt
SORTING (σ):	650.1	15.08	4.056	19.26	4.267	Extremely Poorly Sorted
SKEWNESS (Sk):	1.416	0.851	-0.579	0.386	-0.386	Very Coarse Skewed
KURTOSIS (K):	3.064	2.374	1.866	0.517	0.517	Very Platykurtic

86.5 cm



SAMPLE STATISTICS

SAMPLE IDENTITY: **HE23T4C4B 86.5 cm**

ANALYST & DATE: K Drew,

SAMPLE TYPE: Trimodal, Poorly Sorted

TEXTURAL GROUP: Mud

SEDIMENT NAME: Coarse Silt

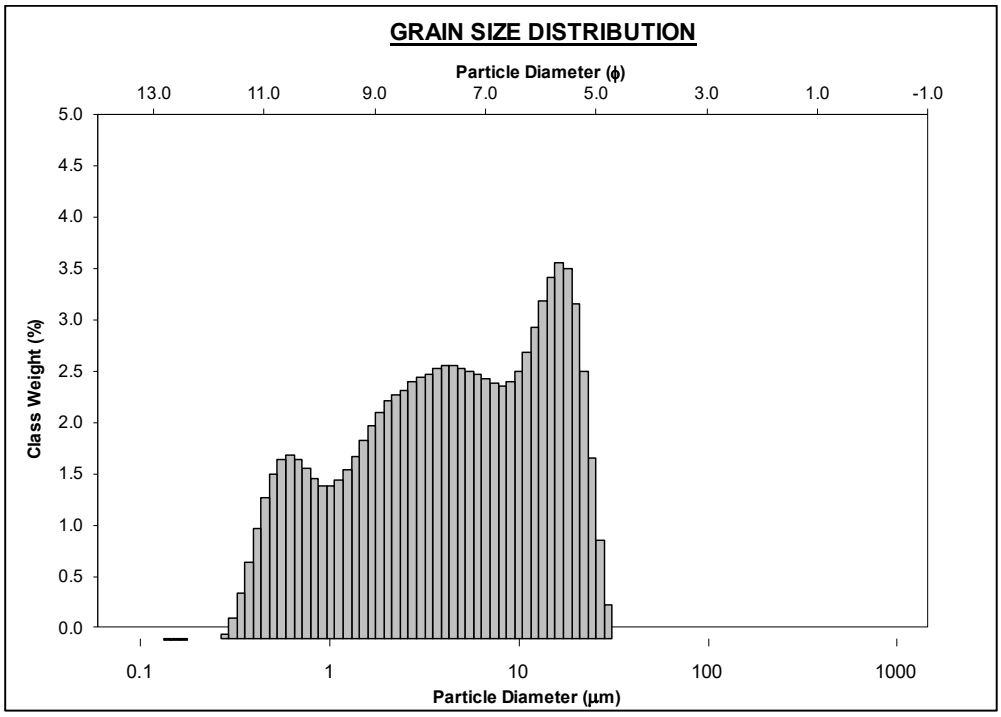
	µm	ϕ
MODE 1:	24.29	5.365
MODE 2:	4.484	7.803
MODE 3:	0.615	10.67
D_{10}:	0.842	5.307
MEDIAN or D_{50}:	6.124	7.351
D_{90}:	25.25	10.21
(D_{90} / D_{10}):	29.99	1.924
(D_{90} - D_{10}):	24.41	4.907
(D_{75} / D_{25}):	7.032	1.471
(D_{75} - D_{25}):	13.60	2.814

GRAIN SIZE DISTRIBUTION

GRAVEL: 0.0%	COARSE SAND: 0.0%
SAND: 0.0%	MEDIUM SAND: 0.0%
MUD: 100.0%	FINE SAND: 0.0%
	V FINE SAND: 0.0%
V COARSE GRAVEL: 0.0%	V COARSE SILT: 3.4%
COARSE GRAVEL: 0.0%	COARSE SILT: 22.0%
MEDIUM GRAVEL: 0.0%	MEDIUM SILT: 18.4%
FINE GRAVEL: 0.0%	FINE SILT: 18.1%
V FINE GRAVEL: 0.0%	V FINE SILT: 16.1%
V COARSE SAND: 0.0%	CLAY: 22.0%

	METHOD OF MOMENTS			FOLK & WARD METHOD		
	Arithmetic	Geometric	Logarithmic	Geometric	Logarithmic	Description
	µm	µm	ϕ	µm	ϕ	
MEAN ($\bar{x}$):	9.950	5.462	7.516	5.639	7.470	Fine Silt
SORTING (σ):	9.537	3.420	1.774	3.601	1.848	Poorly Sorted
SKEWNESS (Sk):	1.044	-0.387	0.387	-0.147	0.147	Fine Skewed
KURTOSIS (K):	3.066	2.157	2.157	0.830	0.830	Platykurtic

112 cm



SAMPLE STATISTICS

SAMPLE IDENTITY: **HE23T4C4B 112 cm**

ANALYST & DATE: K Drew,

SAMPLE TYPE: Trimodal, Poorly Sorted

TEXTURAL GROUP: Mud

SEDIMENT NAME: Medium Silt

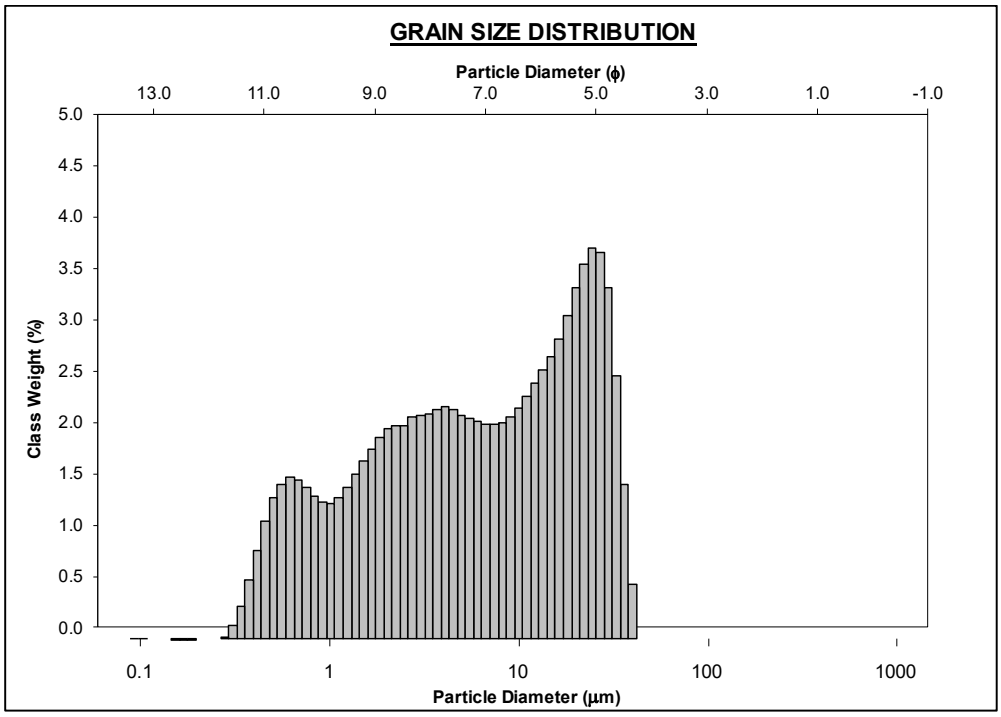
	µm	ϕ
MODE 1:	16.32	5.939
MODE 2:	4.060	7.946
MODE 3:	0.615	10.67
D_{10}:	0.682	5.768
MEDIAN or D_{50}:	4.562	7.776
D_{90}:	18.36	10.52
(D_{90} / D_{10}):	26.93	1.824
(D_{90} - D_{10}):	17.67	4.751
(D_{75} / D_{25}):	7.138	1.443
(D_{75} - D_{25}):	10.23	2.835

GRAIN SIZE DISTRIBUTION

GRAVEL: 0.0%	COARSE SAND: 0.0%
SAND: 0.0%	MEDIUM SAND: 0.0%
MUD: 100.0%	FINE SAND: 0.0%
	V FINE SAND: 0.0%
V COARSE GRAVEL: 0.0%	V COARSE SILT: 0.0%
COARSE GRAVEL: 0.0%	COARSE SILT: 15.9%
MEDIUM GRAVEL: 0.0%	MEDIUM SILT: 20.2%
FINE GRAVEL: 0.0%	FINE SILT: 18.1%
V FINE GRAVEL: 0.0%	V FINE SILT: 17.4%
V COARSE SAND: 0.0%	CLAY: 28.5%

	METHOD OF MOMENTS			FOLK & WARD METHOD		
	Arithmetic	Geometric	Logarithmic	Geometric	Logarithmic	Description
	µm	µm	ϕ	µm	ϕ	
MEAN ($\bar{x}$):	7.333	4.114	7.925	4.132	7.919	Fine Silt
SORTING (σ):	6.959	3.292	1.719	3.503	1.809	Poorly Sorted
SKEWNESS (Sk):	1.024	-0.305	0.305	-0.140	0.140	Fine Skewed
KURTOSIS (K):	3.030	1.995	1.995	0.778	0.778	Platykurtic

136 cm



SAMPLE STATISTICS

SAMPLE IDENTITY: **HE23T4C4B 136 cm**

ANALYST & DATE: K Drew,

SAMPLE TYPE: Trimodal, Poorly Sorted

TEXTURAL GROUP: Mud

SEDIMENT NAME: Coarse Silt

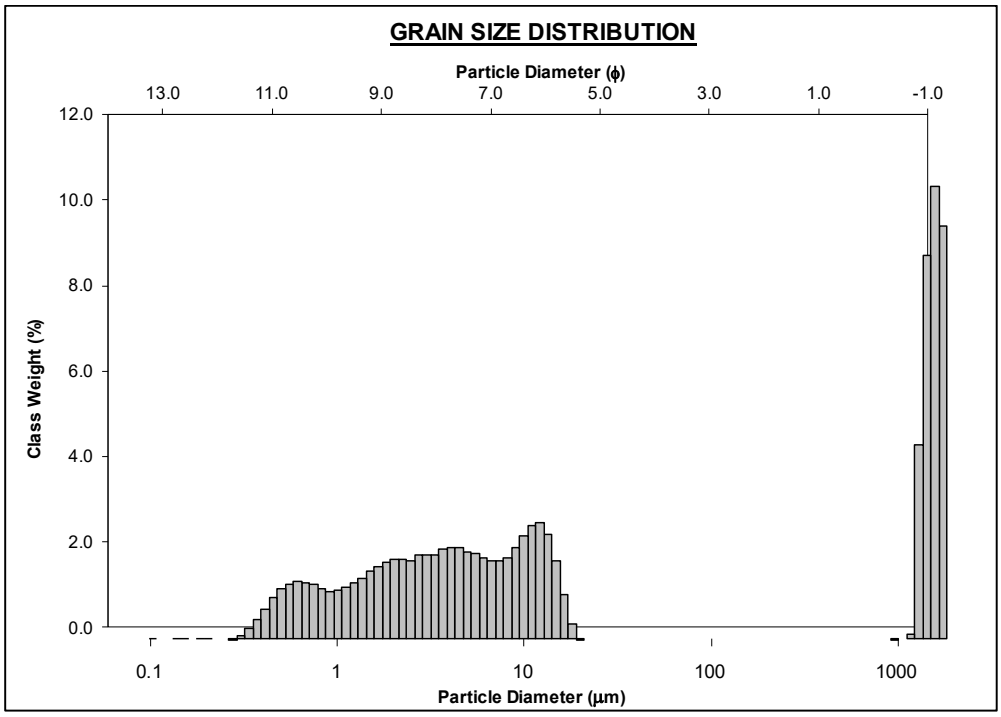
	µm	ϕ
MODE 1:	24.29	5.365
MODE 2:	4.060	7.946
MODE 3:	0.615	10.67
D_{10}:	0.760	5.226
MEDIAN or D_{50}:	6.215	7.330
D_{90}:	26.71	10.36
(D_{90} / D_{10}):	35.15	1.983
(D_{90} - D_{10}):	25.95	5.136
(D_{75} / D_{25}):	8.922	1.541
(D_{75} - D_{25}):	15.59	3.157

GRAIN SIZE DISTRIBUTION

GRAVEL: 0.0%	COARSE SAND: 0.0%
SAND: 0.0%	MEDIUM SAND: 0.0%
MUD: 100.0%	FINE SAND: 0.0%
	V FINE SAND: 0.0%
V COARSE GRAVEL: 0.0%	V COARSE SILT: 4.5%
COARSE GRAVEL: 0.0%	COARSE SILT: 24.0%
MEDIUM GRAVEL: 0.0%	MEDIUM SILT: 16.7%
FINE GRAVEL: 0.0%	FINE SILT: 15.0%
V FINE GRAVEL: 0.0%	V FINE SILT: 14.9%
V COARSE SAND: 0.0%	CLAY: 24.8%

	METHOD OF MOMENTS			FOLK & WARD METHOD		
	Arithmetic	Geometric	Logarithmic	Geometric	Logarithmic	Description
	µm	µm	ϕ	µm	ϕ	
MEAN ($\bar{x}$):	10.46	5.418	7.528	5.504	7.505	Fine Silt
SORTING (σ):	10.17	3.664	1.873	3.861	1.949	Poorly Sorted
SKEWNESS (Sk):	0.937	-0.343	0.343	-0.164	0.164	Fine Skewed
KURTOSIS (K):	2.730	1.960	1.960	0.754	0.754	Platykurtic

138 cm



SAMPLE STATISTICS

SAMPLE IDENTITY: **HE23T4C4B 138 cm** ANALYST & DATE: K Drew,

SAMPLE TYPE: Polymodal, Extremely Poorly Sorted TEXTURAL GROUP: Sandy Mud

SEDIMENT NAME: Very Coarse Sandy Medium Silt

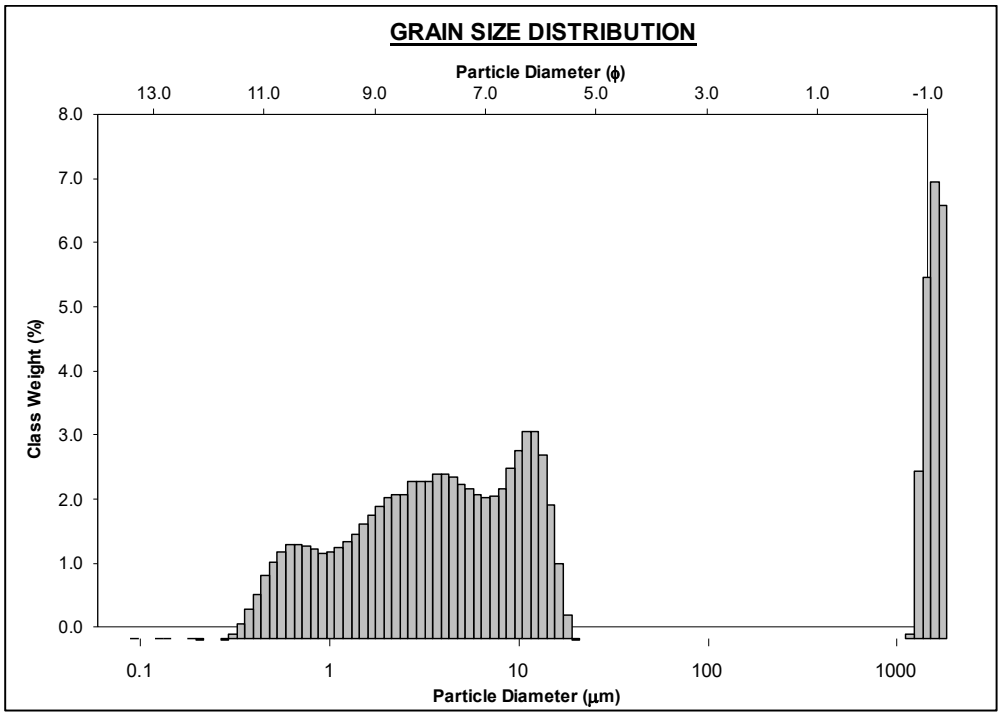
	µm	ϕ
MODE 1:	1577.6	-0.656
MODE 2:	12.11	6.369
MODE 3:	4.060	7.946
D_{10}:	0.924	-0.819
MEDIAN or D_{50}:	9.769	6.678
D_{90}:	1764.3	10.08
(D_{90} / D_{10}):	1909.1	-12.306
(D_{90} - D_{10}):	1763.4	10.90
(D_{75} / D_{25}):	583.2	-14.507
(D_{75} - D_{25}):	1505.3	9.188

GRAIN SIZE DISTRIBUTION

GRAVEL: 0.0%	COARSE SAND: 0.0%
SAND: 38.3%	MEDIUM SAND: 0.0%
MUD: 61.7%	FINE SAND: 0.0%
	V FINE SAND: 0.0%
V COARSE GRAVEL: 0.0%	V COARSE SILT: 0.0%
COARSE GRAVEL: 0.0%	COARSE SILT: 1.2%
MEDIUM GRAVEL: 0.0%	MEDIUM SILT: 14.9%
FINE GRAVEL: 0.0%	FINE SILT: 12.9%
V FINE GRAVEL: 0.0%	V FINE SILT: 12.6%
V COARSE SAND: 38.3%	CLAY: 20.1%

	METHOD OF MOMENTS			FOLK & WARD METHOD		
	Arithmetic µm	Geometric µm	Logarithmic ϕ	Geometric µm	Logarithmic ϕ	Description
MEAN ($\bar{x}$):	490.1	20.77	4.917	29.01	5.107	Coarse Silt
SORTING (σ):	721.0	21.07	4.438	18.91	4.241	Extremely Poorly Sorted
SKEWNESS (Sk):	0.842	0.538	-0.265	0.379	-0.379	Very Coarse Skewed
KURTOSIS (K):	1.773	1.610	1.359	0.506	0.506	Very Platykurtic

140 cm



SAMPLE STATISTICS

SAMPLE IDENTITY: **HE23T4C4B 140 cm** ANALYST & DATE: K Drew,

SAMPLE TYPE: Polymodal, Extremely Poorly Sorted TEXTURAL GROUP: Sandy Mud

SEDIMENT NAME: Very Coarse Sandy Medium Silt

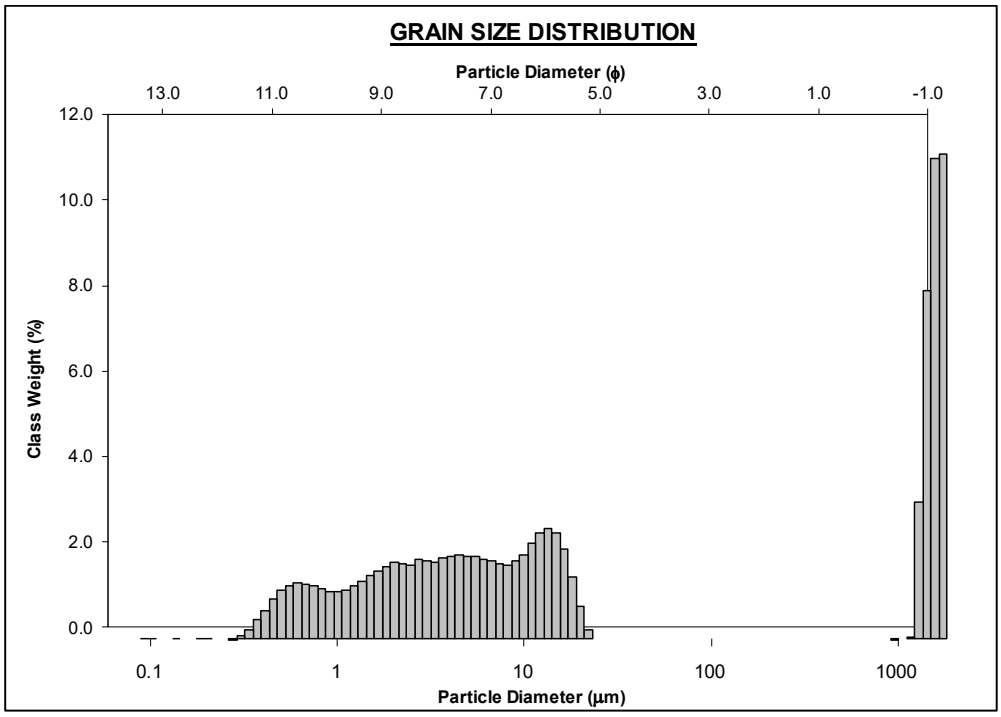
	μm	ϕ
MODE 1:	12.11	6.369
MODE 2:	4.060	7.946
MODE 3:	3.014	8.376
D_{10}:	0.852	-0.758
MEDIAN or D_{50}:	6.371	7.294
D_{90}:	1691.6	10.20
(D_{90} / D_{10}):	1985.3	-13.446
(D_{90} - D_{10}):	1690.7	10.96
(D_{75} / D_{25}):	594.0	-25.114
(D_{75} - D_{25}):	1274.9	9.214

GRAIN SIZE DISTRIBUTION

GRAVEL: 0.0%	COARSE SAND: 0.0%
SAND: 26.0%	MEDIUM SAND: 0.0%
MUD: 74.0%	FINE SAND: 0.0%
	V FINE SAND: 0.0%
V COARSE GRAVEL: 0.0%	V COARSE SILT: 0.0%
COARSE GRAVEL: 0.0%	COARSE SILT: 1.4%
MEDIUM GRAVEL: 0.0%	MEDIUM SILT: 18.2%
FINE GRAVEL: 0.0%	FINE SILT: 15.6%
V FINE GRAVEL: 0.0%	V FINE SILT: 15.8%
V COARSE SAND: 26.0%	CLAY: 23.0%

	METHOD OF MOMENTS			FOLK & WARD METHOD		
	Arithmetic	Geometric	Logarithmic	Geometric	Logarithmic	Description
	μm	μm	ϕ	μm	ϕ	
MEAN ($\bar{x}$):	331.3	11.40	5.960	23.55	5.408	Coarse Silt
SORTING (σ):	636.0	14.87	4.047	19.74	4.303	Extremely Poorly Sorted
SKEWNESS (Sk):	1.463	1.000	-0.756	0.482	-0.482	Very Coarse Skewed
KURTOSIS (K):	3.210	2.568	2.035	0.515	0.515	Very Platykurtic

145 cm



SAMPLE STATISTICS

SAMPLE IDENTITY: **HE23T4C4B 145 cm** ANALYST & DATE: K Drew,

SAMPLE TYPE: Polymodal, Extremely Poorly Sorted TEXTURAL GROUP: Sandy Mud

SEDIMENT NAME: Very Coarse Sandy Medium Silt

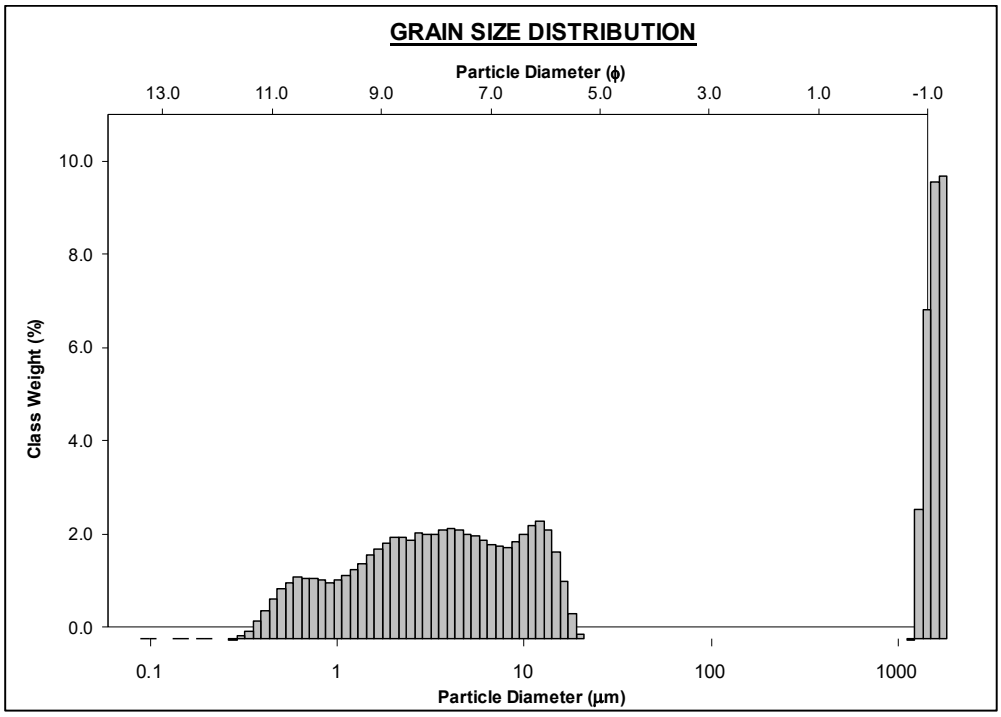
	µm	ϕ
MODE 1:	1742.4	-0.799
MODE 2:	13.38	6.226
MODE 3:	4.484	7.803
D_{10}:	0.963	-0.849
MEDIAN or D_{50}:	11.76	6.410
D_{90}:	1801.7	10.02
(D_{90} / D_{10}):	1870.1	-11.797
(D_{90} - D_{10}):	1800.7	10.87
(D_{75} / D_{25}):	552.1	-13.211
(D_{75} - D_{25}):	1556.5	9.109

GRAIN SIZE DISTRIBUTION

GRAVEL: 0.0%	COARSE SAND: 0.0%
SAND: 39.5%	MEDIUM SAND: 0.0%
MUD: 60.5%	FINE SAND: 0.0%
	V FINE SAND: 0.0%
V COARSE GRAVEL: 0.0%	V COARSE SILT: 0.0%
COARSE GRAVEL: 0.0%	COARSE SILT: 4.0%
MEDIUM GRAVEL: 0.0%	MEDIUM SILT: 14.0%
FINE GRAVEL: 0.0%	FINE SILT: 12.0%
V FINE GRAVEL: 0.0%	V FINE SILT: 11.5%
V COARSE SAND: 39.5%	CLAY: 19.0%

	METHOD OF MOMENTS			FOLK & WARD METHOD		
	Arithmetic	Geometric	Logarithmic	Geometric	Logarithmic	Description
	µm	µm	ϕ	µm	ϕ	
MEAN ($\bar{x}$):	490.4	20.89	4.741	31.78	4.976	Very Coarse Silt
SORTING (σ):	728.4	20.84	4.415	18.46	4.207	Extremely Poorly Sorted
SKEWNESS (Sk):	0.861	0.533	-0.196	0.334	-0.334	Very Coarse Skewed
KURTOSIS (K):	1.797	1.629	1.345	0.503	0.503	Very Platykurtic

148 cm



SAMPLE STATISTICS

SAMPLE IDENTITY: **HE23T4C4B 148 cm** ANALYST & DATE: K Drew,

SAMPLE TYPE: Polymodal, Extremely Poorly Sorted TEXTURAL GROUP: Sandy Mud

SEDIMENT NAME: Very Coarse Sandy Very Fine Silt

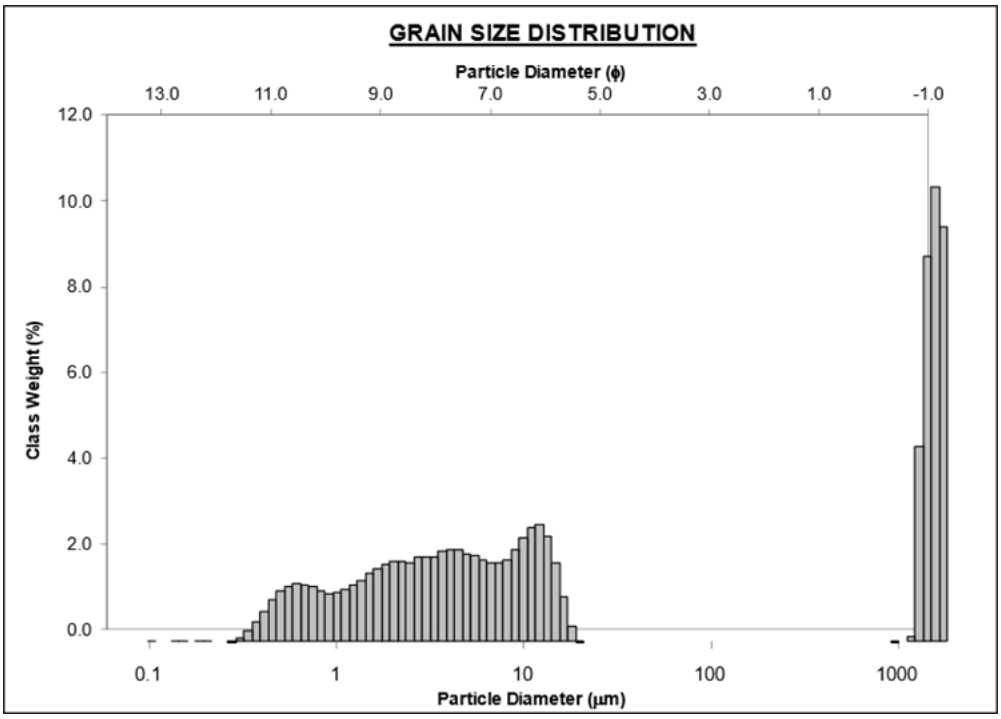
	µm	ϕ
MODE 1:	1742.4	-0.799
MODE 2:	12.11	6.369
MODE 3:	4.060	7.946
D_{10}:	0.961	-0.831
MEDIAN or D_{50}:	8.089	6.950
D_{90}:	1778.7	10.02
(D_{90} / D_{10}):	1850.3	-12.064
(D_{90} - D_{10}):	1777.7	10.85
(D_{75} / D_{25}):	632.2	-14.657
(D_{75} - D_{25}):	1507.3	9.304

GRAIN SIZE DISTRIBUTION

GRAVEL: 0.0%	COARSE SAND: 0.0%
SAND: 34.7%	MEDIUM SAND: 0.0%
MUD: 65.3%	FINE SAND: 0.0%
	V FINE SAND: 0.0%
V COARSE GRAVEL: 0.0%	V COARSE SILT: 0.0%
COARSE GRAVEL: 0.0%	COARSE SILT: 1.7%
MEDIUM GRAVEL: 0.0%	MEDIUM SILT: 14.2%
FINE GRAVEL: 0.0%	FINE SILT: 14.1%
V FINE GRAVEL: 0.0%	V FINE SILT: 14.4%
V COARSE SAND: 34.7%	CLAY: 20.9%

	METHOD OF MOMENTS			FOLK & WARD METHOD		
	Arithmetic	Geometric	Logarithmic	Geometric	Logarithmic	Description
	µm	µm	ϕ	µm	ϕ	
MEAN ($\bar{x}$):	432.1	16.00	5.225	27.20	5.200	Coarse Silt
SORTING (σ):	701.9	18.95	4.350	18.77	4.231	Extremely Poorly Sorted
SKEWNESS (Sk):	1.059	0.730	-0.412	0.431	-0.431	Very Coarse Skewed
KURTOSIS (K):	2.177	1.898	1.475	0.494	0.494	Very Platykurtic

150 cm



SAMPLE STATISTICS

SAMPLE IDENTITY: **HE23T4C4B 150 cm** ANALYST & DATE: K Drew,

SAMPLE TYPE: Polymodal, Extremely Poorly Sorted TEXTURAL GROUP: Sandy Mud

SEDIMENT NAME: Very Coarse Sandy Mud

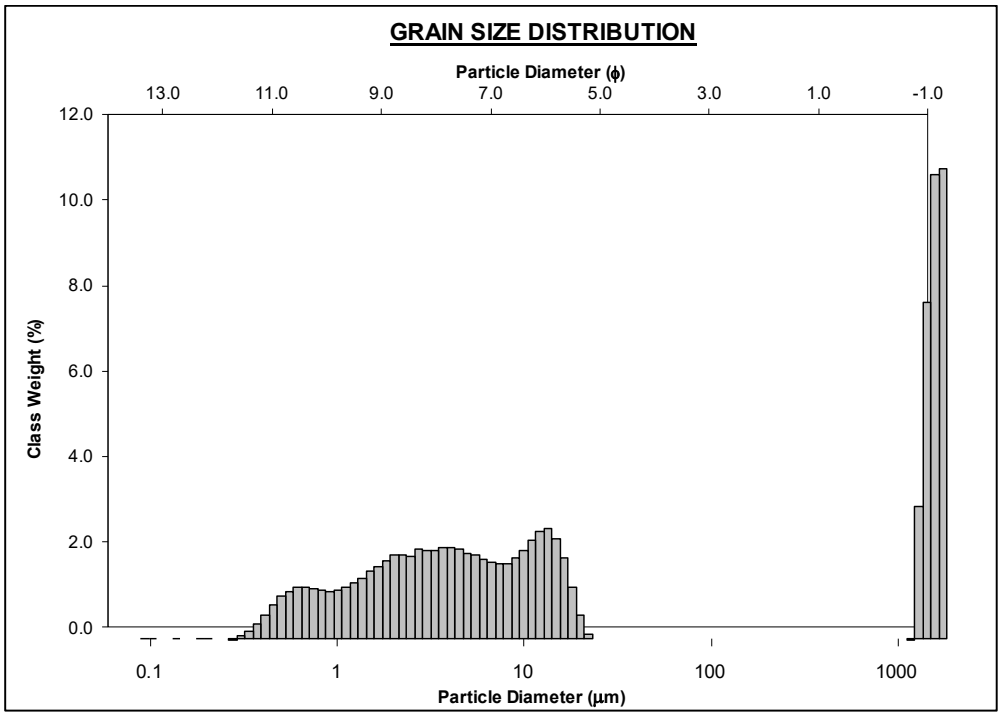
	µm	ϕ
MODE 1:	12.11	6.369
MODE 2:	2.728	8.519
MODE 3:	3.676	8.089
D_{10}:	0.879	-0.802
MEDIAN or D_{50}:	6.288	7.313
D_{90}:	1744.0	10.15
(D_{90} / D_{10}):	1984.5	-12.652
(D_{90} - D_{10}):	1743.1	10.95
(D_{75} / D_{25}):	682.4	-17.977
(D_{75} - D_{25}):	1408.3	9.414

GRAIN SIZE DISTRIBUTION

GRAVEL: 0.0%	COARSE SAND: 0.0%
SAND: 29.2%	MEDIUM SAND: 0.0%
MUD: 70.8%	FINE SAND: 0.0%
	V FINE SAND: 0.0%
V COARSE GRAVEL: 0.0%	V COARSE SILT: 0.0%
COARSE GRAVEL: 0.0%	COARSE SILT: 1.4%
MEDIUM GRAVEL: 0.0%	MEDIUM SILT: 15.3%
FINE GRAVEL: 0.0%	FINE SILT: 14.4%
V FINE GRAVEL: 0.0%	V FINE SILT: 16.0%
V COARSE SAND: 29.2%	CLAY: 23.7%

	METHOD OF MOMENTS			FOLK & WARD METHOD		
	Arithmetic	Geometric	Logarithmic	Geometric	Logarithmic	Description
	µm	µm	ϕ	µm	ϕ	
MEAN ($\bar{x}$):	363.2	12.04	5.748	23.82	5.391	Coarse Silt
SORTING (σ):	662.3	16.43	4.203	19.50	4.285	Extremely Poorly Sorted
SKEWNESS (Sk):	1.330	0.937	-0.639	0.485	-0.485	Very Coarse Skewed
KURTOSIS (K):	2.829	2.341	1.780	0.495	0.495	Very Platykurtic

157 cm



SAMPLE STATISTICS

SAMPLE IDENTITY: **HE23T4C4B 157 cm** ANALYST & DATE: K Drew,

SAMPLE TYPE: Polymodal, Extremely Poorly Sorted TEXTURAL GROUP: Sandy Mud

SEDIMENT NAME: Very Coarse Sandy Medium Silt

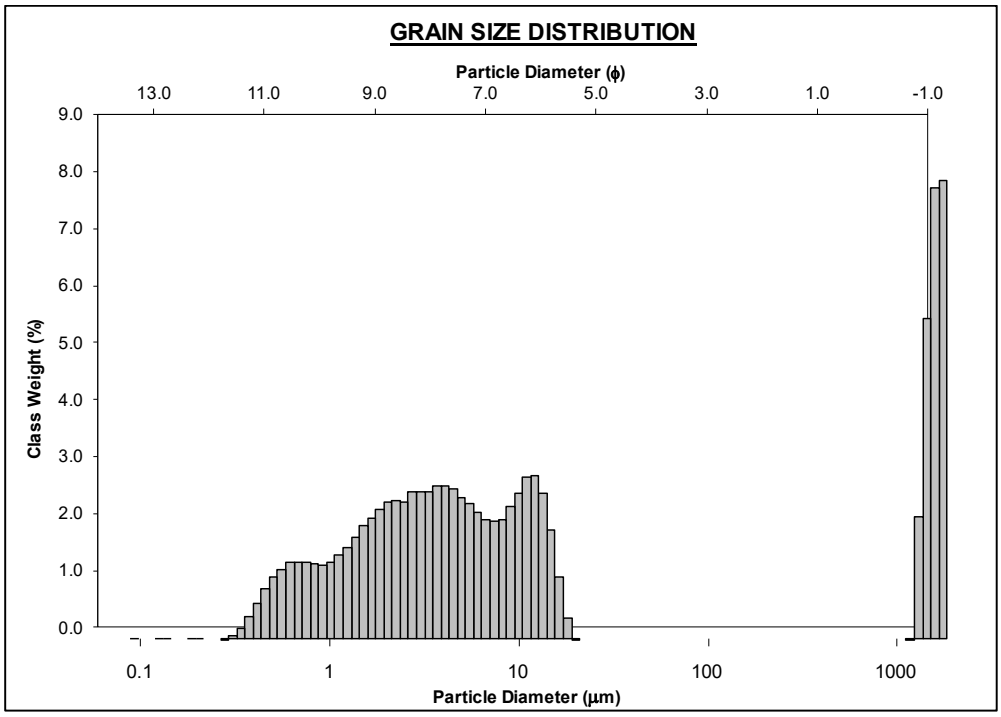
	µm	ϕ
MODE 1:	1742.4	-0.799
MODE 2:	13.38	6.226
MODE 3:	4.060	7.946
D_{10}:	1.042	-0.845
MEDIAN or D_{50}:	10.77	6.537
D_{90}:	1796.4	9.906
(D_{90} / D_{10}):	1723.6	-11.722
(D_{90} - D_{10}):	1795.4	10.75
(D_{75} / D_{25}):	563.0	-13.493
(D_{75} - D_{25}):	1545.3	9.137

GRAIN SIZE DISTRIBUTION

GRAVEL: 0.0%	COARSE SAND: 0.0%
SAND: 38.3%	MEDIUM SAND: 0.0%
MUD: 61.7%	FINE SAND: 0.0%
	V FINE SAND: 0.0%
V COARSE GRAVEL: 0.0%	V COARSE SILT: 0.0%
COARSE GRAVEL: 0.0%	COARSE SILT: 3.4%
MEDIUM GRAVEL: 0.0%	MEDIUM SILT: 14.1%
FINE GRAVEL: 0.0%	FINE SILT: 12.4%
V FINE GRAVEL: 0.0%	V FINE SILT: 13.1%
V COARSE SAND: 38.3%	CLAY: 18.7%

	METHOD OF MOMENTS			FOLK & WARD METHOD		
	Arithmetic	Geometric	Logarithmic	Geometric	Logarithmic	Description
	µm	µm	ϕ	µm	ϕ	
MEAN ($\bar{x}$):	475.7	19.78	4.845	31.15	5.005	Coarse Silt
SORTING (σ):	722.3	20.15	4.383	18.16	4.183	Extremely Poorly Sorted
SKEWNESS (Sk):	0.909	0.588	-0.257	0.366	-0.366	Very Coarse Skewed
KURTOSIS (K):	1.882	1.689	1.363	0.499	0.499	Very Platykurtic

160 cm



SAMPLE STATISTICS

SAMPLE IDENTITY: **HE23T4C4B 160 cm** ANALYST & DATE: K Drew,

SAMPLE TYPE: Polymodal, Extremely Poorly Sorted TEXTURAL GROUP: Sandy Mud

SEDIMENT NAME: Very Coarse Sandy Very Fine Silt

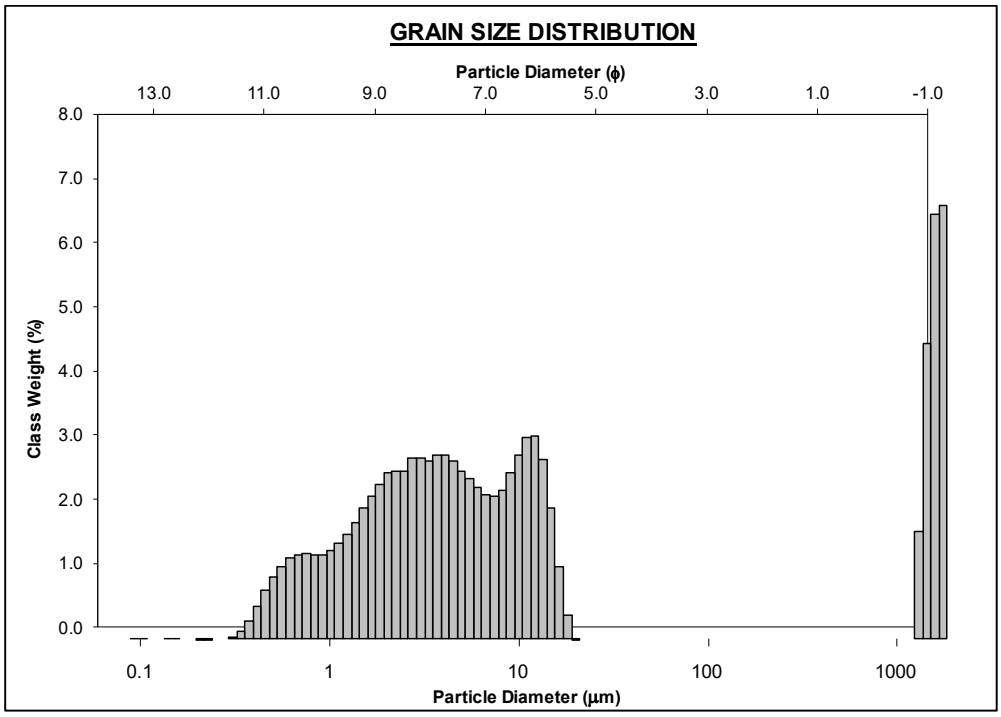
	µm	ϕ
MODE 1:	12.11	6.369
MODE 2:	4.060	7.946
MODE 3:	2.728	8.519
D_{10}:	0.931	-0.798
MEDIAN or D_{50}:	6.239	7.324
D_{90}:	1738.6	10.07
(D_{90} / D_{10}):	1867.8	-12.620
(D_{90} - D_{10}):	1737.6	10.87
(D_{75} / D_{25}):	639.4	-18.511
(D_{75} - D_{25}):	1390.4	9.321

GRAIN SIZE DISTRIBUTION

GRAVEL: 0.0%	COARSE SAND: 0.0%
SAND: 28.4%	MEDIUM SAND: 0.0%
MUD: 71.6%	FINE SAND: 0.0%
	V FINE SAND: 0.0%
V COARSE GRAVEL: 0.0%	V COARSE SILT: 0.0%
COARSE GRAVEL: 0.0%	COARSE SILT: 1.3%
MEDIUM GRAVEL: 0.0%	MEDIUM SILT: 15.9%
FINE GRAVEL: 0.0%	FINE SILT: 15.4%
V FINE GRAVEL: 0.0%	V FINE SILT: 16.5%
V COARSE SAND: 28.4%	CLAY: 22.5%

	METHOD OF MOMENTS			FOLK & WARD METHOD		
	Arithmetic µm	Geometric µm	Logarithmic ϕ	Geometric µm	Logarithmic ϕ	Description
MEAN ($\bar{x}$):	352.5	11.86	5.784	24.17	5.370	Coarse Silt
SORTING (σ):	655.2	15.73	4.143	19.14	4.258	Extremely Poorly Sorted
SKEWNESS (Sk):	1.378	0.973	-0.678	0.496	-0.496	Very Coarse Skewed
KURTOSIS (K):	2.958	2.435	1.847	0.499	0.499	Very Platykurtic

165 cm



SAMPLE STATISTICS

SAMPLE IDENTITY: **HE23T4C4B 165 cm** ANALYST & DATE: K Drew,

SAMPLE TYPE: Polymodal, Extremely Poorly Sorted TEXTURAL GROUP: Sandy Mud

SEDIMENT NAME: Very Coarse Sandy Very Fine Silt

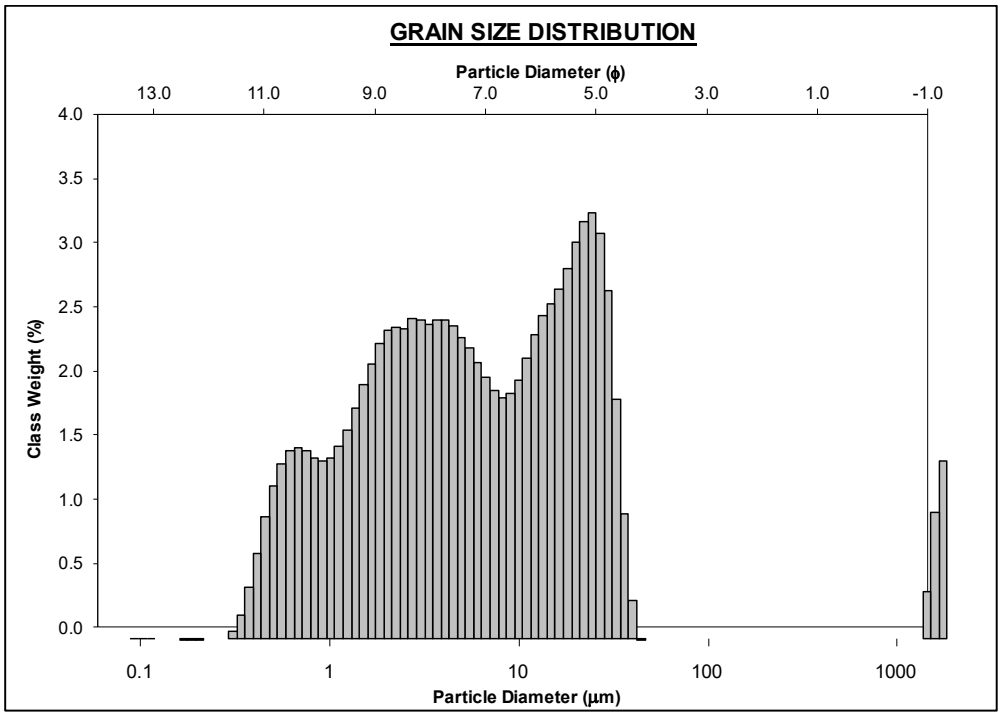
	µm	ϕ
MODE 1:	12.11	6.369
MODE 2:	4.060	7.946
MODE 3:	2.728	8.519
D_{10}:	0.976	-0.765
MEDIAN or D_{50}:	5.658	7.465
D_{90}:	1699.6	10.00
(D_{90} / D_{10}):	1742.2	-13.070
(D_{90} - D_{10}):	1698.6	10.77
(D_{75} / D_{25}):	7.347	1.482
(D_{75} - D_{25}):	13.75	2.877

GRAIN SIZE DISTRIBUTION

GRAVEL: 0.0%	COARSE SAND: 0.0%
SAND: 23.9%	MEDIUM SAND: 0.0%
MUD: 76.1%	FINE SAND: 0.0%
	V FINE SAND: 0.0%
V COARSE GRAVEL: 0.0%	V COARSE SILT: 0.0%
COARSE GRAVEL: 0.0%	COARSE SILT: 1.3%
MEDIUM GRAVEL: 0.0%	MEDIUM SILT: 17.8%
FINE GRAVEL: 0.0%	FINE SILT: 16.6%
V FINE GRAVEL: 0.0%	V FINE SILT: 18.0%
V COARSE SAND: 23.9%	CLAY: 22.4%

	METHOD OF MOMENTS			FOLK & WARD METHOD		
	Arithmetic	Geometric	Logarithmic	Geometric	Logarithmic	Description
	µm	µm	ϕ	µm	ϕ	
MEAN ($\bar{x}$):	296.5	9.926	6.128	23.29	5.424	Coarse Silt
SORTING (σ):	614.0	13.17	3.913	18.94	4.243	Extremely Poorly Sorted
SKEWNESS (Sk):	1.656	1.166	-0.887	0.531	-0.531	Very Coarse Skewed
KURTOSIS (K):	3.805	2.990	2.267	1.624	1.624	Very Leptokurtic

166 cm



SAMPLE STATISTICS

SAMPLE IDENTITY: **HE23T4C4B 166 cm**

ANALYST & DATE: K Drew,

SAMPLE TYPE: Polymodal, Poorly Sorted

TEXTURAL GROUP: Mud

SEDIMENT NAME: Coarse Silt

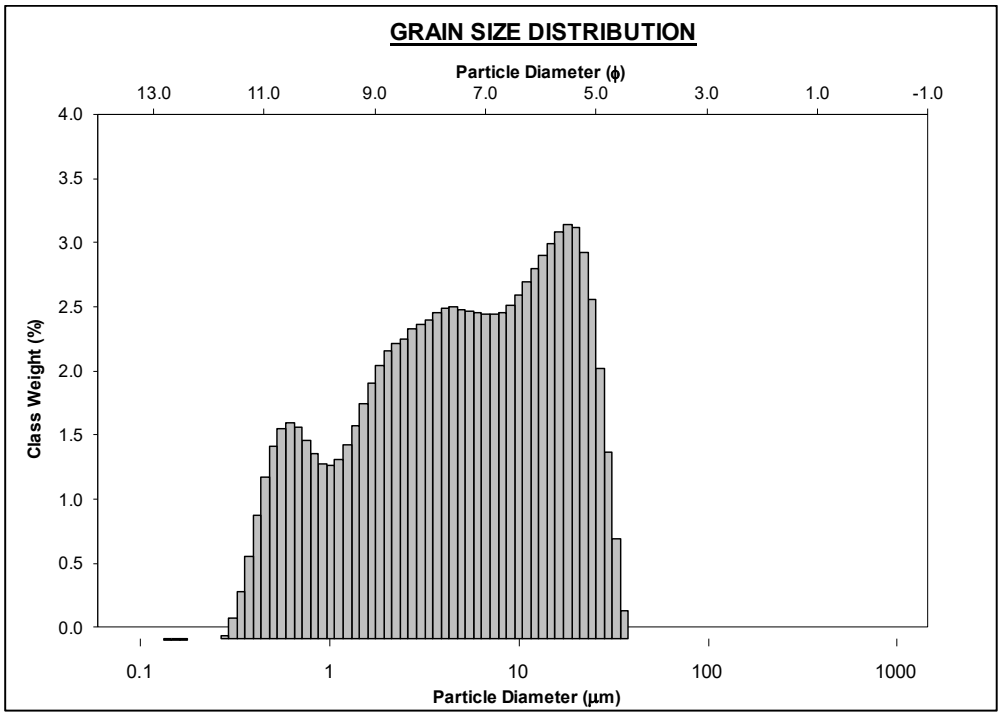
	µm	ϕ
MODE 1:	24.29	5.365
MODE 2:	2.728	8.519
MODE 3:	4.060	7.946
D_{10}:	0.840	5.157
MEDIAN or D_{50}:	5.563	7.490
D_{90}:	28.02	10.22
(D_{90} / D_{10}):	33.37	1.981
(D_{90} - D_{10}):	27.19	5.061
(D_{75} / D_{25}):	8.779	1.536
(D_{75} - D_{25}):	15.34	3.134

GRAIN SIZE DISTRIBUTION

GRAVEL: 0.0%	COARSE SAND: 0.0%
SAND: 4.1%	MEDIUM SAND: 0.0%
MUD: 95.9%	FINE SAND: 0.0%
	V FINE SAND: 0.0%
V COARSE GRAVEL: 0.0%	V COARSE SILT: 3.0%
COARSE GRAVEL: 0.0%	COARSE SILT: 20.7%
MEDIUM GRAVEL: 0.0%	MEDIUM SILT: 15.3%
FINE GRAVEL: 0.0%	FINE SILT: 15.3%
V FINE GRAVEL: 0.0%	V FINE SILT: 16.8%
V COARSE SAND: 4.1%	CLAY: 24.8%

	METHOD OF MOMENTS			FOLK & WARD METHOD		
	Arithmetic	Geometric	Logarithmic	Geometric	Logarithmic	Description
	µm	µm	ϕ	µm	ϕ	
MEAN ($\bar{x}$):	53.23	5.678	7.321	5.473	7.513	Fine Silt
SORTING (σ):	264.9	4.731	2.387	3.847	1.944	Poorly Sorted
SKEWNESS (Sk):	5.879	1.018	-1.111	-0.055	0.055	Symmetrical
KURTOSIS (K):	35.78	5.606	5.400	0.772	0.772	Platykurtic

169.5 cm



SAMPLE STATISTICS

SAMPLE IDENTITY: **HE23T4C4B 169.5 cm**

ANALYST & DATE: K Drew,

SAMPLE TYPE: Trimodal, Poorly Sorted

TEXTURAL GROUP: Mud

SEDIMENT NAME: Medium Silt

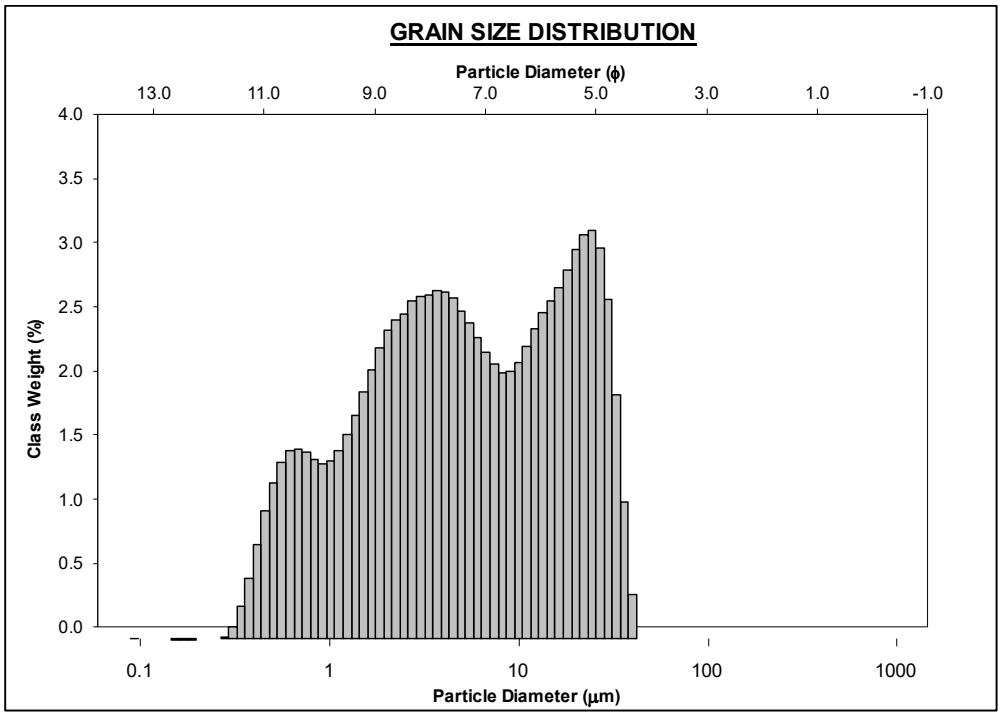
	µm	ϕ
MODE 1:	18.03	5.796
MODE 2:	4.484	7.803
MODE 3:	0.615	10.67
D_{10}:	0.718	5.570
MEDIAN or D_{50}:	5.091	7.618
D_{90}:	21.05	10.44
(D_{90} / D_{10}):	29.32	1.875
(D_{90} - D_{10}):	20.33	4.874
(D_{75} / D_{25}):	7.153	1.454
(D_{75} - D_{25}):	11.25	2.838

GRAIN SIZE DISTRIBUTION

GRAVEL: 0.0%	COARSE SAND: 0.0%
SAND: 0.0%	MEDIUM SAND: 0.0%
MUD: 100.0%	FINE SAND: 0.0%
	V FINE SAND: 0.0%
V COARSE GRAVEL: 0.0%	V COARSE SILT: 1.0%
COARSE GRAVEL: 0.0%	COARSE SILT: 18.6%
MEDIUM GRAVEL: 0.0%	MEDIUM SILT: 19.5%
FINE GRAVEL: 0.0%	FINE SILT: 17.8%
V FINE GRAVEL: 0.0%	V FINE SILT: 16.7%
V COARSE SAND: 0.0%	CLAY: 26.4%

	METHOD OF MOMENTS			FOLK & WARD METHOD		
	Arithmetic	Geometric	Logarithmic	Geometric	Logarithmic	Description
	µm	µm	ϕ	µm	ϕ	
MEAN ($\bar{x}$):	8.305	4.555	7.778	4.597	7.765	Fine Silt
SORTING (σ):	8.091	3.379	1.756	3.586	1.842	Poorly Sorted
SKEWNESS (Sk):	1.124	-0.313	0.313	-0.141	0.141	Fine Skewed
KURTOSIS (K):	3.366	2.036	2.036	0.803	0.803	Platykurtic

186 cm



SAMPLE STATISTICS

SAMPLE IDENTITY: **HE23T4C4B 186 cm**

ANALYST & DATE: K Drew,

SAMPLE TYPE: Trimodal, Poorly Sorted

TEXTURAL GROUP: Mud

SEDIMENT NAME: Coarse Silt

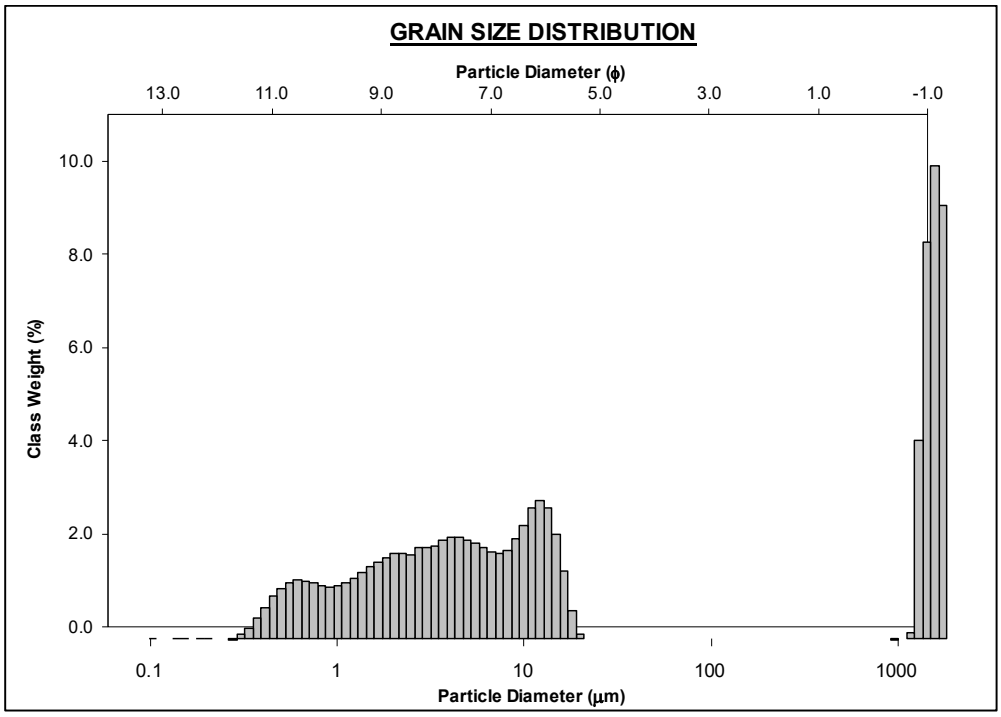
	µm	ϕ
MODE 1:	24.29	5.365
MODE 2:	3.676	8.089
MODE 3:	0.679	10.53
D_{10}:	0.813	5.339
MEDIAN or D_{50}:	5.048	7.630
D_{90}:	24.71	10.27
(D_{90} / D_{10}):	30.40	1.923
(D_{90} - D_{10}):	23.90	4.926
(D_{75} / D_{25}):	7.667	1.484
(D_{75} - D_{25}):	12.96	2.939

GRAIN SIZE DISTRIBUTION

GRAVEL: 0.0%	COARSE SAND: 0.0%
SAND: 0.0%	MEDIUM SAND: 0.0%
MUD: 100.0%	FINE SAND: 0.0%
	V FINE SAND: 0.0%
V COARSE GRAVEL: 0.0%	V COARSE SILT: 3.2%
COARSE GRAVEL: 0.0%	COARSE SILT: 20.5%
MEDIUM GRAVEL: 0.0%	MEDIUM SILT: 16.1%
FINE GRAVEL: 0.0%	FINE SILT: 16.9%
V FINE GRAVEL: 0.0%	V FINE SILT: 18.1%
V COARSE SAND: 0.0%	CLAY: 25.1%

	METHOD OF MOMENTS			FOLK & WARD METHOD		
	Arithmetic	Geometric	Logarithmic	Geometric	Logarithmic	Description
	µm	µm	ϕ	µm	ϕ	
MEAN ($\bar{x}$):	9.311	4.932	7.663	5.030	7.635	Fine Silt
SORTING (σ):	9.466	3.447	1.785	3.655	1.870	Poorly Sorted
SKEWNESS (Sk):	1.146	-0.221	0.221	-0.055	0.055	Symmetrical
KURTOSIS (K):	3.274	2.000	2.000	0.789	0.789	Platykurtic

191 cm



SAMPLE STATISTICS

SAMPLE IDENTITY: **HE23T4C4B 191 cm** ANALYST & DATE: K Drew,

SAMPLE TYPE: Polymodal, Extremely Poorly Sorted TEXTURAL GROUP: Sandy Mud

SEDIMENT NAME: Very Coarse Sandy Medium Silt

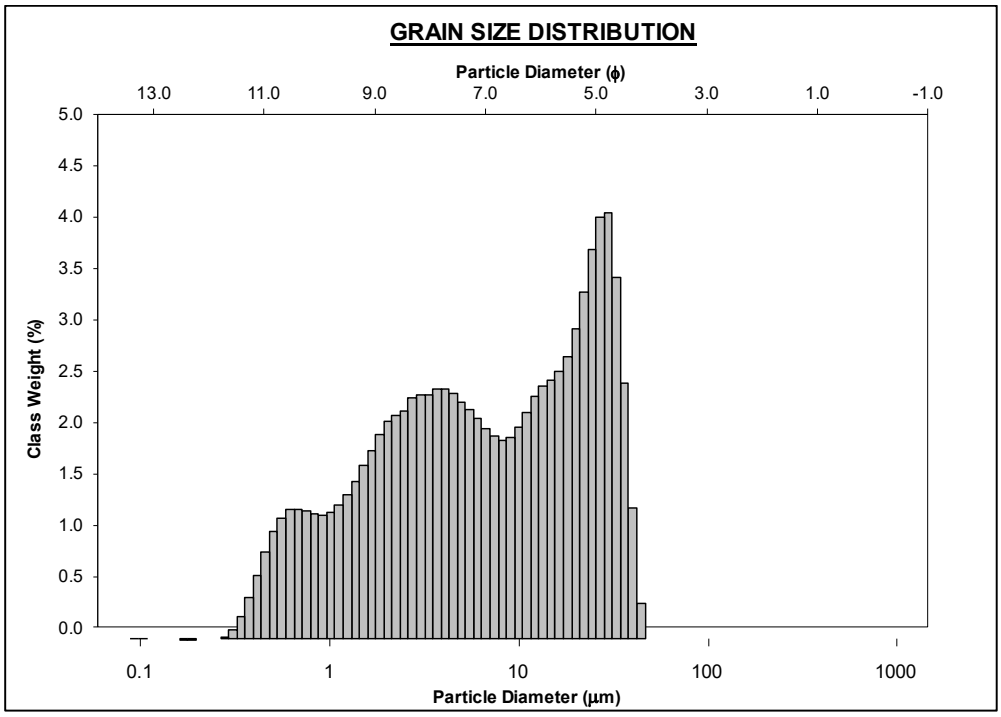
	μm	ϕ
MODE 1:	1577.6	-0.656
MODE 2:	12.11	6.369
MODE 3:	4.484	7.803
D_{10}:	0.968	-0.814
MEDIAN or D_{50}:	9.920	6.655
D_{90}:	1758.6	10.01
(D_{90} / D_{10}):	1817.2	-12.295
(D_{90} - D_{10}):	1757.6	10.83
(D_{75} / D_{25}):	556.0	-14.758
(D_{75} - D_{25}):	1490.8	9.119

GRAIN SIZE DISTRIBUTION

GRAVEL: 0.0%	COARSE SAND: 0.0%
SAND: 36.7%	MEDIUM SAND: 0.0%
MUD: 63.3%	FINE SAND: 0.0%
	V FINE SAND: 0.0%
V COARSE GRAVEL: 0.0%	V COARSE SILT: 0.0%
COARSE GRAVEL: 0.0%	COARSE SILT: 1.9%
MEDIUM GRAVEL: 0.0%	MEDIUM SILT: 16.1%
FINE GRAVEL: 0.0%	FINE SILT: 13.2%
V FINE GRAVEL: 0.0%	V FINE SILT: 12.6%
V COARSE SAND: 36.7%	CLAY: 19.5%

	METHOD OF MOMENTS			FOLK & WARD METHOD		
	Arithmetic	Geometric	Logarithmic	Geometric	Logarithmic	Description
	μm	μm	ϕ	μm	ϕ	
MEAN ($\bar{x}$):	469.7	19.91	4.995	29.46	5.085	Coarse Silt
SORTING (σ):	712.6	19.94	4.369	18.68	4.224	Extremely Poorly Sorted
SKEWNESS (Sk):	0.911	0.581	-0.313	0.381	-0.381	Very Coarse Skewed
KURTOSIS (K):	1.893	1.693	1.413	0.509	0.509	Very Platykurtic

193 cm



SAMPLE STATISTICS

SAMPLE IDENTITY: **HE23T4C4B 193 cm**

ANALYST & DATE: K Drew,

SAMPLE TYPE: Trimodal, Poorly Sorted

TEXTURAL GROUP: Mud

SEDIMENT NAME: Coarse Silt

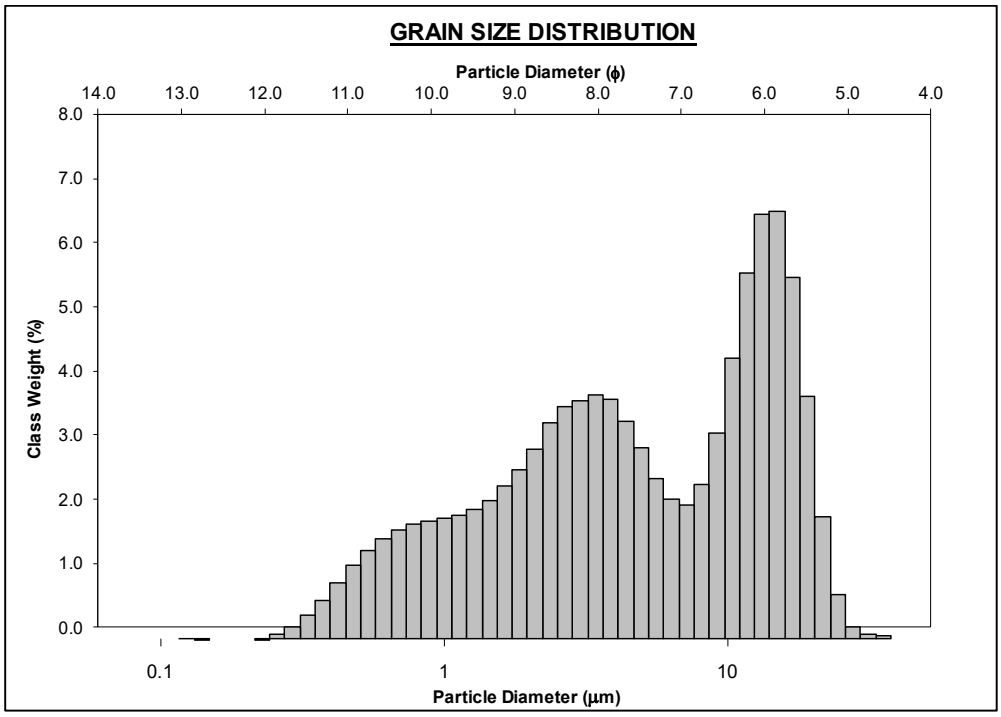
	µm	ϕ
MODE 1:	29.63	5.079
MODE 2:	4.060	7.946
MODE 3:	0.679	10.53
D_{10}:	0.913	5.089
MEDIAN or D_{50}:	6.618	7.239
D_{90}:	29.37	10.10
(D_{90} / D_{10}):	32.15	1.984
(D_{90} - D_{10}):	28.46	5.007
(D_{75} / D_{25}):	8.680	1.549
(D_{75} - D_{25}):	17.31	3.118

GRAIN SIZE DISTRIBUTION

GRAVEL: 0.0%	COARSE SAND: 0.0%
SAND: 0.0%	MEDIUM SAND: 0.0%
MUD: 100.0%	FINE SAND: 0.0%
	V FINE SAND: 0.0%
V COARSE GRAVEL: 0.0%	V COARSE SILT: 7.4%
COARSE GRAVEL: 0.0%	COARSE SILT: 23.7%
MEDIUM GRAVEL: 0.0%	MEDIUM SILT: 15.5%
FINE GRAVEL: 0.0%	FINE SILT: 15.4%
V FINE GRAVEL: 0.0%	V FINE SILT: 16.0%
V COARSE SAND: 0.0%	CLAY: 21.9%

	METHOD OF MOMENTS			FOLK & WARD METHOD		
	Arithmetic	Geometric	Logarithmic	Geometric	Logarithmic	Description
	µm	µm	ϕ	µm	ϕ	
MEAN ($\bar{x}$):	11.51	6.027	7.374	6.204	7.333	Fine Silt
SORTING (σ):	11.15	3.604	1.850	3.770	1.915	Poorly Sorted
SKEWNESS (Sk):	0.914	-0.337	0.337	-0.128	0.128	Fine Skewed
KURTOSIS (K):	2.632	2.005	2.005	0.759	0.759	Platykurtic

195 cm



SAMPLE STATISTICS

SAMPLE IDENTITY: **HE23T4C4B 195 cm**

ANALYST & DATE: K Drew,

SAMPLE TYPE: Bimodal, Poorly Sorted

TEXTURAL GROUP: Mud

SEDIMENT NAME: Medium Silt

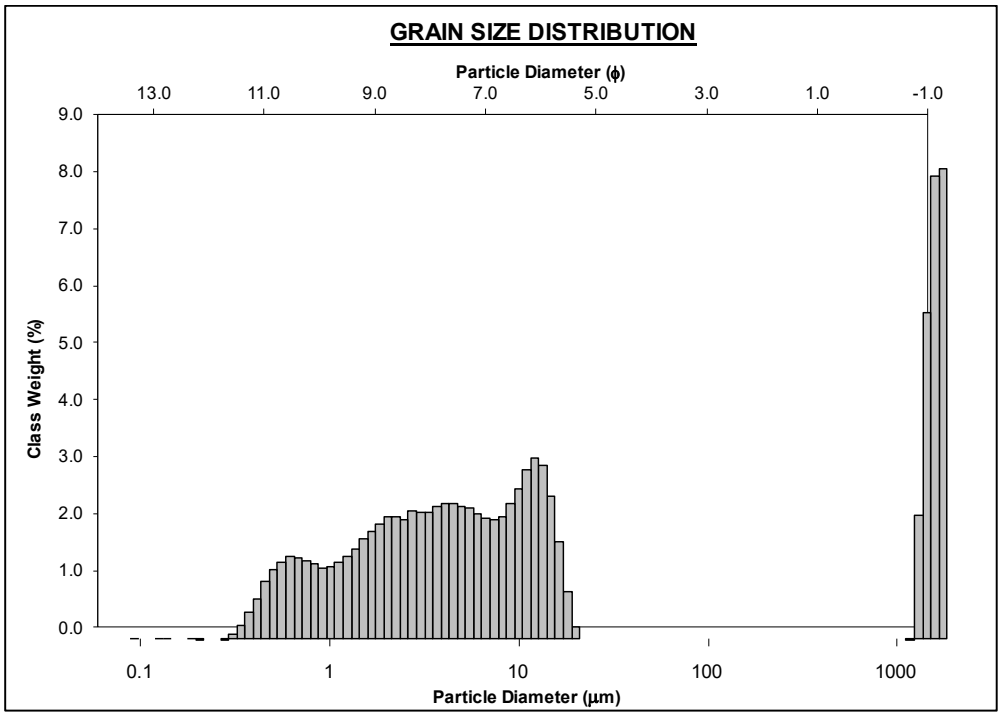
	µm	ϕ
MODE 1:	14.87	6.074
MODE 2:	3.402	8.202
MODE 3:		
D_{10}:	0.845	5.911
MEDIAN or D_{50}:	4.807	7.701
D_{90}:	16.62	10.21
(D_{90} / D_{10}):	19.69	1.727
(D_{90} - D_{10}):	15.78	4.299
(D_{75} / D_{25}):	6.262	1.419
(D_{75} - D_{25}):	10.49	2.647

GRAIN SIZE DISTRIBUTION

GRAVEL: 0.0%	COARSE SAND: 0.0%
SAND: 0.0%	MEDIUM SAND: 0.0%
MUD: 100.0%	FINE SAND: 0.0%
	V FINE SAND: 0.0%
V COARSE GRAVEL: 0.0%	V COARSE SILT: 0.1%
COARSE GRAVEL: 0.0%	COARSE SILT: 12.8%
MEDIUM GRAVEL: 0.0%	MEDIUM SILT: 27.7%
FINE GRAVEL: 0.0%	FINE SILT: 15.1%
V FINE GRAVEL: 0.0%	V FINE SILT: 19.8%
V COARSE SAND: 0.0%	CLAY: 24.5%

	METHOD OF MOMENTS			FOLK & WARD METHOD		
	Arithmetic	Geometric	Logarithmic	Geometric	Logarithmic	Description
	µm	µm	ϕ	µm	ϕ	
MEAN ($\bar{x}$):	7.381	4.473	7.800	4.455	7.810	Fine Silt
SORTING (σ):	6.306	3.065	1.624	3.139	1.650	Poorly Sorted
SKEWNESS (Sk):	0.776	-0.427	0.374	-0.152	0.152	Fine Skewed
KURTOSIS (K):	2.656	2.115	2.334	0.775	0.775	Platykurtic

197 cm



SAMPLE STATISTICS

SAMPLE IDENTITY: **HE23T4C4B 197 cm** ANALYST & DATE: K Drew,

SAMPLE TYPE: Polymodal, Extremely Poorly Sorted TEXTURAL GROUP: Sandy Mud

SEDIMENT NAME: Very Coarse Sandy Medium Silt

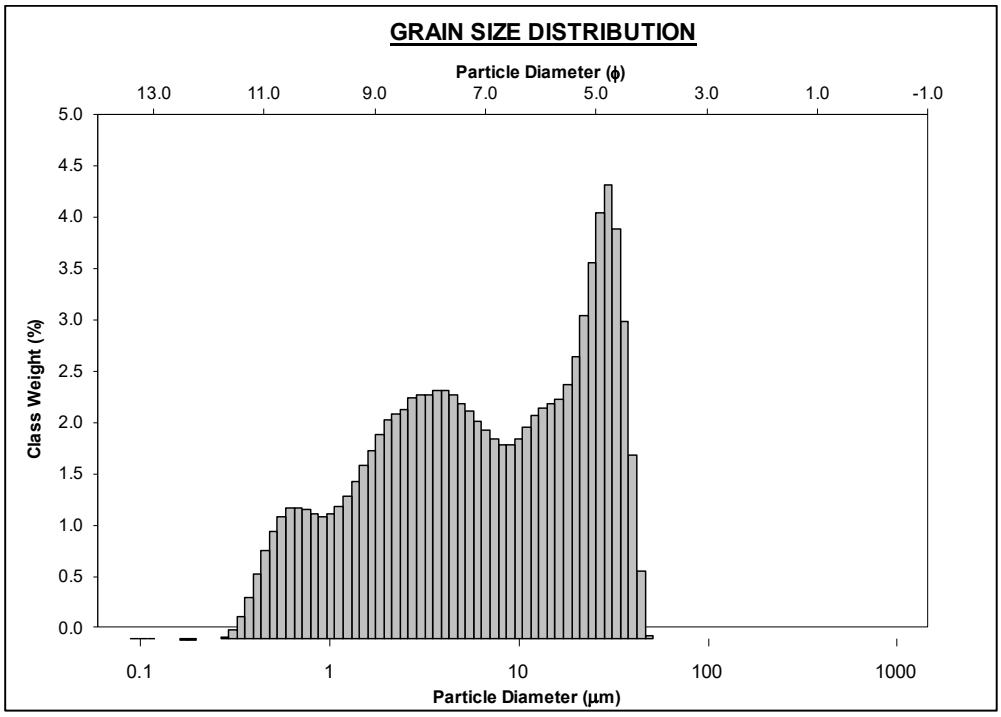
	µm	ϕ
MODE 1:	12.11	6.369
MODE 2:	4.484	7.803
MODE 3:	2.728	8.519
D_{10}:	0.873	-0.803
MEDIAN or D_{50}:	7.413	7.076
D_{90}:	1744.1	10.16
(D_{90} / D_{10}):	1997.4	-12.662
(D_{90} - D_{10}):	1743.3	10.96
(D_{75} / D_{25}):	620.0	-17.804
(D_{75} - D_{25}):	1405.4	9.276

GRAIN SIZE DISTRIBUTION

GRAVEL: 0.0%	COARSE SAND: 0.0%
SAND: 29.0%	MEDIUM SAND: 0.0%
MUD: 71.0%	FINE SAND: 0.0%
	V FINE SAND: 0.0%
V COARSE GRAVEL: 0.0%	V COARSE SILT: 0.0%
COARSE GRAVEL: 0.0%	COARSE SILT: 2.4%
MEDIUM GRAVEL: 0.0%	MEDIUM SILT: 17.5%
FINE GRAVEL: 0.0%	FINE SILT: 14.7%
V FINE GRAVEL: 0.0%	V FINE SILT: 14.4%
V COARSE SAND: 29.0%	CLAY: 22.0%

	METHOD OF MOMENTS			FOLK & WARD METHOD		
	Arithmetic	Geometric	Logarithmic	Geometric	Logarithmic	Description
	µm	µm	ϕ	µm	ϕ	
MEAN ($\bar{x}$):	360.4	12.67	5.673	25.53	5.292	Coarse Silt
SORTING (σ):	660.2	15.98	4.153	19.33	4.273	Extremely Poorly Sorted
SKEWNESS (Sk):	1.345	0.908	-0.616	0.444	-0.444	Very Coarse Skewed
KURTOSIS (K):	2.868	2.344	1.798	0.504	0.504	Very Platykurtic

197.5 cm



SAMPLE STATISTICS

SAMPLE IDENTITY: **HE23T4C4B 197.5 cm** ANALYST & DATE: K Drew,

SAMPLE TYPE: Polymodal, Poorly Sorted TEXTURAL GROUP: Mud

SEDIMENT NAME: Coarse Silt

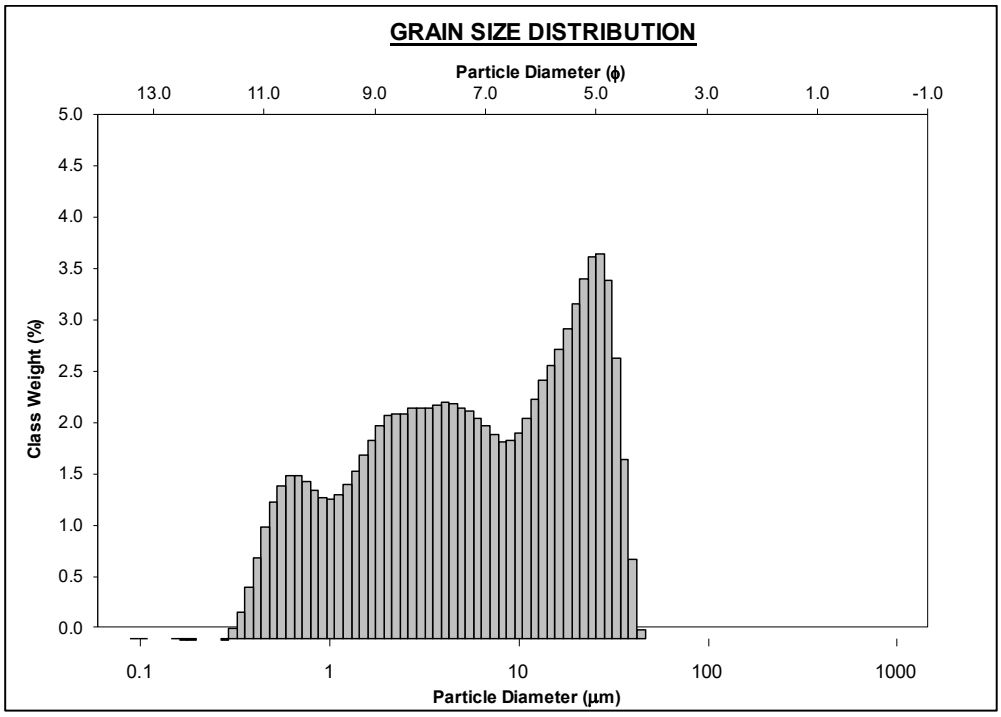
	µm	ϕ
MODE 1:	29.63	5.079
MODE 2:	4.060	7.946
MODE 3:	3.014	8.376
D_{10}:	0.907	5.021
MEDIAN or D_{50}:	6.637	7.235
D_{90}:	30.80	10.11
(D_{90} / D_{10}):	33.95	2.013
(D_{90} - D_{10}):	29.89	5.085
(D_{75} / D_{25}):	9.266	1.575
(D_{75} - D_{25}):	18.60	3.212

GRAIN SIZE DISTRIBUTION

GRAVEL: 0.0%	COARSE SAND: 0.0%
SAND: 0.0%	MEDIUM SAND: 0.0%
MUD: 100.0%	FINE SAND: 0.0%
	V FINE SAND: 0.0%
V COARSE GRAVEL: 0.0%	V COARSE SILT: 9.4%
COARSE GRAVEL: 0.0%	COARSE SILT: 22.9%
MEDIUM GRAVEL: 0.0%	MEDIUM SILT: 14.5%
FINE GRAVEL: 0.0%	FINE SILT: 15.3%
V FINE GRAVEL: 0.0%	V FINE SILT: 16.0%
V COARSE SAND: 0.0%	CLAY: 21.9%

	METHOD OF MOMENTS			FOLK & WARD METHOD		
	Arithmetic	Geometric	Logarithmic	Geometric	Logarithmic	Description
	µm	µm	ϕ	µm	ϕ	
MEAN ($\bar{x}$):	11.98	6.143	7.347	6.322	7.305	Fine Silt
SORTING (σ):	11.75	3.682	1.881	3.852	1.946	Poorly Sorted
SKEWNESS (Sk):	0.901	-0.319	0.319	-0.114	0.114	Fine Skewed
KURTOSIS (K):	2.557	1.977	1.977	0.746	0.746	Platykurtic

201 cm



SAMPLE STATISTICS

SAMPLE IDENTITY: **HE23T4C4B 201 cm**

ANALYST & DATE: K Drew,

SAMPLE TYPE: Polymodal, Poorly Sorted

TEXTURAL GROUP: Mud

SEDIMENT NAME: Coarse Silt

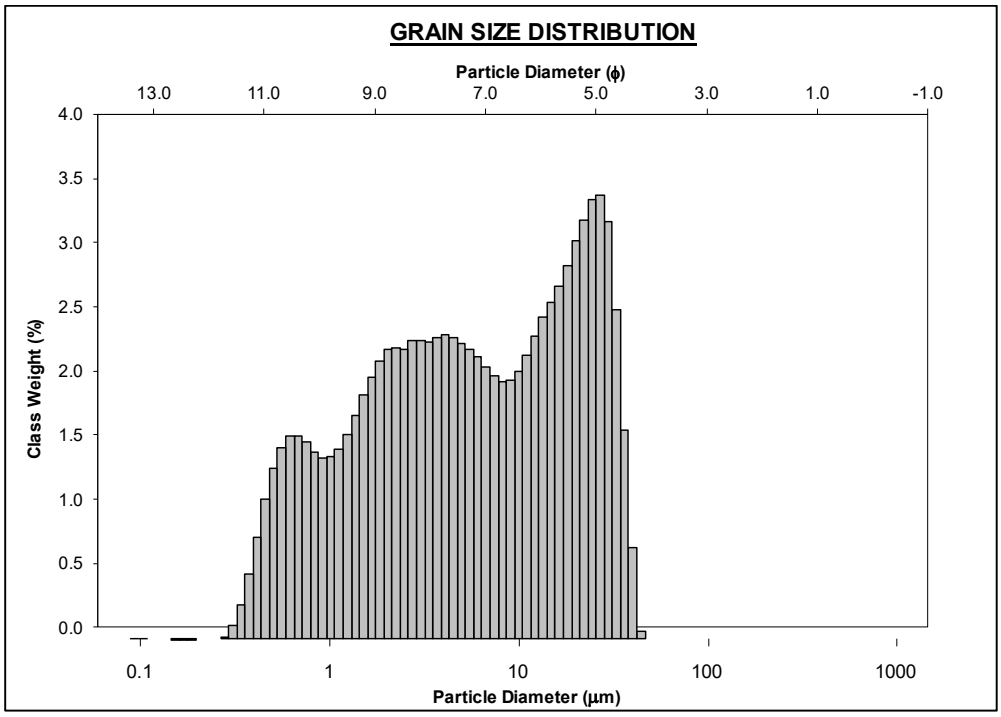
	µm	ϕ
MODE 1:	26.82	5.222
MODE 2:	4.060	7.946
MODE 3:	2.728	8.519
D_{10}:	0.773	5.195
MEDIAN or D_{50}:	5.901	7.405
D_{90}:	27.30	10.34
(D_{90} / D_{10}):	35.29	1.990
(D_{90} - D_{10}):	26.52	5.141
(D_{75} / D_{25}):	9.134	1.549
(D_{75} - D_{25}):	15.80	3.191

GRAIN SIZE DISTRIBUTION

GRAVEL: 0.0%	COARSE SAND: 0.0%
SAND: 0.0%	MEDIUM SAND: 0.0%
MUD: 100.0%	FINE SAND: 0.0%
	V FINE SAND: 0.0%
V COARSE GRAVEL: 0.0%	V COARSE SILT: 5.2%
COARSE GRAVEL: 0.0%	COARSE SILT: 23.5%
MEDIUM GRAVEL: 0.0%	MEDIUM SILT: 15.5%
FINE GRAVEL: 0.0%	FINE SILT: 15.2%
V FINE GRAVEL: 0.0%	V FINE SILT: 15.5%
V COARSE SAND: 0.0%	CLAY: 25.1%

	METHOD OF MOMENTS			FOLK & WARD METHOD		
	Arithmetic	Geometric	Logarithmic	Geometric	Logarithmic	Description
	µm	µm	ϕ	µm	ϕ	
MEAN ($\bar{x}$):	10.54	5.389	7.536	5.453	7.519	Fine Silt
SORTING (σ):	10.45	3.675	1.878	3.876	1.955	Poorly Sorted
SKEWNESS (Sk):	0.973	-0.294	0.294	-0.124	0.124	Fine Skewed
KURTOSIS (K):	2.800	1.925	1.925	0.746	0.746	Platykurtic

212 cm



SAMPLE STATISTICS

SAMPLE IDENTITY: **HE23T4C4B 212 cm**

ANALYST & DATE: K Drew,

SAMPLE TYPE: Polymodal, Poorly Sorted

TEXTURAL GROUP: Mud

SEDIMENT NAME: Coarse Silt

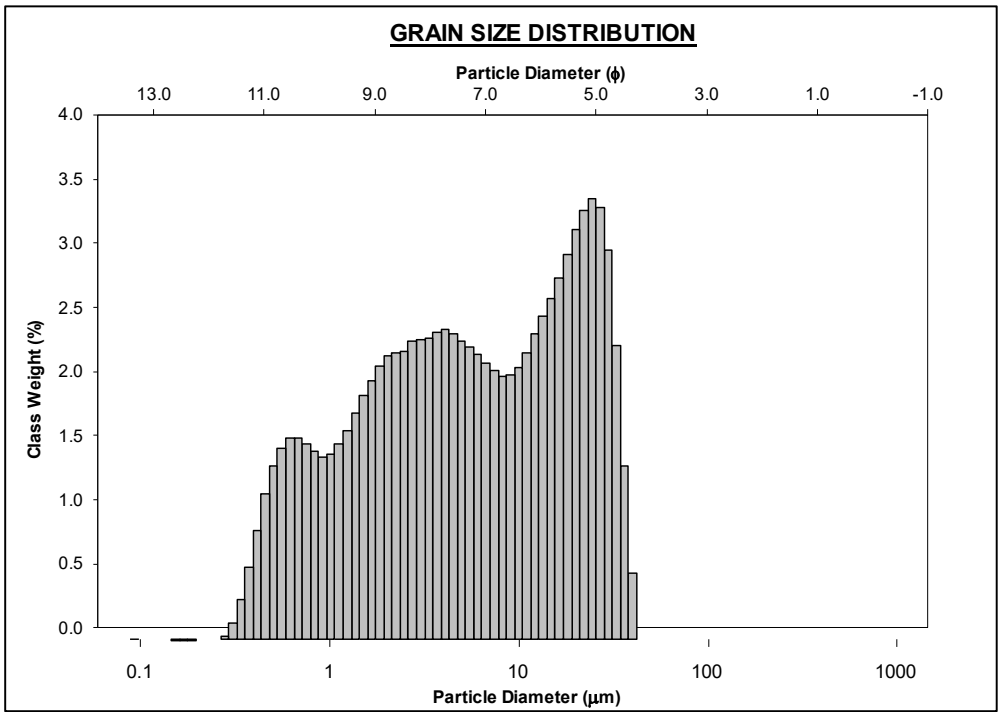
	µm	ϕ
MODE 1:	26.82	5.222
MODE 2:	4.060	7.946
MODE 3:	3.014	8.376
D_{10}:	0.774	5.225
MEDIAN or D_{50}:	5.547	7.494
D_{90}:	26.73	10.34
(D_{90} / D_{10}):	34.55	1.978
(D_{90} - D_{10}):	25.96	5.110
(D_{75} / D_{25}):	8.866	1.533
(D_{75} - D_{25}):	14.83	3.148

GRAIN SIZE DISTRIBUTION

GRAVEL: 0.0%	COARSE SAND: 0.0%
SAND: 0.0%	MEDIUM SAND: 0.0%
MUD: 100.0%	FINE SAND: 0.0%
	V FINE SAND: 0.0%
V COARSE GRAVEL: 0.0%	V COARSE SILT: 4.8%
COARSE GRAVEL: 0.0%	COARSE SILT: 22.0%
MEDIUM GRAVEL: 0.0%	MEDIUM SILT: 15.8%
FINE GRAVEL: 0.0%	FINE SILT: 15.5%
V FINE GRAVEL: 0.0%	V FINE SILT: 16.0%
V COARSE SAND: 0.0%	CLAY: 25.8%

	METHOD OF MOMENTS			FOLK & WARD METHOD		
	Arithmetic	Geometric	Logarithmic	Geometric	Logarithmic	Description
	µm	µm	ϕ	µm	ϕ	
MEAN ($\bar{x}$):	10.13	5.182	7.592	5.261	7.571	Fine Silt
SORTING (σ):	10.23	3.631	1.860	3.843	1.942	Poorly Sorted
SKEWNESS (Sk):	1.048	-0.255	0.255	-0.098	0.098	Symmetrical
KURTOSIS (K):	2.986	1.927	1.927	0.753	0.753	Platykurtic

220 cm



SAMPLE STATISTICS

SAMPLE IDENTITY: **HE23T4C4B 220 cm**

ANALYST & DATE: K Drew,

SAMPLE TYPE: Trimodal, Poorly Sorted

TEXTURAL GROUP: Mud

SEDIMENT NAME: Coarse Silt

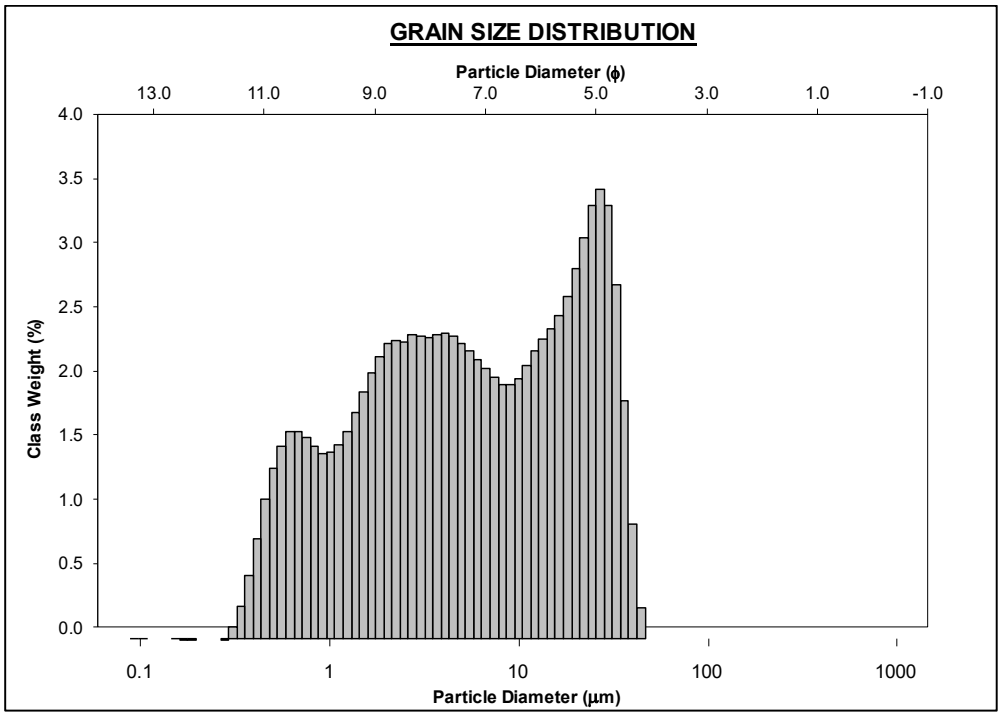
	µm	ϕ
MODE 1:	24.29	5.365
MODE 2:	4.060	7.946
MODE 3:	0.615	10.67
D_{10}:	0.761	5.271
MEDIAN or D_{50}:	5.441	7.522
D_{90}:	25.91	10.36
(D_{90} / D_{10}):	34.05	1.966
(D_{90} - D_{10}):	25.15	5.090
(D_{75} / D_{25}):	8.754	1.527
(D_{75} - D_{25}):	14.39	3.130

GRAIN SIZE DISTRIBUTION

GRAVEL: 0.0%	COARSE SAND: 0.0%
SAND: 0.0%	MEDIUM SAND: 0.0%
MUD: 100.0%	FINE SAND: 0.0%
	V FINE SAND: 0.0%
V COARSE GRAVEL: 0.0%	V COARSE SILT: 4.0%
COARSE GRAVEL: 0.0%	COARSE SILT: 22.1%
MEDIUM GRAVEL: 0.0%	MEDIUM SILT: 16.0%
FINE GRAVEL: 0.0%	FINE SILT: 15.7%
V FINE GRAVEL: 0.0%	V FINE SILT: 16.0%
V COARSE SAND: 0.0%	CLAY: 26.1%

	METHOD OF MOMENTS			FOLK & WARD METHOD		
	Arithmetic	Geometric	Logarithmic	Geometric	Logarithmic	Description
	µm	µm	ϕ	µm	ϕ	
MEAN ($\bar{x}$):	9.851	5.065	7.625	5.132	7.606	Fine Silt
SORTING (σ):	9.927	3.614	1.854	3.830	1.937	Poorly Sorted
SKEWNESS (Sk):	1.052	-0.261	0.261	-0.101	0.101	Fine Skewed
KURTOSIS (K):	3.005	1.938	1.938	0.756	0.756	Platykurtic

230 cm



SAMPLE STATISTICS

SAMPLE IDENTITY: **HE23T4C4B 230 cm**

ANALYST & DATE: K Drew,

SAMPLE TYPE: Polymodal, Poorly Sorted

TEXTURAL GROUP: Mud

SEDIMENT NAME: Coarse Silt

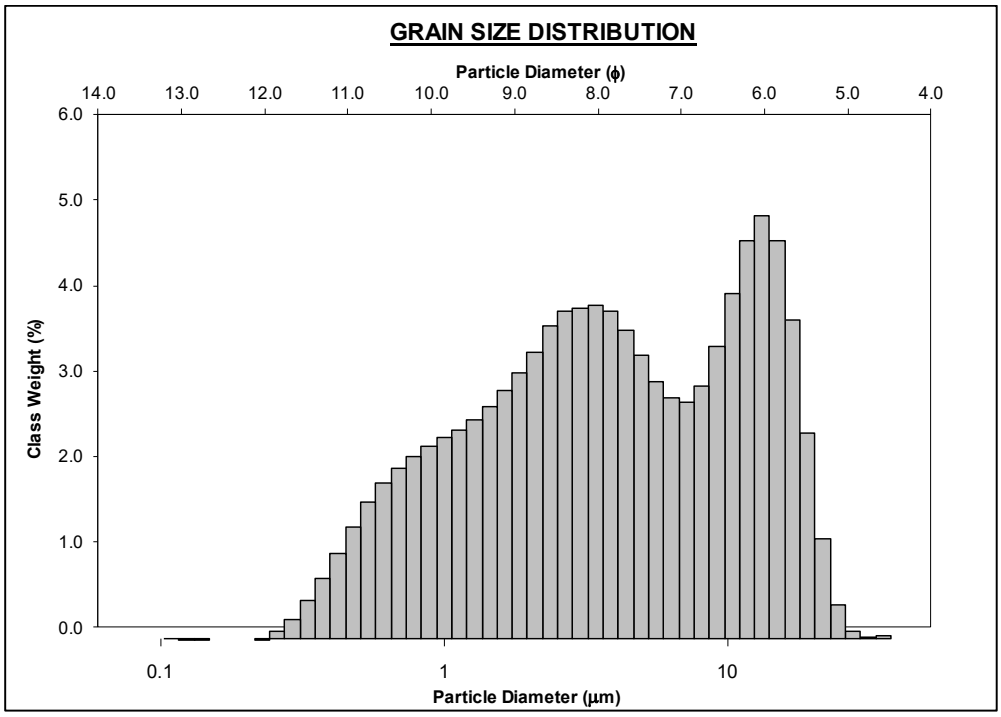
	µm	ϕ
MODE 1:	26.82	5.222
MODE 2:	4.060	7.946
MODE 3:	2.728	8.519
D_{10}:	0.769	5.187
MEDIAN or D_{50}:	5.384	7.537
D_{90}:	27.45	10.34
(D_{90} / D_{10}):	35.69	1.994
(D_{90} - D_{10}):	26.68	5.157
(D_{75} / D_{25}):	9.107	1.541
(D_{75} - D_{25}):	15.03	3.187

GRAIN SIZE DISTRIBUTION

GRAVEL: 0.0%	COARSE SAND: 0.0%
SAND: 0.0%	MEDIUM SAND: 0.0%
MUD: 100.0%	FINE SAND: 0.0%
	V FINE SAND: 0.0%
V COARSE GRAVEL: 0.0%	V COARSE SILT: 5.6%
COARSE GRAVEL: 0.0%	COARSE SILT: 21.4%
MEDIUM GRAVEL: 0.0%	MEDIUM SILT: 15.1%
FINE GRAVEL: 0.0%	FINE SILT: 15.5%
V FINE GRAVEL: 0.0%	V FINE SILT: 16.3%
V COARSE SAND: 0.0%	CLAY: 26.2%

	METHOD OF MOMENTS			FOLK & WARD METHOD		
	Arithmetic µm	Geometric µm	Logarithmic ϕ	Geometric µm	Logarithmic ϕ	Description
MEAN ($\bar{x}$):	10.23	5.144	7.603	5.227	7.580	Fine Silt
SORTING (σ):	10.54	3.669	1.875	3.902	1.964	Poorly Sorted
SKEWNESS (Sk):	1.083	-0.219	0.219	-0.074	0.074	Symmetrical
KURTOSIS (K):	3.053	1.908	1.908	0.749	0.749	Platykurtic

240 cm



SAMPLE STATISTICS

SAMPLE IDENTITY: **HE23T4C4B 240 cm**

ANALYST & DATE: K Drew,

SAMPLE TYPE: Bimodal, Poorly Sorted

TEXTURAL GROUP: Mud

SEDIMENT NAME: Medium Silt

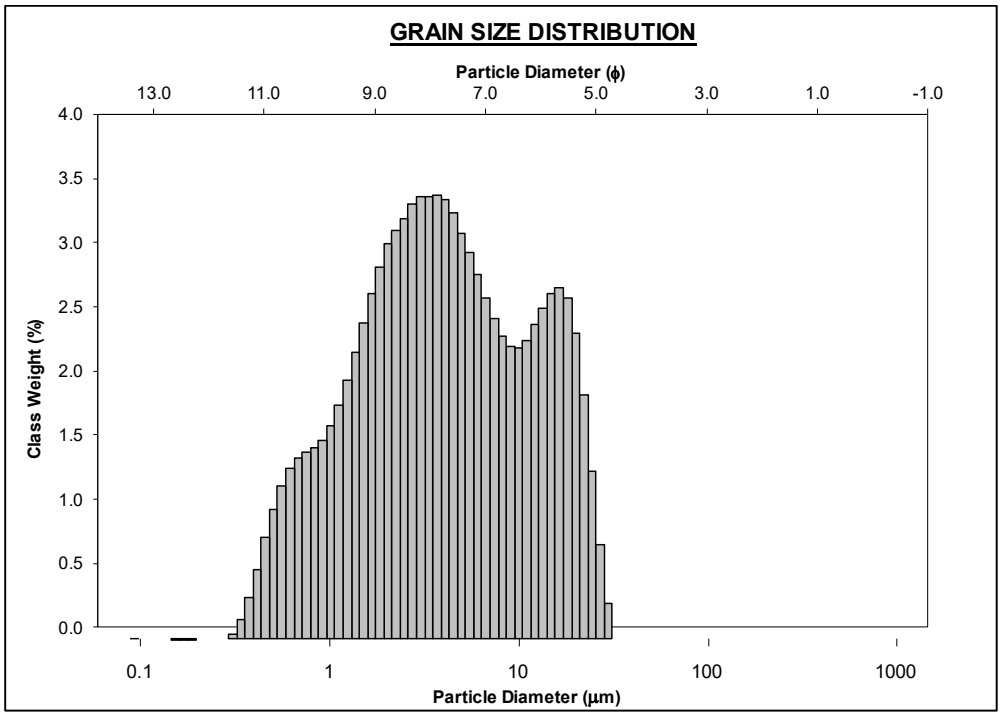
	µm	ϕ
MODE 1:	13.15	6.251
MODE 2:	3.402	8.202
MODE 3:		
D_{10}:	0.765	6.067
MEDIAN or D_{50}:	3.827	8.030
D_{90}:	14.91	10.35
(D_{90} / D_{10}):	19.50	1.706
(D_{90} - D_{10}):	14.15	4.286
(D_{75} / D_{25}):	6.174	1.395
(D_{75} - D_{25}):	8.374	2.626

GRAIN SIZE DISTRIBUTION

GRAVEL: 0.0%	COARSE SAND: 0.0%
SAND: 0.0%	MEDIUM SAND: 0.0%
MUD: 100.0%	FINE SAND: 0.0%
	V FINE SAND: 0.0%
V COARSE GRAVEL: 0.0%	V COARSE SILT: 0.1%
COARSE GRAVEL: 0.0%	COARSE SILT: 8.2%
MEDIUM GRAVEL: 0.0%	MEDIUM SILT: 23.4%
FINE GRAVEL: 0.0%	FINE SILT: 17.7%
V FINE GRAVEL: 0.0%	V FINE SILT: 21.0%
V COARSE SAND: 0.0%	CLAY: 29.6%

	METHOD OF MOMENTS			FOLK & WARD METHOD		
	Arithmetic	Geometric	Logarithmic	Geometric	Logarithmic	Description
	µm	µm	ϕ	µm	ϕ	
MEAN ($\bar{x}$):	6.145	3.691	8.081	3.730	8.067	Very Fine Silt
SORTING (σ):	5.655	2.994	1.584	3.141	1.651	Poorly Sorted
SKEWNESS (Sk):	1.075	-0.258	0.243	-0.077	0.077	Symmetrical
KURTOSIS (K):	3.360	2.059	2.130	0.775	0.775	Platykurtic

250 cm



SAMPLE STATISTICS

SAMPLE IDENTITY: **HE23T4C4B 250 cm**

ANALYST & DATE: K Drew,

SAMPLE TYPE: Bimodal, Poorly Sorted

TEXTURAL GROUP: Mud

SEDIMENT NAME: Very Fine Silt

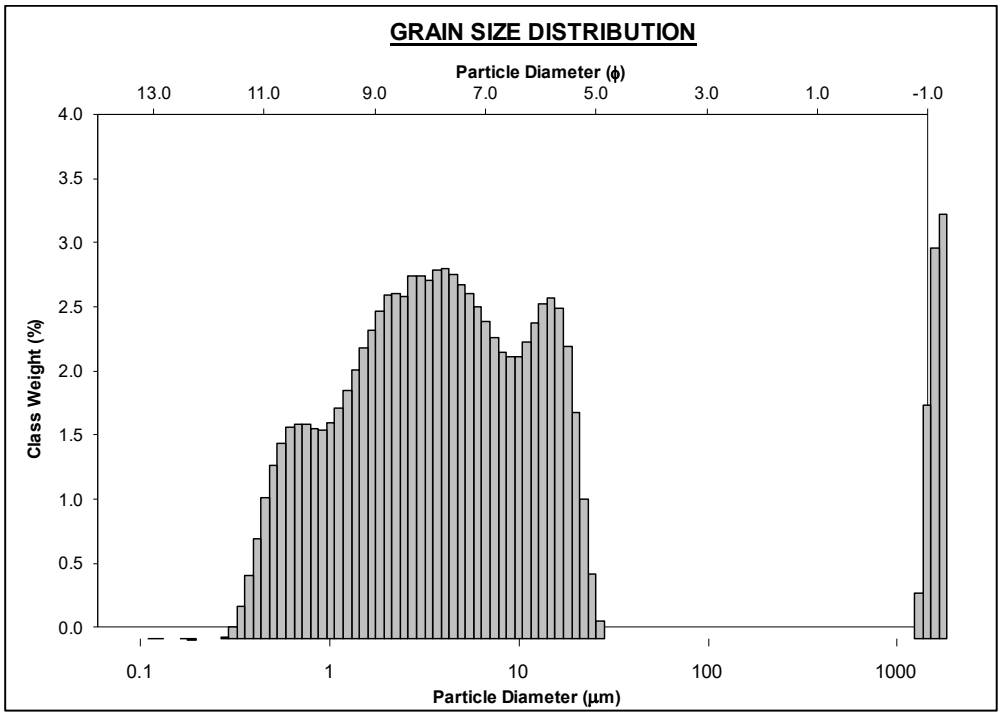
	µm	ϕ
MODE 1:	3.676	8.089
MODE 2:	16.32	5.939
MODE 3:		
D_{10}:	0.885	5.907
MEDIAN or D_{50}:	3.830	8.028
D_{90}:	16.67	10.14
(D_{90} / D_{10}):	18.84	1.717
(D_{90} - D_{10}):	15.78	4.236
(D_{75} / D_{25}):	5.091	1.347
(D_{75} - D_{25}):	7.343	2.348

GRAIN SIZE DISTRIBUTION

GRAVEL: 0.0%	COARSE SAND: 0.0%
SAND: 0.0%	MEDIUM SAND: 0.0%
MUD: 100.0%	FINE SAND: 0.0%
	V FINE SAND: 0.0%
V COARSE GRAVEL: 0.0%	V COARSE SILT: 0.0%
COARSE GRAVEL: 0.0%	COARSE SILT: 11.8%
MEDIUM GRAVEL: 0.0%	MEDIUM SILT: 16.9%
FINE GRAVEL: 0.0%	FINE SILT: 20.7%
V FINE GRAVEL: 0.0%	V FINE SILT: 23.2%
V COARSE SAND: 0.0%	CLAY: 27.5%

	METHOD OF MOMENTS			FOLK & WARD METHOD		
	Arithmetic	Geometric	Logarithmic	Geometric	Logarithmic	Description
	µm	µm	ϕ	µm	ϕ	
MEAN ($\bar{x}$):	6.415	3.867	8.015	3.992	7.969	Fine Silt
SORTING (σ):	6.324	2.886	1.529	3.062	1.614	Poorly Sorted
SKEWNESS (Sk):	1.379	-0.108	0.108	0.005	-0.005	Symmetrical
KURTOSIS (K):	4.102	2.162	2.162	0.875	0.875	Platykurtic

260 cm



SAMPLE STATISTICS

SAMPLE IDENTITY: **HE23T4C4B 260 cm** ANALYST & DATE: K Drew,

SAMPLE TYPE: Polymodal, Very Poorly Sorted TEXTURAL GROUP: Sandy Mud

SEDIMENT NAME: Very Coarse Sandy Very Fine Silt

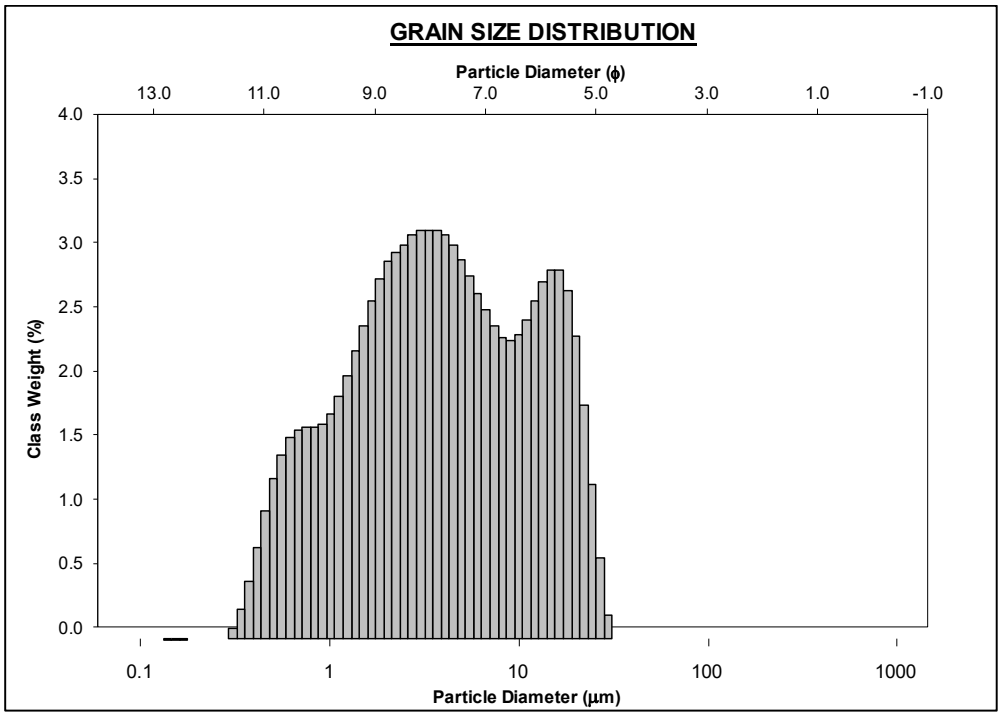
	μm	ϕ
MODE 1:	4.060	7.946
MODE 2:	2.728	8.519
MODE 3:	2.237	8.806
D_{10}:	0.772	-0.493
MEDIAN or D_{50}:	4.351	7.844
D_{90}:	1407.5	10.34
(D_{90} / D_{10}):	1823.4	-20.965
(D_{90} - D_{10}):	1406.8	10.83
(D_{75} / D_{25}):	7.170	1.448
(D_{75} - D_{25}):	10.60	2.842

GRAIN SIZE DISTRIBUTION

GRAVEL: 0.0%	COARSE SAND: 0.0%
SAND: 11.0%	MEDIUM SAND: 0.0%
MUD: 89.0%	FINE SAND: 0.0%
	V FINE SAND: 0.0%
V COARSE GRAVEL: 0.0%	V COARSE SILT: 0.0%
COARSE GRAVEL: 0.0%	COARSE SILT: 7.9%
MEDIUM GRAVEL: 0.0%	MEDIUM SILT: 16.2%
FINE GRAVEL: 0.0%	FINE SILT: 17.9%
V FINE GRAVEL: 0.0%	V FINE SILT: 18.8%
V COARSE SAND: 11.0%	CLAY: 28.2%

	METHOD OF MOMENTS			FOLK & WARD METHOD		
	Arithmetic	Geometric	Logarithmic	Geometric	Logarithmic	Description
	μm	μm	ϕ	μm	ϕ	
MEAN ($\bar{x}$):	137.5	5.561	7.220	4.403	7.827	Fine Silt
SORTING (σ):	440.6	7.361	3.094	6.710	2.746	Very Poorly Sorted
SKEWNESS (Sk):	3.067	1.647	-1.463	0.252	-0.252	Coarse Skewed
KURTOSIS (K):	10.50	5.634	4.590	1.666	1.666	Very Leptokurtic

270 cm



SAMPLE STATISTICS

SAMPLE IDENTITY: **HE23T4C4B 270 cm**

ANALYST & DATE: K Drew,

SAMPLE TYPE: Trimodal, Poorly Sorted

TEXTURAL GROUP: Mud

SEDIMENT NAME: Very Fine Silt

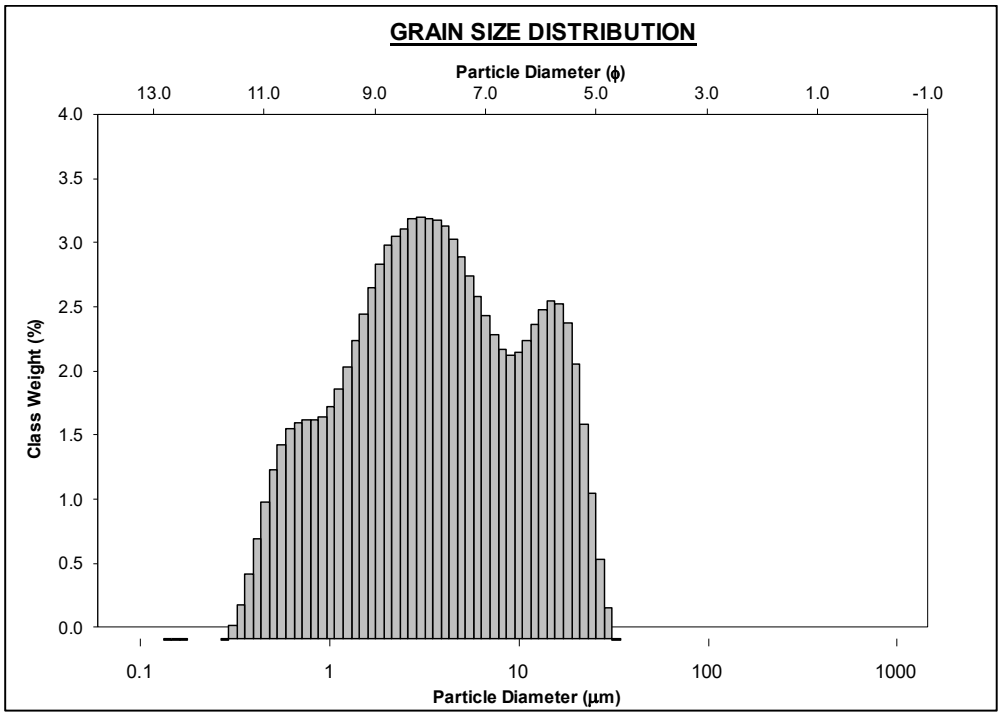
	µm	ϕ
MODE 1:	3.676	8.089
MODE 2:	3.014	8.376
MODE 3:	14.78	6.082
D_{10}:	0.788	5.921
MEDIAN or D_{50}:	3.768	8.052
D_{90}:	16.50	10.31
(D_{90} / D_{10}):	20.93	1.741
(D_{90} - D_{10}):	15.71	4.388
(D_{75} / D_{25}):	5.658	1.371
(D_{75} - D_{25}):	7.734	2.500

GRAIN SIZE DISTRIBUTION

GRAVEL: 0.0%	COARSE SAND: 0.0%
SAND: 0.0%	MEDIUM SAND: 0.0%
MUD: 100.0%	FINE SAND: 0.0%
	V FINE SAND: 0.0%
V COARSE GRAVEL: 0.0%	V COARSE SILT: 0.0%
COARSE GRAVEL: 0.0%	COARSE SILT: 11.6%
MEDIUM GRAVEL: 0.0%	MEDIUM SILT: 17.8%
FINE GRAVEL: 0.0%	FINE SILT: 19.5%
V FINE GRAVEL: 0.0%	V FINE SILT: 21.6%
V COARSE SAND: 0.0%	CLAY: 29.5%

	METHOD OF MOMENTS			FOLK & WARD METHOD		
	Arithmetic µm	Geometric µm	Logarithmic ϕ	Geometric µm	Logarithmic ϕ	Description
MEAN ($\bar{x}$):	6.362	3.741	8.062	3.831	8.028	Very Fine Silt
SORTING (σ):	6.292	2.991	1.581	3.182	1.670	Poorly Sorted
SKEWNESS (Sk):	1.316	-0.132	0.132	-0.020	0.020	Symmetrical
KURTOSIS (K):	3.902	2.080	2.080	0.837	0.837	Platykurtic

279 cm



SAMPLE STATISTICS

SAMPLE IDENTITY: **HE23T4C4B 279 cm**

ANALYST & DATE: K Drew,

SAMPLE TYPE: Bimodal, Poorly Sorted

TEXTURAL GROUP: Mud

SEDIMENT NAME: Very Fine Silt

	µm	ϕ
MODE 1:	3.014	8.376
MODE 2:	14.78	6.082
MODE 3:		
D_{10}:	0.761	5.962
MEDIAN or D_{50}:	3.542	8.141
D_{90}:	16.04	10.36
(D_{90} / D_{10}):	21.08	1.738
(D_{90} - D_{10}):	15.28	4.398
(D_{75} / D_{25}):	5.427	1.356
(D_{75} - D_{25}):	7.058	2.440

GRAIN SIZE DISTRIBUTION

GRAVEL: 0.0%	COARSE SAND: 0.0%
SAND: 0.0%	MEDIUM SAND: 0.0%
MUD: 100.0%	FINE SAND: 0.0%
	V FINE SAND: 0.0%
V COARSE GRAVEL: 0.0%	V COARSE SILT: 0.0%
COARSE GRAVEL: 0.0%	COARSE SILT: 10.7%
MEDIUM GRAVEL: 0.0%	MEDIUM SILT: 16.6%
FINE GRAVEL: 0.0%	FINE SILT: 19.5%
V FINE GRAVEL: 0.0%	V FINE SILT: 22.4%
V COARSE SAND: 0.0%	CLAY: 30.8%

	METHOD OF MOMENTS			FOLK & WARD METHOD		
	Arithmetic	Geometric	Logarithmic	Geometric	Logarithmic	Description
	µm	µm	ϕ	µm	ϕ	
MEAN ($\bar{x}$):	6.091	3.560	8.134	3.643	8.101	Very Fine Silt
SORTING (σ):	6.189	2.982	1.576	3.182	1.670	Poorly Sorted
SKEWNESS (Sk):	1.431	-0.086	0.086	-0.001	0.001	Symmetrical
KURTOSIS (K):	4.312	2.104	2.104	0.861	0.861	Platykurtic